

A Cross Section of Amplitudes

by

Timothy M. Olson

A dissertation submitted in partial fulfillment
of the requirements for the degree of
Doctor of Philosophy
(Physics)
in the University of Michigan
2016

Doctoral Committee:

Associate Professor Henriette D. Elvang, Chair
Professor Dante E. Amidei
Professor Thomas Lam
Professor Finn Larsen
Professor James T. Liu

Acknowledgements

I am grateful to Henriette Elvang for guidance and collaboration on many projects. Much gratitude is due also to collaborators Nikolay Bobev, Yu-tin Huang, Cindy Keeler, Thomas Lam, Samuel Roland, and David E Speyer. Additional thanks to Ratin Akhoury, Nima Arkani-Hamed, Jake Bourjaily, Dan Freedman, Rachel Karpman, Michael Kiermaier, Finn Larsen, Jim Liu, Stefan Theisen, and Jaroslav Trnka for useful discussions. I would also like to thank all the graduate students and postdocs in the University of Michigan physics department whose interactions have been invaluable throughout my degree. Finally, I would like to thank Emily Olson for providing feedback and comments and for her constant support and love!

I have been supported by a Regents Graduate Fellowship at the University of Michigan and a National Science Foundation Graduate Research Fellowship under Grant No. F031543.

Table of Contents

Acknowledgements	ii
List of Tables	v
List of Figures	vi
List of Appendices	ix
Abstract	x
Chapter 1: Introduction	1
1.1 Overview	1
1.2 Background for Part I	3
1.3 New Results in Part I	9
1.4 Background for Part II	12
1.5 New Results in Part II	20
1.6 Summary of Results and Publications	24
Part I Constraining QFTs: Dilaton Effective Action and the a-theorem	26
Chapter 2: RG Flows in d Dimensions and the Dilaton Effective Action	26
2.1 Motivation and Preview	26
2.2 Dilaton Effective Action and Scattering in d Dimensions	30
2.3 Example: Free Scalar in 8d	40
2.4 Scalar Anomaly from Zeta-Function Regularization of the Free Energy	43
2.5 Free Scalar in d Dimensions and the Dilaton Effective Action	45

Chapter 3: Dilaton Effective Action with $\mathcal{N} = 1$ Supersymmetry	50
3.1 Motivation and Preview	50
3.2 Scattering Constraints from Supersymmetry	54
3.3 Dilaton Effective Action	56
3.4 Matching to Superspace Calculation	58
3.5 Dilaton and Axion Scattering in Flat Space	60
Part II Modern Methods for Amplitudes: Grassmannians and Plabic Graphs	65
Chapter 4: Grassmannians for Amplitudes	65
4.1 Motivation and Preview	65
4.2 $\mathcal{N} = 4$ SYM and the Grassmannian	67
4.3 Relating the Three Grassmannian Formulations	75
4.4 NMHV Integrals and Residues	80
4.5 3d ABJM Grassmannian	95
4.6 Outlook	110
Chapter 5: Orientations of BCFW Charts on the Grassmannian	113
5.1 Motivation and Preview	113
5.2 Background	117
5.3 Relating Distinct Charts	125
5.4 Applications	137
Appendices	144
Bibliography	176

List of Tables

1.1	Examples of the rapidly growing number of diagrams required to compute the n -gluon color-ordered tree amplitude.	13
2.1	Results for the coefficients α , β , γ , and $\tilde{\gamma}$ of the effective action (2.49) for the case of the d -dimensional free massive scalar flow. The subscript \circ in the table indicates that a factor of $(4\pi)^{-\lfloor d/2 \rfloor}$ was taken out, e.g. $\alpha = \alpha_{\circ}(4\pi)^{-\lfloor d/2 \rfloor}$. The label “div” indicates that the 1-loop scalar integral diverges at and beyond this order. The boxed results are those encoding the $d = 4, 6, 8$ anomaly flows for the free massive scalar; see (2.76). Terms with negative mass-dimension are not needed for our study of RG flows, but we include them here to illustrate that the amplitudes match even in those higher-derivative cases	47
D.1	Diagrams contributing to the 4-point 1-loop amplitude at $\mathcal{O}(p^8)$ in $8d$	153

List of Figures

1.1	A schematic diagram of a generic scattering amplitude \mathcal{A} . Particles in the initial state $ i\rangle$ are incoming from the left and the outgoing particles form the final state $\langle f $ on the right.	2
1.2	Illustration of an RG flow interpolating between an ultraviolet fixed point at high energy and an infrared fixed point at low energy.	4
1.3	A choice of contour avoiding the simple pole at the origin.	10
1.4	A collection of puzzle pieces that make a circular disk when they are properly joined together. Feynman diagrams are similar insofar as they tend to obfuscate the underlying structure.	14
1.5	A collection of rotationally symmetric puzzle pieces that also make a circular disk when they are properly assembled. Using symmetry as a guide can reveal the fundamental structure more clearly from the start.	14
1.6	The poset paths and dlog forms for a pair of distinct 2-dimensional charts on a submanifold. On the left, coordinate α corresponding to (ab) was added first, while on the right, coordinate β corresponding to (cd) was added first.	23
1.7	A suitable choice of edge weights. The product of weights around the quadrilateral must be -1	23
4.1	An on-shell diagram representation of the permutation $\tilde{\sigma} = \{3, 5, 6, 7, 9, 8, 11\}$. The ‘left-right path’ between external vertices 4 and 7 shows $\tilde{\sigma}(4) = 7$	91
4.2	An on-shell diagram representation of the permutation $\tilde{\sigma} = \{4, 5, 6, 7, 9, 10, 8\}$. External legs 1 and 7 are connected by a path with all white vertices, which forces their respective momenta to be parallel.	92
4.3	Two diagrams representing cells of the appropriate dimension for which the 6 th and 7 th minors vanish. Only the left diagram has kinematical support for generic momenta.	94
5.1	Two distinct sequences of transpositions connecting the 0-dimensional cell σ_0 to the 2-dimensional cell σ	115

5.2	A choice of edge weights such that the product around the loop is -1	115
5.3	Different types of paths through the poset of cells.	116
5.4	A $GL(1)$ transformation with scaling factor f	120
5.5	A merge operation.	120
5.6	A square move operation.	121
5.7	Adding a BCFW bridge.	123
5.8	The sequence of diagrams produced by (5.11). We have added a black vertex between the first two bridges to make the graph bipartite; it is drawn slightly smaller to distinguish it from the bridge vertices.	123
5.9	Two paths representing sequences of transpositions connecting the permutations σ_0 and σ . Together the paths form a closed loop.	126
5.10	Graphs representing the sequences defined in step (2i) of Algorithm 1.	130
5.11	Boundaries of a 1-dimensional cell σ_1	131
5.12	A sequence of equivalence moves relating the two representative graphs for a 1d cell.	131
5.13	Two sequences that are identical except for the first transposition.	132
5.14	Reference paths from Algorithm 1 and interior quadrilaterals.	134
5.15	The two 0d cells at the end of the paths are connected by a sawtooth path between 1d and 0d cells. Combining this path with the input paths yields a closed loop.	136
5.16	A set of edge weights that locally match the signs obtained by direct computation.	138
5.17	A factorization channel representing a physical, local pole.	140
5.18	A diagram for the permutation $\{4, 5, 6, 8, 9, 10, 14\}$. It represents an unphysical, nonlocal singularity.	141
5.19	Grouping legs 6 and 7 in Figure 5.18 leads to a diagram of the form in Figure 5.17.	142
5.20	A closeup of the left-hand subamplitude in Figure 5.19.	142
D.1	All external momenta are outgoing. Loop momentum flows clockwise.	150
D.2	Two distinct $n = 6$ box diagrams with canonical labels.	151
I.1	Graph manipulations used to compare the transposition sequences in case (ii).	168
I.2	Graph manipulations used to compare the transposition sequences in case (iii).	169
I.3	Simple graph manipulations used to compare the transposition sequences in case (iv). A square move is required to complete the transformation.	170
I.4	Graph manipulations used to compare the transposition sequences in case (v).	171

I.5	An on-shell diagram with bridges (ad) and (bc)	172
I.6	Graph manipulations used to compare the transposition sequences in case (vi), where we have defined $\Delta = 1/(\alpha_j + \alpha_{j+3})$	173

List of Appendices

Appendix A: Euler Density and the WZ Action	144
Appendix B: $\text{Diff} \times \text{Weyl}$ Invariants in d Dimensions	145
Appendix C: Dilaton Amplitudes in d Dimensions	148
Appendix D: Free Massive Scalar: 1-Loop Dilaton Scattering	150
Appendix E: Conformal Anomaly	154
Appendix F: Matrix Q Details	157
F.1 Derivation of $\det Q$	157
F.2 Verification of Q^{-1}	159
Appendix G: Calculations of Higher-Dimensional Residues	161
Appendix H: Pole Structure of 6-Point ABJM Amplitude	165
Appendix I: Details for Algorithm 1	167
Appendix J: Assigning Edge Weights	174
J.1 Reduced Words	174
J.2 Decorating Edges	175

Abstract

Scattering amplitudes provide a handle for testing and constraining quantum field theories. In this thesis, I explore two directions within the topic: 1) using amplitudes to probe how the number of degrees of freedom evolves as the energy scale changes along renormalization group flows, and 2) extending a new modern approach to computing amplitudes that reveals the intriguing underlying mathematical structure. In the first part, I generalize a method that encodes the flow of degrees of freedom into certain scattering amplitudes from four dimensions to arbitrary dimensions and uncover new structures that become relevant in eight dimensions. I also demonstrate that scattering of other massless modes cannot interfere with the 4d method. In the second part, I explore a reformulation of tree-level amplitudes in 4d $\mathcal{N} = 4$ super Yang-Mills (SYM) theory in terms of a contour integral over the space of $k \times n$ matrices and show how to extend several aspects beyond $\mathcal{N} = 4$ SYM theory. A key new result is an algorithm I developed to resolve an important sign ambiguity in calculating residues of the contour integral.

Chapter 1

Introduction

1.1 Overview

Particle physics constantly pushes the limits of experimental and theoretical understanding. The unceasing development of higher energy and higher precision experiments has driven the pursuit of more advanced descriptions of the physics. This in turn has led to new insights and revealed unexpected connections between physics and mathematics, especially through the study of quantum field theories (QFTs). Examples of such insights will become apparent as the main contribution of this thesis is to collect and synthesize new theoretical results in the subject of *scattering amplitudes*.

Scattering occurs when an initial quantum state $|i\rangle$ of incident particles interact and transition into an outgoing final state $\langle f|$. It can be pictured intuitively as in Figure 1.1. The probability amplitude of the interaction, i.e., the scattering amplitude, mathematically represents that transition:

$$\mathcal{A} = \langle f|i\rangle. \tag{1.1}$$

Amplitudes provide an essential link between theory and experiment, allowing proposed QFT descriptions of fundamental physics to be tested and constrained. In scattering experiments, one measures the probability of a given final state occurring given the known initial state. The probability measurements are then translated to scattering cross sections σ . These are compared to theoretical predictions derived from amplitudes as an integral over moduli squared amplitudes:

$$\sigma \sim \int |\mathcal{A}|^2. \tag{1.2}$$

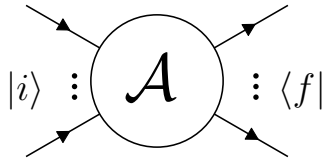


Figure 1.1: A schematic diagram of a generic scattering amplitude \mathcal{A} . Particles in the initial state $|i\rangle$ are incoming from the left and the outgoing particles form the final state $\langle f|$ on the right.

New physics beyond the Standard Model will likely be hidden in tiny signals among Standard Model backgrounds, so in order to unravel the new phenomena, it is crucial to have a solid theoretical understanding of the known amplitudes and efficient techniques for computing them.

The traditional method for computing an amplitude is to encode the possible interactions pictorially in Feynman diagrams and then sum over all diagrams that can contribute to the process. The Feynman approach can be very useful for computations in weakly coupled theories with simple interactions where one can in principle expand perturbatively in the small coupling constant (the parameter that encodes the strength of interaction) and solve the problem order-by-order in the expansion.

The Feynman approach emphasizes the properties of locality and unitarity, which are thought to be fundamental to any QFT that describes our universe. By exploiting these properties, one can discover strong constraints on scattering amplitudes and the dynamical evolution of QFTs. For example, unitarity implies the optical theorem, which relates the imaginary part of a scattering amplitude to a sum over scattering cross sections. Similar analytic features can (and will in Part I of this thesis) be exploited to construct essential conditions for important intrinsic quantities of unitary QFTs.

While Feynman diagrams can provide useful results, in many theories the calculations quickly become intractable due to the inordinate number of diagrams that must be evaluated and the myriad of cancellations that tend to occur. The issue stems from the focus on locality and unitarity at the cost of serious unphysical redundancies in intermediate steps. For example, scalar theories can be modified by field redefinitions that are invisible from the point of view of amplitudes, but can significantly change the values of individual Feynman diagrams. Theories with higher spin have increasingly complex gauge redundancies that are respected only by the sum over Feynman diagrams, but not necessarily by each diagram alone. Complicated symmetry transformations often exhibit similar behavior. All of these actions shuffle information around between different diagrams in just such a way as to leave the total amplitude invariant. This begs the question: could there be a different way to

compute amplitudes such that symmetry and gauge invariance are manifest from the start? Rather than imposing unitarity and locality on individual pieces, perhaps one can instead construct building blocks of the amplitude that each obey the symmetries and combine them such that locality and unitarity emerge in the sum. This objective has spurred the development of new computational techniques and revised geometric interpretations of amplitudes in specific QFTs. Aspects of these modern methods are the subject of Part II.

This thesis is divided into two parts, which together provide progress toward two goals of the amplitudes program: using scattering amplitudes to understand fundamental properties, structures, and symmetries of QFTs; and developing efficient methods for computing them. In Part I, the former goal is central. The primary objective is to use analyticity properties of scattering amplitudes to study how degrees of freedom evolve as the energy scale changes in a QFT. Part II primarily deals with the latter goal. The main focus is to clarify and extend the development of a matrix-integral approach to computing amplitudes while filling in some gaps in the logic. A secondary focus is to provide a crisp geometric interpretation of the results. The remainder of this introduction will be organized to parallel the bipartite structure of the main text. For each part, essential background will be presented first, followed by an overview of my contributions to the field.

1.2 Background for Part I

1.2.1 RG Flows and CFTs

The dynamics of quantum field theories will generally vary depending on the relevant scales in the problem. Intuitively, at energies much smaller than a particle's mass M , there will be insufficient energy to create the particle. It can only be exchanged internally in Feynman diagrams, so its effect can be encoded in an effective low energy description in which lower mass particles will have extra interaction terms with small coefficients determined essentially by the ratio of the momenta to the mass M . Scattering amplitudes can be computed perturbatively as long as the couplings remain small. As the momentum rises however, the perturbative expansion in the effective theory will break down because the ratios become larger. To obtain sensible results at and above energies of the order of M , one needs to return to the full theory with both the light and heavy particles.¹

This intuitive example demonstrates a theory evolving under changes in energy. More

¹A classic example from particle physics is Fermi's interaction for beta decay. At the energy scales relevant to nuclear decay, Fermi's interaction treats the neutron, proton, electron, and antineutrino as directly coupled. At higher energies, however, one must account for the full electroweak theory and incorporate the exchange of a W -boson.

generally, the dependence of parameters on energy is a fundamental feature of QFTs and leads to the subject of renormalization group (RG) flows. Energy dependence of the coupling constants g_i is encoded in the beta functions

$$\beta_i(\mu) = \frac{dg_i}{d \log \mu}, \quad (1.3)$$

where μ represents the energy scale. Typically, if the beta function for some coupling is positive, then the theory becomes strongly coupled at high energies and perturbation theory breaks down. Quantum electrodynamics (QED) has this feature; calculations performed assuming a small coupling are invalid at very high scales. Conversely a negative beta function indicates that the coupling weakens with energy. For example, quantum chromodynamics (QCD) is strongly coupled at low energy and asymptotically approaches a free theory at high energy.

A QFT with generic values of the couplings can be thought of as a point along some RG flow. Fundamentally, the beta functions governing the flow are differential equations, so it is not surprising that in many theories certain configurations of the couplings can define fixed points at which the beta functions vanish. The flow parameter is energy, so fixed points represent theories with no energy dependence. Since RG flows describe the evolution of theories under changes in energy, fixed points of the beta functions correspond to endpoints of RG flows. Thus many RG flows can be understood as interpolating between ultraviolet (UV) and infrared (IR) fixed points, as shown schematically in Figure 1.2

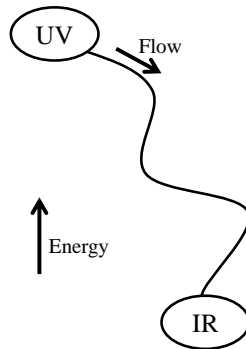


Figure 1.2: Illustration of an RG flow interpolating between an ultraviolet fixed point at high energy and an infrared fixed point at low energy.

There is another reason why fixed points are especially interesting to study. When the beta functions are zero, the theory dynamically generates a new symmetry: scale (dilatation) invariance. Extra symmetry means extra constraints on observables, which allows stronger results concerning properties of the theory. The dilatation symmetry is doubly significant be-

cause scale invariance is often accompanied by additional symmetries under angle-preserving diffeomorphisms known collectively as conformal invariance. Indeed, it has been proven in 2d that scale invariance implies conformal invariance under very general assumptions [1, 2], and a similar theorem has been conjectured in four dimensions, e.g., see [3, 4] for arguments in favor of the 4d conjecture.

Conformally invariant QFTs, known as conformal field theories (CFTs), are highly constrained due to the large amount of symmetry they obey. When RG flows end at CFTs, one can hope to leverage some of the CFT results to gain insight into properties of the flows. In particular, the presence of a conformal anomaly in curved spaces has been used to prove irreversibility theorems in 2d and 4d for RG flows in a very broad class of QFTs [2, 5]. The motivation stems from the Wilsonian intuition that as the energy decreases along RG flows, degrees of freedom that would require more energy than the RG scale should be effectively eliminated. The example described at the beginning of this section illustrates this intuition as the degrees of freedom associated with the massive field are kinematically inaccessible at low energies. Since the low energy theory has fewer degrees of freedom than the high energy theory, there is no way to flow back to the original theory from the low energy one. In that sense, RG flows are expected to be irreversible, as proven directly in 2d and 4d. Chapters 2 and 3 are based on the ideas presented in [5, 6], so it will be worthwhile to review the framework now.

1.2.2 Irreversibility of RG Flows

The original 2d theorem due to Zamolodchikov can be stated as follows [2]:

Theorem 1 (*c*-theorem). *For any unitary, Lorentz-invariant 2d QFT with a conserved stress tensor, there exists a positive definite real function $c(g)$ which is*

1. *Monotonically decreasing along RG flows*
2. *Stationary at fixed points*
3. *Equal to the central charges of the CFTs at the fixed points*

Zamolodchikov's *c*-theorem is so called due to the close connection to a fundamental 2d CFT parameter traditionally denoted *c*. In a generic CFT, the stress tensor $T_{\mu\nu}$ is classically traceless, but a quantum anomaly will generally spoil the tracelessness condition in curved space. For example, the 2d trace anomaly may be familiar from its ubiquitous presence in string theory,

$$\langle T_{\mu}^{\mu} \rangle = -\frac{c}{24}R, \tag{1.4}$$

where R is the Ricci curvature of the background spacetime and c is a pure number that is characteristic of the theory in question. Perturbatively, c is closely related to the field content of the theory, so the intuition is to interpret the central charge as a measure of the degrees of freedom in the CFT. This idea seems to be borne out in practice as the central charge is intimately tied to the entanglement entropy of quantum systems, e.g., in 2d, the entanglement entropy S_{EE} between a line segment and the rest of the universe is [7, 8]

$$S_{EE} = \frac{c + \bar{c}}{6} \log \frac{\Sigma}{\epsilon}, \quad (1.5)$$

where c and \bar{c} are the left and right moving central charges, Σ is the size of the region, and ϵ is a UV cutoff. The entropy S_{EE} naively measures the entanglement between separated regions, but it has since been shown to carry additional fundamental information. For example, holographic calculations demonstrate that the Bekenstein-Hawking entropy of a BTZ black hole is completely captured by entanglement entropy in a dual 2d CFT [9]. The Bekenstein-Hawking entropy is usually interpreted as a thermal entropy, but a relationship between 2d thermal and entanglement entropies was proposed in [9] and subsequently proven in [10]. Since thermal entropy is supposed to provide a count of the number of microstates, i.e., degrees of freedom in a system, the key takeaway is that the 2d central charge provides a genuine measure of the degrees of freedom in a system. The c -theorem guarantees the number always decreases along RG flows, thus realizing the Wilsonian intuition that degrees of freedom are lost along RG flows.

A similar story is expected to be true in higher dimensions, and a version of the c -theorem has been generalized to all dimensions for theories that obey a gauge/gravity duality [11, 12]. However, not all RG flows have dual gravitational descriptions, so an alternative method will be required for those cases. Zamolodchikov's approach cannot be directly extended beyond 2d due to obstructions whose source depends on the number of dimensions; in odd dimensions there is no trace anomaly, which rules out an odd-dimensional version,² while in even dimensions there are additional contributions to Zamolodchikov's $c(g)$ function that interfere with the proof.

Nevertheless, the trace of the stress tensor in even dimensions is still expected to carry some measure of degrees of freedom. The trick will be to isolate the appropriate quantities. The full trace anomaly takes the following general form in even dimensions [19, 20]:

$$\langle T^\mu_\mu \rangle = \sum_i c_i I_i - (-1)^{d/2} a E_d, \quad (1.6)$$

²Alternative measures of degrees of freedom such as the free energy have been proposed, and a related F -theorem was proven in 3d [13, 14, 15, 16, 17, 18].

where $\sqrt{-g}I_i$ are dimension-specific Weyl invariants, c_i are the corresponding central charges, and a is the central charge associated with the d -dimensional Euler density E_d .³ In 2d, there are no c_i , and the so-called a -anomaly is the only contribution (for historical reasons it is customary to use c instead of a in that case). The c_i cannot provide higher-dimensional generalizations of the c -theorem as they are not generally monotonic along RG flows [21, 22, 23]. However, on the basis of 1-loop monotonicity evidence, Cardy conjectured that the a -anomaly could ultimately provide a higher-dimensional version of the theorem [24].

Over two decades after the 2d c -theorem was proven [2] and the a -theorem conjectured [24], the 4d version was proven in [5] using analytic properties of scattering amplitudes. A fairly detailed sketch of the proof follows since my work in Chapter 2 is a direct extension of this method, and Chapter 3 addresses a subtlety that was not explicitly considered in the original papers.

Proof Sketch. Consider two CFTs related by an RG flow as in Figure 1.2. The flow from CFT_{UV} can be ignited two ways, both of which lead to the presence of a particle called the *dilaton*:

1. **Spontaneously:** If the conformal symmetry is broken spontaneously, then there will be a massless scalar Goldstone boson for the broken scale symmetry. It is the dilaton.
2. **Explicitly:** If the conformal symmetry is broken explicitly by the insertion of a relevant operator (such as a mass term), then one can restore the symmetry by introducing the dilaton τ as a compensator field $\Omega = f e^{-2\tau}$ with $\langle \Omega \rangle = f$. For example,

$$M^2 \rightarrow M^2 e^{-2\tau} = (M^2/f^2) \Omega^2. \quad (1.7)$$

The modified theory is conformal and has a moduli space for the compensator. Now the mass term is induced by letting Ω take its VEV f , which spontaneously breaks the restored conformal symmetry as in the previous case. Hence the dilaton again appears as a Goldstone boson in the low energy theory.

The goal is to use the low energy dilaton effective action S_τ to extract information about the flow of the trace anomaly (in particular the a -anomaly). Specifically, it will be shown that the $2 \rightarrow 2$ dilaton scattering amplitude is proportional to the difference in anomaly between the 4d CFTs at the end points of the RG flow. By considering the analytic structure of the $2 \rightarrow 2$ amplitude, it follows that the change in anomaly must be nonnegative. Consequently, any RG flow between two CFTs is irreversible, and the intuition is borne out that the a -anomaly represents the effective degrees of freedom.

³The Euler density and Weyl invariants are constructed out of the metric $g_{\mu\nu}$ and its derivatives.

At high energy, the action is given by that of the UV CFT, while at low energy, the IR CFT and dilaton effective action decouple [25], so the total action is the sum:

$$\begin{aligned} S_{\text{UV}} &= \text{CFT}_{\text{UV}} \\ S_{\text{IR}} &= \text{CFT}_{\text{IR}} + S_\tau. \end{aligned} \tag{1.8}$$

A Ward identity $\langle T_\mu^\mu \rangle = 0$ remains valid when conformal symmetry is spontaneously broken [26], which implies that the total anomaly in S_{UV} must agree with the total anomaly in S_{IR} . This means the actions must satisfy a consistency condition similar to 't Hooft anomaly matching [27]. For the CFTs, the UV anomaly a_{UV} and IR anomaly a_{IR} are generally unequal, so the difference must be captured by the dilaton effective action: $a_\tau = a_{\text{UV}} - a_{\text{IR}} = \Delta a$.

Goldstone symmetries imply that the dilaton effective action must be classically scale invariant, but the symmetry is violated by precisely the trace anomaly (1.6). Under a scale transformation, $g_{\mu\nu} \rightarrow e^{2\sigma} g_{\mu\nu}$ and $\tau \rightarrow \tau + \sigma$, the action is invariant up to an anomaly-dependent term:

$$\delta_\sigma S_\tau = \int d^4x \sqrt{-g} \sigma \langle T_\mu^\mu \rangle = \int d^4x \sqrt{-g} \sigma (c_\tau W^2 - a_\tau E_4), \tag{1.9}$$

where W^2 is the square of the Weyl tensor.

In order to compute the relevant scattering amplitudes for the dilaton, it will be necessary to reconstruct the full dilaton effective action up to the appropriate order in derivatives. Starting from a simple ansatz whose variation gives (1.9) and iteratively adding terms to cancel extra variations, one eventually arrives at the so-called Wess-Zumino action for the dilaton:

$$\begin{aligned} S_{\text{WZ}} &= -a_\tau \int d^4x \sqrt{-g} \left(\tau E_4 + 4(R^{\mu\nu} - \frac{1}{2}g^{\mu\nu}R) \partial_\mu \tau \partial_\nu \tau - 4(\partial\tau)^2 \square\tau + 2(\partial\tau)^4 \right) \\ &\quad + c_\tau \int d^4x \sqrt{-g} \tau W^2. \end{aligned} \tag{1.10}$$

The curvature tensors are defined for the metric $g_{\mu\nu}$. The Wess-Zumino action is defined up to scale-invariant terms, so one should add all other terms consistent with the scale symmetry and allow arbitrary coefficients. However, in four dimensions none of those extra terms will contribute to the relevant $2 \rightarrow 2$ dilaton amplitude.

The discussion so far has allowed the metric $g_{\mu\nu}$ to be general, but the remainder will focus on flat space by taking $g_{\mu\nu} \rightarrow \eta_{\mu\nu}$, so $\hat{g}_{\mu\nu} \rightarrow e^{-2\tau} \eta_{\mu\nu}$. Taking the flat space limit of (1.10) and imposing the equation of motion $\square\tau = (\partial\tau)^2$ leads to the on-shell action for the

dilaton:

$$S_\tau \xrightarrow[\eta_{\mu\nu}]{EOM} 2 \Delta a \int d^4x \left[(\partial\tau)^4 + O(\partial^6) \right]. \quad (1.11)$$

It is short work to translate this to the 4-dilaton amplitude in terms of the familiar s, t, u Mandelstam invariants,

$$\mathcal{A}_4(s, t) = \Delta a \frac{4}{f^4} (s^2 + t^2 + u^2). \quad (1.12)$$

The last step is to prove the positivity of Δa by a contour integral argument. In the forward limit $t \rightarrow 0$, $\mathcal{A}_4(s, 0)/s^3$ has a simple pole at the origin of the complex s -plane with residue $4 \Delta a / f^4$. Choosing a contour as in Figure 1.3 yields a dispersion relation

$$\Delta a = \frac{f^4}{4\pi} \int_0^\infty ds \frac{\text{Im } \mathcal{A}_4(s, 0)}{s^3}. \quad (1.13)$$

By the optical theorem, $\text{Im } \mathcal{A}_4$ is proportional to the full scattering cross section, which is manifestly nonnegative. This establishes the 4d a -theorem: $\Delta a \geq 0$. \square

A similar approach can also provide an alternative proof of the 2d c -theorem [6]. Subsequently, an extension to six dimensions was considered in [28]. In 6d, the anomaly (1.6) enters at the level of six derivatives. An obstruction to a direct extension of the 4d proof arises because the 6-derivative component of the $2 \rightarrow 2$ dilaton amplitude vanishes in the forward limit ($\mathcal{A}_4 \sim stu \rightarrow 0$), which prevents the straightforward derivation of a positive sum rule like (1.13). Nevertheless, many interesting details of the 6d story were worked out and further evidence for a 6d a -theorem was provided [28, 29, 30, 31]. More importantly for this thesis, it was pointed out in [28] that the forward limit of the $2 \rightarrow 2$ amplitude would likely be nonvanishing in eight dimensions, which means the 6d obstruction would be absent. This is where my work enters the scene.

1.3 New Results in Part I

1.3.1 Preview

Part I covers two directions of my work on the subject of dilaton effective actions and RG flows. The first objective is to see how far the methods of [5] can be extended and explore how to combine the higher-dimensional extensions into a shared framework. In Chapter 2, we work out the dilaton effective action in arbitrary dimensions up to eight derivatives. This

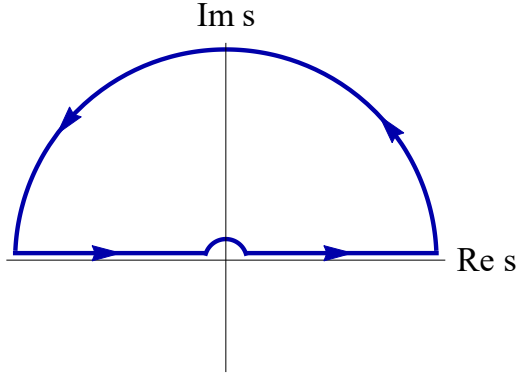


Figure 1.3: A choice of contour avoiding the simple pole at the origin.

is sufficiently high order to extend the methods from the 4d a -theorem to eight dimensions, where we uncover new structures that complicate the story. It is important to note that no nontrivial CFTs are known in eight dimensions, and there can be no superconformal theories [32], but the intuition regarding degrees of freedom would still be expected to apply if any are discovered in the future, and an 8d a -theorem would guarantee this behavior.

Chapter 3 describes the other direction of my work on the dilaton effective action in which we address an implicit subtlety in the 4d proof of the a -theorem. In the presence of broken symmetries beyond conformal symmetry, one expects additional massless Goldstone bosons to appear in the low energy theory. If these interfere with the $2 \rightarrow 2$ dilaton amplitude, then this could cause problems for the proof of the a -theorem. However, we classify all terms that could affect the amplitude and explicitly show that no problematic quantities survive the restrictions imposed by the a -theorem proof. The discussion in Chapter 3 is specific to four dimensions, but if higher dimensional a -theorems are eventually proven, similar considerations will be important in those cases as well.

1.3.2 Chapter 2

In eight dimensions, the relevant 8-derivative portion of the 4-point amplitude survives the forward limit ($\mathcal{A}_4 \sim s^4 + t^4 + u^4$), which suggests that an 8d a -theorem might be attainable by direct extension of the methods from [5]. With this in mind, we construct the dilaton effective action up to eight derivatives in Chapter 2. Although motivated by the 8d story, most of my work in Chapter 2 is presented in arbitrary d dimensions. As a result, much of the previous work on the dilaton effective actions in four and six dimensions is wrapped into a common framework.⁴ In particular, combining the previous stories into the unified

⁴Of course, the dilaton effective action in odd (and fractional) dimensions is also contained in these results, but there is no anomaly in those cases, so one should not expect a corresponding a -theorem.

d -dimensional action makes it very clear that things are fundamentally different in 8d than in 4d and 6d as we are about to see.

The on-shell dilaton effective action through 8-derivative order can be completely and compactly specified solely in terms of a special class of functions \mathcal{W}_k ,

$$S_\tau = \int d^d x \sqrt{-g} \left[\frac{(d-2)^2}{8} f^{d-2} \mathcal{W}_1 + \alpha^{(d)} \mathcal{W}_2 + \beta^{(d)} \mathcal{W}_3 + \gamma^{(d)} \mathcal{W}_4 + \tilde{\gamma}^{(d)} \frac{(d-4)^2}{4} e^{d\tau} (\mathcal{W}_2)^2 + \dots \right] \Big|_{g_{\mu\nu} = \eta_{\mu\nu}}$$

with $\mathcal{W}_k = \left(\frac{2}{d-2k} \right)^2 e^{-(d/2-k)\tau} P_k e^{-(d/2-k)\tau}$, (1.14)

where the dots stand for higher derivatives and terms that vanish on-shell, and $P_k = (\square^k + \text{curvature terms})$ is a GJMS operator (named for the mathematicians who discovered these operators, Graham, Jenne, Mason, and Sparling [33]). The GJMS operators P_k are higher-derivative generalizations of the conformal Laplacian ($k = 1$); in flat space they are simply \square^k . From the action (1.14), one can see that there is exactly one nonvanishing operator at each order in derivatives up to and including six derivatives,⁵ which is why the $2 \rightarrow 2$ amplitudes in 4d and 6d were specified completely by the anomaly. However, with eight derivatives a new feature appears in the form of a second nonvanishing term, $e^{d\tau} (\mathcal{W}_2)^2$. This structure has important consequences for the a -theorem analysis. In fewer than eight dimensions, the only contribution to the on-shell action at the relevant derivative order comes from $\mathcal{W}_{d/2}$ with a coefficient fixed by the a -anomaly, e.g., (1.11) in 4d, while in eight dimensions there is an anomaly-fixed piece from \mathcal{W}_4 plus additional contributions from the other nonvanishing term. Crucially, the coefficient of the latter piece is generally unrelated to the anomaly. Hence the 4-point dilaton amplitude still provides a sum rule similar to (1.13), but the resulting positive quantity is not obviously connected to the anomaly flow. Nonetheless, we show that Δa can be disentangled from the new structures through higher-point amplitudes, which suggests it may be possible to prove an 8d a -theorem with only a slight generalization of the methods.

As a consistency check, we work out the example of a free massive scalar in $d = 3, 4, \dots, 10$ dimensions and match the dilaton effective action up to eight derivatives. This is a highly nontrivial check because it requires matching the coefficients of 19 independent polynomials with just three parameters. In addition, we derive a zeta-regularized expression for the anomaly of a scalar in d -dimensions and verify the results against known values from the literature. One of the parameters used to match the free massive scalar example with the dilaton effective action in 8d is the anomaly flow Δa , and we show that it agrees exactly with the zeta-regularized expression as expected.

⁵The zeroth order cosmological constant must be zero or else the dilaton would be massive [5].

Key takeaways: The dilaton effective action is constructed and checked in d dimensions; connections to GJMS operators are observed; and obstructions to direct extension of 4d a -theorem methods to eight dimensions are identified.

1.3.3 Chapter 3

In Chapter 3, we discuss and close a small potential loophole in the 4d a -theorem. Conceivably, the presence of other massless modes in the IR theory (perhaps arising from other broken symmetries) could pollute the dilaton amplitudes and potentially invalidate the proof in such situations. However, we show in Chapter 3 that no such conspiracy can occur. After writing down all possible contributions from other massless Goldstone bosons arising from broken $U(1)$ symmetries, we work out the flat space limit under the equations of motion. As expected, none of the new terms affect the $2 \rightarrow 2$ dilaton amplitude, so the a -theorem remains valid. In the special case of broken R -symmetry in $\mathcal{N} = 1$ supersymmetric theories, a complicated expression for the joint dilaton-axion action was worked out from superspace in [26]. Using the framework developed in Chapter 3, a more compact form is presented. As a bonus, the amplitude arising from scattering four axions provides an alternate route to the a -theorem.

Key takeaways: The 4d a -theorem is shown to be unaffected by other massless modes from broken $U(1)$ symmetries; the joint dilaton-axion action is matched to existing literature and collected into a compact form.

1.4 Background for Part II

So far, the primary use of amplitudes in this thesis has been to constrain QFTs and RG flows. In the second part, the focus shifts to using symmetries and other properties of specific QFTs to expand on a new formulation of scattering amplitudes and gain greater insight into the underlying mathematical structure.

1.4.1 Symmetry as a Guiding Principle

The 4d dilaton effective action from Part I has a fairly restricted form due to the strong constraints imposed by scale symmetry and because the dilaton is a single scalar. In more general theories, there can be additional interactions that contribute to the dynamics, making it much more difficult to compute amplitudes in the traditional way using Feynman diagrams. For instance, the self-interactions of pure gluons (gauge bosons transforming in the adjoint of $SU(N)$) are complicated enough to make even tree level calculations with Feynman diagrams

impractical. Table 1.1 counts the minimal number of Feynman diagrams needed to compute the n -gluon tree amplitude; the actual number required would be higher if not for the fact that a single-trace group theory factor can be split off so that one needs only to compute the *color-ordered (tree) amplitude*, $\mathcal{A}_n(1\ 2\ \dots\ n)$, for a fixed labeling of the external legs and then sum over permutations,

$$\mathcal{A}_n^{\text{full (tree)}} = g^{n-2} \sum_{\text{perms } \sigma} \mathcal{A}_n(1\ \sigma(2\ 3\ \dots\ n)) \text{Tr} (T^{a_1} T^{\sigma(a_2)} \dots T^{a_n}), \quad (1.15)$$

where the Yang-Mills (YM) coupling g has been factored out, and T^a are the gauge group generators.⁶

Table 1.1: Examples of the rapidly growing number of diagrams required to compute the n -gluon color-ordered tree amplitude.

External gluons (n):	3	4	5	6	7	...	10	...	15	...
Diagrams for \mathcal{A}_n :	1	3	10	38	154	...	12,925	...	30,142,360	...

Despite the enormous number of Feynman diagrams, maximally helicity violating (MHV) gluon amplitudes actually take a very compact form (1.16) discovered by Parke and Taylor [35]. MHV amplitudes are color-ordered amplitudes in which $n - 2$ external gluons have positive helicity, and the other two have negative helicity.⁷ If i and j label the two negative helicity legs, then the Parke-Taylor amplitude is

$$\mathcal{A}_n^{\text{MHV}}(1^+ 2^+ \dots i^- \dots j^- \dots n^+) = \frac{\langle ij \rangle^4}{\langle 12 \rangle \langle 23 \rangle \dots \langle n1 \rangle}. \quad (1.16)$$

The angle bracket notation is explained below in the [Box](#) on spinor-helicity formalism.

The incredible simplicity of the Parke-Taylor amplitude (1.16) despite the rapidly growing number of diagrams in Table 1.1 is an indication that Feynman diagrams are highly redundant and therefore not the optimal tools for computing scattering amplitudes. The principal source of redundancy is the dependence of individual diagrams on gauge choices. Information can be shuffled between diagrams by gauge/symmetry transformations and field redefinitions, even though the sum of diagrams (i.e., the amplitude) must remain invariant. The situation is analogous to holding a collection of misshapen pieces and finding that, al-

⁶At loop-level, additional trace structures appear. More details and references can be found in [34].

⁷Other gluon helicity configurations are named by how close they are to MHV. Next-to-MHV, or NMHV, amplitudes have three negative helicity gluons, and in general N^k MHV amplitudes have $k+2$ negative helicity gluons. One can equivalently count from the anti-MHV amplitude which has exactly two positive helicity gluons. Amplitudes with fewer than two positive or negative helicities vanish at tree-level in Yang-Mills theories and at all loop orders in super Yang-Mills theories [34].

most miraculously, they combine into a perfect disk (Figure 1.4). If, on the other hand, the initial pieces were annular, then it would be no great surprise that the final shape is a circular disk (Figure 1.5).

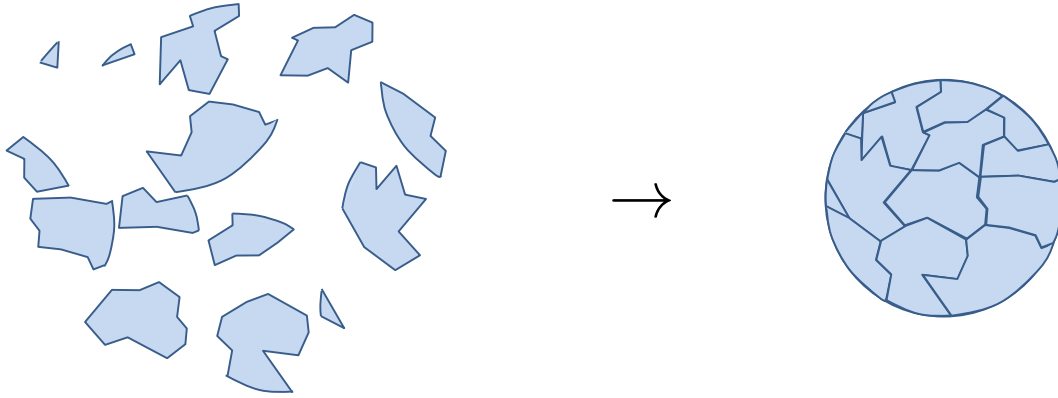


Figure 1.4: A collection of puzzle pieces that make a circular disk when they are properly joined together. Feynman diagrams are similar insofar as they tend to obfuscate the underlying structure.

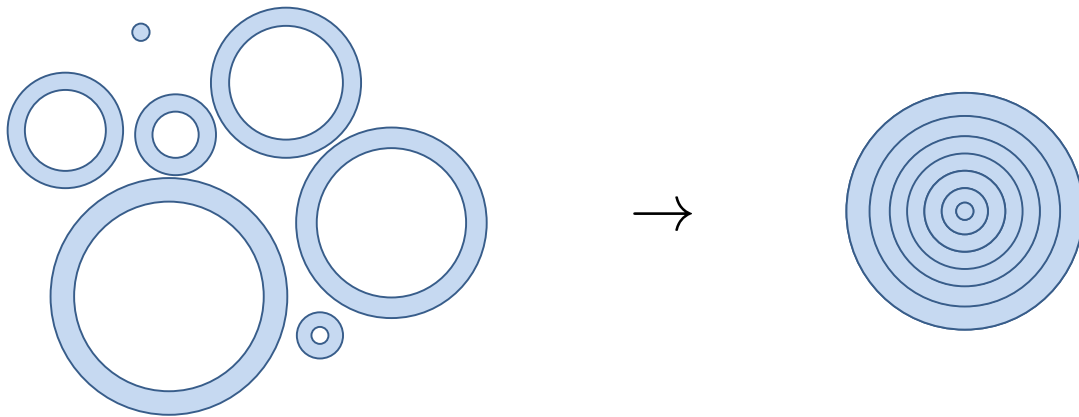


Figure 1.5: A collection of rotationally symmetric puzzle pieces that also make a circular disk when they are properly assembled. Using symmetry as a guide can reveal the fundamental structure more clearly from the start.

The key is symmetry. Building blocks that individually obey the rotational symmetry of a circle are much more easily merged into a circular disk than a jumble of random-edged pieces. Likewise, one can seek to calculate scattering amplitudes in terms of objects that independently obey the symmetries of the theory so that the final answer is guaranteed to have the right properties.

Box: Spinor-Helicity Formalism

The angle brackets in (1.16) represent momentum contractions via the 4d spinor-helicity formalism through which the 4-momentum p_μ of the i^{th} massless gluon is represented as a product of 2-component spinors λ^a and $\tilde{\lambda}^b$:

$$p^{ab} = p^\mu (\sigma_\mu)^{ab} = \lambda^a \tilde{\lambda}^b, \quad (1.17)$$

and similarly for p_{ab} . Indices are raised and lowered with 2-index Levi Civita symbols $\epsilon_{\dot{a}\dot{b}}$ and ϵ_{ab} . Closed pairs of angle and square brackets are shorthand for contracted indices:

$$\langle i j \rangle = \epsilon_{ab} \lambda^a \lambda^b = \det(\lambda^a \lambda^b), \quad \text{and} \quad [i j] = \epsilon_{\dot{a}\dot{b}} \tilde{\lambda}^{\dot{a}} \tilde{\lambda}^{\dot{b}} = \det(\tilde{\lambda}^{\dot{a}} \tilde{\lambda}^{\dot{b}}). \quad (1.18)$$

They are antisymmetric in the labels i and j . More details about the spinor helicity formalism can be found in the reviews [34, 36]. The brief appearance of momentum spinors in Chapter 3 uses the conventions defined in [34], while the conventions in Chapters 4 and 5 agree with [37].

1.4.2 Superamplitudes in $\mathcal{N} = 4$ SYM

More symmetry implies more constraints on the building blocks, so it makes sense to start in a theory with the maximal amount of symmetry. In four dimensions, that theory is $\mathcal{N} = 4$ Super Yang-Mills (SYM) theory, and it is especially constraining in the planar limit.⁸ Although our universe does not obey $\mathcal{N} = 4$ SYM theory, as a toy model it serves as a useful testing ground for new theoretical approaches. It is a superconformal field theory with four supersymmetries ($\mathcal{N} = 4$). The on-shell field content consists of positive and negative helicity gluons g^\pm , gluinos Λ^A, Λ^{ABC} , and scalars S^{AB} . The antisymmetric indices $A = 1, 2, 3, 4$ encode their symmetry transformation properties.⁹

Supersymmetry implies relations among the amplitudes known as supersymmetric Ward Identities (which coincidentally appear also in the a -theorem discussion of Chapter 3). Supersymmetrically related amplitudes can be combined into a single quantity called the scattering *superamplitude* that encodes all of the individual component amplitudes and their relations. The field content is organized into an on-shell superfield Ω via the introduction of

⁸The planar limit of a gauge theory means observables depend only on planar Feynman diagrams while nonplanar diagrams are suppressed [38]. In this context, the gauge group is $SU(N)$, and $N \rightarrow \infty$ leads to the planar limit.

⁹The fields transform in the antisymmetric representation of the $SU(4)_{\mathcal{R}}$ \mathcal{R} -symmetry.

anticommuting Grassmann variables $\tilde{\eta}_A$ whose indices match those of the fields [34]:

$$\Omega = g^+ + \tilde{\eta}_A \Lambda^A - \frac{1}{2!} \tilde{\eta}_A \tilde{\eta}_B S^{AB} - \frac{1}{3!} \tilde{\eta}_A \tilde{\eta}_B \tilde{\eta}_C \Lambda^{ABC} + \tilde{\eta}_1 \tilde{\eta}_2 \tilde{\eta}_3 \tilde{\eta}_4 g^-. \quad (1.19)$$

Acting with a supersymmetry transformation on a particular component has the effect of adding or removing an $\tilde{\eta}_A$, so reading from left to right in (1.19) is like climbing a ladder defined by the four supersymmetries. We write the superamplitude as $\mathcal{A}_n(\Omega_1, \Omega_2, \dots, \Omega_n)$ to indicate that it encodes all scattering amplitudes for the components of the superfields Ω_i .

Particle states are in correspondence with Grassmann monomials, so for instance $\tilde{\eta}_{i1} \tilde{\eta}_{i3}$ means particle i is a scalar S^{13} . In momentum space using the spinor-helicity formalism (see the [Box](#) for details), the external data for each particle is therefore specified by a set of bosonic momentum spinors and fermionic state variables, $(\lambda_i^a, \tilde{\lambda}_i^{\dot{a}} | \tilde{\eta}_{iA})$. For example, the Parke-Taylor amplitude (1.16) has $n - 2$ positive helicity gluons and two negative helicity gluons. The latter pair each contribute exactly four $\tilde{\eta}$'s from (1.19) while the positive helicity gluons have no $\tilde{\eta}$'s. Therefore, the Parke-Taylor amplitude (1.16) appears in the expansion of the superamplitude as the coefficient of $\tilde{\eta}_{i1} \tilde{\eta}_{i2} \tilde{\eta}_{i3} \tilde{\eta}_{i4} \tilde{\eta}_{j1} \tilde{\eta}_{j2} \tilde{\eta}_{j3} \tilde{\eta}_{j4}$:

$$\mathcal{A}_n(\Omega_1, \Omega_2, \dots, \Omega_n) = \dots + \sum_{i,j} \frac{\langle i j \rangle^4}{\langle 1 2 \rangle \langle 2 3 \rangle \dots \langle n 1 \rangle} \tilde{\eta}_{i1} \tilde{\eta}_{i2} \tilde{\eta}_{i3} \tilde{\eta}_{i4} \tilde{\eta}_{j1} \tilde{\eta}_{j2} \tilde{\eta}_{j3} \tilde{\eta}_{j4} + \dots, \quad (1.20)$$

where the sum over i and j appears because the superamplitude contains the Parke-Taylor amplitude for any i and j . The dots to the left and right denote other components of the superamplitude with different Grassmann monomials.

Just as the MHV Parke-Taylor amplitude appears as a component in the superamplitude, supersymmetry implies that all N^k MHV gluon scattering amplitudes $\mathcal{A}_n(1, 2, \dots, n)$ are components of complete N^k MHV superamplitudes $\mathcal{A}_n^{(k)}(\Omega_1, \Omega_2, \dots, \Omega_n)$:

$$\mathcal{A}_n(\Omega_1, \Omega_2, \dots, \Omega_n) = \sum_{k=2}^{n-2} \mathcal{A}_n^{(k)}(\Omega_1, \Omega_2, \dots, \Omega_n). \quad (1.21)$$

Each N^k MHV superamplitude $\mathcal{A}_n^{(k)}$ is a degree- $4(k + 2)$ polynomial in the Grassmann variables; for example, the Parke-Taylor amplitude has $k = 0$, and the sum in (1.20) denotes a degree- $4(0 + 2) = 8$ polynomial in the $\tilde{\eta}$ variables.

Recall that the goal is to write down building blocks of amplitudes that are invariant under the symmetries of a theory. This is a highly nontrivial problem because many of the symmetry operators act nonlinearly on the momentum space data. Consequently the building blocks may need to be fairly complicated in order to remain invariant under the

nonlinear symmetries. To partially address that problem, there are two other common ways of representing the external data that at least simplify a subset of the symmetries:

- The *(super)twistor* space representation linearizes the action of the standard superconformal symmetry.¹⁰ It employs a half-Fourier transform of the momentum data, so the twistors \mathcal{W}_i are defined as $\mathcal{W}_i(\tilde{\mu}_i^a, \tilde{\lambda}_i^{\dot{a}}|\tilde{\eta}_{iA})$ where $\tilde{\mu}_i^a$ is the Fourier conjugate to λ_i^a . When the amplitude is written in twistor space, the superconformal symmetry is manifest.
- Tree level amplitudes and loop-level integrands in planar $\mathcal{N} = 4$ SYM also have a hidden symmetry called dual superconformal symmetry that is completely independent of the standard superconformal symmetry. The *momentum (super)twistor* representation linearizes the dual symmetry. Momentum twistors $\mathcal{Z}_i(\lambda_i, \mu_i|\eta_i)$ are related to the momentum space data by algebraic incidence relations defined in Section 4.2.2.

A thorough review of the three descriptions and their relationships is presented in Chapter 4, including a streamlined proof of the equivalence between amplitudes computed in twistor and momentum twistor space. The momentum twistor representation tends to produce more compact expressions, so for the remainder of this introduction the formulas will be displayed in those variables. See Chapter 4 for the other variables.

1.4.3 Grassmannian Integral Representation

We now turn to constructing $\mathcal{N} = 4$ SYM scattering superamplitudes from the symmetry-oriented point of view (from now on we will use “amplitude” interchangeably with “superamplitude” unless the context requires extra clarity). Tree-level amplitudes should be invariant under the joint superconformal \times dual superconformal symmetry, which together form an infinite dimensional symmetry group called the Yangian [39]. Furthermore, tree amplitudes should be cyclically symmetric, meaning that the amplitude does not change under relabeling all external legs $i \rightarrow (i + 1) \bmod n$, cf. the super-Parke-Taylor amplitude (1.20).

It was shown in [37] that starting from a simple 3-point amplitude and recursively adding legs and changing the MHV degree k through a well-defined procedure, one arrives at a contour integral representation (1.22) of the n -point N^k MHV tree-level amplitude. Residues of the integral have exactly the right symmetry properties to be building blocks of the amplitude:

$$\mathcal{A}_n^{(k)} = \mathcal{A}_n^{\text{MHV}} \oint_{\Gamma} \frac{d^{k \times n} C}{GL(k) M_1 M_2 \dots M_n} \delta^{4k|4k}(C \cdot \mathcal{Z}). \quad (1.22)$$

¹⁰“There is another...” –Yoda

Each piece is explained in the following list:

- The $\mathcal{A}_n^{\text{MHV}}$ prefactor is the supersymmetric Parke-Taylor amplitude (the sum in (1.20) along with momentum-conserving delta functions). It ensures that for MHV amplitudes ($k = 0$), the integral is trivial and the result is simply the super Parke-Taylor amplitude.
- The C in the numerator is a full-rank $k \times n$ matrix whose entries are to be integrated over.
- The denominator contains a product of the n consecutive minors M_i of C , which are determinants of $k \times k$ submatrices of C constructed out of cyclically consecutive columns \vec{c}_a ,

$$M_i = \det \left(\vec{c}_i \vec{c}_{i+1} \dots \vec{c}_{i+k-1} \right). \quad (1.23)$$

- The notation $\frac{1}{GL(k)}$ is shorthand for modding out the left action of $GL(k)$. This is essential¹¹ because in order to properly encode scattering amplitudes, the matrix C actually needs to be an element of the Grassmannian $\text{Gr}(k, n)$, which is the space of k -planes in n dimensions. The equivalence with $k \times n$ matrices modulo $GL(k)$ follows by treating the rows of a given matrix C as k vectors defining a k -plane, and any rotation of those vectors by a $GL(k)$ matrix defines the same plane.
- The $4k$ bosonic and $4k$ fermionic delta functions encode the external data in terms of momentum twistors $\mathcal{Z}_i = (Z_i | \eta_i)$.
- The bosonic delta functions impose $4k$ constraints on the integral, and modding out the $GL(k)$ fixes an additional k^2 degrees of freedom. Therefore, since tree amplitudes contain no free integrals, the remaining $(k(n - k - 4))$ degrees of freedom must be fixed by the contour Γ wrapping poles where the minors M_i vanish. The set of wrapped poles is determined by locality considerations discussed below. Thus the amplitude is a sum over residues at the poles enclosed by the contour Γ :

$$\mathcal{A}_n^{(k)} = \sum_{\text{poles } p} \text{Residue}[p]. \quad (1.24)$$

At MHV level ($k = 0$), the integral (1.22) is trivial, and the answer is just the Parke-Taylor prefactor. For $k > 1$ in the $N^k\text{MHV}$ classification, the minors in the denominator

¹¹That is, it follows from the derivation of the integral representation [40].

are nonlinear functions of the variables; hence the pole structure is very complicated and standard contour integral techniques are insufficient. At NMHV level ($k = 1$), however, C is a $1 \times n$ matrix whose consecutive minors are simply its entries,

$$\text{NMHV: } C = (c_1 \ c_2 \ \dots \ c_n), \quad M_i = c_i, \quad (1.25)$$

so the integral can be evaluated directly. That calculation is one of the results presented in Chapter 4.

Beyond NMHV level ($k > 1$) the nonlinear pole structure introduces composite singularities and other obstructions to straightforward evaluation of the integral [40]. Nevertheless, a technique was developed in [37] to generate coordinate charts from which codimension-1 residues can be reached as simple logarithmic singularities. By recursively applying the method to submanifolds of the Grassmannian, the complicated measure¹² in (1.22) is converted to a product of $d\alpha/\alpha = \text{dlog } \alpha$ forms:

$$\frac{d^{k \times n} C}{GL(k) M_1 M_2 \dots M_n} \rightarrow \text{dlog } \alpha_d \wedge \text{dlog } \alpha_{d-1} \wedge \dots \wedge \text{dlog } \alpha_1. \quad (1.26)$$

This structure leads to an alternative technique for evaluating residues that leads to the problem and solution of Chapter 5.

Aside from evaluating the residues themselves, we also want to combine them into the amplitude sum (1.24) by proper choice of the contour Γ . However, as part of the search for symmetric building blocks, we had to give up the manifest locality provided by Feynman diagrams. Individual residues of (1.22) can have nonlocal and hence unphysical singularities, but the sum (1.24) should not have any such nonlocalities. In principle, the contour Γ restores locality by selecting residues such that all nonlocal poles cancel in the sum. The locality constraints are explained in [37] and reviewed here in Chapter 4 for NMHV amplitudes and in Chapter 5 for general N^k MHV amplitudes. It was shown in [37] that using their method for simplifying the measure (1.26), all nonlocal poles would necessarily appear in pairs so they at least cancel mod 2, but it remained to prove that the signs are always correct to cancel exactly. The issue of exact cancellation is the subject of Chapter 5.

Contour integrals also imply relations among residues through Cauchy-like residue theorems. By extension, the residue theorems produce relationships among amplitudes which resolves the puzzle of why a single amplitude can have many distinct but equivalent representations [37, 41]. The residue theorems play a crucial role in the locality discussion of Chapter 5.

¹²The measure in (1.22) is everything inside the integral except the delta functions.

Ultimately, it is hoped that these developments lead to a new understanding of the physics that describes our universe, perhaps even a reformulation of quantum field theory itself [37]. Although such a dream is seemingly very distant, we can begin by exploring which features of the new formulation are specific to $\mathcal{N} = 4$ SYM theory and which are more broadly applicable. Along this line of thought, it is very intriguing that many of the Grassmannian calculations in 4d $\mathcal{N} = 4$ SYM have analogues in a 3-dimensional $\mathcal{N} = 6$ superconformal field theory called ABJM theory. The main difference is that the 3d version requires an additional orthogonality constraint on the matrices, $CC^T = 0$, which defines a submanifold of $Gr(k, n)$ known as the *orthogonal Grassmannian* $OG(k, n)$ [42, 43, 44]. In Chapter 4 of this thesis, several additional ideas from 4d $\mathcal{N} = 4$ SYM are extended to 3d ABJM theory.

1.5 New Results in Part II

1.5.1 Preview

Many interesting discoveries have arisen out of research into properties of the Grassmannian and its connections to physics, including unexpected combinatorial relations among amplitudes [37], the geometrization of tree and loop-level amplitudes in the amplituhedron [45, 46], and much more. While my work has overlap with the above categories, it is mostly complementary. My main contributions are to clarify the mathematical structure underlying the connection between amplitudes and the Grassmannian and extend the formalism beyond 4d $\mathcal{N} = 4$ SYM theory, and to resolve a sign ambiguity in the calculation of residues thereby leading to a proof that the tree amplitude computed from the Grassmannian contour integral (1.22) has no unphysical singularities.

1.5.2 Chapter 4

This chapter covers two separate Grassmannian formulations of amplitudes: one is relevant to 4d $\mathcal{N} = 4$ SYM theory and the other applies to 3d ABJM theory.

4d Results

The 4d section contains a detailed review of the three representations of the external data for $\mathcal{N} = 4$ SYM theory: momentum space, twistor space, and momentum twistor space. It was previously known that amplitudes can be equivalently derived in any of the three formulations, but we provide a new streamlined presentation of the relationship between the Grassmannian contour integrals in twistor and momentum twistor space.

In addition, we present the first complete and self-contained derivation of the general n -point NMHV amplitude directly from the contour integral (1.22). In Section 4.4 we explain how to consistently choose the contour Γ and impose the $GL(1)$ and delta function constraints to explicitly evaluate (1.22); Appendix G provides a more careful derivation including the sign of each residue. A key observation that allow the integral to be solved in general is that any five 4-dimensional vectors Z_a are linearly dependent,¹³

$$\langle ijkl \rangle Z_m + \langle jklm \rangle Z_i + \langle klmi \rangle Z_j + \langle lmi j \rangle Z_k + \langle mij k \rangle Z_l = 0. \quad (1.27)$$

The 4-bracket coefficient of each vector in (1.27) denotes the determinant of the other four vectors,

$$\langle ijkl \rangle = \det \begin{pmatrix} Z_i & Z_j & Z_k & Z_l \end{pmatrix}. \quad (1.28)$$

To see why this is useful, suppose the contour Γ fixes all $c_i = 0$ except for $i \in \{a, b, c, d, e\}$. Then the bosonic delta functions simplify to $\delta^4(c_a Z_a + c_b Z_b + c_c Z_c + c_d Z_d + c_e Z_e)$. The Schouten identity (1.27) guarantees that the argument vanishes if the matrix entries $c_{a,b,c,d,e}$ are chosen to be the complementary 4-brackets. This leaves the residue,

$$\frac{\delta^{(4)} \left(\langle bcde \rangle \eta_a + \langle cdea \rangle \eta_b + \langle deab \rangle \eta_c + \langle eabc \rangle \eta_d + \langle abcd \rangle \eta_e \right)}{\langle bcde \rangle \langle cdea \rangle \langle deab \rangle \langle eabc \rangle \langle abcd \rangle} =: [abcde]. \quad (1.29)$$

In general, the contour Γ can enclose multiple poles, so the general NMHV amplitude derived from (1.22) will be

$$\mathcal{A}_n^{(1)} = \sum c_{abcde} [abcde], \quad (1.30)$$

where the coefficients c_{abcde} are ± 1 or 0 depending on whether the pole is enclosed by Γ . The contour is chosen such that the linear combination satisfies the locality constraints explained in Section 4.4.3.

Since (1.22) is a contour integral, there are residue theorems that relate the residues (1.29). We provide a new geometric interpretation of the residue theorems in terms of hyperplane arrangements in Section 4.4.2, and connections to known identities among 5-brackets are derived in Section 4.4.3. An interpretation of the NMHV results from a combinatorial perspective a la [37] is discussed in Section 4.4.4.

¹³This is also known as a 5-term Schouten identity (or more generally Cramer's rule).

3d Results

As mentioned in the background section above, it is interesting to ask what aspects of the Grassmannian formulation generalize beyond 4d $\mathcal{N} = 4$ SYM theory. A framework for computing 3d ABJM theory amplitudes from the orthogonal Grassmannian is known in momentum space [42, 43, 44]. However, a corresponding momentum twistor representation was previously unknown. Fortunately, a similar strategy to the streamlined derivation of the $\mathcal{N} = 4$ SYM momentum twistor Grassmannian (Section 4.3) can be applied to derive a novel 3d ABJM version of momentum twistors. The details are worked out in Section 4.5. Moreover, just as NMHV amplitudes in $\mathcal{N} = 4$ SYM theory are calculable by direct evaluation of (1.22), the ABJM counterparts are also attainable from the 3d ABJM momentum twistor space integral; the derivation is presented in Section 4.5 with a few additional subtleties discussed in Appendix H.

Key takeaways: Aspects of the Grassmannian representation of 4d $\mathcal{N} = 4$ SYM theory amplitudes are clarified and extended to 3d ABJM theory

1.5.3 Chapter 5

Chapter 5 returns to 4d $\mathcal{N} = 4$ SYM theory to carefully derive the signs of residues from (1.22) and prove that indeed all nonlocal poles cancel exactly in the amplitude sum, not just mod 2. The sign question arises because the procedure of converting the measure to a simple dlog form (1.26) does not preserve orientation information. Relating a given pair of coordinate charts (i.e., dlog forms) generated by the procedure is not trivial, which can introduce critical sign ambiguities in the amplitude sum (1.24). Without the appropriate signs, certain unphysical nonlocalities would not cancel appropriately in the sum. Previously it was shown that the problematic nonlocalities appear in pairs, so they at least cancel mod 2 [37], but a proof of exact cancellation was not known. This issue is resolved in Chapter 5 where an algorithm is developed that reconstructs the relative orientation between a pair of dlog charts. Furthermore, consistency with residue theorems unambiguously fixes the signs of all residues appearing in the amplitude (up to an overall sign) and guarantees the cancellation of all nonlocal poles.

The proof that the algorithm generates the correct signs relies on the fact that the relevant submanifolds of the Grassmannian can be arranged into a partially ordered set (poset) according to the consecutive linear dependencies in the matrix C that define each submanifold. The vertices represent submanifolds, and edges indicate that the vertex at one end represents a codimension-1 residue attainable from the other vertex. Each dlog chart corresponds to a path through the poset, and the paths representing a pair of distinct charts

on a given submanifold together define a closed loop, e.g., Figure 1.6. Edges in the poset are assigned weights ± 1 such that the product of signs around every quadrilateral is -1 (Figure 1.7), and the relative orientation of the two charts is the product of those weights on the edges in the closed loop defined by the paths.¹⁴

To illustrate that this convention produces the correct signs, a simple example is in order. Every step in the construction of a dlog chart is labeled by an ordered pair of indices, so charts can be represented as sequences of ordered pairs. Each step also appends a corresponding coordinate and its dlog form to the chart. The meaning behind the labeling is explained in Chapter 5. For this example, suppose two charts on a given submanifold are defined by the sequences $(ab)(cd)$ and $(cd)(ab)$. Let α represent the coordinate corresponding to (ab) and β represent the coordinate corresponding to (cd) . Then the two charts form a closed quadrilateral in the poset as shown in Figure 1.6 together with their respective forms.

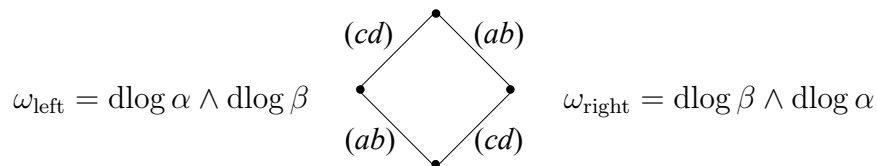


Figure 1.6: The poset paths and dlog forms for a pair of distinct 2-dimensional charts on a submanifold. On the left, coordinate α corresponding to (ab) was added first, while on the right, coordinate β corresponding to (cd) was added first.

The wedge product is antisymmetric, so it is clear that $\omega_{\text{left}} = -\omega_{\text{right}}$. This is also encoded in the poset because the edges are weighted such that the product around the quadrilateral is -1 ; Figure 1.7 shows a possible set of weights. Thus the product of signs around the closed loop formed by the paths (the quadrilateral) is equivalent to the relative orientation between the forms.

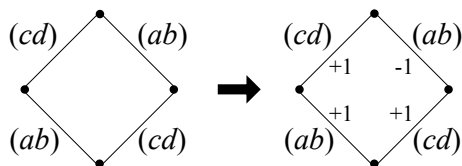


Figure 1.7: A suitable choice of edge weights. The product of weights around the quadrilateral must be -1 .

¹⁴A method for generating a consistent set of edge weights was developed by University of Michigan mathematicians Lam and Speyer [47]. It is reviewed in Appendix J.

In the context of the Grassmannian poset, two vertices (i.e., residues) are related by a residue theorem if they have a common neighbor of higher dimension in the poset. This allows the edge weights to serve a second purpose beyond relating charts on a single submanifold. The relative sign between two residues is equal to the product of signs on the edges connecting them to the shared parent. A similar argument fixes the signs between the residues’ children, which represent singularities of the amplitude. Every nonphysical singularity appears twice [37], and this edge-weighting procedure guarantees that they always appear with opposite signs (I prove that this is a consistent assignment in Section 5.4.1). Hence amplitudes derived from the Grassmannian contour integral (1.22) are always local as required.

The algorithm has been verified by implementing it in Mathematica and applying it to a variety of charts whose orientations are known by other methods. This includes 500 distinct charts on the 10d cell $\{5, 3, 8, 9, 6, 7, 12, 10, 14, 11\} \in \text{Gr}(3, 10)$ whose orientations were computed using an independent method due to J. Bourjaily and A. Postnikov [48]. The results agreed perfectly with my algorithm.

Key takeaways: Orientation information is reconstructed for dlog coordinate charts on the Grassmannian; and locality of the tree amplitude is proven to be exact.

1.6 Summary of Results and Publications

- In Chapter 2, we extend the dilaton-based methods of the 4d a -theorem to higher dimensions. In eight dimensions, new structures appear at the relevant order in the dilaton effective action and interfere with a direct extension of the 4d proof, but we show that the anomaly flow can be disentangled in higher-point amplitudes. The intermediate results are presented in a compact form that depends on the dimension d only as a parameter. This facilitates a connection between the new material and existing literature on the a -theorem in four and six dimensions. We check the results through a highly non-trivial match to an explicit example in multiple dimensions and work out a zeta-regularized expression for the scalar anomaly in d -dimensions.
 - Based on H. Elvang and **T. M. Olson**, “RG flows in d dimensions, the dilaton effective action, and the a -theorem,” JHEP **1303**, 034 (2013) [arXiv:1209.3424 [hep-th]] [49].
- In Chapter 3, the focus returns to the a -theorem in four dimensions where we consider the effect of other massless modes in the low energy theory. A supersymmetric Ward identity relates dilaton and axion scattering amplitudes in $\mathcal{N} = 1$ theories with broken R -symmetry, and we work out a compact version of the low energy dilaton-axion

effective action. Furthermore, we prove that no Goldstone bosons arising from broken $U(1)$ symmetries in the UV can affect the essential 4-dilaton amplitude.

— Based on N. Bobev, H. Elvang, and **T. M. Olson**, “Dilaton effective action with $\mathcal{N} = 1$ supersymmetry,” JHEP **1404**, 157 (2014) [arXiv:1312.2925 [hep-th]] [50].

- Chapter 4 turns to calculations of tree-level scattering amplitudes in 4d $\mathcal{N} = 4$ SYM theory via a correspondence with the Grassmannian $\text{Gr}(k, n)$. The relationships between three different formulations of the external data are clarified and presented in a streamlined manner. Our approach facilitates an extension to 3d ABJM theory and the orthogonal Grassmannian $\text{OG}(k, n)$. The latter result leads us to introduce a novel momentum twistor formalism in 3d. To demonstrate the technology in both ABJM and $\mathcal{N} = 4$ SYM, we explicitly calculate the first nontrivial amplitudes corresponding to $k = 1$ in the N^kMHV classification. We also discuss geometric and combinatorial interpretations of the results.

— Based on H. Elvang, Y-t. Huang, C. Keeler, T. Lam, **T. M. Olson**, S. Roland, and D. E Speyer, “Grassmannians for scattering amplitudes in 4d $\mathcal{N} = 4$ SYM and 3d ABJM,” JHEP **1412**, 181 (2014) [arXiv:1410.0621 [hep-th]] [51].

- In Chapter 5, I resolve an important puzzle in $\mathcal{N} = 4$ SYM regarding the relative signs of residues from the Grassmannian integrals. I develop and prove correctness of an algorithm that reconstructs the relative orientation of distinct charts by identifying an intuitive relationship between the charts and an underlying weighted poset structure. Furthermore, by requiring consistency with residue theorems I prove conclusively that nonlocal poles will always appear with opposite signs and cancel exactly in the amplitude sum.

— Based on **T. M. Olson**, “Orientations of BCFW Charts on the Grassmannian,” JHEP **1508**, 120 (2015) [arXiv:1411.6363 [hep-th]] [52].

Part I

Constraining QFTs: Dilaton Effective Action and the a -theorem

Chapter 2

RG Flows in d Dimensions and the Dilaton Effective Action

2.1 Motivation and Preview

The proof of the 4d a -theorem by Komargodski and Schwimmer (KS) [5] makes exquisite use of the low-energy effective interactions of the dilaton, a field that can be thought of as the Goldstone mode of spontaneously broken conformal symmetry or as a compensator background field. KS showed, following earlier work [26], that the form of the dilaton effective action is dictated by its Weyl-transformation properties and that the low-energy behavior of the 4-point dilaton scattering amplitude

$$\mathcal{A}_4(s, t) = \Delta a \frac{4}{f^4} (s^2 + t^2 + u^2) \tag{2.1}$$

encodes the flow of the a -anomaly $\Delta a = a_{\text{UV}} - a_{\text{IR}}$. In the forward limit $t \rightarrow 0$, $A_4(s, 0)/s^3$ has a simple pole at $s = 0$ whose residue is $4\Delta a/f^4$. A contour integral argument then gives

$$\Delta a = \frac{f^4}{4\pi} \int_0^\infty ds \frac{\text{Im} A(s, 0)}{s^3} > 0. \quad (2.2)$$

Since the integrand on the RHS is positive definite, this proves $a_{\text{IR}} < a_{\text{UV}}$ for an RG flow from a 4d UV CFT to a 4d IR CFT. The convergence of the dispersion integral has been clarified in [6, 25].

Zamolodchikov’s c -theorem [2] and the Cardy-KS a -theorem [5, 24] demonstrate the irreversibility of the RG flow between 2d and 4d CFT fixed points, respectively. It is interesting to ask if this property generalizes to other dimensions. Holographic arguments indicate that it does generalize, and they provide an interesting connection to entanglement entropy [11, 12, 53]. In even dimensions, the irreversibility of the flow can be encoded in an a -theorem for the ‘type A’ anomaly a associated with the Euler density term in the trace anomaly polynomial [20]¹

$$\langle T_\mu^\mu \rangle = \sum_i c_i I_i - (-)^{d/2} a E_d. \quad (2.4)$$

In odd dimensions, the constant term in the free energy $F = -\log Z$ offers a candidate for an analogous F -theorem; for recent work see [13, 14, 15, 16, 17, 18].

The dilaton can be introduced in even as well as in odd dimensions, and one may ask what information can be extracted from its low-energy effective action: in particular if it can be used to prove a higher- d a -theorem and whether it plays a role for odd- d RG flows. The focus of this chapter is to study the structure of the dilaton effective action in general d dimensions.

The dilaton-based approach [5, 6] to the a -theorem was examined recently in [55] for RG flows between 6-dimensional CFTs. The 6d dilaton effective action was constructed up to 6-derivative order and its structure verified in explicit examples. The examples also served to clarify the distinctive roles of the dilaton in the cases of spontaneous and explicit breaking of the conformal symmetry. In the former case, the dilaton is a dynamical field of the low-energy theory and it contributes as such to the scattering amplitudes via Feynman diagrams with internal dilaton lines; this was demonstrated explicitly with the example of the 6d (2,0)

¹We normalize the $d = 2k$ -dimensional Euler density as

$$E_{2k}(g_{\mu\nu}) = \frac{1}{2^k} R_{\mu_1\nu_1}{}^{\rho_1\sigma_1} \dots R_{\mu_k\nu_k}{}^{\rho_k\sigma_k} \epsilon_{\rho_1\sigma_1\dots\rho_k\sigma_k} e^{\mu_1\nu_1\dots\mu_k\nu_k}. \quad (2.3)$$

The ‘type B’ anomalies c_i multiply a set of independent Weyl-invariant scalars $\sqrt{-g}I_i$; there is 1 in 4d, 3 in 6d, and [54] found 12 in 8d. The c -anomalies do not always decrease along an RG flow.

theory on the Coulomb branch [55]. (See also [56].) On the other hand, when the conformal symmetry is broken explicitly, the dilaton is introduced as a compensator field which can be made arbitrarily weakly coupled such that in the low-energy scattering amplitudes it may be treated as a source field. This case was illustrated in [55] by the example of the 6d free massive scalar.

The simple KS approach to proving $a_{\text{IR}} < a_{\text{UV}}$ in 4d does not directly carry over to 6d [55], and no general proof of the 6d a -‘theorem’ has yet been offered. One technical difficulty with generalizing the KS dispersion relation argument is that in 6d the anomaly flow Δa is associated with the 6-derivative terms in the action: the 4-dilaton amplitude is then $A_4(s, t) \sim \Delta a stu$, and since it vanishes in the forward limit no clean positivity statement is extracted; for details see [55].

It would seem easier to derive a positivity result based on a 4-point amplitude of the form $A_4(s, t) \sim (s^4 + t^4 + u^4)$. Indeed in 8d, the a -anomaly is associated with 8-derivative terms in the action, and at order $O(p^8)$ the 4-dilaton amplitude takes this form. However, the 8d dilaton effective action also contains an 8-derivative Weyl-invariant that contributes non-trivially to the scattering amplitudes [55]. In fact, proving positivity of the coefficient of the $O(p^8)$ -terms in the 4-dilaton amplitude amounts to proving only that the coefficient of this new Weyl-invariant is positive and does not yield $\Delta a > 0$.

One purpose of this chapter is to clarify the structure of the terms in the dilaton effective action in 8d up to and including 8-derivative terms. We will also show that despite the pollution from the 8-derivative Weyl-invariant, the flow Δa can be extracted systematically. We demonstrate this explicitly for the example of the 8d free massive scalar. The result for $\Delta a = a_{\text{scalar}, 8d}$ agrees with that found using zeta-function regularization of the coefficient of the log-term in the free energy.

It must be noted that the study of 8d RG flows is motivated by the wish to understand the structure of the dilaton effective action and the generality of the dilaton-based approach of KS in even dimensions. We know of no examples of interacting 8-dimensional conformal theories (and there can be no superconformal ones [32]), so an 8d (or higher- d) a -theorem may be of limited applicability.

The analysis in 8d is part of our more general study of the dilaton effective action in d dimensions, with d even or odd. The trace-anomaly exists only for even d , and therefore it is *a priori* clear that for d odd, the low-energy dilaton effective action simply consists of a derivative-expansion of Weyl-invariants.² Such Weyl-invariants must also be included when writing down the dilaton effective action in even d , in addition to the Wess-Zumino action whose Weyl-variation produces the integral of the trace anomaly polynomial (2.4).

²A holographic approach to the dilaton effective action in d -dimensions was recently discussed in [57].

Despite the obvious difference between even and odd d , we find a compact unifying form for the terms in the dilaton effective action that contribute with non-vanishing local matrix elements to the on-shell dilaton amplitudes; these are the terms that are non-vanishing under the equations of motion. For flows induced by explicit breaking of conformal symmetry this is all that is needed. The unified form is given in terms of

$$\mathcal{W}_k = \left(\frac{2}{d-2k}\right)^2 e^{-(d/2-k)\tau} P_k e^{-(d/2-k)\tau}, \quad (2.5)$$

where τ is the dilaton field and $P_k = (\square^k + \text{curvature terms})$ is a GJMS-operator [33]. The GJMS operators P_k are higher-derivative generalizations of the conformal Laplacian ($k = 1$) and the Paneitz operator ($k = 2$) [58].³ The ‘covariance’ of P_k under conformal transformations (see (2.46)) ensures that \mathcal{W}_k behaves well under Weyl-transformations, $\tau \rightarrow \tau + \sigma$ and $g_{\mu\nu} \rightarrow e^{2\sigma} g_{\mu\nu}$: for $k \neq d/2$ it transforms as $\mathcal{W}_k \rightarrow e^{-d\sigma} \mathcal{W}_k$ so that $\sqrt{-g} \mathcal{W}_k$ is Weyl-invariant. We find that up to and including 8-derivative terms, the d -dimensional action in flat space can be written

$$S_\tau = \int d^d x \sqrt{-g} \left[\frac{(d-2)^2}{8} f^{d-2} \mathcal{W}_1 + \alpha^{(d)} \mathcal{W}_2 + \beta^{(d)} \mathcal{W}_3 + \gamma^{(d)} \mathcal{W}_4 + \tilde{\gamma}^{(d)} \frac{(d-4)^2}{4} e^{d\tau} (\mathcal{W}_2)^2 + \dots \right] \Big|_{g_{\mu\nu} = \eta_{\mu\nu}}, \quad (2.6)$$

where the ellipses stand for terms that vanish on-shell. If d is even, $\sqrt{-g} \mathcal{W}_{d/2}$ reduces to $\tau \square^{d/2} \tau$ in flat space. This is not Weyl-invariant, and it is known from $d = 4$ [6] and $d = 6$ [55] that this form encodes⁴ the anomaly flow as $\frac{d}{2} \Delta a \tau \square^{d/2} \tau$. We demonstrate it in this chapter for $d = 8$. So in $d = 4, 6, 8$ one simply re-interprets the coefficient of $\mathcal{W}_{d/2}$ as $\frac{d}{2} \Delta a$.

The action (2.6) should be thought of as a generator of the dilaton amplitudes for the case of flows induced by explicit breaking of conformal symmetry. In general backgrounds, the GJMS-operators P_k exist for all k for d odd, but only for $k \leq d/2$ when d is even [33]; $k = d/2$ is of course the order where the trace anomaly enters. However, for conformally flat backgrounds, the GJMS-operators exist for all k in both even and odd dimensions [63].

We carry out a non-trivial test of the result for the dilaton effective action (2.6) using the example of the d -dimensional free massive scalar. In this example, the dilaton is introduced as a compensator to restore conformal symmetry. The massive scalar couples quadratically to the dilaton, so the n -dilaton amplitudes can be calculated as 1-loop amplitudes with the massive scalar running in the loop. The low-energy expansion of these 1-loop amplitudes can

³Although commonly referred to as the Paneitz operator in the math literature, this 4-derivative operator actually first appeared in Fradkin and Tseytlin’s work [59, 60] from 1982.

⁴The d -dimensional results can be obtained from a generalization of the analysis in Section 2 of [6]; or it can be motivated by an argument [61] based on Branson’s Q -curvature [62].

then be compared with the dilaton amplitudes produced by S in (2.6). We obtain a perfect match; the specific coefficients $\alpha^{(d)}$, $\beta^{(d)}$, $\gamma^{(d)}$ and $\tilde{\gamma}^{(d)}$ of the action (2.6) are listed in table 2.1 in Section 2.5 for $d = 3, 4, 5, \dots, 10$.

We discuss the structure of the action (2.6) further in Sections 2.2.5 and 2.5.2; and we show that at the order of 10- and 12-derivatives, the GJMS-based building blocks \mathcal{W}_k are not sufficient and new structures are needed. Perhaps this points to possible generalizations of the GJMS-operators.

The chapter is structured as follows. In Section 2.2 we analyze the dilaton effective action in d dimensions order by order in derivatives up to $O(\partial^8)$ and calculate the corresponding dilaton matrix elements, assuming the context of explicit breaking and hence an arbitrarily weakly coupled dilaton. In Section 2.3 we study the example of the free massive scalar in 8d and show how to systematically extract Δa from the dilaton amplitudes. We review in Section 2.4 how the d -dimensional anomaly can be calculated as the coefficient of the log-term in the free energy for the free massive scalar and explicitly verify a compact formula for a_{scalar} by Diaz [64] for $d = 4, 6, \dots, 20$. In particular, the $d = 8$ result matches that of our dilaton amplitude calculation in Section 2.3. We generalize the analysis of the free massive scalar to d -dimensions in Section 2.5 and use it to verify the general result for the dilaton effective action. Details of our calculations can be found in four appendices.

2.2 Dilaton Effective Action and Scattering in d Dimensions

The dilaton effective action S consists of diff×Weyl invariant terms and in even dimensions the Wess-Zumino action whose Weyl variation produces the trace anomaly,

$$\delta_\sigma S_{\text{WZ}} = \int d^d x \sqrt{-g} \sigma \langle T_\mu^\mu \rangle = \int d^d x \sqrt{-g} \sigma \left(\sum_i c_i I_i - (-)^{d/2} a E_d \right). \quad (2.7)$$

The construction of S_{WZ} was detailed in [5, 26, 55] and results given explicitly for $d = 4, 6$; we outline the construction for $d = 8$ in appendix A and discuss the result in Section 2.2.4.

In a spacetime with fixed background metric $g_{\mu\nu}$, the diff×Weyl invariant terms are curvature scalars constructed from the ‘hatted’ metric $\hat{g}_{\mu\nu} = e^{-2\tau} g_{\mu\nu}$, where τ is the dilaton field. Here we are concerned with the dilaton effective action in flat space, so in the following we take

$$\hat{g}_{\mu\nu} = e^{-2\tau} \eta_{\mu\nu}. \quad (2.8)$$

For a conformally flat background, any appearance of the Riemann tensor can be replaced

by the Weyl tensor plus Ricci scalar and tensor terms via (A.2). Thus we can construct our Weyl-invariants from the Ricci scalar, Ricci tensor and covariant derivatives thereof. Examples are $\hat{R}_{\mu\nu}\hat{R}^{\mu\nu}$ and $\hat{R}\square\hat{R}$.

We organize the dilaton low-energy effective action as a derivative expansion

$$S = \underbrace{S^{\partial^2}}_{(2.15)} + \underbrace{S^{\partial^4}}_{(2.17)} + \underbrace{S^{\partial^6}}_{(2.26)} + \underbrace{S^{\partial^8}}_{(2.34)} + \dots \quad (2.9)$$

compact form: (2.20) (2.29) (2.42)

S_{WZ} is included as part of the d -derivative action for d even. In the following, we systematically construct $S^{\partial^{2k}}$ for $k = 1, 2, 3, 4$ in d -dimensions.⁵ The equation reference given below each term in (2.9) indicates where to find the result at order $O(\partial^{2k})$. The compact form refers to the terms in GJMS-form (2.6) discussed in the Introduction. Before we analyze each $S^{(\partial^{2k})}$ and calculate the $O(p^{2k})$ scattering amplitudes, let us make a few general comments:

- **Physical dilaton.** In order to calculate dilaton scattering amplitudes, we introduce the physical dilaton field φ defined by

$$e^{-\frac{d-2}{2}\tau} = 1 - \frac{\varphi}{f^{(d-2)/2}} = \Omega f^{-(d-2)/2}. \quad (2.10)$$

This definition ensures that the physical dilaton has on-shell condition $k^2 = 0$.

- **Explicitly broken conformal symmetry.** In this chapter, we focus entirely on the scenario of explicitly broken conformal symmetry. This means that we treat the dilaton as arbitrarily weakly coupled, so that any contributions to the dilaton amplitudes from diagrams with internal dilaton lines are suppressed [55]. As a result, the low-energy dilaton amplitudes at $O(p^{2k})$ derive solely from the contact-terms with $2k$ derivatives. The only terms in the action that contribute to the amplitudes are therefore those that do not vanish on the leading order (i.e. 2-derivative) dilaton equations of motion.
- **From action to amplitudes.** In the dilaton effective action we find terms such as

$$e^{-\frac{d-2k}{2}\tau} \square^k e^{-\frac{d-2k}{2}\tau}. \quad (2.11)$$

Expanding (2.11) in powers of φ gives terms $\varphi^{n_2}\square^k\varphi^{n_1}$ whose contributions to the

⁵All tensor manipulations were done through a combination of pencil, paper, and the Mathematica package xAct [65].

n -point matrix elements are easy to compute:

$$\varphi^{n_2} \square^k \varphi^{n_1} \rightarrow n_1! n_2! \sum_{1 \leq i_1 < i_2 < \dots < i_{n_1} \leq n} s_{i_1 i_2 \dots i_{n_1}}^k. \quad (2.12)$$

Here $n = n_1 + n_2$ and the Mandelstam invariants are defined as

$$s_{i_1 i_2 \dots i_\ell} = -(p_{i_1} + p_{i_2} + \dots + p_{i_\ell})^2. \quad (2.13)$$

The simplicity of (2.12) was exploited previously in [55] for the calculation of the dilaton matrix elements in 4d and 6d. In this chapter, the action also contains terms such as $\varphi \square^2 \varphi^2 \square^2 \varphi^2$ which produce polynomials of the form $(s_{12}^2 s_{34}^2 + \text{perms})$.

2.2.1 Kinetic Term and Dilaton Equations of Motion

The kinetic term for the dilaton is generated by the unique 2-derivative diff \times Weyl invariant $\sqrt{-\hat{g}} \hat{R}$. In a flat background we have

$$\sqrt{-\hat{g}} \hat{R} = 2(d-1) \left(\square \tau - \frac{d-2}{2} (\partial \tau)^2 \right) e^{-(d-2)\tau}, \quad (2.14)$$

so after partial integration we can write

$$\begin{aligned} S^{\partial^2} &= -\frac{1}{8} \frac{d-2}{d-1} f^{d-2} \int d^d x \sqrt{-\hat{g}} \hat{R} \\ &= -\frac{(d-2)^2}{8} f^{d-2} \int d^d x (\partial \tau)^2 e^{-(d-2)\tau} = -\frac{1}{2} \int d^d x (\partial \varphi)^2. \end{aligned} \quad (2.15)$$

The constant f has dimension of mass, and the overall factor is chosen such that the physical dilaton, φ defined in (2.10), has a canonically normalized kinetic term.

It follows from (2.15) that the dilaton equation of motion is

$$\square \tau = \frac{d-2}{2} (\partial \tau)^2 \quad \text{or} \quad \square \varphi = 0. \quad (2.16)$$

The latter form tells us that the on-shell condition for the physical dilaton is $k^2 = 0$, as noted below (2.10). Note that by (2.14), \hat{R} vanishes on-shell.

2.2.2 4-Derivative Action

There are two 4-derivative Weyl-invariants, $\sqrt{-\hat{g}} \hat{R}^2$ and $\sqrt{-\hat{g}} (\hat{R}_{\mu\nu})^2 \equiv \sqrt{-\hat{g}} \hat{R}_{\mu\nu} \hat{R}^{\mu\nu}$, so we write the 4-derivative action

$$S^{\partial^4} = \int d^d x \sqrt{-\hat{g}} \left[\alpha_1 \hat{R}^2 + \alpha_2 (\hat{R}_{\mu\nu})^2 \right] - \delta_{d,4} \Delta a S_{\text{WZ}}, \quad (2.17)$$

where α_i are constants. In 4d, the flat-space limit of S_{WZ} is [5, 26]

$$S_{\text{WZ}} = \int d^4 x \left[-4(\partial\tau)^2 \square\tau + 2(\partial\tau)^4 \right]. \quad (2.18)$$

The Weyl-invariant \hat{R}^2 is zero on-shell, but

$$\begin{aligned} \sqrt{-\hat{g}} (\hat{R}_{\mu\nu})^2 &= \frac{(d-2)^2}{2} \left[\frac{2d(d-1)}{(d-2)^2} (\square\tau)^2 - \frac{3d^2-8d+8}{(d-2)} (\square\tau)(\partial\tau)^2 + (d^2-4d+6)(\partial\tau)^4 \right] e^{-(d-4)\tau} \\ &\xrightarrow{\text{EOM}} -\frac{1}{4}(d-4)(d-2)^2 (\partial\tau)^4 e^{-(d-4)\tau}. \end{aligned} \quad (2.19)$$

This vanishes in $d=4$, as found in [5], so the WZ term is the only contribution to the $O(p^4)$ matrix elements in 4d. This feature facilitated KS's proof of the a -theorem. For $d \neq 4$, the Weyl-invariant (2.19) gives non-vanishing contributions to the $O(p^4)$ matrix elements, as in 6d [55].

The 4-derivative action (2.17) can be written compactly as

$$S^{\partial^4} = \int d^d x \left[\alpha \left(\frac{2}{d-4} \right)^2 e^{-\frac{d-4}{2}\tau} \square^2 e^{-\frac{d-4}{2}\tau} + \dots \right], \quad (2.20)$$

where the “...” refer to terms that vanish on-shell. To see how (2.20) can be compatible with the WZ term, note:

- For $d \neq 4$, the WZ term is absent, and straightforward algebra with the expressions in (B.2) shows that $e^{-\frac{d-4}{2}\tau} \square^2 e^{-\frac{d-4}{2}\tau} = \frac{4-d}{(d-2)^2} \sqrt{-\hat{g}} (\hat{R}_{\mu\nu})^2 +$ terms that vanish on-shell.
- In $d=4$, the only contributions to the $O(p^4)$ dilaton matrix elements come from the WZ action. As noted in [6], the flat-space limit of the S_{WZ} can be written in terms of $-2\Delta a \tau \square^2 \tau +$ terms that vanish on-shell. But this is exactly the expression recovered in the limit $d \rightarrow 4$ of (2.20) with $\alpha = 2\Delta a$.

Practically both cases above require solving a system of 3 equations, matching the coefficients of each unique type of term in (B.2) — $(\square\tau)^2$, $(\partial\tau)^2 \square\tau$, and $(\partial\tau)^4$ — with (2.20), using only the 2 variables α_1 and α_2 [6]. It is noteworthy that a solution exists.

The n -point matrix elements at order $O(p^4)$ can be expressed in terms of a basis of polynomials in the Mandelstam invariants (2.13) as

$$P_n^{(4)} \equiv \sum_{1 \leq i < j \leq n} s_{ij}^2. \quad (2.21)$$

As an example, consider the $O(p^4)$ to the amplitudes determined by S^{∂^4} in (2.20). Changing variables from τ to φ via (2.10) gives

$$\alpha \left(\frac{2}{(d-2)^2} \right)^2 \frac{1}{f^{2d-4}} \varphi^2 \square^2 \varphi^2 + O(\varphi^5), \quad (2.22)$$

so using (2.12) we can directly read off the 4-point amplitude

$$\mathcal{A}_4^{(4)} = \alpha \left(\frac{2}{(d-2)^2} \right)^2 \frac{1}{f^{2d-4}} 2! 2! \sum_{1 \leq i < j \leq 4} s_{ij}^2 = \alpha \frac{32}{(d-2)^4} \frac{1}{f^{2d-4}} (s^2 + t^2 + u^2). \quad (2.23)$$

For $d = 4$, we identify $\alpha = 2\Delta a$, so (2.23) agrees with the result (2.1). Taking $d = 6$, we find $\mathcal{A}_4^{(4)} = \frac{\alpha}{8f^8} (s^2 + t^2 + u^2)$. This matches the result in eq. (3.18) of [55] in which $\mathcal{A}_4^{(4)}$ was expressed in terms of a coefficient b related to α by $\alpha = 4b$.

The higher-point matrix elements of S^{∂^4} are straightforward to extract from (2.20). To avoid cluttering the main text, we list the $O(p^4)$ matrix elements in (C.1) for the general d -dimensional case.

2.2.3 6-Derivative Action

For a d -dimensional conformally flat metric, any 6-derivative Weyl-invariant can be written in terms of

$$\hat{R}^3, \quad \hat{R}(\hat{R}_{\mu\nu})^2 \equiv \hat{R}(\hat{R}^\mu{}_\nu \hat{R}^\nu{}_\mu), \quad \hat{R} \hat{\square} \hat{R}, \quad \text{and} \quad (\hat{R}_{\mu\nu})^3 \equiv (\hat{R}^\mu{}_\nu \hat{R}^\nu{}_\rho \hat{R}^\rho{}_\mu), \quad (2.24)$$

up to total derivatives. For example [66],

$$\begin{aligned} \hat{R}_{\mu\nu} \hat{\square} \hat{R}^{\mu\nu} &= \frac{1}{(d-2)(d-1)} \hat{R}^3 - \frac{2d-1}{(d-2)(d-1)} \hat{R}(\hat{R}_{\mu\nu})^2 \\ &\quad + \frac{d}{4(d-1)} \hat{R} \hat{\square} \hat{R} + \frac{d}{d-2} (\hat{R}_{\mu\nu})^3 + \text{total derivatives}. \end{aligned} \quad (2.25)$$

Using the basis (2.24), the 6-derivative action takes the form:

$$S^{\partial^6} = \int d^d x \sqrt{-\hat{g}} \left[\beta_1 \hat{R}^3 + \beta_2 \hat{R} (\hat{R}_{\mu\nu})^2 + \beta_3 \hat{R} \hat{\square} \hat{R} + \beta_4 (\hat{R}_{\mu\nu})^3 \right] + \delta_{d,6} \Delta a S_{\text{WZ}}, \quad (2.26)$$

where β_i are constants.⁶ A curved-space derivation of the WZ action in $d = 6$ dimensions is given in [55] and [56]. The flat space limit is

$$S_{\text{WZ}} = \int d^6 x \left[-24(\square\tau)^2(\partial\tau)^2 + 24(\partial\tau)^2(\partial\partial\tau)^2 + 36\square\tau(\partial\tau)^4 - 24(\partial\tau)^6 \right]. \quad (2.27)$$

Explicit expressions for each of the four Weyl-invariants are available in appendix B. The three invariants proportional to \hat{R} vanish on-shell, so only $(\hat{R}_{\mu\nu})^3$ contributes to the $O(p^6)$ dilaton matrix elements:

$$(\hat{R}_{\mu\nu})^3 \xrightarrow{\text{EOM}} -\frac{1}{4} e^{-(d-6)\tau} (d-6)(d-2)^3 \left((\partial\partial\tau)^2(\partial\tau)^2 - 2(\partial\tau)^6 \right). \quad (2.28)$$

This vanishes in $d = 6$, hence for the case of explicitly broken conformal symmetry, only the WZ action generates contact-term contributions to the 6d matrix elements at $O(p^6)$.⁷

The 6-derivative action (2.26) can be written in the compact form

$$S^{\partial^6} = \int d^d x \left[\beta \left(\frac{2}{d-6} \right)^2 e^{-\frac{d-6}{2}\tau} \square^3 e^{-\frac{d-6}{2}\tau} + \dots \right], \quad (2.29)$$

where the “...” refer to terms that vanish on-shell. When $d \rightarrow 6$, the action (2.29) reduces to $3\Delta a \tau \square^3 \tau$ and we identify $\beta = 3\Delta a$. The equivalence of (2.26) and (2.29) requires a solution to an overconstrained system of 8 equations (from matching the coefficients of the 8 distinct terms in the expressions of (B.3)-(B.6), e.g. $(\square\tau)(\square^2\tau)$, with (2.29)) using only the 4 variables β_1, \dots, β_4 from (2.26).

The local matrix elements with $n \leq 8$ external dilatons can at $O(p^6)$ be expressed in terms of two linearly independent symmetric Mandelstam polynomials,

$$P_{n,A}^{(6)} = \sum_{1 \leq i < j \leq n} s_{ij}^3, \quad P_{n,B}^{(6)} = \sum_{1 \leq i < j < k \leq n} s_{ijk}^3. \quad (2.30)$$

⁶The observant reader may notice that the 6-derivative action for $d = 6$ in [55] contains only three curvature invariants. This is sufficient in 6d because one can use that the Euler density E_6 is a total derivative to eliminate one of the four invariants.

⁷In the case of spontaneous breaking, the 4-derivative terms also contribute through pole diagrams [55].

Writing the amplitudes in this basis requires identities such as

$$\sum_{1 \leq i < j < k < l \leq 8} s_{ijkl}^3 = -2P_{8,A}^{(6)} + 2P_{8,B}^{(6)}. \quad (2.31)$$

We list the $O(p^6)$ amplitudes in (C.2). In 6d, the 4-, 5- and 6-point amplitudes reproduce (3.19)-(3.21) of [55] with $\beta = 3\Delta a$. For example,

$$\mathcal{A}_6^{(6)} = \frac{64(d+2)}{(d-2)^6} \frac{\beta}{f^{3d-6}} \left(4d P_{6,A}^{(6)} + (d+2) P_{6,B}^{(6)} \right) \xrightarrow{d \rightarrow 6} \frac{3\Delta a}{f^{12}} \left(3 P_{6,A}^{(6)} + P_{6,B}^{(6)} \right). \quad (2.32)$$

In 8d, we have

$$\mathcal{A}_6^{(6)} \xrightarrow{d \rightarrow 8} \frac{20\beta}{729 f^{18}} \left(16 P_{6,A}^{(6)} + 5 P_{6,B}^{(6)} \right). \quad (2.33)$$

We match this and the other $O(p^6)$ n -point amplitudes, $n \leq 8$, for the example of the free massive scalar in Sections 2.3 and 2.5.

2.2.4 8-Derivative Action

For a d -dimensional, conformally flat metric, we find nine independent Weyl-invariants (up to total derivatives) by explicit calculation, so the off-shell action can be written as

$$S^{\partial^8} = \int d^d x \sqrt{-\hat{g}} \left[\gamma_1 \hat{R}^4 + \gamma_2 \hat{R}^2 (\hat{R}_{\mu\nu})^2 + \gamma_3 \hat{R} (\hat{R}_{\mu\nu})^3 + \gamma_4 ((\hat{R}_{\mu\nu})^2)^2 + \gamma_5 (\hat{R}_{\mu\nu})^4 + \gamma_6 (\hat{\square} \hat{R})^2 \right. \\ \left. + \gamma_7 (\hat{\square} \hat{R}_{\mu\nu})^2 + \gamma_8 \hat{R} (\hat{\nabla}_\mu \hat{R})^2 + \gamma_9 (\hat{R}_{\mu\nu})^2 \hat{\square} \hat{R} \right] - \delta_{d,8} \Delta a S_{\text{WZ}}, \quad (2.34)$$

with constants γ_i . We have abbreviated some index contractions using the conventions defined in equation (B.8), e.g. $(\hat{R}_{\mu\nu})^4 \equiv (\hat{R}^\mu{}_\nu \hat{R}^\nu{}_\rho \hat{R}^\rho{}_\lambda \hat{R}^\lambda{}_\mu)$.

In flat space, the 8d WZ action is

$$S_{\text{WZ}} = 48 \int d^8 x \left[3(\square^2 \tau)(\partial\tau)^4 + 6(\square\tau)^3(\partial\tau)^2 + 36(\square\tau)^2(\partial\partial\tau\partial\tau\partial\tau) + 16(\square\tau)(\partial\partial\partial\tau\partial\tau\partial\tau\partial\tau) \right. \\ \left. - 12(\square\tau)(\partial\partial\tau)^2(\partial\tau)^2 - 24(\partial\partial\tau\partial\tau\partial\tau)(\partial\partial\tau)^2 \right. \\ \left. + 12(\square\tau)^2(\partial\tau)^4 - 12(\partial\partial\tau)^2(\partial\tau)^4 - 20(\square\tau)(\partial\tau)^6 + 15(\partial\tau)^8 \right]. \quad (2.35)$$

Details of the derivation are described in appendix A. Applying the equations of motion, we find

$$S_{\text{WZ}} \xrightarrow{\text{EOM}} 144 \int d^8 x \left[-8(\partial\partial\tau\partial\tau\partial\tau)(\partial\partial\tau)^2 - 32(\partial\partial\tau\partial\tau\partial\tau)^2 - 2(\partial\partial\tau)^2(\partial\tau)^4 + 3(\partial\tau)^8 \right]. \quad (2.36)$$

It is clear from (2.35) and (2.36) that S_{WZ} contributes to 5- and higher-point amplitudes, but not to the 4-point amplitude.

We have obtained explicit expressions for the d -dimensional Weyl-invariants in (2.34); the procedure for calculating them is straightforward, though to simplify them requires some effort with multiple applications of partial integration. Since the general- d results are rather involved, we present them in appendix B only for $d = 8$.

Six of the nine Weyl-invariants in (2.34) vanish on-shell; the only non-vanishing ones are $((\hat{R}_{\mu\nu})^2)^2$, $(\hat{R}_{\mu\nu})^4$, and $(\hat{\square}\hat{R}_{\mu\nu})^2$. These three are also related on-shell; for $d > 2$:

$$\sqrt{-\hat{g}}(\hat{\square}\hat{R}_{\mu\nu})^2 \xleftarrow{\text{EOM}} \frac{d}{(d-2)^2} \left(-\sqrt{-\hat{g}}((\hat{R}_{\mu\nu})^2)^2 + d\sqrt{-\hat{g}}(\hat{R}_{\mu\nu})^4 \right). \quad (2.37)$$

The two Weyl-invariants on the RHS give distinct expressions

$$\begin{aligned} \sqrt{-\hat{g}}((\hat{R}_{\mu\nu})^2)^2 \xrightarrow{\text{EOM}} \frac{1}{48} e^{-(d-8)\tau} (d-2)^4 & \left(48(\partial\partial\tau)^4 + 192(\partial\partial\tau\partial\tau\partial\tau) (\partial\partial\tau)^2 + 192(\partial\partial\tau\partial\tau\partial\tau)^2 \right. \\ & \left. - 24(d-4)(\partial\tau)^4 (\partial\partial\tau)^2 - (d-4)(d-44)(\partial\tau)^8 \right), \end{aligned} \quad (2.38)$$

$$\begin{aligned} \sqrt{-\hat{g}}(\hat{R}_{\mu\nu})^4 \xrightarrow{\text{EOM}} \frac{1}{96} e^{-(d-8)\tau} (d-2)^4 & \left(48(\partial\partial\tau)^4 - 48(d-12)(\partial\partial\tau\partial\tau\partial\tau) (\partial\partial\tau)^2 \right. \\ & \left. - 192(d-9)(\partial\partial\tau\partial\tau\partial\tau)^2 + 6(d^2 - 22d + 96) (\partial\tau)^4 (\partial\partial\tau)^2 \right. \\ & \left. + (d^3 - 48d^2 + 626d - 2304) (\partial\tau)^8 \right), \end{aligned} \quad (2.39)$$

except in $d = 8$:

$$\begin{aligned} \sqrt{-\hat{g}}(\hat{R}_{\mu\nu})^4 \xleftarrow[d=8]{\text{EOM}} \frac{1}{2} \sqrt{-\hat{g}}((\hat{R}_{\mu\nu})^2)^2 \\ \xrightarrow[d=8]{\text{EOM}} 648 \left((\partial\partial\tau)^4 + 4(\partial\partial\tau\partial\tau\partial\tau)(\partial\partial\tau)^2 + 4(\partial\partial\tau\partial\tau\partial\tau)^2 - 2(\partial\partial\tau)^2 (\partial\tau)^4 + 3(\partial\tau)^8 \right). \end{aligned} \quad (2.40)$$

So in general $d > 2$, the on-shell matrix elements at $O(p^8)$ depend on two free parameters: for $d = 8$ they are Δa and the coefficient of (say) $(\hat{R}_{\mu\nu})^4$, while for $d \neq 8$ they are the coefficients of $(\hat{R}_{\mu\nu})^4$ and $((\hat{R}_{\mu\nu})^2)^2$. We can summarize this as

$$S^{\partial^8} = \int d^d x \left[\Gamma_1 ((\hat{R}_{\mu\nu})^2)^2 + \Gamma_2 (\hat{R}_{\mu\nu})^4 + \dots \right] - \delta_{d,8} \Delta a S_{\text{WZ}}, \quad (2.41)$$

where the “...” stand for terms that vanish on-shell. In 8d the amplitudes depend only on Δa and the combination $\Gamma_{8d} \equiv 2\Gamma_1 + \Gamma_2$.

As with 4- and 6-derivatives, the 8-derivative action can also be written in an alternative

form,

$$S^{\partial^8} = \int d^d x \left[\gamma \left(\frac{2}{d-8} \right)^2 e^{-(d-8)\tau/2} \square^4 e^{-(d-8)\tau/2} + \tilde{\gamma} \left(\frac{2}{d-4} \right)^2 e^{4\tau} \left(\square^2 e^{-\frac{d-4}{2}\tau} \right)^2 + \dots \right], \quad (2.42)$$

which encodes the same $O(p^8)$ on-shell amplitudes as (2.41), with the understanding that for $d = 8$ we have $\gamma = 4\Delta a$ and $\tilde{\gamma} = 162(\Gamma_{8d} - \frac{2}{9}\Delta a)$. The equality of (2.41) and (2.42) is found by matching the coefficients of the 23 distinct terms in (B.9)-(B.17) with the similar terms in (2.42) using only 9 variables, $\gamma_1, \dots, \gamma_9$.

For $d \neq 8$, the translation between coefficients in (2.41) and (2.42) is

$$\Gamma_1 = \frac{36d}{(d-8)(d-2)^4} \gamma + \frac{4}{(d-2)^4} \tilde{\gamma}, \quad \Gamma_2 = -\frac{576}{(d-8)(d-2)^4} \gamma. \quad (2.43)$$

Note that the linear combination Γ_{8d} is finite in the limit $d \rightarrow 8$.

The $n = 4, 5, \dots, 8$ -point amplitudes at $O(p^8)$ are given in general d dimensions in (C.3). Let us here list the results for $d = 8$, using $\gamma = 4\Delta a$:

$$\begin{aligned} \mathcal{A}_4^{(8)} &= \frac{2}{81f^{12}} (36\Delta a + \tilde{\gamma}) (s^4 + t^4 + u^4) = \Gamma_{8d} \frac{4}{f^{12}} (s^4 + t^4 + u^4), \\ \mathcal{A}_5^{(8)} &= \frac{8}{243f^{15}} \left[(54\Delta a + \tilde{\gamma}) P_{5,A}^{(8)} + \tilde{\gamma} P_{5,B}^{(8)} \right], \\ \mathcal{A}_6^{(8)} &= \frac{8}{729f^{18}} \left[(486\Delta a + 7\tilde{\gamma}) P_{6,A}^{(8)} + 2(81\Delta a + \tilde{\gamma}) P_{6,B}^{(8)} + 7\tilde{\gamma} P_{6,C}^{(8)} + 4\tilde{\gamma} P_{6,D}^{(8)} \right], \\ \mathcal{A}_7^{(8)} &= \frac{16}{243f^{21}} \left[(324\Delta a + 7\tilde{\gamma}) P_{7,A}^{(8)} + 162\Delta a P_{7,B}^{(8)} + 7\tilde{\gamma} P_{7,C}^{(8)} + 4\tilde{\gamma} P_{7,D}^{(8)} \right], \\ \mathcal{A}_8^{(8)} &= \frac{16}{2187f^{24}} \left[(14580\Delta a + 301\tilde{\gamma}) P_{8,A}^{(8)} + (5832\Delta a + 77\tilde{\gamma}) P_{8,B}^{(8)} + (2187\Delta a - 7\tilde{\gamma}) P_{8,C}^{(8)} \right. \\ &\quad \left. + 189\tilde{\gamma} P_{8,D}^{(8)} + 126\tilde{\gamma} P_{8,E}^{(8)} \right], \end{aligned} \quad (2.44)$$

where for instance,

$$P_{5,A}^{(8)} = \sum_{1 \leq i < j \leq 5} s_{ij}^4, \quad P_{5,B}^{(8)} = s_{12}^2 s_{34}^2 + \text{perms}, \quad (2.45)$$

and the definitions of the other basis polynomials for $n \geq 6$ are given in (C.5)-(C.7).

We noted below (2.36) that information about the anomaly cannot enter until the 5-point amplitude. This is verified by the second equality for the 4-point amplitude in (2.44) where we used $\tilde{\gamma} = 162(\Gamma_{8d} - \frac{2}{9}\Delta a)$ to demonstrate that the 4-dilaton amplitude indeed captures no information about the anomaly flow Δa .

It is a new feature in 8d, compared with 4d and 6d, that there is a non-vanishing contribu-

tion from the Weyl-invariants at the same order in momentum as the flow in the a -anomaly. In 4d and 6d, the WZ action provided the unique contributions to, respectively, the $O(p^4)$ and $O(p^6)$ matrix elements. In 8d, the $O(p^8)$ dilaton matrix elements are “polluted” by the Weyl-invariant, which does not contain information about the flow of a in general. However, note that even from just the 5-dilaton amplitude one can determine Δa and $\tilde{\gamma}$ uniquely, since there are two independent Mandelstam polynomials. The match to the higher-point amplitudes is then a strong consistency check. We check consistency explicitly in Section 2.3.

2.2.5 Dilaton Effective Action and GJMS Operators

We found above that the relevant terms in the flat-space dilaton effective action were expressed in terms of \square^k up to and including $O(p^8)$. The derivation required solutions to over-constrained systems of equations. A solution could be found in each case because \square^k is the flat-space limit of the GJMS operator, P_k , which transforms in the following simple manner under conformal transformations:

$$P_k[e^{2\sigma}g] = e^{-(d/2+k)\sigma} P_k[g] e^{(d/2-k)\sigma} ; \quad P_k[\eta] = \square^k . \quad (2.46)$$

The GJMS operators are the higher-order generalizations of the well-known conformal Laplacian (the Yamabe operator) $P_1 = \square - \frac{(d-2)}{4(d-1)}R$ and the Paneitz operator $P_2 = \square^2 + \dots$ [58, 59, 60].

Let us define

$$\mathcal{W}_k \equiv \left(\frac{2}{d-2k}\right)^2 e^{-(d/2-k)\tau} P_k e^{-(d/2-k)\tau} . \quad (2.47)$$

Under a Weyl-transformation, $\tau \rightarrow \tau + \sigma$ and $g_{\mu\nu} \rightarrow e^{2\sigma}g_{\mu\nu}$, and it follows from (2.46) that

$$\mathcal{W}_k \xrightarrow{\text{Weyl}} e^{-d\sigma} \mathcal{W}_k , \quad (k \neq d/2) , \quad (2.48)$$

so that $\sqrt{-g}\mathcal{W}_k$ is a Weyl-invariant for $k \neq d/2$. It is the flat-space limit of $\sqrt{-g}\mathcal{W}_k$ we have encountered in the our analysis of the $O(\partial^{2k})$ -derivative terms.

The results for the $2k$ -derivative actions of the previous subsections can now be summarized as

$$S = \int d^d x \sqrt{-g} \left[\frac{(d-2)^2}{8} f^{d-2} \mathcal{W}_1 + \alpha \mathcal{W}_2 + \beta \mathcal{W}_3 + \gamma \mathcal{W}_4 + \tilde{\gamma} \frac{(d-4)^2}{4} e^{d\tau} (\mathcal{W}_2)^2 + \dots \right] \Big|_{g_{\mu\nu}=\eta_{\mu\nu}} \quad (2.49)$$

where the ellipses stand for 1) terms that vanish upon application on the equations of motion, and 2) terms with more than 8 derivatives.

The normalization in (2.47) was chosen such that for even d we get

$$\int d^d x \sqrt{-g} \mathcal{W}_{d/2} \xrightarrow{\text{flat space}} \int d^d x \tau \square^{d/2} \tau. \quad (2.50)$$

As discussed in the previous subsections, this means the coefficient of $\mathcal{W}_{d/2}$ is $(d/2)\Delta a$ for d even; i.e. $\alpha = 2\Delta a$ for $d = 4$, $\beta = 3\Delta a$ for $d = 6$, and $\gamma = 4\Delta a$ for $d = 8$.⁸

Note also that

$$\frac{(d-4)^2}{4} e^{d\tau} (\mathcal{W}_2)^2 = \left(\frac{2}{d-4}\right)^2 e^{4\tau} \left(P_2 e^{-\frac{d-4}{2}\tau}\right)^2 \xrightarrow{\text{flat space}} \left(\frac{2}{d-4}\right)^2 e^{4\tau} \left(\square^2 e^{-\frac{d-4}{2}\tau}\right)^2. \quad (2.51)$$

In the limit $d \rightarrow 4$, this simply becomes $e^{4\tau} (\square^2 \tau)^2$.

In this section, we have shown that in the case of flows induced by explicit breaking of the conformal symmetry, the terms that matter for extracting the on-shell dilaton amplitudes from the flat-space dilaton effective action can be written in the ‘‘GJMS-form’’ (2.49). In the following sections, we will verify this form explicitly using the example of the RG flow of the free massive scalar field. It is tempting to propose that this is also the form of the action that matters in the conformally flat case, for example the d -sphere, for which the GJMS operators exist for all k [63].

2.3 Example: Free Scalar in 8d

The example of the free conformal scalar was studied for $d = 4$ in [5] and $d = 6$ in [55]. Here we consider $d = 8$ with the purpose of testing the 8d form of the dilaton effective action derived in the previous section. We also show how the flow of the anomaly, Δa , can be separated systematically from the non-vanishing contribution of the 8-derivative Weyl-invariant $e^{8\tau} (\mathcal{W}_2)^2$.

Consider the action for a free massive scalar in 8d,

$$S = \int d^8 x \left(-\frac{1}{2} (\partial\Phi)^2 - \frac{1}{2} M^2 \Phi^2 \right). \quad (2.52)$$

The presence of the mass-term operator explicitly breaks the conformal symmetry of the action. We can restore that symmetry by promoting the coupling to a scalar function of

⁸One should be aware that terms like $\tau \square^{d/2} \tau$ can be produced by more than just the $\mathcal{W}_{d/2}$ operator. For instance, when $d = 8$, $e^{d\tau} (\mathcal{W}_2)^2$ contains $\tau \square^4 \tau$. However, the Weyl transformation of this term is compensated by the other terms produced by that operator so that the whole expression is invariant.

spacetime as

$$M^2 \rightarrow M^2 e^{-2\tau} = \lambda \Omega^{2/3}, \quad (2.53)$$

with $\lambda = M^2/f^2$.

Introducing a kinetic term for the compensator field Ω , we write

$$S = \int d^8x \left(-\frac{1}{2}(\partial\Phi)^2 - \frac{1}{2}(\partial\Omega)^2 - \frac{1}{2}\lambda\Omega^{2/3}\Phi^2 \right). \quad (2.54)$$

The 8d scalar fields Φ and Ω have mass dimension 3, so the exponent of 2/3 in (2.53) is compatible with the coupling λ being dimensionless.

When the compensator acquires a VEV, $\langle\Omega\rangle = f^3$, the mass-term for Φ is recovered. The fluctuation, φ , defined as $\Omega = f^3 - \varphi$ (cf. (2.10)) is the physical dilaton. This way the explicitly broken conformal symmetry can be treated as spontaneously broken and the anomaly matching argument of KS [5, 6] applies. The key difference between the truly spontaneously broken scenario and explicit breaking is that in the latter case we are free to choose the scale f such that the dilaton is arbitrarily weakly coupled.

The fractional exponent of $\Omega = f^3 - \varphi$ means that unlike the 4d and 6d cases [5, 55], there are an infinite number of interaction vertices $\Phi^2\varphi^k$ in the action (2.54):

$$S = \int d^8x \left[-\frac{1}{2}(\partial\Phi)^2 - \frac{1}{2}M^2\Phi^2 - \frac{1}{2}(\partial\varphi)^2 + \frac{M^2}{3f}\Phi^2\varphi + \frac{M^2}{18f^2}\Phi^2\varphi^2 + \frac{2M^2}{81f^3}\Phi^2\varphi^3 + \dots \right]. \quad (2.55)$$

The massive Φ can be integrated out to leave the effective action for the dilaton φ . To compare with our general 8d action, an easy approach [55] is to calculate the n -point on-shell dilaton scattering amplitudes from (2.55) and compare with those of the general 8d dilaton effective action (2.44). Taking $f \gg M$ means that the calculation is effectively 1-loop: no internal φ 's are exchanged. (This is the case of explicit breaking, and we can view the dilaton as a source [55].) The low-energy expansion of the amplitudes in powers of external momenta results in divergent diagrams at $O(p^4)$; the coupling of the $O(\partial^4)$ terms are renormalized in 8d, and we do not attempt to match them to the general effective action. At order $O(p^6)$ and $O(p^8)$ (and higher) the results of the 1-loop calculation are finite and a precise match is obtained up to 8-point order.

As an example of the match, consider the 6-point $O(p^6)$ amplitudes. The calculation of the 1-loop amplitude with 6 external φ 's and an internal loop of Φ 's makes use of 3-, 4-, 5-, and 6-point interactions from (2.55) and involves sums of hexagon diagrams, pentagon diagrams, 3 types of box diagrams (with topology of “1-mass”, “2-mass-easy” and “2-mass-

hard”), 3 types of triangle diagrams, and 2 types of bubble diagrams.⁹ The result can be expressed in terms of the Mandelstam basis polynomials (2.30) as

$$d = 8: \quad \mathcal{A}_6^{(6)} = \frac{2^3 M^2}{3^{10} 7 (4\pi)^4 f^{18}} \left(16 P_{6,A}^{(6)} + 5 P_{6,B}^{(6)} \right). \quad (2.56)$$

Comparing this with (2.33) one immediately sees that the functional form matches, and we can read off $\beta = 2M^2/(2835(4\pi)^4)$. We have explicitly checked that all the other $n = 4, 5, 6, 7, 8$ -point amplitudes (C.1) with $d = 8$ are also reproduced exactly with this value of β . While β itself has no particular interest to us¹⁰ — it is a model-dependent dimensional coefficient — the fact that we reproduce the $O(p^6)$ amplitudes is a strong consistency check on the 1-loop calculation and on the structure of the dilaton effective action at $O(\partial^6)$.

Next, move ahead to the $O(p^8)$ amplitudes which in $d = 8$ contain information about the flow of the trace anomaly. Details of the calculation are given in appendix D; here we quote the 4- and 5-point 1-loop amplitudes:

$$\begin{aligned} \mathcal{A}_4^{(8)} &= \frac{17}{3\,061\,800 (4\pi)^4 f^{12}} (s^4 + t^4 + u^4), \\ \mathcal{A}_5^{(8)} &= \frac{16}{27 f^{15}} \left[\frac{13}{777\,600 (4\pi)^4} P_{5,A}^{(8)} + \frac{11}{5\,443\,200 (4\pi)^4} P_{5,B}^{(8)} \right]. \end{aligned} \quad (2.57)$$

Comparing $\mathcal{A}_5^{(8)}$ in (2.57) and (2.44), we find both Δa and $\tilde{\gamma}$ thanks to the two independent Mandelstam polynomials. The result is

$$\Delta a = \frac{23}{5\,443\,200 (4\pi)^4} = \frac{23}{2^7 3^5 5^2 7 (4\pi)^4} \quad (2.58)$$

and

$$\tilde{\gamma} = \frac{11}{151\,200 (4\pi)^4}. \quad (2.59)$$

This is consistent with the matching of $\mathcal{A}_4^{(8)}$ in (2.57) and (2.44) with

$$\Gamma_{\text{sd}} = \frac{\tilde{\gamma}}{162} + \frac{2}{9} \Delta a = \frac{17}{12\,247\,200 (4\pi)^4}. \quad (2.60)$$

Note that $\Delta a > 0$ in accordance with a possible 8d a -theorem. Also, the coefficient of

⁹For comparison, the equivalent calculation [55] in 6d was much easier since with only a cubic vertex, the only diagram involved was the hexagon diagram.

¹⁰Other than we note that β is positive.

$(s^4 + t^4 + u^4)$ is positive as expected, $\Gamma_{8d} > 0$ (cf. discussion in the Introduction). As a further non-trivial consistency check, we have calculated the 1-loop 6, 7, 8-point amplitudes and matched them exactly to the $O(p^8)$ amplitudes in (2.44) with the same values (2.58) and (2.59).

The UV theory is that of a free massless scalar with the corresponding Weyl anomaly $a_{\text{UV}} = a_{\text{scalar},8d}$. The mass term ignites the flow and in the deep IR the massive scalar Φ decouples. Hence the IR theory is trivial, $a_{\text{IR}} = 0$. Thus we expect that $\Delta a = a_{\text{UV}} - a_{\text{IR}} = a_{\text{scalar},8d}$. The anomaly $a_{\text{scalar},8d}$ of a free conformal scalar can be calculated from the free energy on a d -sphere, so our value (2.58) for $\Delta a = a_{\text{scalar},8d}$ is easily checked. Read on.

2.4 Scalar Anomaly from Zeta-Function Regularization of the Free Energy

The action for a free conformal scalar is

$$S = \int d^d x \sqrt{-g} \left(-\frac{1}{2} (\nabla \Phi)^2 - \frac{d-2}{4(d-1)} R \Phi^2 \right). \quad (2.61)$$

Consider now the theory on a d -sphere S^d . In the notation of [15], we can write the free energy

$$\begin{aligned} F &= -\log |Z| = \frac{1}{2} \log \det \mu_0^{-2} \left(-\nabla^2 + \frac{d-2}{4(d-1)} R \right) \\ &= \frac{1}{2} \sum_{n=0}^{\infty} m_n \left[-2 \log(\mu_0 r_0) + \log(n + d/2) + \log(n - 1 + d/2) \right], \end{aligned} \quad (2.62)$$

where r_0 is the radius of the S^d , μ_0 is the UV cutoff, and

$$m_n = \frac{(2n + d - 1)(n + d - 1)!}{(d - 1)! n!} \quad (2.63)$$

are the multiplicities of the eigenvalues $\{\lambda_n\}_{n \geq 0}$ of the conformal Laplacian on S^d . The coefficient of the $\log(\mu_0 r_0)$ -term in (2.62) is the a -anomaly of the free conformal scalar. Normalizing by the integral of the Euler density over S^d , we have

$$a_{\text{scalar},d} = -\frac{\sum_{n=0}^{\infty} m_n}{\int_{S^d} \sqrt{g} E_d}. \quad (2.64)$$

In our conventions (2.3) for the Euler density this is

$$\int_{S^d} \sqrt{g} E_d = d! \Omega_d, \quad (2.65)$$

where $\Omega_d = 2\pi^{(d+1)/2} / \Gamma(\frac{d+1}{2})$ is the surface volume of the d -sphere.

The sum in (2.64) is formally divergent, but can be evaluated via zeta-function regularization. This gives $a_{\text{scalar},d \text{ odd}} = 0$ as well as the familiar values

$$a_{\text{scalar},4d} = \frac{1}{360 (4\pi)^2}, \quad \text{and} \quad a_{\text{scalar},6d} = \frac{1}{9072 (4\pi)^3}. \quad (2.66)$$

This method was used already in 1979 to calculate the functional determinant (2.62) [67]; explicit values for $d = 4, 6, 8, 10$ were given by Copeland and Toms in 1986 [68].¹¹ More recently, Cappelli and D'Appollonio [69] extended the list of explicit values up to $d = 14$. A compact formula for $a_{\text{scalar},d}$ was presented by Diaz [64], and it is easily translated to our conventions using (2.65):

$$d \text{ even:} \quad a_{\text{scalar},d} = \frac{a(d)}{d! \left(\frac{d}{2}\right)! (4\pi)^{d/2}}, \quad \text{with} \quad a(d) = - \int_0^1 dt \prod_{i=0}^{d/2-1} (i^2 - t^2). \quad (2.67)$$

For $d = 4, 6, \dots, 20$ one finds

$$a(d) = \left\{ \frac{2}{15}, \frac{10}{21}, \frac{184}{45}, \frac{2104}{33}, \frac{2140592}{1365}, \frac{2512144}{45}, \frac{2075529088}{765}, \frac{344250108032}{1995}, \frac{6884638343936}{495} \right\}. \quad (2.68)$$

We have checked explicitly that these values agree with the result of zeta-function regularization of the sum (2.64).

Note that for $d = 8$, we have

$$a_{\text{scalar},8d} = \frac{1}{8! 4! (4\pi)^4} \times \frac{184}{45} = \frac{23}{5443200 (4\pi)^4}. \quad (2.69)$$

This is in perfect agreement with our 1-loop calculation (2.58).¹²

¹¹Table 1 in [68] quotes an incorrect value for $d = 12$.

¹²Let us note that for odd- d , the $O((r_0)^0)$ -terms in (2.62) produce the F -coefficient for a free conformal scalar; this is also evaluated using zeta-function regularization and explicit values can be found in [15]. An approach using entanglement entropy for even- d and odd- d spheres was studied in [70] and [71].

2.5 Free Scalar in d Dimensions and the Dilaton Effective Action

In this section, we generalize to d dimensions the example of the 8d free scalar from Section 2.3. We match the dilaton effective action up to 8-derivative terms for $d = 3, 4, \dots, 10$. Finally, we comment on the structure of higher-derivative terms.

2.5.1 Free Scalar in d Dimensions

Consider a free massless scalar, Φ . Introducing a mass term in the action,

$$S = \int d^d x \left(-\frac{1}{2}(\partial\Phi)^2 - \frac{1}{2}M^2\Phi^2 \right), \quad (2.70)$$

breaks the conformal symmetry explicitly. The symmetry can be restored by promoting the mass to a spacetime dependent quantity with the introduction of a compensator field Ω :

$$S = \int d^d x \left(-\frac{1}{2}(\partial\Phi)^2 - \frac{1}{2}(\partial\Omega)^2 - \frac{1}{2}\lambda\Omega^{\frac{4}{d-2}}\Phi^2 \right). \quad (2.71)$$

The coupling $\lambda = M^2/f^2$ is dimensionless (as is compatible with the mass-dimension $(d-2)/2$ of d -dimensional scalars). To see that this makes the classical theory conformal, calculate the stress tensor from the action (2.71),

$$T_{\mu\nu} = -\frac{2}{\sqrt{-g}}\frac{\delta S}{\delta g^{\mu\nu}} = \partial_\mu\Phi\partial_\nu\Phi + \partial_\mu\Omega\partial_\nu\Omega - \frac{1}{2}\eta_{\mu\nu}\left[(\partial\Phi)^2 + (\partial\Omega)^2 + \lambda\Omega^{\frac{4}{d-2}}\Phi^2\right], \quad (2.72)$$

and improve it to

$$\Theta_{\mu\nu} = T_{\mu\nu} - \frac{1}{4}\frac{d-2}{d-1}(\partial_\mu\partial_\nu - \eta_{\mu\nu}\square)(\Phi^2 + \Omega^2). \quad (2.73)$$

Then upon application of the equations of motion

$$\square\Phi = \lambda\Omega^{\frac{4}{d-2}}\Phi \quad \text{and} \quad \square\Omega = \lambda\frac{2}{d-2}\Omega^{\frac{4}{d-2}-1}\Phi^2 \quad (2.74)$$

one finds $\Theta_\mu{}^\mu = 0$.

The model (2.71) has a moduli space along Ω when $\langle\Phi\rangle = 0$. At the origin, $\langle\Omega\rangle = 0$, the theory is conformal, but the conformal symmetry is spontaneously broken at $\langle\Omega\rangle = f^{(d-2)/2} \neq 0$. In this vacuum, the original mass term is recovered since $\lambda = M^2/f^2$, and the physical dilaton φ is the fluctuation, $\Omega = f^{(d-2)/2} - \varphi$. The scale of f is unrelated to M , so

we choose $f \gg M$ to make the model perturbative, $\lambda \ll 1$.

We are interested in calculating the n -point dilaton amplitudes in a leading order (in λ) low-energy expansion and comparing the results with the matrix elements extracted from the dilaton effective action in Section 2.2. With $\Omega = f^{(d-2)/2} - \varphi$, the action (2.71) gives n -point interaction terms between Φ and φ for all n , unless $d = 3, 4, 6$ when there are a finite number of terms. At leading order in λ , the dilaton scattering amplitudes are given by the 1-loop diagrams with n -external dilatons φ and the massive scalar Φ running in the loop. The Feynman rule for the vertex with two Φ 's and k φ 's is

$$V_k = i(-1)^{k+1} \frac{M^2}{f^{k(d-2)/2}} \left(\prod_{n=0}^{k-1} \left(\frac{4}{d-2} - n \right) \right). \quad (2.75)$$

We refer the reader to appendix D for practical details of the 1-loop calculation.

The results of the 1-loop calculation of the n -point dilaton amplitudes for the free massive scalar can be compared to the general form of the amplitudes discussed in Section 2.2 and listed in appendix C. Since to $O(\partial^8)$ there are only few parameters, α , β , γ , and $\tilde{\gamma}$, in the dilaton effective action (2.49), this provides a very non-trivial check of the structure. We find perfect consistency for $d = 3, 4, 5, \dots, 10$. Specifically:

- At $O(p^4)$ and $O(p^6)$ we have checked the form of the action (2.49) for $d = 3, 4, \dots, 7$ (and also $d = 8, 9$ for $O(p^6)$) by matching the amplitudes with $n = 4, 5, 6, 7, 8$ external dilatons. To illustrate the non-triviality of the match, note that for $O(p^6)$ this requires matching the coefficients of a total of 8 independent momentum polynomials of (C.2) in terms of just a single free parameter, β .
- At $O(p^8)$, we have matched the $d = 3, 4, \dots, 10$ dilaton n -point amplitudes with $n = 4, 5, 6, 7$. This requires matching the coefficients of 11 independent Mandelstam polynomials in (C.3) using just two parameters γ and $\tilde{\gamma}$.¹³ For $d = 8$, we also matched the 8-point amplitude with its 5 independent momentum polynomials. And as noted in Sections 2.3-2.4, the 8d anomaly flow $\Delta a = \gamma/4$ for the free massive scalar was correctly reproduced by this calculation.

Thus the 1-loop calculation for the free massive scalar offers a highly non-trivial check of the dilaton effective action.

In Table 2.1, we summarize the results for the coefficients α , β , γ , and $\tilde{\gamma}$ in $d =$

¹³Note that the constrained 3d kinematics leave fewer independent Mandelstam polynomials than for $d > 3$.

Table 2.1: Results for the coefficients α , β , γ , and $\tilde{\gamma}$ of the effective action (2.49) for the case of the d -dimensional free massive scalar flow. The subscript \circ in the table indicates that a factor of $(4\pi)^{-[d/2]}$ was taken out, e.g. $\alpha = \alpha_\circ(4\pi)^{-[d/2]}$. The label “div” indicates that the 1-loop scalar integral diverges at and beyond this order. The boxed results are those encoding the $d = 4, 6, 8$ anomaly flows for the free massive scalar; see (2.76). Terms with negative mass-dimension are not needed for our study of RG flows, but we include them here to illustrate that the amplitudes match even in those higher-derivative cases

d	α_\circ	β_\circ	γ_\circ	$\tilde{\gamma}_\circ$
3	$\frac{1}{960 M}$	$-\frac{1}{43\,008 M^3}$	$-\frac{1}{92\,160 M^5}$	$\frac{1}{7\,680 M^5}$
4	$\frac{1}{180}$	$\frac{1}{7\,560 M^2}$	$-\frac{1}{85\,050 M^4}$	$\frac{11}{37\,800 M^4}$
5	$\frac{M}{480}$	$\frac{67}{967\,680 M}$	$\frac{1}{1\,935\,360 M^3}$	$\frac{1}{18\,432 M^3}$
6	$\frac{M^2}{90}$	$\frac{1}{3\,024}$	$\frac{1}{113\,400 M^2}$	$\frac{1}{7\,560 M^2}$
7	$\frac{M^3}{144}$	$\frac{61 M}{483\,840}$	$\frac{1}{272\,160 M}$	$\frac{13}{483\,840 M}$
8	div	$\frac{2 M^2}{2\,835}$	$\frac{23}{1\,360\,800}$	$\frac{11}{151\,200}$
9		$\frac{113 M^3}{241\,920}$	$\frac{47 M}{7\,257\,600}$	$\frac{41 M}{2\,419\,200}$
10		div	$\frac{151 M^2}{4\,082\,400}$	$\frac{M^2}{18\,144}$

3, 4, 5, ..., 10. Note that the boxed values in the table correspond to the anomaly flows

$$\begin{aligned}
\Delta a_{4d} &= \frac{1}{2} \alpha_\circ (4\pi)^{-2} = \frac{1}{360 (4\pi)^2}, \\
\Delta a_{6d} &= \frac{1}{3} \beta_\circ (4\pi)^{-3} = \frac{1}{9072 (4\pi)^3}, \\
\Delta a_{8d} &= \frac{1}{4} \gamma_\circ (4\pi)^{-4} = \frac{23}{5\,443\,200 (4\pi)^4}.
\end{aligned} \tag{2.76}$$

The successful match of the amplitudes for the free massive scalar and the simplicity of the dilaton effective action S in the form (2.49) encourages us to speculate about the higher-derivative terms in S . We outline some ideas and tests of this in the following section.

2.5.2 Higher-Order Effective Action?

In Section 2.2.5 we wrote the flat space dilaton effective action

$$S = \int d^d x \sqrt{-g} \left[\frac{(d-2)^2}{8} f^{d-2} \mathcal{W}_1 + \alpha \mathcal{W}_2 + \beta \mathcal{W}_3 + \gamma \mathcal{W}_4 + \tilde{\gamma} \frac{(d-4)^2}{4} e^{d\tau} (\mathcal{W}_2)^2 + \dots \right] \Big|_{g_{\mu\nu} = \eta_{\mu\nu}}, \tag{2.77}$$

with the ellipses standing for terms that vanish upon application on the equations of motion, plus terms with more than 8 derivatives. Recall that its definition in terms of the GJMS operators P_k in (2.46) makes the behavior of $\mathcal{W}_k \equiv \left(\frac{2}{d-2k}\right)^2 e^{-(d/2-k)\tau} P_k e^{-(d/2-k)\tau}$ under Weyl transformations particularly simple, $\mathcal{W}_k \xrightarrow{\text{Weyl}} e^{-d\sigma} \mathcal{W}_k$. This ensures Weyl-invariance of the action (2.77), except for $d = 2k$ where it produces the correct trace anomaly; the relation between the coefficients in (2.77) and the anomaly flow was given in (2.76).

The simplicity of (2.77) encourages a guess for the 10-derivative terms, namely

$$S^{\partial^{10}} = \int d^d x \sqrt{-g} \left[\delta \mathcal{W}_5 + \tilde{\delta} \frac{(d-4)(d-6)}{4} e^{d\tau} \mathcal{W}_2 \mathcal{W}_3 + \dots \right] \Big|_{g_{\mu\nu}=\eta_{\mu\nu}}. \quad (2.78)$$

The “...” denote terms that vanish on-shell.¹⁴ For $d = 3, 4, \dots, 10$, we have checked explicitly that the 4, 5, 6-point amplitudes produced by the action (2.78) are matched exactly by the $O(p^{10})$ dilaton amplitudes produced by the free massive scalar 1-loop computation. For each d , this requires the coefficient of 9 distinct Mandelstam polynomials to be matched using just two constants, δ and $\tilde{\delta}$, and it is therefore encouraging that this guess works. However, those two constants are not sufficient to match the 7-point amplitude; the guess in (2.78) is incomplete. Moreover, following the pattern of the lower-order terms, we would expect the anomaly flow in $d = 10$ to be encoded as $\Delta a = \frac{1}{5}\delta$. Instead, we find that $\frac{1}{5}\delta \neq \Delta a_{10d}$. Hence at least one other term is required in (2.78).

A further complication (or feature) arises for the 12-derivative terms. The GJMS construction suggests that we can write

$$S^{\partial^{12}} = \int d^d x \sqrt{-g} \left[\epsilon_1 \mathcal{W}_6 + \epsilon_2 \frac{(d-6)^2}{4} e^{d\tau} (\mathcal{W}_3)^2 + \epsilon_3 \frac{(d-4)(d-8)}{4} e^{d\tau} \mathcal{W}_2 \mathcal{W}_4 + \epsilon_4 \frac{(d-4)^3}{8} e^{2d\tau} (\mathcal{W}_2)^3 + \dots \right] \Big|_{g_{\mu\nu}=\eta_{\mu\nu}}. \quad (2.79)$$

However, this *cannot* be the full answer, because starting at $O(p^{12})$, the 4-point amplitude has two independent Mandelstam polynomials.¹⁵ For example in $d = 12$ we find for the free massive scalar flow:

$$\mathcal{A}_4^{(12)} = \frac{1}{2^5 3^3 5^7 7^2 11^1 13^1} \left(-7s^2 t^2 u^2 + 2250(s^6 + t^6 + u^6) \right). \quad (2.80)$$

The polynomial $s^6 + t^6 + u^6$ can be produced by the terms in (2.79), but $s^2 t^2 u^2$ cannot. This means that new structures appear in the effective action at 12-derivative order. This

¹⁴Note that terms with \mathcal{W}_1 vanish on-shell.

¹⁵This follows the same structure as the matrix elements of the candidate counterterm operators $D^{2k} R^4$ in supergravity; see for example Table 1 in [28].

may be evidence for the existence of a new class of curved-space GJMS-type operators whose “leading” components are not \square^k but are perhaps composed of various contractions of $G_{\mu\nu\rho} = (\nabla_\mu \nabla_\nu \nabla_\rho)$. For instance, a term in the action that also produces $s^2 t^2 u^2$ could be:

$$\varphi G_{\mu\nu\rho} \varphi G^{\mu\nu\rho} G^{\sigma\lambda\kappa} \varphi G_{\sigma\lambda\kappa} \varphi. \quad (2.81)$$

Such new operators may also enter the 10-derivative action and account for the mismatch of the 1-loop amplitudes predicted by extrapolating the GJMS-type action. It would be interesting to explore further the connections between RG flows, conformal geometry, functional determinants, and the a - and F -theorems.

Chapter 3

Dilaton Effective Action with $\mathcal{N} = 1$ Supersymmetry

3.1 Motivation and Preview

The dilaton-based proof [5, 6] of the four-dimensional a -theorem has provided new insights into the behavior of quantum field theories under renormalization group (RG) flows. The arguments in [5, 6, 25] exploit that the structure of the effective action for the dilaton — introduced as a conformal compensator or as the Goldstone boson for spontaneously broken conformal symmetry — is determined by symmetries up to and including four-derivative terms. This is used to extract the change in the Euler central charge $\Delta a = a_{\text{UV}} - a_{\text{IR}}$ in an RG flow between UV and IR CFTs. The form of the dilaton action shows that the low-energy expansion of the scattering process of four dilatons is proportional to Δa and a sum rule then allowed the authors of [5] to argue that $\Delta a > 0$, thus proving the a -theorem.

It is worth exploring if this argument can be affected by the presence of other massless modes in the low-energy theory, such as Goldstone bosons arising from the spontaneous breaking of other continuous global symmetries. This situation arises in $\mathcal{N} = 1$ supersymmetric theories, because the stress tensor is in the same supermultiplet as the R-current, so the Goldstone boson β for the broken $U(1)$ R-symmetry accompanies the dilaton τ . In the low-energy effective action, there are couplings between τ and β , even in the flat-space limit, so one may wonder if this affects the proof of the a -theorem.

Since the Goldstone boson β is a pseudo-scalar (an axion), we are quickly relieved of our worries: its presence cannot change the scattering of four scalars (the dilatons) through single-axion exchanges, which would be the only option in the low-energy effective action. But precisely how this works is less trivial, since the “naive” dilaton field τ is non-linearly

coupled to the axion β , and to identify the physical modes one must disentangle the fields via a field redefinition. The result of course still holds true: the axion does not spoil the proof of the four-dimensional a -theorem presented in [5].

In this chapter, we consider in detail the form of the bosonic terms in the $\mathcal{N} = 1$ supersymmetric extension of the four-dimensional dilaton effective action in order to fully illuminate the above questions and to clarify results in the previous work [26].¹ Our focus is four-dimensional $\mathcal{N} = 1$ superconformal theories in which the conformal symmetry is broken by a relevant operator that preserves the $\mathcal{N} = 1$ supersymmetry. We assume that the induced flow terminates in another $\mathcal{N} = 1$ superconformal theory in the deep IR. The fields τ and β form a complex scalar field which is the lowest component of a chiral Goldstone superfield $\Phi = (\tau + i\beta) + \dots$. We are interested in writing down the most general low-energy effective action for τ and β in a general rigid four-dimensional curved space with background metric $g_{\mu\nu}$ and background $U(1)$ R-symmetry gauge potential A_μ . Such an action has been studied previously by Schwimmer and Theisen using a superspace approach [26]. One of our goals is to derive the action in component form from basic symmetry principles and use this to clarify the structure of the result presented in [26].

The fundamental ideas we use to determine the effective action $S[\tau, \beta]$ are diffeomorphism invariance and the following three properties:

1. Weyl variation ($\delta_\sigma g_{\mu\nu} = 2\sigma g_{\mu\nu}$ and $\delta_\sigma \tau = \sigma$) produces the trace anomaly, i.e.

$$\delta_\sigma S = \int d^4x \sqrt{-g} \sigma \langle T_\mu{}^\mu \rangle. \quad (3.1)$$

The expectation value of the trace of the stress tensor, $\langle T_\mu{}^\mu \rangle$, is a functional of the background fields, namely the metric $g_{\mu\nu}$ and the $U(1)_R$ gauge field A_μ . It does not depend on τ or β . The full trace anomaly for an $\mathcal{N} = 1$ SCFT with central charges a and c is²

$$\langle T_\mu{}^\mu \rangle = cW^2 - aE_4 + b'\square R - 6c(F_{\mu\nu})^2. \quad (3.2)$$

The coefficient of $\square R$ is non-physical as it can be removed by adding a local counterterm in the UV theory. Thus it is not an anomaly and we drop it henceforth.

¹See also [72] for important early work on the subject as well as [73] for a discussion of the dilaton effective action in four-dimensional theories with $\mathcal{N} = 2$ supersymmetry.

²In Appendix E we discuss why no other terms involving the gauge field are allowed.

2. Gauge transformations ($\delta_\alpha A_\mu = \nabla_\mu \alpha$ and $\delta_\alpha \beta = \alpha$) generate the gauge anomaly:

$$\delta_\alpha S = \int d^4x \sqrt{-g} \alpha \left(2(5a - 3c) F_{\mu\nu} \tilde{F}^{\mu\nu} + (c - a) R_{\mu\nu\rho\sigma} \tilde{R}^{\mu\nu\rho\sigma} \right), \quad (3.3)$$

where the tilde denotes Hodge dualization with respect to the curved metric $g_{\mu\nu}$,

$$\tilde{R}_{\mu\nu\rho\sigma} \equiv \frac{1}{2} \epsilon_{\mu\nu\lambda\delta} R^{\lambda\delta}{}_{\rho\sigma}, \quad \tilde{F}_{\mu\nu} \equiv \frac{1}{2} \epsilon_{\mu\nu\rho\sigma} F^{\rho\sigma}. \quad (3.4)$$

The second line of (3.3) gives the gauge anomaly³ for the case of an $\mathcal{N} = 1$ superconformal theory; it was derived in [22] with slightly different normalization of a and c (see also [26, 74, 75]).

3. The low-energy effective action must be invariant under $\mathcal{N} = 1$ supersymmetry. In this chapter, we mostly ignore the fermionic degrees of freedom and focus entirely on the bosonic part of the action.

The first and second properties allow us to split the action into two parts $S = S_{\text{WZ}} + S_{\text{inv}}$ where Weyl and gauge variations of S_{WZ} produce the trace and gauge anomalies, respectively, while S_{inv} is gauge and Weyl invariant. The general form of S_{inv} is a linear combination of all possible gauge and Weyl invariant operators and the principles 1 and 2 above do not allow us to constrain the constant coefficients in this linear combination. However, the third property (supersymmetry) does fix certain relationships between the two parts of the action: some of the coefficients in S_{inv} are determined in terms of the central charges a and c . This still leaves the possible freedom of having gauge and Weyl invariant operators that are independently supersymmetric. We will show that no such operators contribute to the flat-space scattering process of four-particle dilaton and Goldstone modes at the four-derivative order. This means that such independently supersymmetric terms in the dilaton effective action (if they exist) cannot affect the proof of the a -theorem.

It is not easy to check whether a given four-derivative operator is supersymmetrizable. Thankfully the power of supersymmetry Ward identities allow us to test this question indirectly and to the extent we need it. As we show in Section 3.2, the supersymmetry Ward identities require that the scattering process of four dilatons is identical to the scattering process of the four associated R-symmetry Goldstone modes. This means that if an operator contributes only to one of these processes, it cannot possibly be supersymmetrizable on its own. We use this to exclude contributions from Weyl and gauge invariant operators that

³This is the 't Hooft anomaly for the global $U(1)_R$ symmetry present in any $\mathcal{N} = 1$ SCFT. With slight abuse of notation we will refer to it as the gauge anomaly.

could otherwise affect the proof of the a -theorem in four-dimensional $\mathcal{N} = 1$ supersymmetric theories.⁴

Our work suggests several natural avenues for further exploration. First it will be interesting to analyze the effective actions for conformal field theories (not necessarily supersymmetric) with larger continuous global symmetry groups. For superconformal theories with $\mathcal{N} = 1$ supersymmetry and more than one Abelian global symmetry one may hope that such an effective action will offer a new perspective on the principle of a -maximization [74]. It will also be of great interest to construct the dilation effective action for four-dimensional SCFTs with extended supersymmetry, in particular for $\mathcal{N} = 4$ SYM. In this context, one may be able to establish a more precise connection between the dilation effective action and the Dirac-Born-Infeld action for SCFTs with holographic duals. Finally, one can also study the supersymmetric dilation effective action for SCFTs in two and six dimensions.⁵ The methods of this chapter should extend readily to two-dimensional SCFTs with $(0, 2)$ or $(2, 2)$ supersymmetry since these theories have Abelian R-symmetry. The extension to six-dimensional $(1, 0)$ or $(2, 0)$ SCFTs may prove more subtle, although in the latter case holography should provide useful insights.

Before delving into the construction of the dilaton effective action, we start by deriving supersymmetry Ward identities for on-shell scattering amplitudes in Section 3.2. In Section 3.3 we derive the most general form of the dilaton effective action for $\mathcal{N} = 1$ SCFTs up to four-derivative terms. We compare this action to the results of Schwimmer-Theisen in Section 3.4 to clarify the structure of their superspace-based result. In Section 3.5, we show that the Ward identities from Section 3.2 confirm the supersymmetry of our result for the action in the flat-space limit. The resulting dilaton-axion effective action gives an explicit verification that the dilaton-based proof is not affected by β . Furthermore, we show that supersymmetry is actually not needed to reach this conclusion: the Goldstone mode of any broken global $U(1)$ symmetry cannot spoil the proof of the a -theorem. Finally, we note that supersymmetry requires that the $2 \rightarrow 2$ axion scattering amplitude must equal the $2 \rightarrow 2$ dilaton amplitude, and this allows for a proof of the a -theorem based on the axion scattering for $\mathcal{N} = 1$ SCFTs. In Appendix E, we present a way to derive the conformal anomaly for four-dimensional CFTs from basic principles.

⁴Very similar arguments were developed in [28] to test supersymmetrization of candidate counterterms in $\mathcal{N} = 8$ supergravity.

⁵There are no SCFTs in dimension greater than six and there are no conformal anomalies in odd dimensions. thus dimensions two, four and six exhaust all cases of interest.

3.2 Scattering Constraints from Supersymmetry

Scattering amplitudes in supersymmetric theories obey supersymmetry Ward identities [76, 77]. We consider here an $\mathcal{N} = 1$ chiral model with a complex scalar ζ and its fermionic superpartner λ . In Section 3.5, the chiral scalar will be related to the dilaton and $U(1)$ Goldstone modes. As a result of the supersymmetry transformations of the free fields, it can be shown [34] that the supersymmetry generators Q and Q^\dagger act on the states as⁶

$$\begin{aligned} [Q, \zeta] &= [p| \lambda, & [Q^\dagger, \lambda] &= |p\rangle \zeta, \\ [Q, \lambda] &= 0, & [Q^\dagger, \zeta] &= 0, \\ [Q, \bar{\zeta}] &= 0, & [Q^\dagger, \bar{\lambda}] &= 0, \\ [Q, \bar{\lambda}] &= [p| \bar{\zeta}, & [Q^\dagger, \bar{\zeta}] &= |p\rangle \bar{\lambda}, \end{aligned} \tag{3.5}$$

where the (anti)commutators are graded Lie brackets. The two-component spinors $|p\rangle$ and $[p|$ represent components of the particle momentum in the spinor-helicity formalism.⁷ More precisely, the on-shell four-momentum p_μ for a massless particle can be written in terms of a pair of two-component spinors $|p\rangle^{\dot{a}}$ and $[p|^b$ as

$$p_\mu (\bar{\sigma}^\mu)^{\dot{a}b} = -|p\rangle^{\dot{a}} [p|^b, \quad \text{and} \quad p_\mu (\sigma^\mu)_{ab} = -[p]_a \langle p|_b. \tag{3.6}$$

For two light-like four-vectors, p^μ and q^μ , angle- and square-brackets are defined as

$$[pq] = [p|^a |q]_a, \quad \text{and} \quad \langle pq \rangle = \langle p|_{\dot{a}} |q\rangle^{\dot{a}}. \tag{3.7}$$

These brackets are antisymmetric, $[pq] = -[qp]$ and $\langle pq \rangle = -\langle qp \rangle$, because spinor indices are raised and lowered with the two-dimensional Levi-Civita symbol.

Now assuming the vacuum is supersymmetric, i.e. $Q|\mathbf{0}\rangle = Q^\dagger|\mathbf{0}\rangle = 0$, we can derive supersymmetry Ward identities for the amplitudes. For example (treating λ and ζ as creation operators),⁸

$$0 = \langle \mathbf{0} | [Q^\dagger, \lambda \zeta \zeta \zeta] | \mathbf{0} \rangle = \langle \mathbf{0} | [Q^\dagger, \lambda] \zeta \zeta \zeta | \mathbf{0} \rangle = |p_1\rangle \langle \mathbf{0} | \zeta \zeta \zeta \zeta | \mathbf{0} \rangle, \tag{3.8}$$

where we have used that Q^\dagger annihilates ζ . The free-field commutators (3.5) can be used here

⁶We are abusing notation by using the same symbols to represent the fields and their corresponding creation and annihilation operators. Hopefully it is clear enough from context what we mean.

⁷See the reviews [34, 36] for more details about the spinor-helicity formalism and supersymmetry Ward identities.

⁸We are not including explicit momentum labels, but assume that the first state in the list has momentum p_1^μ , the next p_2^μ etc.

because the supercharges are acting on the asymptotic states. This is simply the statement that at any loop-order, the on-shell four-scalar amplitude $\mathcal{A}_4(\zeta\zeta\zeta\zeta)$ must vanish (where now we mean the particles created by the field ζ). Similarly, $\mathcal{A}_4(\bar{\zeta}\bar{\zeta}\bar{\zeta}\bar{\zeta}) = 0$.

The four-scalar amplitudes with three ζ and one $\bar{\zeta}$ also vanish. To see this, we write

$$0 = \langle \mathbf{0} | [Q^\dagger, \bar{\zeta} \lambda \zeta \zeta] | \mathbf{0} \rangle = |p_1\rangle \langle \mathbf{0} | \bar{\lambda} \lambda \zeta \zeta | \mathbf{0} \rangle + |p_2\rangle \langle \mathbf{0} | \bar{\zeta} \zeta \zeta \zeta | \mathbf{0} \rangle. \quad (3.9)$$

Now dot in $\langle p_1 |$ and use the antisymmetry of the angle bracket to eliminate the first term on the right hand side in (3.9). For generic momenta, this leads to the statement that $\mathcal{A}_4(\bar{\zeta}\zeta\zeta\zeta) = 0$.

A similar story applies to scalar amplitudes with three $\bar{\zeta}$'s. Altogether, supersymmetry requires the following amplitudes to vanish:

$$\begin{aligned} \mathcal{A}_4(\zeta\zeta\zeta\zeta) &= \mathcal{A}_4(\bar{\zeta}\bar{\zeta}\bar{\zeta}\bar{\zeta}) = 0, \\ \mathcal{A}_4(\bar{\zeta}\zeta\zeta\zeta) &= \mathcal{A}_4(\zeta\bar{\zeta}\bar{\zeta}\bar{\zeta}) = \dots = \mathcal{A}_4(\bar{\zeta}\bar{\zeta}\bar{\zeta}\zeta) = 0. \end{aligned} \quad (3.10)$$

The second line includes all four-point amplitudes with an odd number of ζ 's. Amplitudes with two ζ 's and two $\bar{\zeta}$'s, such as $\mathcal{A}_4(\bar{\zeta}\bar{\zeta}\zeta\zeta)$, are permitted to be non-vanishing by supersymmetry. The reader may be puzzled: surely a supersymmetric Lagrangian can have interactions terms of the form $\zeta^4 + \bar{\zeta}^4$, so how can that be compatible with our claim above that for massless scalars $\mathcal{A}_4(\zeta\zeta\zeta\zeta) = 0$? To see this in an example, consider an $\mathcal{N} = 1$ theory with a canonical kinetic term $\Phi^\dagger\Phi$ and a superpotential $W = f\Phi + \frac{1}{5}\Phi^5$. The scalar potential $V = |dW/d\zeta|^2 = |f|^2 + f\zeta^4 + \bar{f}\bar{\zeta}^4 + \zeta^4\bar{\zeta}^4$ has exactly the four-scalar interaction terms that our supersymmetry Ward identity argument appears to be incompatible with. However, the origin $\zeta = \bar{\zeta} = 0$ is obviously not a supersymmetric vacuum, so the Ward identity — which used $Q^\dagger|\mathbf{0}\rangle = 0$ — is not valid. If we expand around another vacuum, we generate mass-terms and we are only interested in the case of massless particles. This resolves the puzzle.

Now suppose we decompose the complex scalar field ζ into its real and imaginary parts, $\zeta = \varphi + i\xi$ and denote the corresponding scalar, φ , and pseudo-scalar, ξ , states by the same symbols. Expanding the supersymmetry constraints (3.10) then leads to the following

non-trivial constraints on the amplitudes:⁹

$$\mathcal{A}_4(\varphi\varphi\varphi\varphi) = \mathcal{A}_4(\xi\xi\xi\xi), \quad (3.11)$$

$$\mathcal{A}_4(\varphi\varphi\varphi\varphi) = \mathcal{A}_4(\varphi\varphi\xi\xi) + \mathcal{A}_4(\varphi\xi\varphi\xi) + \mathcal{A}_4(\varphi\xi\xi\varphi). \quad (3.12)$$

These linear relations between amplitudes will be very valuable in the analysis of the $\mathcal{N} = 1$ low-energy effective action for the dilaton. In this context, φ will be associated with the physical dilaton and ξ with the R-symmetry Goldstone mode. Thus, without knowing any details of the form of the $\mathcal{N} = 1$ supersymmetric dilaton effective action, we have already learned from the first identity (3.11) that the four-dilaton amplitude must be equal to the four-axion amplitude. The second identity (3.12) is important for testing that the explicit action we derive in Section 3.5 is supersymmetric.

The identities in (3.11)–(3.12) can also be used to test if a given candidate Weyl and gauge invariant operator is compatible with supersymmetry. If the on-shell four-point amplitudes resulting from the operator do not satisfy (3.11)–(3.12), then the operator cannot be supersymmetrized. On the other hand, if the resulting amplitudes are compatible with (3.11)–(3.12), then the operator has a supersymmetric extension at the level of four fields (though not necessarily beyond that order).

3.3 Dilaton Effective Action

We turn now to the construction of an $\mathcal{N} = 1$ supersymmetric effective action for the dilaton and axion fields τ and β in the presence of a curved background metric $g_{\mu\nu}$ and background gauge field A_μ . As noted in the Introduction, the dilaton effective action can be split into two parts

$$S = S_{\text{WZ}} + S_{\text{inv}}, \quad (3.13)$$

depending on whether gauge and Weyl transformations act non-trivially.

3.3.1 Wess-Zumino Action

The Wess-Zumino part of the action is defined such that its gauge variation produces the anomaly for the $U(1)_R$ symmetry and its Weyl variation results in the conformal anomaly. It

⁹The Ward identities also imply certain relationships between the four-point amplitudes containing only one φ or one ξ , e.g. $\mathcal{A}_4(\varphi\varphi\varphi\xi) = -\mathcal{A}_4(\xi\xi\xi\varphi)$. These relations are independent from those in (3.11)–(3.12). However, they are trivially satisfied for our application because any amplitude with an odd number of pseudo-scalars ξ vanishes in a parity-invariant theory.

can be obtained either by iteratively applying transformations and adding terms to cancel extra variations, or by integrating the anomalies directly [78]. The result is the four-dimensional Wess-Zumino action for the dilaton and axion:

$$\begin{aligned}
S_{\text{WZ}} = \int d^4x \sqrt{-g} & \left[\Delta c \tau W^2 - \Delta a \tau E_4 - 6 \Delta c \tau F^2 \right. \\
& + \beta \left(2(5 \Delta a - 3 \Delta c) F \tilde{F} + (\Delta c - \Delta a) R \tilde{R} \right) \\
& \left. - \Delta a \left(4 \left(R^{\mu\nu} - \frac{1}{2} R g^{\mu\nu} \right) \nabla_\mu \tau \nabla_\nu \tau - 2 (\nabla \tau)^2 \left(2 \square \tau - (\nabla \tau)^2 \right) \right) \right].
\end{aligned} \tag{3.14}$$

Here $F = dA$ is the flux for the background $U(1)_R$ gauge field. Under a Weyl transformation, the variation of τ on the first line produces the conformal anomaly, while the Weyl tensor and field strength are inert. However, E_4 is not inert, but the Weyl variation of the third line cancels the contributions from $\tau \delta_\sigma(\sqrt{-g}E_4)$. The second line is Weyl invariant. Gauge transformations shift $\beta \rightarrow \beta + \alpha$, hence the second line in (3.14) produces the $U(1)_R$ anomaly. When the flux and the axion vanish, one recovers the WZ action for the dilaton [5, 6, 26]. The coefficients $\Delta a = a_{\text{UV}} - a_{\text{IR}}$ and $\Delta c = c_{\text{UV}} - c_{\text{IR}}$ are the difference between the corresponding central charges of the UV and IR SCFTs, as required by the anomaly matching conditions [5, 26].

3.3.2 Gauge and Weyl invariants

Since S_{WZ} is determined by its variation, it is only specified up to terms whose gauge and Weyl variations vanish. We define S_{inv} to be the sum of all independent gauge and Weyl invariant combinations of τ , β , $g_{\mu\nu}$, and A_μ . To facilitate the analysis, we define a Weyl invariant metric $\hat{g}_{\mu\nu} = e^{-2\tau} g_{\mu\nu}$, so that any curvature terms computed in terms of $\hat{g}_{\mu\nu}$ will be invariant. This procedure appeared in the analysis in [5] (see also [49, 55, 79] for analogues in higher dimensions) where there were three possible four-derivative Weyl invariants with independent coefficients: $\sqrt{-\hat{g}} \hat{W}^2$, $\sqrt{-\hat{g}} \hat{R}^2$, and $\sqrt{-\hat{g}} \hat{E}_4$. (The Euler density \hat{E}_4 is total derivative in four dimensions so it can be dropped.) In the present context, there are additional fields that can be used to construct invariants. Specifically, the combination $(A - \nabla \beta)_\mu$ is both gauge and Weyl invariant. This combination also suggests that we should treat A_μ on the same footing as a derivative in the low-energy effective action. With these building blocks we find the most general Ansatz for S_{inv} including terms with at most four

derivatives:

$$S_{\text{inv}} = \int d^4x \sqrt{-\hat{g}} \left[-\frac{f^2}{2} \left(\frac{\hat{R}}{6} + \hat{g}^{\mu\nu} (A - \nabla\beta)_\mu (A - \nabla\beta)_\nu \right) + \sum_{i=1}^9 \gamma_i W_i + \mathcal{O}(\nabla^6) \right], \quad (3.15)$$

where we have dropped total derivatives such as $\sqrt{-\hat{g}}\hat{E}_4$. The hatted two-derivative gauge-Weyl invariants produce the kinetic terms for the scalars when expanded in terms of the unhatted metric and the dilaton. The real constants $\gamma_1, \dots, \gamma_9$ are arbitrary coefficients of the independent four-derivative gauge and Weyl invariant terms, $\sqrt{-\hat{g}}W_i$, defined by

$$\begin{aligned} W_1 &\equiv \hat{W}^2, & W_2 &\equiv \hat{R}^2, \\ W_3 &\equiv (A - \nabla\beta)_\mu \hat{\nabla}^\mu \hat{R}, & W_4 &\equiv \left(\hat{\nabla}^\mu (A - \nabla\beta)_\mu \right)^2, \\ W_5 &\equiv \hat{g}^{\mu\nu} (A - \nabla\beta)_\mu \hat{\square} (A - \nabla\beta)_\nu, & W_6 &\equiv \hat{R}^{\mu\nu} (A - \nabla\beta)_\mu (A - \nabla\beta)_\nu, \\ W_7 &\equiv \hat{R} \hat{g}^{\mu\nu} (A - \nabla\beta)_\mu (A - \nabla\beta)_\nu, & W_8 &\equiv \left(\hat{g}^{\mu\nu} (A - \nabla\beta)_\mu (A - \nabla\beta)_\nu \right)^2, \\ W_9 &\equiv \hat{g}^{\mu\nu} (A - \nabla\beta)_\mu (A - \nabla\beta)_\nu \hat{\nabla}^\lambda (A - \nabla\beta)_\lambda. \end{aligned} \quad (3.16)$$

All other invariants can be written as linear combination of the W_i and total derivatives, e.g. the Bianchi identity implies $\hat{R}^{\mu\nu} \hat{\nabla}_\mu (A - \nabla\beta)_\nu = \hat{\nabla}_\mu \left(\hat{R}^{\mu\nu} (A - \nabla\beta)_\nu \right) - \frac{1}{2}W_3$.

This is the most general possible action written in terms of natural gauge and Weyl invariant objects constructed from the basic fields. So far, we have not imposed any supersymmetry on the Weyl+gauge invariant action S_{inv} . As we will see in the following sections, the constraints implied by $\mathcal{N} = 1$ supersymmetry and the consequences for the a -theorem are easily expressed and understood in terms of the W_i and their coefficients.

3.4 Matching to Superspace Calculation

The bosonic terms in the $\mathcal{N} = 1$ supersymmetric version of the Wess-Zumino action were derived earlier by Schwimmer and Theisen [26]. They started with the Weyl anomaly in superspace and integrated it directly using the Wess-Zumino method [78]. This gives a superspace form of the Wess-Zumino action which was then expanded in component fields; the result is given in equation (3.23) of [26]. In that expression, it is easy to pick out the terms that match S_{WZ} in (3.14). The two-derivative terms in (3.15) are also easily recognized. However, it is not *a priori* clear how to interpret the rest of the 4-derivative terms in (3.23) of [26]. Indeed, at first sight it may seem almost miraculous that these additional terms would not contribute to the anomaly under a gauge/Weyl transformation.

The correct interpretation of the rest of the terms in (3.23) of [26] is that they are a combination of gauge and Weyl invariants required for the supersymmetric completion of S_{WZ} in (3.14). Thus, the extra terms in (3.23) of [26] are a particular linear combination of the operators W_i from (3.16): there is a unique choice of γ_i in S_{inv} (3.15) such that our action $S = S_{\text{WZ}} + S_{\text{inv}}$ agrees with (3.23) in [26].¹⁰ This choice is to set

$$\gamma_6 = -6\gamma_7 = 2\gamma_8 = -4\Delta a \quad (3.17)$$

and drop the other W_i 's. This yields the following action:

$$\begin{aligned} S_0 = \int d^4x \left\{ -f^2 \sqrt{-\hat{g}} \left[\frac{1}{12} \hat{R} + \frac{1}{2} \left(\hat{g}^{\mu\nu} (A - \nabla\beta)_\mu (A - \nabla\beta)_\nu \right) \right] \right. \\ + \sqrt{-g} \left[\Delta c \tau W^2 - \Delta a \tau E_4 - 6 \Delta c \tau F^2 \right. \\ + \beta \left(2(5\Delta a - 3\Delta c) F \tilde{F} + (\Delta c - \Delta a) R \tilde{R} \right) \\ - \Delta a \left(4 \left(R^{\mu\nu} - \frac{1}{2} R g^{\mu\nu} \right) \nabla_\mu \tau \nabla_\nu \tau - 2 (\nabla\tau)^2 \left(2 \square\tau - (\nabla\tau)^2 \right) \right) \left. \right] \\ - 4 \Delta a \sqrt{-\hat{g}} \left[\left(\hat{R}^{\mu\nu} - \frac{1}{6} \hat{R} \hat{g}^{\mu\nu} \right) (A - \nabla\beta)_\mu (A - \nabla\beta)_\nu \right. \\ \left. + \frac{1}{2} \left(\hat{g}^{\mu\nu} (A - \nabla\beta)_\mu (A - \nabla\beta)_\nu \right)^2 \right] + \mathcal{O}(\nabla^6) \left. \right\}. \end{aligned} \quad (3.18)$$

The first line contains the kinetic terms. The second through fourth lines are the WZ action, (3.14), whose Weyl and gauge variations respectively produce the conformal and $U(1)_R$ anomaly. The last two lines are gauge and Weyl invariant and can be viewed as the supersymmetric completion of the Wess-Zumino action.

Although the other γ_i and W_i do not appear in (3.18), this should not be interpreted as setting them equal to zero. Rather, the remaining γ_i do not contribute to (3.18) because the superspace calculation in [26] derived only the terms related to the anomaly in a general $\mathcal{N} = 1$ theory. At present, the rest of the γ_i are not fixed. We will see later that the supersymmetry Ward identities imply additional constraints.

¹⁰Our sign conventions differ from those of [26]. We use the curvature convention $[\nabla_\mu, \nabla_\nu] V^\rho = R_{\mu\nu}{}^\rho{}_\sigma V^\sigma$. All equations shown here can be translated into the conventions of [26] by flipping the signs of the curvature tensors. We use a different normalization for f and A_μ , namely $f_{\text{here}}^2 = 2f_{\text{ST}}^2$ and $A_{\text{here}} = \frac{2}{3}A_{\text{ST}}$. Also, our result (3.19) fixes minor typos in [26].

One can now expand (3.18) to facilitate comparison with equation (3.23) in [26]:

$$\begin{aligned}
S_0 = & -f^2 \int d^4x \sqrt{-g} e^{-2\tau} \left(\frac{1}{2} (\nabla\tau)^2 + \frac{1}{12} R + \frac{1}{2} (\nabla\beta - A)^2 \right) \\
& + \int d^4x \sqrt{-g} \left[\Delta c \tau W^2 - \Delta a \tau E_4 - 6 \Delta c \tau (F_{\mu\nu})^2 \right. \\
& \quad \left. + \beta \left(2(5\Delta a - 3\Delta c) F^{\mu\nu} \tilde{F}_{\mu\nu} + (\Delta c - \Delta a) R^{\mu\nu\rho\sigma} \tilde{R}_{\mu\nu\rho\sigma} \right) \right] \\
& + 8\Delta a \int d^4x \sqrt{-g} \left(\left[R^{\mu\nu} A_\nu - \frac{1}{6} R A^\mu + A^2 A^\mu \right] \nabla_\mu \beta - A^\mu A^\nu \nabla_\mu \nabla_\nu \tau \right) \\
& + 2\Delta a \int d^4x \sqrt{-g} \left\{ \left[(R + 2A^2) g^{\mu\nu} - 2(R^{\mu\nu} + 2A^\mu A^\nu) \right] \nabla_\mu \tau \nabla_\nu \tau \right. \\
& \quad \left. + \left[\left(\frac{1}{3} R - 2A^2 \right) g^{\mu\nu} - 2(R^{\mu\nu} + 2A^\mu A^\nu) \right] \nabla_\mu \beta \nabla_\nu \beta + 8 A^\nu \nabla^\mu \beta \nabla_\nu \nabla_\mu \tau \right\} + \dots .
\end{aligned} \tag{3.19}$$

Here the dots denote terms with either no β 's and τ 's, or more than two of them. Higher-derivative terms are also suppressed.

The comparison between our dilaton effective action and the result in [26] uniquely selects the three gauge-Weyl invariants W_6 , W_7 , and W_8 and fixes their coefficients as in (3.17). If there are any other gauge-Weyl invariants in the low-energy dilaton-axion effective action, then their linear combination must be independently supersymmetrizable. We analyze this in the next section.

3.5 Dilaton and Axion Scattering in Flat Space

For the purposes of testing supersymmetry and investigating the a -theorem, we now take the theory on a flat background with vanishing gauge field. Then τ and β will be the only fields involved. For the moment, we continue to ignore the other W_i that did not contribute to (3.18). We will explain later why this is justified. The action (3.18) encodes the familiar dilaton interactions, as well as new couplings to the axion β . These new interactions are present even in the flat-space limit with no background gauge field. Up to total derivatives, we find

$$\begin{aligned}
S_0 = \int d^4x \left\{ -\frac{f^2}{2} e^{-2\tau} \left[(\partial\tau)^2 + (\partial\beta)^2 \right] + 2\Delta a \left[2\Box\tau \left((\partial\tau)^2 - (\partial\beta)^2 \right) + 4\Box\beta (\partial\tau \cdot \partial\beta) \right. \right. \\
\quad \left. \left. - 4(\partial\tau \cdot \partial\beta)^2 - \left((\partial\tau)^2 - (\partial\beta)^2 \right)^2 \right] + \mathcal{O}(\partial^6) \right\} .
\end{aligned} \tag{3.20}$$

The fields τ and β are coupled already at the two-derivative level through $e^{-2\tau}(\partial\beta)^2$, so the equations of motion mix τ and β :

$$\square\tau = (\partial\tau)^2 - (\partial\beta)^2, \quad \text{and} \quad \square\beta = 2(\partial\tau \cdot \partial\beta). \quad (3.21)$$

3.5.1 Field Redefinition

To facilitate the calculation of scattering amplitudes, we make a field redefinition to decouple the kinetic terms. This is easiest when we identify the complex scalar field Z that produces the kinetic terms

$$Z \equiv e^{-(\tau+i\beta)} \Rightarrow |\partial Z|^2 = e^{-2\tau} \left((\partial\tau)^2 + (\partial\beta)^2 \right). \quad (3.22)$$

The action (3.20) can be rewritten in terms of Z and its complex conjugate \bar{Z} and takes a very simple form

$$S_0 = \int d^4x \left\{ -\frac{f^2}{2} |\partial Z|^2 + 2\Delta a \left[-\left(\frac{\partial Z}{Z}\right)^2 \frac{\square\bar{Z}}{\bar{Z}} - \left(\frac{\partial\bar{Z}}{\bar{Z}}\right)^2 \frac{\square Z}{Z} + \left|\frac{\partial Z}{Z}\right|^4 \right] + \mathcal{O}(\partial^6) \right\}. \quad (3.23)$$

Note that when the Goldstone mode β vanishes we have a real scalar $Z \rightarrow e^{-\tau} \equiv \Omega$ and the action (3.23) reduces to the familiar form for the dilaton effective action in the flat space limit (see, for example, equation (2.8) in [25]).

The field Z is the compensator we introduce to restore the broken symmetries. We can expand about its constant vev¹¹ f with the fluctuating field ζ ,

$$Z = 1 - \frac{\zeta}{f}, \quad \zeta = \varphi + i\xi, \quad (3.24)$$

where φ and ξ are real scalar fields. Plugging this into the action (3.23) and expanding up

¹¹Note that one can always choose the vev of Z to be real using the global $U(1)$ symmetry in the action (3.23).

to fourth order in the fields, we find

$$\begin{aligned}
S_0 \rightarrow \int d^4x \left\{ -\frac{1}{2} \left((\partial\varphi)^2 + (\partial\xi)^2 \right) + \frac{4\Delta a}{f^3} \left(\square\varphi \left((\partial\varphi)^2 - (\partial\xi)^2 \right) + 2\square\xi (\partial\varphi \cdot \partial\xi) \right) \right. \\
+ \frac{2\Delta a}{f^4} \left[2\square\varphi \left(3\varphi \left((\partial\varphi)^2 - (\partial\xi)^2 \right) - 2\xi (\partial\varphi \cdot \partial\xi) \right) \right. \\
+ 2\square\xi \left(\xi \left((\partial\varphi)^2 - (\partial\xi)^2 \right) + 6\varphi (\partial\varphi \cdot \partial\xi) \right) \left. \right] \\
+ \left. \left((\partial\varphi)^2 - (\partial\xi)^2 \right)^2 + 4(\partial\varphi \cdot \partial\xi)^2 \right] + \mathcal{O}(\partial^6) \left. \right\}.
\end{aligned} \tag{3.25}$$

This parameterization decouples the equations of motion into those of free massless scalars

$$\square\varphi = 0, \quad \square\xi = 0. \tag{3.26}$$

Treating this as an effective action with a derivative expansion, we only include the two-derivative quadratic terms in the equations of motion. All other terms in the action involve three or more fields and give rise to interaction terms in the quantized theory. In (3.25), all such interactions involve at least four derivatives, so the amplitudes have no local contributions from pole diagrams until at least $\mathcal{O}(p^6)$.

3.5.2 Amplitudes

We are interested in the four-point amplitudes. From the action (3.25), we see that the low-energy expansion starts at $\mathcal{O}(p^4)$. The equations of motion (3.26) make it easy to read off the amplitudes from the contact terms in the last line of (3.25), which yield at $\mathcal{O}(p^4)$:

$$\begin{aligned}
\mathcal{A}_4(\varphi\varphi\varphi\varphi) &= \frac{4\Delta a}{f^4}(s^2 + t^2 + u^2), \\
\mathcal{A}_4(\xi\xi\xi\xi) &= \frac{4\Delta a}{f^4}(s^2 + t^2 + u^2), \\
\mathcal{A}_4(\varphi\varphi\xi\xi) &= \frac{4\Delta a}{f^4}(-s^2 + t^2 + u^2), \\
\mathcal{A}_4(\varphi\xi\varphi\xi) &= \frac{4\Delta a}{f^4}(s^2 - t^2 + u^2), \\
\mathcal{A}_4(\varphi\xi\xi\varphi) &= \frac{4\Delta a}{f^4}(s^2 + t^2 - u^2).
\end{aligned} \tag{3.27}$$

We can now use these results to check if the action (3.23) is compatible with supersymmetry. Combining the corresponding results from (3.27), we see that indeed the constraints (3.11)–

(3.12) from the supersymmetry Ward identities are obeyed.

All three Weyl invariants, $W_{6,7,8}$, contributed to the amplitudes (3.27) in a non-trivial way that ensures that the supersymmetry Ward identities are satisfied. Hence, this tests the supersymmetry of (3.18). The combination of Weyl invariants W_i in (3.18)-(3.19) was fixed via comparison with the superspace form given by Schwimmer and Theisen [26]. The match was obtained by comparing the last three lines of (3.19) with the corresponding expressions in [26]. Note that all the terms used explicitly in the match vanish in the flat-space limit with the background gauge potential turned off. However, as we have seen, $W_{6,7,8}$ also have flat-space contributions, so supersymmetry could also be tested via the Ward identities. Thus, in that limit, we have tested that our completion of the Schwimmer-Theisen terms does obey the supersymmetry constraints.

3.5.3 Supersymmetry and the Other Weyl Invariants

So far we have considered only the part of the action that matched the superspace derivation of the Wess-Zumino action, fixing the values of γ_6 , γ_7 , and γ_8 . The full dilaton effective action may have contributions from the other invariants W_i as well. This is important because their flat-space limits could include additional dilaton and axion scattering beyond what we have considered so far, with potentially dangerous consequences for the a -theorem.

With that in mind, let us return to the list of gauge-Weyl invariants (3.16) and evaluate them in the flat background. Applying the equations of motion (3.26), we find:

$$\begin{aligned}
W_1 &\rightarrow 0, & W_2 &\rightarrow \frac{36}{f^4}(\partial\xi)^4, \\
W_3 &\rightarrow 0, & W_4 &\rightarrow 0, \\
W_5 &\rightarrow -\frac{2}{f^4}\left((\partial\xi)^4 + (\partial\varphi \cdot \partial\xi)^2\right), & \mathbf{W}_6 &\rightarrow -\frac{2}{f^4}\left((\partial\xi)^4 + (\partial\varphi \cdot \partial\xi)^2\right), \\
\mathbf{W}_7 &\rightarrow -\frac{6}{f^4}(\partial\xi)^4, & \mathbf{W}_8 &\rightarrow \frac{1}{f^4}(\partial\xi)^4, \\
W_9 &\rightarrow 0, & &
\end{aligned} \tag{3.28}$$

where the three expressions in boldface are those already included in (3.18).

The first key feature to notice is that none of the invariants contain a $(\partial\varphi)^4$ interaction. Hence the four-scalar amplitude, $\mathcal{A}_4(\varphi\varphi\varphi\varphi)$ in (3.27), receives contributions only from the dilaton part of the Wess-Zumino action. It is completely blind to the presence of the axion. Thus it is not surprising that the resulting amplitude in (3.27) matches exactly the one found in [5]. Moreover, this implies that the proof of the a -theorem using the four-dilaton amplitude is unaffected by the presence of the axion.

The second key feature is that any gauge+Weyl+supersymmetry invariant four-derivative term has to be a linear combination of the W_i 's, say $\mathcal{W} = \sum_{i=1}^9 b_i W_i$. Since (3.28) tells us that

the four-dilaton amplitude has zero contribution from \mathcal{W} , the supersymmetry Ward identity (3.12) requires $b_5 + b_6 = 0$, and consequently (3.11) enforces $b_2 - 6b_7 + 36b_8 = 0$. There are no constraints on the other b_i 's from four-particle supersymmetry Ward identities. In conclusion, any gauge+Weyl+supersymmetry invariant four-derivative operator (if it exists) does not contribute at all to the four-particle scattering processes, so from that point of view we can completely neglect it.

Using general principles, we have shown that — up to four-derivative terms — the dilaton-axion effective action for $\mathcal{N} = 1$ SCFTs takes the form $S = S_{\text{WZ}} + S_{\text{inv}}$, with S_{WZ} and S_{inv} given by (3.14) and (3.15) respectively. The results of [26] fix the coefficients γ_i as in (3.17) to complete the Wess-Zumino action to an $\mathcal{N} = 1$ supersymmetric form. The supersymmetry Ward identities can be applied in the flat-space limit to see that no supersymmetric linear combination of the W_i 's contribute to any four-particle process. However, we cannot eliminate the possibility of such supersymmetric combinations; we can only say that in the flat-space limit their four-field terms must be proportional to total derivatives and the EOM. It would be curious to know if such fully supersymmetric operators do exist, although we have established that for the proof of the a -theorem in four dimensions they do not matter.

We have demonstrated that the four-point axion scattering amplitude is given by the second line in (3.27). One can now use the same positivity arguments as in [5, 6] to show that for $\mathcal{N} = 1$ SCFTs $\Delta a = a_{\text{UV}} - a_{\text{IR}} > 0$. This can be regarded as an alternative route to the a -theorem for four-dimensional SCFTs with $\mathcal{N} = 1$ supersymmetry.

3.5.4 No Supersymmetry

Suppose we do not assume $\mathcal{N} = 1$ supersymmetry. Then the coefficients in the gauge anomaly (3.3) are no longer fixed in terms of the trace anomalies a and c . This affects only the second line of the WZ action (3.14), now with β interpreted as the Goldstone mode of *some* broken $U(1)$ symmetry. Nothing else changes in the WZ action. The general form of the Weyl and gauge invariant action (3.15) is unchanged in the flat-space limit with $A_\mu = 0$. (The relative normalization between A_μ and β may change, but we do not have to worry about this when $A_\mu = 0$.) Of course, there is no supersymmetry or other principle to fix the coefficients γ_i . However, that is not important for the Komargodski-Schwimmer proof of the a -theorem because (3.28) shows that none of the Weyl+gauge invariants W_i affect the $2 \rightarrow 2$ scattering amplitude of the physical dilaton at order p^4 . Hence we conclude that even in the absence of supersymmetry the proof of the a -theorem is unaffected by the presence of Goldstone bosons for Abelian global symmetries.¹²

¹²The fact that the presence of extra Goldstone bosons will not affect the $2 \rightarrow 2$ dilaton scattering was also mentioned in [80] as well as in Section 3.5.1 of [81].

Part II

Modern Methods for Amplitudes: Grassmannians and Plabic Graphs

Chapter 4

Grassmannians for Amplitudes

4.1 Motivation and Preview

Recent years have brought remarkable progress in our understanding of the mathematical structure of scattering amplitudes, especially in the planar limit of $\mathcal{N} = 4$ super Yang-Mills theory (SYM). Among the new approaches are the Grassmannian formulations [40, 82, 83], on-shell diagrams [37], and the geometrization of amplitudes in the “amplituhedron” [45, 46, 84]. Many of the ideas from planar $\mathcal{N} = 4$ SYM carry over to the superconformal 3d $\mathcal{N} = 6$ Chern-Simons matter theory constructed by Aharony, Bergman, Jafferis and Maldacena (ABJM) [85]; see also [86]. In this chapter we study the Grassmannian descriptions of amplitudes in both 4d $\mathcal{N} = 4$ SYM and in 3d ABJM theory.

The Grassmannian $\text{Gr}(k, n)$ is the set of all k -planes in n -dimensional space; in the context of scattering amplitudes, n counts the number of external particles while k refers to a classification of amplitudes. The Grassmannian description of amplitudes depends on

how the external data — particle momenta and type — are encoded. For n -particle N^k MHV amplitudes in 4d planar $\mathcal{N} = 4$ SYM there are three formulations [40, 82]:

- The *momentum space* formulation uses the spinor helicity representation for the external momenta, e.g. $p_{ab} = \lambda_a \tilde{\lambda}_b$. The relevant Grassmannian is $\text{Gr}(k + 2, n)$.
- The *twistor space* formulation encodes the data via a half-Fourier transform of the external momenta, i.e. a Fourier transform of λ , but not $\tilde{\lambda}$. This representation makes the superconformal symmetry $SU(2, 2|4)$ manifest. As in momentum space, the Grassmannian is $\text{Gr}(k + 2, n)$.
- The *momentum twistor* formulation is applicable in the planar limit and makes the *dual* superconformal symmetry $SU(2, 2|4)$ manifest. The relevant Grassmannian is $\text{Gr}(k, n)$.

In Section 4.2, we provide a pedagogical review of these three representations of the 4d external data and present the corresponding Grassmannian integrals explicitly.

The three Grassmannian descriptions are directly related. The relation between the 4d SYM twistor space and momentum space integrals was utilized already in the early literature [40] on the subject. The momentum twistor Grassmannian was introduced shortly after in [82]. Its relation to the two other formulations was given in [83] using a set of intricate integral manipulations. In particular, the argument of [83] uses a gauge fixing that breaks little group scaling and therefore results in very complicated Jacobians that are difficult to write explicitly. In Section 4.3, we present a new version of the proof, valid for all n and k , that manifestly preserves the little group scaling at each step of the calculation and yields all Jacobians as simple explicit expressions.

In Section 4.4 we address how the Grassmannian integrals are evaluated as contour integrals and demonstrate this with the explicit computation of the residues in the n -point NMHV sector using the momentum twistor Grassmannian integral. The results for the individual residues are known to be the dual superconformal invariant building blocks of the tree amplitudes, i.e. the “ R -invariants” [87] or “5-brackets” [82]. These invariants obey a set of linear relations, which in the Grassmannian formulation simply follow from global residue theorems. We provide a homological interpretation of the residue theorems for the NMHV residues. We then review the structure of physical versus spurious (unphysical) poles of the residues and how this gives a specification of contours for which the Grassmannian integral exactly produces the tree-level amplitudes. The results are then rephrased in the context of on-shell diagrams and the positroid stratification of the Grassmannian, and we show how the ‘boundary operation’ in the Grassmannian integral is related to both the residue theorems and the pole structure.

In Section 4.5, we turn to the Grassmannian descriptions of amplitudes in 3d ABJM theory. We briefly review the momentum space spinor helicity formalism in 3d and the associated Grassmannian integral for ABJM amplitudes, which was introduced previously in [42, 43, 44, 88]. It encodes the $n=(2k+4)$ -point N^k MHV amplitudes of ABJM theory as contour integrals in the *orthogonal Grassmannian* $OG(k+2, 2k+4)$. The space $OG(k, n)$ is equipped with the metric $g_{ij} = \delta_{ij}$, $i, j = 1, 2, \dots, n$, and consists of k -dimensional null planes in \mathbb{C}^n ; in other words, the $k \times n$ matrices $B \in OG(k, n)$ satisfy $BgB^T = 0$.

A momentum twistor version of the ABJM Grassmannian integral has not previously been constructed. We achieve this goal in Section 4.5, which is an important first step towards developing an amplituhedron for the ABJM theory. To this end, we first introduce another formulation of the 3d spinor helicity formalism that facilitates the definition of 3d momentum twistors. They are simply the 4d momentum twistors Z_i^A ($A = 1, 2, 3, 4$) subject to the bi-local $SO(2, 3) \sim Sp(4)$ -invariant constraint $Z_i^A Z_{i+1}^B \Omega_{AB} = 0$ for all $i = 1, 2, \dots, n$.

Next, our streamlined proof of the relation between the 4d Grassmannian integral representations in Section 4.3 allows us to derive the desired momentum twistor version of the Grassmannian integral for ABJM theory. Just like the momentum space Grassmannian integral, the new integral has an orthogonality constraint, but a novel feature is that the k -dimensional planes are now null with respect to a metric defined by $Sp(4)$ -invariant inner products of the momentum twistors, $Z_i^A Z_j^B \Omega_{AB}$.

Orthogonal Grassmannians defined by non-trivial metrics for Grassmannians have been encountered previously in the mathematics literature in the context of electrical networks and related combinatorics [89, 90]. However, the dependence of the metric on external data appears to be a new property that would be exciting to explore further. In particular, it plays a crucial role for the boundary properties needed for the physical poles of the 6-point ABJM tree-amplitude, as we discuss in some detail.

We end in Section 4.6 with a brief outlook to Grassmannians beyond the NMHV level and open questions. A few technical results are relegated to appendices.

4.2 $\mathcal{N} = 4$ SYM and the Grassmannian

This section is intended as a short review of the Grassmannian formulation of amplitudes in planar $\mathcal{N} = 4$ SYM. Sections 4.2.1 and 4.2.2 introduce the basic definitions and concepts needed for (super)amplitudes in $\mathcal{N} = 4$ and present the three different forms of the external data: momentum space, twistor space, and momentum twistor space. See (4.12) for an overview. Section 4.2.3 presents the Grassmannian integrals. Experts can skip ahead to Section 4.3.

4.2.1 External Data: Momentum Space and Superamplitudes

The external data for an amplitude encodes the information about the initial and final state particles in the scattering process; practically we take all states to be outgoing. We are here considering only amplitudes in $\mathcal{N} = 4$ SYM, so each of the n external particles — labeled $i = 1, 2, \dots, n$ — is specified by a null momentum p_i , i.e. $p_i^2 = 0$, along with a specification of the particle type (e.g. gluon, gluino, or scalar). The scattering amplitude A_n takes this external data as input and returns a complex number on the support of a delta function that enforces momentum conservation $\delta^4(p_1 + \dots + p_n)$.

In 4d, a null vector p_i^μ is conveniently written as a 2×2 matrix $p_i^{\dot{a}a}$ with vanishing determinant. Because it has rank 1, the matrix can be expressed as a product of two 2-component vectors:¹ $p_i^{\dot{a}a} = \lambda^a \tilde{\lambda}^{\dot{a}}$. Thus, for an n -particle amplitude with n external massless particles, the on-shell momenta p_i with $p_i^2 = 0$ are specified as $(\lambda_i, \tilde{\lambda}_i)$. For the purpose of exploring the mathematical properties of amplitudes, it is useful to work with complex-valued momenta. In that case, λ_i and $\tilde{\lambda}_i$ are independent. (Alternatively, we can keep p_i real and work with a metric with signature $(-, -, +, +)$.)

The scattering amplitudes are built from Lorentz-invariant contractions of the spinors, such as the angle bracket

$$\langle ij \rangle := \epsilon_{ab} \lambda_i^a \lambda_j^b, \quad (4.1)$$

constructed with the help of the antisymmetric Levi-Civita symbol, here $\epsilon^{12} = -\epsilon^{21} = 1 = -\epsilon_{12} = \epsilon_{21}$, of the $SL(2)$ subgroup of the 4d Lorentz group $SO(3, 1)$. Lorentz indices are often suppressed in our presentation.

The physical spectrum of $\mathcal{N} = 4$ SYM consists of 16 massless particles: the gluon g^\pm with helicity states $h = \pm 1$, four gluinos Λ^A and Λ_A with $h = \pm \frac{1}{2}$, and six scalars S^{AB} with $h = 0$; $A, B = 1, 2, 3, 4$. The helicity h states transform in rank $r = 2 - 2h$ fully antisymmetric representations of the global $SU(4)$ R -symmetry of $\mathcal{N} = 4$ SYM. It is very convenient to encode the states using anticommuting Grassmann variables $\tilde{\eta}_{iA}$, with fundamental $SU(4)$ index $A = 1, 2, 3, 4$ and particle label $i = 1, 2, \dots, n$; Grassmann monomials are in one-to-one correspondence with the states, e.g. $\tilde{\eta}_{31} \tilde{\eta}_{33} \tilde{\eta}_{34}$ means that particle 3 is a negative helicity gluino $\Lambda^{134} \sim \Lambda_2$.

The n -point component amplitudes A_n combine into **superamplitudes** $\mathcal{A}_n^{\text{N}^k\text{MHV}}$ (or more generally \mathcal{A}_n), which are polynomials of degree $4(k + 2)$ in the Grassmann variables. R -symmetry requires \mathcal{A}_n to be an $SU(4)$ singlet, hence the Grassmann degree of each term must be a multiple of 4. The label N^kMHV stands for (Next-to) ^{k} Maximally Helicity Vi-

¹The spinor helicity conventions used in this chapter are chosen to conform with much of the literature on Grassmannians. They differ from those used in the recent review [34].

olating — this sector of amplitudes consists of all gluon amplitudes with $k + 2$ negative helicity gluons and $n - k - 2$ positive helicity gluons, as well as all amplitudes related to those via supersymmetry. The sector with $k = 0$ is simply called MHV. The coefficient of a given Grassmann monomial in \mathcal{A}_n is a component amplitude whose external states are those dictated by the Grassmann variables; for example, the coefficient of the monomial $(\tilde{\eta}_{11}\tilde{\eta}_{12}\tilde{\eta}_{13}\tilde{\eta}_{14})(\tilde{\eta}_{23}\tilde{\eta}_{24})(\tilde{\eta}_{41}\tilde{\eta}_{42})$ is the component amplitude

$$A_n [g^-(p_1)S^{34}(p_2)g^+(p_3)S^{12}(p_4)g^+(p_6) \dots g^+(p_n)]. \quad (4.2)$$

The $SU(N)$ gauge group of $\mathcal{N} = 4$ SYM dresses the amplitudes with a color-structure that factorizes from the kinematic information. Amplitudes in the *planar* theory have a single trace of $SU(N)$ generators,² and as a result the planar n -particle superamplitudes are invariant under *cyclic permutations* of the external labels, i.e. under $i \rightarrow i + 1 \bmod n$.

The MHV sector is the simplest. The tree-level MHV superamplitude is given by the supersymmetrization of the Parke-Taylor gluon amplitude [35, 91]:

$$\mathcal{A}_n^{\text{MHV}} = \frac{\delta^4(\sum_{i=1}^n \lambda_i \tilde{\lambda}_i) \delta^{(8)}(\sum_{i=1}^n \lambda_i \tilde{\eta}_i)}{\langle 12 \rangle \langle 23 \rangle \dots \langle n1 \rangle}. \quad (4.3)$$

The four bosonic delta functions in (4.3) encode momentum conservation via $p_i = \lambda_i \tilde{\lambda}_i$, while the Grassmann delta function,³ defined as

$$\delta^{(8)}\left(\sum_{i=1}^n \lambda_i \tilde{\eta}_i\right) := \frac{1}{2^4} \prod_{A=1}^4 \sum_{i,j=1}^n \langle ij \rangle \tilde{\eta}_{iA} \tilde{\eta}_{jA}, \quad (4.4)$$

ensures conservation of $\mathcal{N} = 4$ supermomentum, $q_{iA} := \lambda_i \tilde{\eta}_{iA}$. The superamplitude (4.3) clearly has cyclic symmetry.

To summarize, for n -particle superamplitudes in $\mathcal{N} = 4$ SYM, the external data is specified in terms of the set $(\lambda_i, \tilde{\lambda}_i | \tilde{\eta}_{iA})$ for $i = 1, 2, \dots, n$. We call this the **momentum space** representation of the external data (or sometimes ‘on-shell superspace’).

²For further details, see Section 2.5 of the review [34].

³The bosonic delta functions are defined as standard in distribution theory [92], i.e. they have the property that $\int_{\mathbb{R}^m} d^m x \delta^m(x - x_0) f(x) = f(x_0)$ for any suitable test function f . Similarly, we use $\int d^m x d^n y \delta^n(g(x, y)) f(x, y) = \int d^m x \sum_{g(x, y)=0} f(x, y) / \det(dg/dy)$. The Grassmann delta functions are defined by the same property, $\int d\eta \delta^{(1)}(\eta - \eta_0) f(\eta) = f(\eta_0)$, but using the Berezin integral $\int d\eta \eta = 1$ and $\int d\eta 1 = 0$. Thus, the Grassmann delta function is simply $\delta^{(1)}(\eta) = \eta$ and $\delta^{(2)}(\sum_i \lambda_i \eta_i) = \frac{1}{2} \sum_{i,j} \langle ij \rangle \eta_i \eta_j$. The superscript on the Grassmann delta-function indicates its polynomial Grassmann degree.

The momentum space external data has a redundancy known as *little group scaling*:

$$\lambda_i \rightarrow t_i \lambda_i, \quad \tilde{\lambda}_i \rightarrow t_i^{-1} \tilde{\lambda}_i, \quad \tilde{\eta}_i \rightarrow t_i^{-1} \tilde{\eta}_i, \quad (4.5)$$

for each $i = 1, 2, \dots, n$. A component amplitude scales homogeneously under little group scaling with weight $t_i^{-2h_i}$, where h_i is the helicity of the i^{th} particle. The scaling of the Grassmann variables ensures uniform weight for all external states in a superamplitude:

$$\mathcal{A}_n \rightarrow t_i^{-2} \mathcal{A}_n. \quad (4.6)$$

for each $i = 1, 2, \dots, n$. Little group scaling plays a key role in several explorations of scattering amplitudes, including the work we present in this chapter.

4.2.2 External Data: Twistors and Momentum Twistors

In addition to the momentum space representation, we will be using two other formulations for the 4d external data, namely twistor space and momentum twistor space. We describe each in turn.

Twistor space is obtained from momentum space via a Fourier transform of λ_j , formally via

$$\int d^2 \lambda_j \exp(-i \tilde{\mu}_j^a \lambda_{ja}) \bullet, \quad (4.7)$$

for each $j = 1, 2, \dots, n$. The bullet indicates the expression that is Fourier transformed. (We are ignoring factors of 2π in all Fourier transforms here and henceforth as these only amount to overall normalizations.) The external data is then encoded in the 4-component twistor $W_i = (\tilde{\mu}_i, \tilde{\lambda}_i)$ and its companion, the supertwistor $\mathcal{W}_i = (\tilde{\mu}_i, \tilde{\lambda}_i | \tilde{\eta}_i)$. Under little group scaling (4.5), we have $\tilde{\mu}_i \rightarrow t_i^{-1} \tilde{\mu}_i$, so the (super)twistor scales uniformly, e.g. $\mathcal{W}_i \rightarrow t_i^{-1} \mathcal{W}_i$. The measure in the integral (4.7) scales as t_i^2 , so this exactly compensates the little group scaling of the superamplitude (4.6). Thus, after the half-Fourier transformation for all $j = 1, 2, \dots, n$, the superamplitude is invariant under little group scaling. In other words, the superamplitude in twistor space is defined projectively, and the twistors W_i and supertwistors \mathcal{W}_i are homogeneous coordinates of projective space, \mathbb{CP}^3 and $\mathbb{CP}^{3|4}$, respectively.

The third description of the external data uses the 4-component *momentum twistors* $Z_i = (\lambda_i, \mu_i)$ [93] and their momentum supertwistor extensions $\mathcal{Z}_i = (\lambda_i, \mu_i | \eta_i)$. The 2-component spinors μ_i are defined via incidence relations⁴

$$\mu_i := \lambda_i y_i = \lambda_i y_{i+1}, \quad (4.8)$$

⁴For a more comprehensive review of dual space and momentum twistors, see Section 5.4 of [34].

where the dual space coordinates y_i are defined in terms of the momenta as

$$p_i = y_i - y_{i+1}. \quad (4.9)$$

The second relation in (4.8) follows from the Weyl equation, $p_i \lambda_i = 0$. The definition (4.9) makes momentum conservation automatic via the identification $y_{n+1} = y_1$. The on-shell condition $p_i^2 = 0$ requires ‘adjacent’ points y_i and y_{i+1} to be null separated. Dual conformal symmetry acts on the dual space variables y_i in the familiar way, e.g. under dual inversion we have $y_i \rightarrow y_i/y_i^2$.

The geometric interpretation of the incidence relations (4.8) is that a point $Z_i = (\lambda_i, \mu_i)$ in momentum twistor space corresponds to a null line defined by the points y_i and y_{i+1} in dual space. Similarly, the line defined by Z_{i-1} and Z_i in momentum twistor space maps to a point in dual space via

$$y_i = \frac{\lambda_i \mu_{i-1} - \lambda_{i-1} \mu_i}{\langle i-1, i \rangle}. \quad (4.10)$$

This follows from (4.8).

In our applications, we need to be able to map directly from momentum space variables $(\lambda_i, \tilde{\lambda}_i | \tilde{\eta}_i)$ to momentum twistor variables $\mathcal{Z}_i = (\lambda_i, \mu_i | \eta_i)$. This is done via the relations

$$\begin{aligned} \tilde{\lambda}_i &= \frac{\langle i+1, i \rangle \mu_{i-1} + \langle i, i-1 \rangle \mu_{i+1} + \langle i-1, i+1 \rangle \mu_i}{\langle i-1, i \rangle \langle i, i+1 \rangle}, \\ \tilde{\eta}_{iA} &= \frac{\langle i+1, i \rangle \eta_{i-1,A} + \langle i, i-1 \rangle \eta_{i+1,A} + \langle i-1, i+1 \rangle \eta_{iA}}{\langle i-1, i \rangle \langle i, i+1 \rangle}. \end{aligned} \quad (4.11)$$

It follows from (4.11) that both μ_i and η_i scale linearly with t_i under little group transformations, so the momentum (super)twistors scale uniformly, e.g. $\mathcal{Z}_i \rightarrow t_i \mathcal{Z}_i$. Therefore, the \mathcal{Z}_i naturally live in projective space, \mathbb{CP}^3 and $\mathbb{CP}^{3|4}$. With the external data given in momentum twistor space, the superamplitude still scales uniformly as in (4.6). However, as we shall see, one can split off the MHV superamplitude (4.3) as an overall factor; it takes care of the scaling properties and leaves behind an object that is invariant under little group scaling and therefore projectively well-defined.

The relations between the three different forms of the external data can be summarized compactly as follows:

twistor space	momentum space	momentum twistor space	
$\mathcal{W}_i = (\tilde{\mu}_i, \tilde{\lambda}_i \tilde{\eta}_i)$	$(\lambda_i, \tilde{\lambda}_i \tilde{\eta}_i)$	$\mathcal{Z}_i = (\lambda_i, \mu_i \eta_i)$	(4.12)
	\longleftrightarrow	\longleftrightarrow	
	Fourier transform eq (4.7)	incidence relations eq (4.11)	

Superamplitudes in $\mathcal{N} = 4$ SYM enjoy superconformal symmetry $SU(2, 2|4)$; the action of this symmetry is linearized in (super)twistor variables. In the planar limit, the superamplitudes (at tree-level or more generally the loop-*integrand*s) also have dual superconformal symmetry $SU(2, 2|4)$ whose action is linearized in the momentum twistor description. The generators of the ‘ordinary’ and dual superconformal symmetries can be arranged to generate an infinite-dimensional algebra called the $SU(2, 2|4)$ Yangian. Further details of the representation of the amplitudes and their symmetries can be found in [34].

4.2.3 Grassmannian Integrals

The complex Grassmannian $\text{Gr}(k, n)$ is the space of k -planes in \mathbb{C}^n . A k -plane can be described as a collection of k n -component vectors. Since any $GL(k)$ rotation of the vectors yield the same k -plane, the Grassmannian $\text{Gr}(k, n)$ can be given equivalently in terms of $k \times n$ matrices modulo $GL(k)$. The dimension of $\text{Gr}(k, n)$ is therefore $kn - k^2 = k(n - k)$. Here, we will list and briefly describe the three Grassmannian integrals relevant for amplitudes in $\mathcal{N} = 4$ SYM; the actual connection to the amplitudes is made in Section 4.4.

Grassmannian with Twistor Space Data \mathcal{W}

In terms of twistor variables, \mathcal{W} , the relevant Grassmannian integral was first presented in [40]. For the $N^k\text{MHV}$ sector of n -point superamplitudes, the associated Grassmannian is $\text{Gr}(k + 2, n)$ and in this space we study the integral

$$\tilde{\mathcal{L}}_{n;k}(\mathcal{W}) = \int \frac{d^{\tilde{k} \times n} B}{GL(\tilde{k})} \frac{\delta^{4\tilde{k}|4\tilde{k}}(B \cdot \mathcal{W})}{m_1 m_2 \dots m_n}. \quad (4.13)$$

Here $\tilde{k} = k + 2$ and the m_i ’s are the $\tilde{k} \times \tilde{k}$ consecutive minors of the matrix B , i.e. $m_1 = (1 2 \dots \tilde{k})_B$, $m_2 = (2 3 \dots \tilde{k} + 1)_B$, \dots , $m_n = (n 1 \dots \tilde{k} - 1)_B$. The integral (4.13) should be understood as a contour integral; this will be discussed in Section 4.2.3 and more concretely in Section 4.4.1.⁵ The external data enters the integral (4.13) only via the argument of the

⁵The integral (4.13) exhibits two conventions typical of this field. First, we write an integral over a parameter space with r complex parameters to mean that the integral will be taken over a real r -dimensional contour to be specified later. Second, let X be a parameter space on which some connected group G acts, let dX be a G -invariant volume form on X and choose a left invariant volume form μ_G on G . We write dX/G for the volume form on X/G so that, if we locally identify a patch on X with a product of a patch on X/G and a patch on G , then $dX = (dX/G) \times \mu_G$. We do not actually specify the measure μ_G , since it only adds a global constant factor.

delta-functions $B \cdot \mathcal{W} = \sum_{i=1}^n B_{\alpha i} \mathcal{W}_i$ with $\alpha = 1, 2, \dots, \tilde{k}$. Specifically, we have

$$\delta^{4\tilde{k}|4\tilde{k}}(B \cdot \mathcal{W}) = \prod_{\alpha=1}^{\tilde{k}} \delta^4 \left(\sum_i B_{\alpha i} \mathcal{W}_i \right) \delta^{(4)} \left(\sum_i B_{\alpha i} \tilde{\eta}_i \right) \quad (4.14)$$

with the sum over $i = 1, 2, \dots, n$. Note two simple properties of (4.13):

- Little group scaling, $\mathcal{W}_i \rightarrow t_i^{-1} \mathcal{W}_i$, can be absorbed via a scaling of the i^{th} column of B : $B_{\alpha i} \rightarrow t_i B_{\alpha i}$ for all $\alpha = 1, \dots, \tilde{k}$. The i^{th} column is included in exactly \tilde{k} minors, so the scaling of the product of minors is $t_i^{\tilde{k}}$ and this precisely cancels the scaling of the measure $d^{\tilde{k} \times n} B$. Thus, $\tilde{\mathcal{L}}_{n;\tilde{k}}$ is invariant under little group scaling; it is projectively defined, just as are the superamplitudes in twistor space.
- $\tilde{\mathcal{L}}_{n;\tilde{k}}$ produces objects of Grassmann degree $4\tilde{k} = 4(k+2)$ which is the same as for superamplitudes in the $N^k \text{MHV}$ sector.

Grassmannian with Momentum Space Data $(\lambda, \tilde{\lambda} | \tilde{\eta})$

In momentum space, the Grassmannian for n -point $N^k \text{MHV}$ amplitudes is also $\text{Gr}(k+2, n)$.

The integral can be written

$$\mathcal{L}_{n;k}(\lambda, \tilde{\lambda}, \tilde{\eta}) = \int \frac{d^{\tilde{k} \times n} B}{GL(\tilde{k})} \frac{\delta^{2\tilde{k}}(B_{\alpha i} \tilde{\lambda}_i) \delta^{2(n-\tilde{k})}(B_{\alpha i}^{\perp} \lambda_i) \delta^{(4\tilde{k})}(B_{\alpha i} \tilde{\eta}_{iA})}{m_1 m_2 \cdots m_n}, \quad (4.15)$$

where $\tilde{k} = k+2$ and B^{\perp} is the $(n-\tilde{k}) \times n$ matrix parameterizing the $(n-\tilde{k})$ -plane orthogonal to the \tilde{k} -plane defined by B ; i.e. $B(B^{\perp})^T = 0$.⁶

The momentum space Grassmannian integral (4.15) has $2n$ bosonic delta-functions while the twistor space version (4.13) has $4(k+2)$; the difference arises from the Fourier transformations that relate (4.13) and (4.15), as we review in detail in Section 4.3. The first $2\tilde{k}$ delta functions in (4.15) require that the 2-plane defined by the n $\tilde{\lambda}_i$'s must lie in the orthogonal complement to the \tilde{k} -plane defined by B . The remaining $2(n-\tilde{k})$ delta functions require the λ 2-plane to be in the orthogonal complement of B^{\perp} ; i.e. the λ -plane must be contained in B . Hence, the bosonic delta functions require the 2-planes defined by λ and $\tilde{\lambda}$ to be orthogonal: $\sum_i \lambda_i \tilde{\lambda}_i = 0$. This is just momentum conservation. We conclude that 4 of the $2n$ bosonic delta-functions in (4.15) simply enforce a condition on the external data, thus leaving constraints only on $2n-4$ of the integration variables B .

⁶ B^{\perp} is defined only up to a $GL(n-\tilde{k})$ redundancy, but after fixing the $GL(\tilde{k})$ of B we can choose a canonical B^{\perp} to avoid ambiguities.

Grassmannian with Momentum Twistor Space Data \mathcal{Z}

The $\text{Gr}(k, n)$ Grassmannian integral with external data given in momentum twistor space was introduced in [82]. For the $N^k\text{MHV}$ sector with n external particles it is

$$\mathcal{L}_{n;k}(\mathcal{Z}) = \mathcal{A}_n^{\text{MHV}} \int \frac{d^{k \times n} C}{GL(k)} \frac{\delta^{4k|4k}(C \cdot \mathcal{Z})}{M_1 M_2 \cdots M_n}. \quad (4.16)$$

The $k \times k$ minors of the matrix C are $M_1 = (12 \dots k)_C$, etc., and the overall factor is the MHV superamplitude (4.3).

As above we note that

- The integral on the RHS of (4.16) is invariant under little group scaling $\mathcal{Z}_i \rightarrow t_i \mathcal{Z}_i$ after a compensating scaling by t_i^{-1} of the i^{th} column of C . However, the MHV factor scales as t_i^{-2} . Thus $\mathcal{L}_{n;k}(\mathcal{Z}) \rightarrow t_i^{-2} \mathcal{L}_{n;k}(\mathcal{Z})$; this is precisely the scaling (4.6) needed for superamplitudes in momentum twistor space.
- $\mathcal{L}_{n;k}$ produces objects of Grassmann degree $4k + 8$, with the “+8” arising from the MHV factor. This is the correct count for superamplitudes in the $N^k\text{MHV}$ sector.

Contours

Beyond the comments about little group scaling and Grassmann degrees, we have not yet established the connection between the Grassmannian integrals and superamplitudes. The first step is to define what is actually meant by the integrals. The idea is the same in all three cases, so we focus on the momentum twistor integral (4.16).

Fixing the $GL(k)$ invariance of $\mathcal{L}_{n;k}$ in (4.16) leaves an integral over $k(n - k)$ variables. Of these, the bosonic delta functions localize $4k$. Thus, we are left with $k(n - k - 4)$ variables to be integrated. The prescription is to interpret the integrals as $k(n - k - 4)$ -dimensional contour integrals. We can consider contours that select $k(n - k - 4)$ simultaneous zeros of the minors. For each such contour γ , the integral (4.16) computes a $k(n - k - 4)$ -dimensional residue $\mathcal{L}_{n;k}^{(\gamma)}$. The sum of certain sets of such residues turns out to be exactly the $N^k\text{MHV}$ tree superamplitude in momentum twistor space: denoting the corresponding contour Γ_{tree} , we therefore have $\mathcal{L}_{n;k}^{(\Gamma_{\text{tree}})}(\mathcal{Z}) = \mathcal{A}_{n,\text{tree}}^{N^k\text{MHV}}(\mathcal{Z})$. We demonstrate the explicit calculation of the individual NMHV residues in Section 4.4 and discuss the associated global residue theorems in Section 4.4.2. The NMHV ‘tree-contour’ Γ_{tree} is described in Section 4.4.3.

The Grassmannian integrals (4.13), (4.15), and (4.16) are directly related. This was argued in [83] and we now provide a streamlined proof.

4.3 Relating the Three Grassmannian Formulations

The twistor space and momentum space Grassmannian integrals (4.13) and (4.15) are easily related via the half-Fourier transform (4.7); for completeness we review this below. The derivation of the momentum twistor Grassmannian integral (4.16) from either of the other two integrals requires more effort since one needs to reduce the Grassmannian $\text{Gr}(k+2, n)$ to $\text{Gr}(k, n)$. As noted in the Introduction, this was first done in [83]. We present here a streamlined and more explicit version of the proof; this will be useful for deriving the equivalent momentum twistor Grassmannian integral for ABJM theory in Section 4.5.

4.3.1 From Twistor Space to Momentum Space

The Grassmannian integral in twistor space $\tilde{\mathcal{L}}_{n;k}(\mathcal{W})$ is converted to momentum space via the inverse of the Fourier transform (4.7) that relates momentum space and twistor space. Thus, the momentum space Grassmannian integral is given as

$$\mathcal{L}_{n;k}(\lambda, \tilde{\lambda}, \tilde{\eta}) = \left(\prod_{i=1}^n \int d^2 \tilde{\mu}_i e^{i \lambda_i \cdot \tilde{\mu}_i} \right) \tilde{\mathcal{L}}_{n;k}(\mathcal{W}). \quad (4.17)$$

Since $\tilde{\mathcal{L}}_{n;k}(\mathcal{W})$ is invariant under little group scaling, the expression $\mathcal{L}_{n;k}$ scales as t_i^{-2} thanks to the scaling of the measure of the Fourier transform.

The only $\tilde{\mu}$ -dependent part of $\tilde{\mathcal{L}}_{n;k}(\mathcal{W})$ is $\delta^{2\tilde{k}}(B \cdot \tilde{\mu})$, as can be seen from (4.13). This δ -function enforces that B must be orthogonal to the 2-plane defined by $\tilde{\mu}_a$ (viewed as two n -component vectors). It is convenient to introduce the B^\perp as the $(n - \tilde{k}) \times n$ matrix parameterizing the $(n - \tilde{k})$ -plane orthogonal to the \tilde{k} -plane defined by B ; i.e. it satisfies $B(B^\perp)^T = 0$. The constraints of $\delta^{2\tilde{k}}(B \cdot \tilde{\mu})$ can then be reformulated as $\tilde{\mu} \subset B^\perp$. In other words, $\tilde{\mu}_a$ is some linear combination of the rows of B^\perp :

$$\delta^{2\tilde{k}}(B_{\alpha i} \tilde{\mu}_i) = \int d^{2(n-\tilde{k})} \sigma_{\bar{\alpha}} \delta^{2n}(\tilde{\mu}_i - \sigma_{\bar{\alpha}} B_{\bar{\alpha} i}^\perp), \quad (4.18)$$

where $\bar{\alpha} = 1, \dots, n - \tilde{k}$. We can now easily perform the inverse-Fourier transform back to momentum space. The delta functions (4.18) localize the Fourier integral (4.17) to give $e^{i\sigma \cdot B^\perp \cdot \lambda}$, so that integration of the σ 's then yields $2(n - \tilde{k})$ new delta functions $\delta^{2(n-\tilde{k})}(B^\perp \cdot \lambda)$. The result is the momentum space Grassmannian integral (4.15).

4.3.2 Derivation of the Momentum Twistor Grassmannian

Having derived the momentum space integral (4.15) from the twistor space one (4.13), we now continue to momentum twistor space. The key step is the reduction of the integral from $\text{Gr}(k+2, n)$ to $\text{Gr}(k, n)$.

The bosonic delta functions $\delta^{2(n-\tilde{k})}(B^\perp \cdot \lambda)$ in (4.15) require that the λ 2-plane lies in the orthogonal complement of B^\perp , so

$$\prod_{\beta=1}^{\tilde{k}} \int d^2 \rho_\beta \delta^{2n}(\lambda_j - \rho_\alpha B_{\alpha j}), \quad (4.19)$$

where ρ_α^a is a $2 \times \tilde{k}$ array of dummy integration variables.

As an aside, let us note that we could easily have found (4.19) directly from the inverse Fourier integral of the twistor space integral (4.17) by writing $\delta^{2\tilde{k}}(B \cdot \tilde{\mu})$ as $\int d^2 \rho_\alpha e^{-i\rho_\alpha B_{\alpha j} \tilde{\mu}_j}$ and then carrying out the $2n$ Fourier integrals in (4.17) to find (4.19).

The $GL(\tilde{k}) = GL(k+2)$ redundancy of the B 's is transferred to the ρ 's. So we can go ahead and fix part of $GL(k+2)$ by choosing

$$\rho = \begin{pmatrix} 0 & \cdots & 0 & 1 & 0 \\ 0 & \cdots & 0 & 0 & 1 \end{pmatrix}. \quad (4.20)$$

The $2n$ delta functions (4.19) then fix the last two rows of B to be the λ 's:

$$B = \begin{pmatrix} B_{11} & B_{12} & \cdots & B_{1n} \\ \vdots & \vdots & \ddots & \vdots \\ B_{k1} & B_{k2} & \cdots & B_{kn} \\ \lambda_1^1 & \lambda_2^1 & \cdots & \lambda_n^1 \\ \lambda_1^2 & \lambda_2^2 & \cdots & \lambda_n^2 \end{pmatrix}. \quad (4.21)$$

Thus, after evaluating the ρ integrals, we find

$$\mathcal{L}_{n;k}(\lambda, \tilde{\lambda}, \tilde{\eta}) = \delta^4(\lambda_i \tilde{\lambda}_i) \delta^{(8)}(\lambda_i \tilde{\eta}_i) \times \int \frac{d^{k \times n} B_{\hat{\alpha}i}}{GL(k) \times T_k} \frac{\delta^{2k}(B_{\hat{\alpha}i} \tilde{\lambda}_i) \delta^{(4k)}(B_{\hat{\alpha}i} \tilde{\eta}_i)}{m_1 m_2 \cdots m_n}, \quad (4.22)$$

with $\hat{\alpha} = 1, 2, \dots, k$. The gauge choice (4.21) preserves little group scaling. Note that all the delta functions in (4.22) are little group invariant using $B_{\hat{\alpha}i} \rightarrow t_i B_{\hat{\alpha}i}$. Again, the n minors scale as $t_i^{\tilde{k}} = t_i^{k+2}$, but now the measure only contributes t_i^k . So overall, the expression (4.22) for $\mathcal{L}_{n;k}$ scales as t_i^{-2} , as anticipated.

In (4.22), T_k indicates the translational redundancy in the $B_{\hat{\alpha}i}$ -variables. The transla-

tional symmetry acts as

$$B_{\hat{\alpha}i} \rightarrow B_{\hat{\alpha}i} + r_{1\hat{\alpha}}\lambda_i^1 + r_{2\hat{\alpha}}\lambda_i^2 \quad \text{for all } i \text{ simultaneously,} \quad (4.23)$$

where $r_{1\hat{\alpha}}$ and $r_{2\hat{\alpha}}$ are any numbers. This is a mixing of the last two rows in the B -matrix (4.21) with the other rows, and this leaves the minors m_i unchanged. It is also clear that on the support of the two delta functions $\delta^4(\lambda_i\tilde{\lambda}_i)\delta^{(8)}(\lambda_i\tilde{\eta}_i)$ (that encode momentum and supermomentum conservation), the delta-functions in the integral (4.22) are invariant under such a shift.

So far, what we have done parallels the work [83]. At this stage, the authors of [83] fix the translation invariance T_k via $2k$ delta functions $\delta(B_{\hat{\alpha}i}\lambda_i)$. This breaks the little group scaling and the associated Jacobian is therefore unpleasant. We proceed here in a way that preserves little group scaling at every step and gives very simple Jacobians that can be presented explicitly.

We change variables in the external data to go from momentum space to momentum twistor space. The momentum supertwistors $\mathcal{Z}_i = (\lambda_i, \mu_i | \eta_i)$ are related to the momentum space variables via the relations (4.11). Using these relations, we directly find for each $\hat{\alpha} = 1, 2, \dots, k$:

$$\sum_{i=1}^n B_{\hat{\alpha}i}\tilde{\lambda}_i = -\sum_{i=1}^n C_{\hat{\alpha}i}\mu_i, \quad \sum_{i=1}^n B_{\hat{\alpha}i}\tilde{\eta}_i = -\sum_{i=1}^n C_{\hat{\alpha}i}\eta_i, \quad (4.24)$$

where the reorganization on the RHS directly gives

$$C_{\hat{\alpha}i} = \frac{\langle i, i+1 \rangle B_{\hat{\alpha}, i-1} + \langle i-1, i \rangle B_{\hat{\alpha}, i+1} + \langle i+1, i-1 \rangle B_{\hat{\alpha}i}}{\langle i-1, i \rangle \langle i, i+1 \rangle}. \quad (4.25)$$

A sign was absorbed which flipped the angle brackets relative to (4.11). The expression (4.25) implies that $C_{\hat{\alpha}i} \rightarrow t_i^{-1}C_{\hat{\alpha}i}$ under little group scaling.

We can rewrite the $(k+2) \times (k+2)$ minors m_i of the B -matrix in terms of the $k \times k$ minors of the C -matrix as [83]

$$m_1 = (B_1 \dots B_{k+2}) = -\langle 12 \rangle \dots \langle k+1, k+2 \rangle (C_2 \dots C_{k+1}) \quad \text{etc.} \quad (4.26)$$

Defining the $k \times k$ minors of the $k \times n$ C -matrix to be $M_1 := (C_1 \dots C_k)$ etc, we thus have

$$m_1 m_2 \dots m_n = (-1)^n (\langle 12 \rangle \langle 23 \rangle \dots \langle n1 \rangle)^{k+1} M_1 M_2 \dots M_n. \quad (4.27)$$

(We drop the signs $(-1)^n$ just as we drop 2π 's in the Fourier transforms.) Thus, we now

have

$$\mathcal{L}_{n;k}(\lambda, \tilde{\lambda}, \tilde{\eta}) = \frac{\delta^4(\lambda_i \tilde{\lambda}_i) \delta^{(8)}(\lambda_i \tilde{\eta}_i)}{(\langle 12 \rangle \langle 23 \rangle \cdots \langle 1n \rangle)^{k+1}} \int \frac{d^{k \times n} B_{\hat{\alpha}i}}{GL(k) \rtimes T_k} \frac{\delta^{2k}(C_{\hat{\alpha}i} \mu_i) \delta^{(4k)}(C_{\hat{\alpha}i} \eta_i)}{M_1 M_2 \cdots M_n}. \quad (4.28)$$

It is here understood that the C 's are functions of the B 's as given by (4.25).

Note that the Schouten identity guarantees the following two important properties:

- The C 's are invariant under the translations (4.23).
- The expression (4.25) implies that $C_{\hat{\alpha}i} \lambda_i = 0$.

We would now like to do two things: fix the translational redundancy and rewrite the integral in terms of C 's instead of B 's.

Because of the translational invariance, the B 's are not independent variables: for example we can use translations to set $2k$ of them to zero (see below). So after fixing translational invariance, we will have $kn - 2k = k(n - 2)$ variables to integrate over.

Step 1: Fixing translation invariance.

Let us use the translation invariance T_k to fix the first two columns in $B_{\hat{\alpha}i}$ to be zero, i.e. for all $\hat{\alpha} = 1, \dots, k$ we set $B_{\hat{\alpha}1} = B_{\hat{\alpha}2} = 0$. This gives

$$\frac{d^{k \times n} B_{\hat{\alpha}i}}{T_k} = \langle 12 \rangle^k d^{k \times (n-2)} B_{\hat{\alpha}i}, \quad (4.29)$$

where the included prefactor preserves the scaling properties of the measure. (This can be derived more carefully as a Jacobian of the gauge fixing.)

Step 2: Changing variables from B to C

We know how $C_{\hat{\alpha}i}$ is related to $B_{\hat{\alpha}i}$ from equation (4.25). We can use that relation to solve for $k(n - 2)$ of the components of C in terms of the $k(n - 2)$ unfixed components of B . Given our choice to set $B_{\hat{\alpha}1} = B_{\hat{\alpha}2} = 0$, we have the following system of $k(n - 2)$ equations:

$$C_{\hat{\alpha}i} = \begin{cases} \frac{\langle i, i+1 \rangle B_{\hat{\alpha}, i-1} + \langle i+1, i-1 \rangle B_{\hat{\alpha}i} + \langle i-1, i \rangle B_{\hat{\alpha}, i+1}}{\langle i-1, i \rangle \langle i, i+1 \rangle} & \text{for } 3 < i < n \\ \frac{\langle 42 \rangle B_{\hat{\alpha}3} + \langle 23 \rangle B_{\hat{\alpha}4}}{\langle 23 \rangle \langle 34 \rangle} & \text{for } i = 3 \\ \frac{\langle n1 \rangle B_{\hat{\alpha}, n-1} + \langle 1, n-1 \rangle B_{\hat{\alpha}n}}{\langle n-1, n \rangle \langle n1 \rangle} & \text{for } i = n \end{cases}. \quad (4.30)$$

We can write this as $C_{\hat{\alpha}\hat{i}} = B_{\hat{\alpha}\hat{i}} Q_{\hat{i}\hat{j}}$, with $\hat{i}, \hat{j} = 3, \dots, n$, for a square symmetric matrix $Q_{\hat{i}\hat{j}}$ with nonzero entries only on and adjacent to the main diagonal. In Appendix F.1, we show

that

$$|\det Q| = \frac{\langle 12 \rangle^2}{\langle 12 \rangle \langle 23 \rangle \cdots \langle n1 \rangle}. \quad (4.31)$$

Therefore the measure transforms as

$$d^{k(n-2)} B_{\hat{\alpha}\hat{i}} = \frac{d^{k(n-2)} C_{\hat{\alpha}\hat{i}}}{|\det Q|^k} = \left(\frac{\langle 12 \rangle \langle 23 \rangle \cdots \langle n1 \rangle}{\langle 12 \rangle^2} \right)^k d^{k(n-2)} C_{\hat{\alpha}\hat{i}}. \quad (4.32)$$

We take the absolute value of the determinant since the overall sign is irrelevant. Once again, the little group scaling of dC is compensated by the Jacobian factor so that the overall scaling of the right-hand side matches that of dB on the left.

Step 3: Restoring the full set of C variables

With the help of (4.29) and (4.32), the integral (4.28) now takes the form

$$\mathcal{L}_{n;k}(\mathcal{Z}) = \frac{\delta^4(\lambda_i \tilde{\lambda}_i) \delta^{(8)}(\lambda_i \tilde{\eta}_i)}{\langle 12 \rangle \langle 23 \rangle \cdots \langle 1n \rangle} \frac{1}{\langle 12 \rangle^k} \int \frac{d^{k \times (n-2)} C_{\hat{\alpha}\hat{i}}}{GL(k)} \frac{\delta^{2k}(C_{\hat{\alpha}\hat{i}} \mu_i) \delta^{(4k)}(C_{\hat{\alpha}\hat{i}} \eta_i)}{M_1 M_2 \cdots M_n} \Big|_{C_{\hat{\alpha}1,2} = C_{\hat{\alpha}1,2}^{(0)}}. \quad (4.33)$$

We recognize the first factor as the MHV superamplitude $\mathcal{A}_n^{\text{MHV}}$ from (4.3).

The restriction of $C_{\hat{\alpha}1}$ and $C_{\hat{\alpha}2}$ in (4.33) follows from the relation (4.25) between the B and C ; it was used above to solve for $k(n-2)$ components of C in terms of the B 's, but the remaining $2k$ components of C are then fixed as

$$C_{\hat{\alpha}1} = \frac{B_{\hat{\alpha}n}}{\langle n1 \rangle} = \sum_{j=3}^n \frac{\langle 2j \rangle}{\langle 12 \rangle} C_{\hat{\alpha}j} =: C_{\hat{\alpha}1}^{(0)}, \quad C_{\hat{\alpha}2} = \frac{B_{\hat{\alpha}3}}{\langle 23 \rangle} = - \sum_{j=3}^n \frac{\langle 1j \rangle}{\langle 12 \rangle} C_{\hat{\alpha}j} =: C_{\hat{\alpha}2}^{(0)}. \quad (4.34)$$

To verify the second equality in each relation, use (4.30) and rejoice in the beauty of the sum telescoping under the Schouten identity.

Thus, when evaluating the integral (4.33), $C_{\hat{\alpha}1}$ and $C_{\hat{\alpha}2}$ are functions of the other $k(n-2)$ C -components. This is a restriction of the region of integration that we can also impose via $2k$ delta functions $\delta(C_{\hat{\alpha}i} - C_{\hat{\alpha}i}^{(0)})$ for $i = 1, 2$. Moreover, it follows from the explicit solution (4.34) that the constraints are equivalent to $C_{\hat{\alpha}i} \lambda_i = 0$. Thus we can rewrite the delta function restriction as

$$\delta(C_{\hat{\alpha}1} - C_{\hat{\alpha}1}^{(0)}) \delta(C_{\hat{\alpha}2} - C_{\hat{\alpha}2}^{(0)}) = \langle 12 \rangle \delta^2(C_{\hat{\alpha}i} \lambda_i). \quad (4.35)$$

for each $\hat{\alpha} = 1, 2, \dots, k$.

We then have

$$\mathcal{L}_{n;k}(\mathcal{Z}) = \mathcal{A}_n^{\text{MHV}} \int \frac{d^{k \times n} C_{\hat{\alpha}i}}{GL(k)} \frac{\delta^{2k}(C_{\hat{\alpha}i}\lambda_i) \delta^{2k}(C_{\hat{\alpha}i}\mu_i) \delta^{(4k)}(C_{\hat{\alpha}i}\eta_i)}{M_1 M_2 \cdots M_n}. \quad (4.36)$$

Although we chose to fix the first two columns of B to be zero, the answer is independent of that choice; the factors of $\langle 12 \rangle$ cancel out. We can now write the result directly in terms of the momentum supertwistors $\mathcal{Z}_i = (Z_i|\eta_i) = (\lambda_i, \mu_i|\eta_i)$ as

$$\mathcal{L}_{n;k}(\mathcal{Z}) = \mathcal{A}_n^{\text{MHV}} \int \frac{d^{k \times n} C_{\hat{\alpha}i}}{GL(k)} \frac{\delta^{4k}(C_{\hat{\alpha}i}Z_i) \delta^{(4k)}(C_{\hat{\alpha}i}\eta_i)}{M_1 M_2 \cdots M_n} = \mathcal{A}_n^{\text{MHV}} \int \frac{d^{k \times n} C_{\hat{\alpha}i}}{GL(k)} \frac{\delta^{4k|4k}(C_{\hat{\alpha}i}\mathcal{Z}_i)}{M_1 M_2 \cdots M_n}. \quad (4.37)$$

This completes our derivation of the $\mathcal{N} = 4$ SYM Grassmannian integral in momentum twistor space from that in momentum space. A very similar procedure leads to an analogous result in 3d ABJM theory as we explain below in Section 4.5. In the intervening section, we demonstrate an explicit evaluation of the $\mathcal{N} = 4$ SYM momentum twistor integral (4.37) in the NMHV sector.

4.4 NMHV Integrals and Residues

In this section we evaluate the NMHV Grassmannian integral in momentum twistor space and discuss some properties of the residues and their relations to on-shell diagrams. While part of this is review, new material includes recasting the residue theorems in terms of the homology and a precise description of how the residue relations and pole structures relate to the boundary operation and the boundaries of cells in the Grassmannian.

4.4.1 Evaluation of the NMHV Residues

We focus on the momentum twistor Grassmannian, so for NMHV we have $k = 1$ and (4.16) is a contour integral in the Grassmannian $G(1, n)$. The elements $C \in G(1, n)$ are $1 \times n$ matrices modulo a $GL(1)$ scaling,

$$C = [c_1 \quad c_2 \quad \cdots \quad c_n], \quad (4.38)$$

with complex numbers c_i . The Grassmannian integral is $\mathcal{L}_{n;1}(\mathcal{Z}) = \mathcal{A}_n^{\text{MHV}} \mathcal{I}_{n;1}(\mathcal{Z})$ with

$$\mathcal{I}_{n;1}^{(\Gamma)}(\mathcal{Z}) := \oint_{\Gamma} \frac{d^{1 \times n} C}{GL(1) c_1 c_2 \cdots c_n} \delta^4(c_i Z_i) \delta^{(4)}(c_i \eta_i). \quad (4.39)$$

The oriented volume form on \mathbb{C}^n is $d^n C = \bigwedge_{i=1}^n dc^i$, and the contour Γ will be specified below.

The bosonic delta function $\delta^4(c_i Z_i)$ fixes four c_i 's, and the $GL(1)$ redundancy fixes another. This leaves an integral with $n - 5$ variables. Now suppose the contour Γ encircles a pole where exactly $n - 5$ of the c_i 's vanish. Such a contour can be characterized by specifying which five c_i 's are non-vanishing at the pole. Let us denote these five non-vanishing c_i 's by c_a, c_b, c_c, c_d , and c_e , and the corresponding contour γ_{abcde} .

We now evaluate $\mathcal{I}_{n;1}^{\gamma_{abcde}}(\mathcal{Z})$ “by inspection”. Appendix G gives a more careful evaluation that also computes the sign of the residue correctly. It follows from (4.39) that the residue where all c_i vanish for $i \neq a, b, c, d, e$ is, up to a sign, simply

$$\mathcal{I}_{n;1}^{\gamma_{abcde}}(\mathcal{Z}) = \frac{\delta^4(c_a Z_a + c_b Z_b + c_c Z_c + c_d Z_d + c_e Z_e) \delta^{(4)}(c_a \eta_a + c_b \eta_b + c_c \eta_c + c_d \eta_d + c_e \eta_e)}{c_a c_b c_c c_d c_e}. \quad (4.40)$$

Now, the constraint enforced by the bosonic delta-function is trivially solved by

$$c_a = \langle bcde \rangle, \quad c_b = \langle cdea \rangle, \quad c_c = \langle deab \rangle, \quad c_d = \langle eabc \rangle, \quad c_e = \langle abcd \rangle, \quad (4.41)$$

using the 5-term Schouten identity (or Cramer’s rule) that states that five 4-component vectors are necessarily linearly dependent:

$$\langle ijkl \rangle Z_m + \langle jklm \rangle Z_i + \langle klmi \rangle Z_j + \langle lmi j \rangle Z_k + \langle mij k \rangle Z_l = 0. \quad (4.42)$$

The 4-brackets are the fully antisymmetric $SU(2, 2)$ -invariants

$$\langle ijkl \rangle := -\epsilon_{ABCD} Z_i^A Z_j^B Z_k^C Z_l^D = \det(Z_i Z_j Z_k Z_l). \quad (4.43)$$

We conclude that

$$\mathcal{I}_{n;1}^{\gamma_{abcde}} = \frac{\delta^{(4)}(\langle bcde \rangle \eta_a + \langle cdea \rangle \eta_b + \langle deab \rangle \eta_c + \langle eabc \rangle \eta_d + \langle abcd \rangle \eta_e)}{\langle bcde \rangle \langle cdea \rangle \langle deab \rangle \langle eabc \rangle \langle abcd \rangle} =: [abcde], \quad (4.44)$$

The expression (4.44) is manifestly antisymmetric in the five labels a, b, c, d, e . This follows from the standard evaluation of higher-dimensional contour integrals, as we review in Appendix G. In addition, the general results in the appendix tell us that the residue is also fully antisymmetric in the labels $i \neq a, b, c, d, e$. We can incorporate that by labeling the residue (4.40), including the appropriate signs from the appendix, by the $n - 5$ values $i_1, i_2, \dots, i_{n-5} \neq a, b, c, d, e$ as $\{i_1, i_2, \dots, i_{n-5}\}$, which is antisymmetric in its indices. Then

the final answer, which includes all of the signs from Appendix G, is

$$\mathcal{I}_{n;1}^{\gamma abcde} = \frac{1}{(n-5)!} \varepsilon^{abcde i_1 i_2 \dots i_{n-5}} \{i_1, i_2, \dots, i_{n-5}\} = [abcde]. \quad (4.45)$$

This completes the calculation of the residues of the Grassmannian integral $\mathcal{L}_{n;1}$ in momentum twistor space. The result,

$$\mathcal{L}_{n;1}^{\gamma abcde} = \mathcal{A}_n^{\text{MHV}} [abcde], \quad (4.46)$$

shows that the individual residues produced by $\mathcal{L}_{n;1}$ are the 5-brackets $[abcde]$. These are the known building blocks of NMHV amplitudes, both at tree and loop-level.

4.4.2 NMHV Residue Theorems

Since the residues $[abcde]$ of the NMHV Grassmannian integral (G.5) are characterized by five labels, $a, b, c, d, e \in \{1, 2, 3, \dots, n\}$, as in (4.45), it follows that there are a total of $\binom{n}{5}$ NMHV residues. These, however, are not independent. While it is difficult to derive the residue relations — or even verify them — by direct computations, the constraints among them follow quite straightforwardly from the Grassmannian residue theorems, as first noted in [40]. In this section, we count the number of independent NMHV residues $[abcde]$ and examine the linear relations among them. Since the only input is residue theorems, these relationships are also true off the support of the external momentum and supermomentum delta functions in the overall MHV factor in the momentum twistor Grassmannian integral.

Let us begin by taking an abstract view of the integral (G.5). We are integrating over $C = [c_1 \dots c_n]$ modulo a $GL(1)$ that identifies $C \sim sC$ for any $s \in \mathbb{C} - \{0\}$. Thus C can be viewed as homogeneous coordinates of \mathbb{CP}^{n-1} . We are interested in the residues associated with simultaneously vanishing ‘minors’ c_i . Each condition $c_i = 0$ defines a hyperplane in \mathbb{CP}^{n-1} . In other words, we are interested in the n hyperplanes $h_i := \{C \in \mathbb{CP}^{n-1} | c_i = 0\}$. This is called a *hyperplane arrangement* in \mathbb{CP}^{n-1} . Specifically, the residue $[abcde]$ corresponds to picking up the residue from the $(n-5)$ -dimensional toroidal contour $(S^1)^{n-5}$ surrounding the intersection of the $n-5$ hyperplanes h_i with $i \neq a, b, c, d, e$.

The bosonic delta functions in the momentum twistor integral (G.5) impose four conditions among the n components of C . These homogeneous linear relations respect the $GL(1)$ scaling, so they reduce the space of interest from \mathbb{CP}^{n-1} to \mathbb{CP}^{n-5} . Consequently, we are interested in the arrangement of n hyperplanes in \mathbb{CP}^{n-5} .

Now, suppose we focus on the complement of h_n , i.e. $c_n \neq 0$. We fix c_n to be some non-vanishing value to eliminate the projective freedom, so $\mathbb{CP}^{n-5} \rightarrow \mathbb{C}^{n-5}$. The problem

then reduces to the study of $n - 1$ hyperplanes $\{h_i\}_{i=1,\dots,n-1}$ in \mathbb{C}^{n-5} . This step is equivalent to fixing the $GL(1)$ redundancy in the Grassmannian integral. The $(n - 5)$ -dimensional contours of (G.5) must therefore live in the hyperplane arrangement complement

$$X = \mathbb{C}^{n-5} - \bigcup_{i < n} h_i. \quad (4.47)$$

A residue does not change under continuous deformation of the contour, so the result only depends on the homology class of the contour. Thus, the key observation is that the number of possible independent residues is the dimension of the homology class $H_{n-5}(X, \mathbb{C})$.

The geometry of hyperplane arrangements is well-studied in the mathematics literature and the results include the following theorem [94]:

Theorem 2. *Let $X = \mathbb{C}^N - \bigcup_{i=1}^r h_i$ be a hyperplane arrangement complement. Then*

1. *The cohomology $H^*(X, \mathbb{C})$ is generated by the forms $\frac{d\alpha_i}{\alpha_i}$.*
2. *Suppose $\{h_i\}$ is generic.⁷ Then $H^k(X, \mathbb{C})$ is zero for $k \geq N$, and for $k \in \{0, 1, \dots, N\}$, a basis for $H^k(X, \mathbb{C})$ is given by the forms*

$$\frac{d\alpha_{i_1}}{\alpha_{i_1}} \wedge \dots \wedge \frac{d\alpha_{i_k}}{\alpha_{i_k}}$$

ranging over subsets $\{i_1, i_2, \dots, i_k\} \subset \{1, 2, \dots, r\}$. In particular,

$$\dim H^k(X, \mathbb{C}) = \binom{r}{k}. \quad (4.48)$$

The algebra $H^*(X, \mathbb{C})$ (generic arrangement or otherwise) can be described in a combinatorial fashion and is called the Orlik-Solomon algebra.

For our purpose, the ambient space has dimension $N = n - 5$, there are $r = n - 1$ hyperplanes, and we are interested in the dimension of the homology $H_{n-5}(X, \mathbb{C})$. It is of course the same dimension as the corresponding cohomology $H^{n-5}(X, \mathbb{C})$. Hence, by the above theorem, the number of independent residues is

$$R = \dim H_{n-5}(X) = \binom{n-1}{n-5} = \binom{n-1}{4}. \quad (4.49)$$

⁷When the ambient space is \mathbb{C}^N , we say that the hyperplane arrangement is *generic* if $h_{i_1} \cap h_{i_2} \cap \dots \cap h_{i_r}$ has dimension $N - r$, for $r \leq n$. In other words, a hyperplane arrangement is generic if all intersections of hyperplanes have the expected dimension.

The residue relations have a simple geometrical interpretation (see also the discussion in [40]). Let $\{i_1, i_2, \dots, i_{n-5}\}$ denote the residue corresponding to the intersection of $n - 5$ hyperplanes $h_{i_1} \cap h_{i_2} \cap \dots \cap h_{i_{n-5}}$. As explained in the Section 4.4.1, the residue is fully antisymmetric in its labels. For example, when $n = 6$, the “hyperplanes” are just individual points $\{i\}$ in \mathbb{CP}^1 ; there are six such points. Since \mathbb{CP}^1 is isomorphic to a two-sphere S^2 , any contour surrounding all six can be contracted to a point. Hence the residue theorem states that the sum of the six residues is zero. Thus there is one relation among six residues, leaving five independent. This clearly agrees with the counting (4.49) for $n = 6$.

Let us now use this to understand the relations under which only $\binom{n-1}{4}$ of the $\binom{n}{5}$ residues are independent. Consider a choice of $n - 6$ hyperplanes, h_{i_k} with $k = 1, 2, \dots, n - 6$, in \mathbb{CP}^{n-5} . Imagine that we take the S^1 contours surrounding each of these h_i very small so that we effectively look at the subspace $\mathbb{CP}^1 = S^2$ of the intersection of those $n - 6$ hyperplanes. This subspace is (generically) intersected by the other hyperplanes h_j at 6 distinct points. Just as for the $n = 6$ case, a contour in \mathbb{CP}^1 that surrounds these six points can be contracted a point, and the sum of the six residues must vanish: the resulting residue theorem is

$$\sum_{j=1}^n \{i_1, i_2, \dots, i_{n-6}, j\} = 0. \quad (4.50)$$

This holds for any choice of $n - 6$ labels i_1, i_2, \dots, i_{n-6} ; hence we get a web of linear relations among the $\binom{n}{5}$ residues. The statement (4.49) is that under these relations, only $\binom{n-1}{4}$ residues are independent.

The counting of independent residues can be verified directly from the relations (4.50). While there may appear to be $\binom{n}{n-6}$ constraints in (4.50), some of them are redundant. Without loss of generality, consider only those for which all $i_k \neq n$, $k = 1, 2, \dots, n - 6$. There are $\binom{n-1}{n-6}$ distinct constraints of that sort. In each such sum, the index n will appear exactly once, namely when $j = n$, so we can solve for each residue that includes n in terms of residues which do not:

$$\{i_1, i_2, \dots, i_{n-6}, n\} = - \sum_{j=1}^{n-1} \{i_1, i_2, \dots, i_{n-6}, j\} \quad (4.51)$$

where $i_1, i_2, \dots, i_{n-6} \neq n$. This determines all of the residues labeled by n in terms of all of the others. Furthermore, since the first $n - 6$ indices form a unique set, all $\binom{n-1}{n-6}$ equations in (4.51) are independent.

The remaining equations in (4.50) have $i_k = n$ for some k , but they do not provide any

further constraints. To see this, use the antisymmetry and (4.51) to eliminate the index n :

$$\begin{aligned} \sum_{j=1}^n \{i_1, i_2, \dots, i_{n-7}, n, j\} &= - \sum_{j=1}^n \sum_{m=1}^{n-1} \{i_1, i_2, \dots, i_{n-7}, m, j\} \\ &= - \sum_{m=1}^{n-1} \left(\sum_{j=1}^n \{i_1, i_2, \dots, i_{n-7}, m, j\} \right) = 0. \end{aligned} \quad (4.52)$$

We conclude that all of the constraints with a fixed index n are redundant with the ones in (4.51). Hence, the number of independent constraints are $\binom{n-1}{n-6}$ and therefore the number of independent residues is

$$R = \binom{n}{n-5} - \binom{n-1}{n-6} = \binom{n-1}{n-5} = \binom{n-1}{4}, \quad (4.53)$$

in agreement with the dimension of the homology (4.49).

4.4.3 Applications

Residue Theorems as Boundary Operations

Let us now consider some applications of the NMHV residue theorems. The case of $n = 6$ is very well-known. There is just one constraint from (4.50),

$$\{1\} + \{2\} + \{3\} + \{4\} + \{5\} + \{6\} = 0, \quad (4.54)$$

or via (4.45) in terms of the 5-brackets it is the six-term identity

$$[23456] - [13456] + [12456] - [12356] + [12346] - [12345] = 0. \quad (4.55)$$

The LHS of this identity can be succinctly abbreviated as defining the **boundary operation** $\partial[123456]$; the relation to boundaries is explain in Section 4.4.4. More generally, we can write the boundary operation as

$$\partial[abcdef] = 0 \quad \longleftrightarrow \quad \sum_{a',b',c',d',e',f'=1}^n e^{i_1 i_2 \dots i_{n-6} a' b' c' d' e' f'} [a' b' c' d' e'] = 0, \quad (4.56)$$

where $\{i_1, \dots, i_{n-6}\}$ are the complement of $\{a, b, c, d, e, f\}$ in the set $\{1, 2, \dots, n\}$. The relation (4.45) between the 5-brackets and the residues now makes it clear that the boundary

conditions are equivalent to the residue theorems (4.50):

$$\sum_{j=1}^n \{i_1, i_2, \dots, i_{n-6}, j\} = 0 \quad \left\langle \frac{\{i_1, i_2, \dots, i_{n-6}\} = \overline{\{a, b, c, d, e, f\}}}{\phantom{\{i_1, i_2, \dots, i_{n-6}\}}} \right\rangle \quad \partial[abcdef] = 0. \quad (4.57)$$

Identities Among R -Invariants

Prior to the introduction of momentum twistors, the momentum space versions of the 5-brackets were denoted as R -*invariants* [87]:

$$R_{ijk} := [i, j-1, j, k-1, k]. \quad (4.58)$$

It was observed that the R -invariants obey the two identities

$$R_{i, i+2, j} = R_{i+2, j, i+1} \quad \text{and} \quad \sum_{s=3}^{k-2} \sum_{t=s+2}^k R_{1st} = \sum_{s=2}^{k-3} \sum_{t=s+2}^{k-1} R_{kst}. \quad (4.59)$$

for any $k = 1, 2, \dots, n$. These identities have been used in various applications, such as proving dual conformal invariance of the 1-loop ratio function in $\mathcal{N} = 4$ SYM [87, 95, 96]. Let us now review how these arise as a consequence of the symmetries and residue theorems of the 5-brackets.

The first identity in (4.59) follows straightforwardly from the antisymmetry of the 5-bracket [82]:

$$R_{i, i+2, j} = [i, i+1, i+2, j-1, j] = [i+2, j-1, j, i, i+1] = R_{i+2, j, i+1}. \quad (4.60)$$

For the second identity in (4.59), note that $R_{1st} = [1, s-1, s, t-1, t]$ vanishes for $s = 2$, so on the LHS of (4.59) the sum can trivially be extended to include $s = 2$. Then using the six-term identity resulting from $\partial[1, s-1, s, t-1, t, k] = 0$, the 5-bracket $[1, s-1, s, t-1, t]$ can be eliminated in favor of the five other 5-brackets appearing in the identity. This includes $[s-1, s, t-1, t, k] = [k, s-1, s, t-1, t]$, which vanishes trivially for $t = k$ and for $s = k-2$. Hence this part of the sum gives the desired RHS of (4.59). We are left to show that the sum of the remaining four terms vanishes; they are

$$\sum_{s=2}^{k-2} \sum_{t=s+2}^k \left([1, s-1, s, t-1, k] - [1, s-1, s, t, k] + [1, s-1, t-1, t, k] - [1, s, t-1, t, k] \right). \quad (4.61)$$

The sum of the first two terms telescopes to $\sum_{s=3}^{k-2} [1, s-1, s, s+1, k]$ while the sum of the last two terms collapses to $-\sum_{s=2}^{k-3} [1, s, s+1, s+2, k]$. These two sums are identical and

thus the sum (4.61) vanishes. This completes the derivation of the identities (4.59).

Locality and the NMHV Tree Superamplitude

For $k = n$, the second identity in (4.59) can be written

$$\sum_{i < j} [1, i - 1, i, j - 1, j] = \sum_{i < j} [n, i - 1, i, j - 1, j]. \quad (4.62)$$

Note that in this representation, the first label on the LHS plays no special role and can be replaced with any momentum twistor Z_* . Hence the sum of $[*, i - 1, i, j - 1, j]$ over all $i < j$ is independent of Z_* .

Let us now study the *pole structure* of the 5-brackets. A given 5-bracket has five poles, namely where each of the five 4-brackets in the denominator vanish. Consider two 5-brackets that differ by just one momentum twistor, e.g. $[abcdx]$ and $[abcdy]$. They share one common pole, namely $\langle abcd \rangle$. The singularity occurs on the subspace where the four momentum twistors $Z_{a,b,c,d}$ become linearly dependent. Since $Z_y \in \mathbb{CP}^3$ can be expressed as a linear combination of any four other (linearly independent) momentum twistors, we can write $Z_y = w_x Z_x + w_a Z_a + w_b Z_b + w_c Z_c$. Using this, it is straightforward to show that the residue at the pole $\langle abcd \rangle = 0$ is the same for $[abcdx]$ and $[abcdy]$. In other words, the residue of the pole $\langle abcd \rangle$ vanishes in the combination $[abcdx] - [abcdy]$.

It is natural to associate a boundary operation with the residues of the poles of the 5-brackets, written as

$$\partial[abcde] := [bcde] - [acde] + [abde] - [abce] + [abcd]. \quad (4.63)$$

The signs keep track of the relative signs of the residues.

It now follows that the cancellation of $[abcd]$ in $\partial([abcdx] - [abcdy])$ is equivalent to the statement that the residue of the pole at $\langle abcd \rangle = 0$ vanishes in the difference of the two five-brackets.

Physical poles in color-ordered tree-level scattering amplitudes are exactly those associated with vanishing Mandelstam invariants $(p_i + p_{i+1} + \dots)^2$ involving a sum of a subset of adjacent momenta. These are precisely associated with poles in the 5-brackets of the form $\langle i - 1, i, j - 1, j \rangle$ because of the identity [82, 93]

$$(p_i + p_{i+1} + \dots p_{j-1})^2 = \frac{\langle i - 1, i, j - 1, j \rangle}{\langle i - 1, i \rangle \langle j - 1, j \rangle}. \quad (4.64)$$

Poles *not* of the form $\langle i - 1, i, j - 1, j \rangle$ are spurious: they cannot appear in the tree-amplitude.

A straightforward algebraic exercise shows that

$$\partial \sum_{i < j} [* , i - 1, i, j - j, j] = \sum_{i < j} [i - 1, i, j - j, j]. \quad (4.65)$$

This means that all spurious poles in the LHS sum telescope to zero, leaving just the manifestly local poles. For $* = q = 1, 2, \dots, n$, this sum — times the MHV superamplitude — is exactly the expression one finds [97] as the solution to the BCFW recursion relation based on a $[q, q + 1]$ -supershift of the *tree NMHV superamplitude*

$$\mathcal{A}_n^{\text{NMHV}} = \mathcal{A}_n^{\text{MHV}} \sum_{i < j} [* , i - 1, i, j - j, j], \quad (4.66)$$

for $Z_* = Z_q$.⁸ From the point of view of the Grassmannian, we see that (4.66) results from a certain choice of contour. Thus, there are choices of contours for the Grassmannian integral such that the result is exactly the NMHV tree amplitude; such a contour what we called the ‘tree contour’. Note that the insistence of locality, in the sense of having only physical poles, allowed us to identify the tree contours.

It may seem puzzling that only a small subset of the residues produced by the Grassmannian integral appear in the BCFW-form (4.66) of the NMHV tree superamplitude: residues of the form $[q, i - 1, i, j - 1, j]$ are used, while residues such as $[1, 2, 4, 6, 8]$ or $[1, 3, 5, 7, 9]$ do not seem to play a role, other than through the residue theorems. It would be peculiar if the other residues of the same Grassmann degree were not relevant for NMHV amplitudes; it turns out that they are. It has been conjectured [40] that — in addition to the tree superamplitudes — the Grassmannian integral also produces all the Leading Singularities of all amplitudes in planar $\mathcal{N} = 4$ SYM at any loop order. The 1-loop NMHV ratio function [87, 95, 96] can be written in terms of the exactly the same types of residues $[q, i - 1, i, j - 1, j]$ as at tree-level, so one has to go to 2-loop order to encounter ‘non-tree’ residues in the Leading Singularities [40]. Also, it has been demonstrated that no new Leading Singularities appear beyond 3-loop order in the NMHV sector [98, 99], so the first three loop-orders of the NMHV amplitudes are expected to utilize the full set of residues produced by the Grassmannian integral $\mathcal{L}_{n,1}$.

⁸When Z_* is not selected to be one of the n momentum twistors Z_i of the external data, the expression (4.66) is a CSW-like representation of the NMHV superamplitude.

4.4.4 Cells, Permutations, and On-Shell Diagrams

So far we have described the evaluation of NMHV amplitudes in the language of contour integrals and residue theorems, but we find that it is also instructive to take a more abstract view and consider how it fits into the context of on-shell diagrams, permutations, and cells of the Grassmannian. Since the calculations in Section 4.4 were performed in the momentum twistor formulation, we will discuss that case first, and subsequently develop the corresponding story in the momentum space formulation.

Before delving into the details, it will be helpful to quickly review some terminology from [37]. Subspaces of the Grassmannian $\text{Gr}(k, n)$ can be classified into **cells** by specifying the ranks of cyclically consecutive columns C_i , that is $\text{rank}(\text{span}(C_i, C_{i+1}, \dots, C_j))$ for all cyclic intervals $[i, j]$. The *dimension* of a cell is the number of parameters it takes to specify a matrix representative modulo the $GL(k)$ redundancy. Cells are uniquely labeled by decorated permutations, which are “permutations” of the set $\{1, 2, \dots, n\}$ in which k of the elements are shifted beyond n .⁹ Throughout the remainder of this text, we will use ‘permutation’ and ‘decorated permutation’ interchangeably, but we will always mean the latter. Each permutation labels a cell by encoding the linear dependencies of the columns in a representative matrix of the cell. Treating the matrix columns c_i as k -vectors, a given permutation

$$\sigma = \{\sigma(1), \sigma(2), \dots\} = \{a, b, \dots\} \quad (4.67)$$

encodes that c_a is the first column with $a > 1 \pmod{n}$ such that c_1 is in the span of $\{c_2, c_3, \dots, c_a\}$. Similarly, c_2 is spanned by $\{c_3, \dots, c_b\}$, and so on. Entries for which $\sigma(i) = i$ imply that the i^{th} column is identically zero. As an example, consider the 5-dimensional cell in $\text{Gr}(2, 6)$ with representative matrix

$$\begin{pmatrix} 1 & 0 & c_{11} & c_{12} & 0 & c_{14} \\ 0 & 1 & c_{21} & c_{22} & 0 & 0 \end{pmatrix}. \quad (4.68)$$

One can easily verify that this cell is labeled by the permutation $\sigma = \{3, 4, 6, 8, 5, 7\}$.

The cell with maximal dimension $k(n - k)$ in $\text{Gr}(k, n)$ is known as the **top cell**, and it is the unique cell in which at a generic point none of the $k \times k$ minors vanish in a representative matrix. Since none of the consecutive minors vanish, each column must be spanned by the next k columns, and therefore the top cell is labeled by a permutation of the form

$$\sigma_{\text{top}} = \{1 + k, 2 + k, \dots, n + k\}. \quad (4.69)$$

⁹The decorated permutations will be familiar to practitioners of the juggling arts, where they are also referred to as “juggling patterns.” The decoration encodes that balls can only be thrown forward.

Momentum Twistor Space

The n -particle NMHV integral in momentum twistor space (4.39) is an integral over the $(n - 1)$ -dimensional top cell of $\text{Gr}(1, n)$, which has a representative $1 \times n$ matrix C , as in (4.38). Since the minors of C are determinants of 1×1 matrices (i.e. numbers), the top cell is represented by matrices with all non-zero entries.

The external data enters through the delta functions $\delta^{4|4}(C \cdot \mathcal{Z})$. The four independent bosonic delta functions fix all degrees of freedom for any 4-dimensional cell of $\text{Gr}(1, n)$. In order to reach a 4d cell from the top cell, one must set $n - 5$ of the minors to zero. This is done in practice by choosing an $(n - 5)$ -dimensional contour γ_{abcde} that encircles a point where only five of the coordinates, i.e. minors, are non-vanishing. For a given choice of a, b, c, d, e , the result of evaluating the contour integral is an integral (that will be fully localized by the delta functions) over a unique 4d cell labeled by the decorated permutation

$$\sigma_{abcde} = \{1, 2, \dots, \overset{a}{a-1}, \overset{b}{b}, \overset{c}{a+1}, \dots, \overset{c}{c}, \dots, \overset{d}{d}, \dots, \overset{e}{e}, \dots, a+n, \dots, n\}, \quad (4.70)$$

where all entries are self-identified except those at positions a, b, c, d, e (marked above). The bosonic delta functions fix the remaining degrees of freedom and leave the residue $\{i_1, i_2, \dots, i_{n-5}\}$, which is related to the five-bracket $[abcde]$ via equation (4.45). In the momentum twistor Grassmannian integral, all 4d cells meet the support of the delta-function at NMHV level thanks to the 5-term Schouten identity (4.42). (This is specific to NMHV level; it is not the case for higher k amplitudes.)

Momentum Space

The momentum space version of the Grassmannian integral was given in (4.15). For NMHV we have $\tilde{k} = k + 2 = 3$, so the relevant Grassmannian is $\text{Gr}(3, n)$. The top cell of $\text{Gr}(3, n)$ is $(3n - 9)$ -dimensional and is labeled by the decorated permutation

$$\tilde{\sigma}_{\text{top}} = \{4, 5, \dots, n + 3\}. \quad (4.71)$$

The representative matrices are $3 \times n$ and for the top cell all 3×3 minors are non-vanishing.

The momentum space Grassmannian integral (4.15) has $2n$ bosonic delta functions, and as we noted in Section 4.2.3, four of them ensure external momentum conservation; similarly, eight of the fermionic delta functions impose supermomentum conservation. The remaining bosonic delta functions fix all degrees of freedom in $(2n - 4)$ -dimensional cells of $\text{Gr}(3, n)$. Each of these cells is labeled by a unique decorated permutation of the appropriate dimension.

Each permutation is also associated with a representative *on-shell diagram* (or plabic graph) following the techniques introduced in [37]. For example, the permutation $\tilde{\sigma} = \{3, 5, 6, 7, 9, 8, 11\}$ is represented by the graph in Figure 4.1. The permutation is obtained from the graph by following the ‘left-right paths’ from each external leg, turning left at white vertices and right at black vertices; Figure 4.1 shows one such path, yielding $\tilde{\sigma}(4) = 7$.

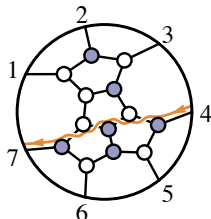


Figure 4.1: An on-shell diagram representation of the permutation $\tilde{\sigma} = \{3, 5, 6, 7, 9, 8, 11\}$. The ‘left-right path’ between external vertices 4 and 7 shows $\tilde{\sigma}(4) = 7$.

The value of each on-shell diagram is computed by associating each black/white vertex with a 3-point superamplitude, MHV or anti-MHV, respectively. External lines carry the information of the external data while for each internal line an integral must be performed over the corresponding momentum and Grassmann-variables. For details, see [37]. The point that will be important for us in the following is that the vertices enforce special 3-particle kinematics, namely a white vertex with legs has $\lambda_a \propto \lambda_b \propto \lambda_c$ while a black vertex imposes the equivalent condition on the $\tilde{\lambda}$ ’s.

In order to go from the $(3n - 9)$ -dimensional top cell in $\text{Gr}(3, n)$ to a $(2n - 4)$ -dimensional cell, we need to eliminate $(3n - 9) - (2n - 4) = n - 5$ degrees of freedom by taking an $(n - 5)$ -dimensional contour around singularities of the integrand. Of course one could evaluate the integral by first changing variables following the procedure of Section 4.3 and treating the resulting integral in momentum twistor space, but we would like to treat the integral directly in momentum space. Unfortunately, this turns out to be a difficult problem due to the non-linear nature of the n consecutive minors in the denominator. It is not *a priori* sufficient to simply take $n - 5$ of the minors to vanish. While this would land in a cell of the correct dimension, there are many $(2n - 4)$ -dimensional cells which cannot be reached by this technique. This failure is due to the appearance of so-called ‘composite singularities’, which occur when one or more of the minors factorize on the zero-locus of a subset of the coordinates [40]. The dlog forms constructed in [37] resolve many of these difficulties, but there are still some challenges associated with such forms as we mention in the Outlook.

Relating the Spaces

In general, there are more $(2n - 4)$ -dimensional cells in $\text{Gr}(3, n)$ than 4-dimensional cells in $\text{Gr}(1, n)$, so it may seem puzzling at first that the twistor and momentum twistor integrals of Section 4.3 are supposed to be equivalent. However, at this point we have not yet imposed the bosonic delta functions. NMHV cells are special because all 4d momentum twistor cells meet the support of the delta function. The same is not true of the momentum space cells; all, and only those, cells which meet the delta function support also have momentum twistor duals, but there are some momentum space cells of the correct dimension $(2n - 4)$ which do not intersect the delta function support and therefore have no corresponding cell in the Grassmannian with momentum twistor formulation.

From the associated on-shell diagrams it is easy to see which NMHV momentum space cells will not be supported for generic momenta: any two external legs that are connected by a path containing vertices of only one color are forced by the delta functions at each vertex to have parallel momenta. This condition is not satisfied for generic external data; hence those residues vanish. For example, consider the 10d cell in $\text{Gr}(3, 7)$ labeled by the permutation $\tilde{\sigma} = \{4, 5, 6, 7, 9, 10, 8\}$. A representative on-shell diagram is shown in Figure 4.2. Since the momenta on legs 1 and 7 are not generically parallel, this cell is not supported by the delta functions.

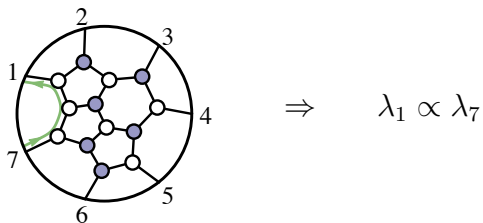


Figure 4.2: An on-shell diagram representation of the permutation $\tilde{\sigma} = \{4, 5, 6, 7, 9, 10, 8\}$. External legs 1 and 7 are connected by a path with all white vertices, which forces their respective momenta to be parallel.

This feature can also be seen from the permutations associated with such cells. Going from twistors to momentum twistors in Section 4.3, we required that the B plane contains the λ 2-plane; see equation (4.21). If B does not contain a generic 2-plane, this imposes a constraint on the external momenta; in other words, this cell does not intersect the delta function support for generic external momenta. In terms of the permutations, the requirement that B contains a generic 2-plane is that $(\tilde{\sigma}(i) - i) \geq 2$ for all i (no column may be in the span of its nearest neighbor, and in particular no column may be zero). To see why, suppose that there exists some i such that $(\tilde{\sigma}(i) - i) = 0$ or 1 . Then $b_i \in \text{span}\{b_{i+1}\}$ where b_i is the i^{th} column of B . Any 2-plane $\lambda \subset B$ would have to satisfy $\langle i, i + 1 \rangle = 0$, which

is clearly not satisfied for generic momenta. Furthermore, recall that the overall Jacobian of the transformation from twistors to momentum twistors, which is just the MHV superamplitude (see equation (4.37)), is singular precisely when $\langle i, i+1 \rangle = 0$ for some i . In the example permutation above, $\tilde{\sigma}(7) = 8$, so for the λ plane to be contained in this cell it would have to satisfy $\langle 71 \rangle = 0$. Hence such a cell cannot have a momentum twistor dual.

Given that the number of cells that meet the support of the delta functions is identical in both spaces, it is not surprising that the permutations which label such cells are related. The permutations for supported momentum space cells $\tilde{\sigma}$ can be obtained directly from momentum twistor labels σ by the following map:

$$\tilde{\sigma}(i) = \sigma(i+1) + 1. \quad (4.72)$$

The inverse map from momentum space permutations to momentum twistor permutations, when it exists, was presented in eq. (8.25) of [37]. Since the momentum space permutations have physically meaningful on-shell diagram representatives, this map also provides a way to associate representative on-shell diagrams with momentum twistor cells of dimension 4.¹⁰

It is perhaps more surprising that non-vanishing residues in momentum space can also be labeled by $(n-5)$ -index sequences similar to those which label the momentum twistor residues (4.45). From (4.26), we see that the vanishing of the i^{th} minor in momentum twistor space implies that the $(i-1)^{\text{th}}$ (consecutive) minor in momentum space vanishes as well. Since there are no composite singularities in NMHV momentum twistor space, those residues are uniquely labeled by the set of vanishing minors, $\{i_1, i_2, \dots, i_{n-5}\}_C$ (not to be confused with a permutation label). By (4.26), we can label the non-vanishing momentum space residues by a similar list of vanishing momentum space minors:

$$\{i_1, i_2, \dots, i_{n-5}\}_C \sim \{i_1 - 1, i_2 - 1, \dots, i_{n-5} - 1\}_B. \quad (4.73)$$

However, setting a collection of $(n-5)$ distinct consecutive minors to vanish in momentum space does not uniquely specify a cell in the Grassmannian. Instead one obtains a union of cells, of which exactly one will have kinematical support. For example, suppose $n = 7$ and we take the cell labeled by $\sigma = \{2, 3, 4, 5, 8, 6, 7\}$, given by the vanishing of the 6th and 7th minors. Then by (4.72), we have $\tilde{\sigma} = \{4, 5, 6, 9, 7, 8, 10\}$, and the minors labeled by columns (5, 6, 7) and (6, 7, 1) vanish. There is exactly one other cell of dimension $2n - 4 = 10$ for which exactly these same minors vanish, namely $\tilde{\sigma}' = \{4, 5, 6, 8, 9, 7, 10\}$. However, $\tilde{\sigma}'$ does not have kinematical support. This can be seen directly from the two corresponding on-shell

¹⁰A diagrammatic representation directly in momentum twistor space has also been recently developed [100].

diagrams in Figure 4.3. The second one vanishes for generic external data since it requires $\lambda_6 \propto \lambda_7$.

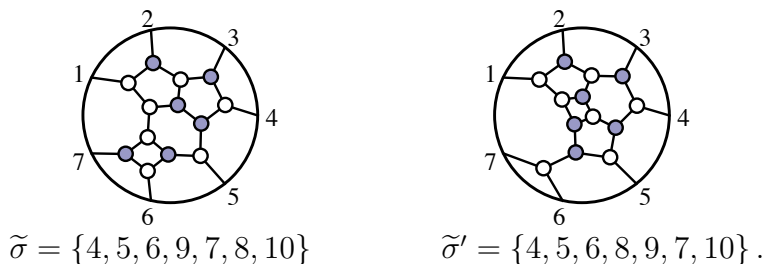


Figure 4.3: Two diagrams representing cells of the appropriate dimension for which the 6th and 7th minors vanish. Only the left diagram has kinematical support for generic momenta.

In general, the momentum space residue $\{i_1 - 1, i_2 - 1, \dots, i_{n-5} - 1\}_B$ is just the residue for the cell $\tilde{\sigma}$. Recalling the Jacobian from Section 4.3, we have the following relationship between residues in momentum twistor and momentum space:

$$\mathcal{A}_n^{\text{MHV}} \{i_1, i_2, \dots, i_{n-5}\}_C = \{i_1 - 1, i_2 - 1, \dots, i_{n-5} - 1\}_B. \quad (4.74)$$

It is also suggestive that, even though the general contours may be difficult to handle, the residues relevant for physics may be easier to study since they will not involve any composite residues. We leave this for future work.

Pushing the Boundaries

In Section 4.4.3 we used the boundary operation in two different contexts: one encoded the residue theorems that give linear relations among 5-brackets, the other selected residues of poles in the five brackets. Let us now see how these arise as boundary limits in the momentum twistor space Grassmannian.

Let us begin with a 4d cell in the NMHV Grassmannian $\text{Gr}(1, n)$. It is characterized by having precisely five non-vanishing entries in the representative matrix, say $c_{a,b,c,d,x}$. The boundaries of this 4d cell are the 3d cells obtained by setting one extra entry of the representative matrix to zero, i.e. there are five 3d boundaries. Suppose we go on the boundary characterized by $c_x = 0$. Then there is not generically support on the delta functions in the Grassmannian integral, because they then enforce $c_a Z_a + c_b Z_b + c_c Z_c + c_d Z_d = 0$. This is a constraint on the external data that requires the momentum twistors $Z_{a,b,c,d}$ to be linearly dependent. That is equivalent to the statement that the 4-bracket $\langle abcd \rangle$ vanishes and, as we know from (4.44), this is precisely one of the poles in 5-bracket $[abcdx]$ associated with the residue of our 4d cell. Similarly, we see that the five poles of $[abcdx]$ are precisely in

1-1 correspondence with the 3d boundaries of the corresponding 4d cell. This justifies the terminology “boundary operation” used in the discussion in Section 4.4.3. The relative signs in (4.63) come from the orientations of the boundaries.

Two 4d cells labeled by non-vanishing entries $c_{a,b,c,d,x}$ and $c_{a,b,c,d,y}$, respectively, share one common 3d boundary characterized by $c_x = 0$ and $c_y = 0$. As we know from the analysis in Section 4.4.3, the residue of the associated pole at $\langle abcd \rangle$ cancels in the difference of the associated 5-brackets, $[abcdx] - [abcdy]$. Analogously, the shared boundary between the cells cancels in the sum if they are oppositely oriented. The locality condition of having no pole $\langle abcd \rangle$ for (a, b, c, d) not of the form $(i, i + 1, j, j + 1)$ translates to the requirement that all shared boundaries not of the corresponding form must be oppositely oriented. These locality conditions, together with the fact that the amplitude is a sum of 4d cells, determine the formula (4.66).

The residue theorems (4.56) also have a boundary interpretation in the Grassmannian: boundaries of 5d cells give different equivalent ways of writing the same amplitude formula. We interpret the 4d cells associated with the 5-bracket residues as the boundary of a 5d cell defined by having precisely six non-vanishing entries in the representative matrices, say $c_{a,b,c,d,e,f}$. The six 4d boundaries of this 5d cell are associated with sending one of these six entries to zero. Meanwhile, the Grassmannian integral on the 5d cell is a contour integral on \mathbb{CP}^1 with six poles, corresponding to the 4d boundaries above. The sum of the residues at these six poles must therefore be zero by Cauchy’s theorem. This is our familiar residue theorem (4.50), and we see now why it is natural to associate it with a boundary operation.

4.5 3d ABJM Grassmannian

The fascinating relation between cells of Grassmannian and scattering amplitudes of 4d $\mathcal{N} = 4$ SYM has a parallel in 3d ABJM theory [85, 86]. Previously, an ABJM Grassmannian was developed for external data in momentum space [42, 43, 44, 88]. The purpose of this section is to apply the strategy from Section 4.3 to derive the ABJM Grassmannian in momentum twistor space.

4.5.1 Momentum Space ABJM Grassmannian

ABJM theory is a 3-dimensional $\mathcal{N} = 6$ superconformal Chern-Simons matter theory with 4 complex fermions ψ^A and 4 complex scalars X^A , transforming in the $\mathbf{4}$ and $\bar{\mathbf{4}}$ under the $SU(4) \sim SO(6)$ R-symmetry. The physical degrees of freedom are the matter fields, and the symmetries imply that the only non-vanishing amplitudes have even multiplicity, in

particular one can show that $n = 2k + 4$ for the N^k MHV sector. (For further discussion of 3d kinematics and ABJM amplitudes, see Chapter 11 of the review [34].)

A 3d momentum vector p_i can be encoded in a symmetric 2×2 matrix p_i^{ab} . The on-shell condition requires it to have vanishing determinant, so we can write $p_i^{ab} = \lambda_i^a \lambda_i^b$, with $a, b = 1, 2$ being $SL(2, \mathbb{R})$ indices. One version of the 3d spinor helicity formalism uses these 2-component commuting spinors λ' to encode the two on-shell degrees of freedom needed for a null 3d momentum vector. As in 4d, we can form the antisymmetric angle-bracket product $\langle ij \rangle := \epsilon_{ab} \lambda_i^a \lambda_j^b$, although in 3d there are no square-spinors. The $\mathcal{N} = 6$ on-shell superspace for 3d ABJM theory involves three Grassmann variables η'_{iI} with $SU(3) \subset SU(4)$ R-symmetry indices $I = 1, 2, 3$. We are denoting the λ'_i s (and η'_{iI} s) with primes to distinguish them from a different formulation of the 3d spinor helicity formalism to be introduced in Section 4.5.2.

In on-shell superspace, the states of ABJM theory are organized in two on-shell supermultiplets

$$\begin{aligned}\Phi &= X_4 + \eta'_A \psi^A - \frac{1}{2} \epsilon^{ABC} \eta'_A \eta'_B X_C - \eta'_1 \eta'_2 \eta'_3 \psi^4, \\ \bar{\Psi} &= \bar{\psi}_4 + \eta'_A \bar{X}^A - \frac{1}{2} \epsilon^{ABC} \eta'_A \eta'_B \bar{\psi}_C - \eta'_1 \eta'_2 \eta'_3 \bar{X}^4.\end{aligned}\tag{4.75}$$

The superfield Φ is thus bosonic in nature while Ψ is fermionic. The states of the color-ordered tree-level superamplitude in planar ABJM are arranged with alternating Φ and Ψ , e.g. $\mathcal{A}_n(\Phi\Psi\Phi\Psi\dots)$, and as a result they do not obey the cyclic invariance $i \rightarrow i + 1$ of superamplitudes in planar $\mathcal{N} = 4$ SYM. Instead, the planar ABJM superamplitudes are invariant under $i \rightarrow i + 2$, up to a sign of $(-1)^{n/2+1}$.

The leading singularities of ABJM theory, and consequently the tree-level amplitudes, enjoy an $OSp(6|4)$ Yangian symmetry [101, 102], and are given as residues of the following Grassmannian integral [42, 43, 44, 88]:

$$\mathcal{L}_{2\tilde{k};\tilde{k}} = \int \frac{d^{2\tilde{k}^2} B'}{GL(\tilde{k})} \frac{\delta^{\tilde{k}(\tilde{k}+1)/2}(B' \cdot B'^T) \delta^{2\tilde{k}|3\tilde{k}}(B' \cdot \Lambda')}{m'_1 m'_2 \cdots m'_k},\tag{4.76}$$

where $\tilde{k} = k + 2 = \frac{n}{2}$ and $\Lambda'_i = (\lambda'_i | \eta'_i)$ is the external data given in 3d momentum space. The denominator contains the product of the first \tilde{k} consecutive minors m'_i of B' .¹¹ The bosonic

¹¹We note here that for k even this means that the states of the superamplitude are $\mathcal{A}_n(\Phi\Psi\Phi\Psi\dots)$ while for k odd they are $\mathcal{A}_n(\Psi\Phi\Psi\Phi\dots)$. This ensures the correct little group scaling in 3d, for which the superamplitude is invariant for Φ states and changes signs for Ψ states. Alternatively, one can replace $m_1 m_2 \cdots m_{\tilde{k}}$ by $\sqrt{m_1 m_2 \cdots m_n}$. The two forms are equivalent up to signs depending on the branch of solutions to the orthogonal constraint [42].

delta-functions enforce the $\frac{1}{2}\tilde{k}(\tilde{k} + 1)$ constraints

$$0 = B' \cdot B'^T = \sum_i B'_{\alpha i} B'_{\beta i} = \sum_{i,j} B'_{\alpha i} B'_{\beta j} g^{ij}, \quad (4.77)$$

with $g^{ij} = \delta^{ij}$ is the trivial metric and $\alpha, \beta = 1, 2, \dots, \tilde{k}$. Thus, in momentum space, the Grassmannian for ABJM theory is an **orthogonal Grassmannian** (also known as an **isotropic Grassmannian** in the mathematics literature) defined as the space of null \tilde{k} -planes in an n -dimensional space equipped with an internal metric g^{ij} . The metric is trivial in momentum space. We will denote an orthogonal Grassmannian as $\text{OG}(\tilde{k}, n)$.¹² Because of the quadratic condition $B' \cdot B'^T = 0$, the orthogonal Grassmannian has two distinct components.

The dimension of the integral (4.76) is

$$2\tilde{k}^2 - \tilde{k}^2 - \frac{1}{2}\tilde{k}(\tilde{k} + 1) - 2\tilde{k} + 3 = \frac{(\tilde{k} - 2)(\tilde{k} - 3)}{2}, \quad (4.78)$$

where the “+3” is because momentum conservation is automatically encoded in the bosonic delta-functions; this will become evident in the following.

Note that in general the metric for a Grassmannian need not be diagonal nor proportional to the identity. For example, positivity for cells of $\text{OG}(\tilde{k}, n)$ is defined with the metric of alternating signs $(+, -, +, \dots, -)$ [44]. In the following we will see that in converting (4.76) into momentum twistor space, we will naturally encounter more general metrics g and denote the corresponding orthogonal Grassmannian as $\text{OG}_g(\tilde{k}, n)$.

4.5.2 3d Momentum Twistors

We would now like to introduce 3d momentum twistors.¹³ A natural way to define momentum twistor variables in 3d is to reduce it from 4d. With the 4d conformal group $SO(2, 4) \sim SU(4)$, a natural way to introduce momentum twistors is to first define 4d spacetime as a projective plane in 6d. This “embedding space” formalism [104, 105, 106, 107] introduces a 6d coordinate Y^{AB} , which is anti-symmetric in the $SU(4)$ indices A, B . 4d spacetime is then defined to be the subspace $Y^2 = \epsilon_{ABCD} Y^{AB} Y^{CD} = 0$ with the projective identification $Y \sim rY$ (for r a real or complex number, depending on the context). A solution to the

¹²We remark that in the theory of planar electrical networks, the orthogonal Grassmannian defined with respect to the metric $g^{ij} = \delta_{i,j+\tilde{k}} + \delta_{i,j-\tilde{k}}$ appears [89, 90]. Curiously, the combinatorics of ABJM amplitudes and of planar electrical networks are very closely related, but there is as yet no conceptual explanation of this.

¹³See [103] for an alternative definition.

constraint $Y^2 = 0$ is to write Y^{AB} as a bi-twistor:

$$Y_i^{AB} = Z_i^A Z_{i-1}^B. \quad (4.79)$$

To honor the projective constraint $Y_i \sim rY_i$, the Z_i s must be defined projectively, $Z_i \sim rZ_i$. Here $i = 1, 2, \dots, n$ label n points Y_i in the embedding space.

Consider now the 3d analogue for which the embedding space is 5d. We can start with the 6d space and introduce an $SO(2, 3)$ -invariant constraint to remove the extra degree of freedom. A natural choice is to impose a $SO(2, 3) \sim Sp(4)$ tracelessness condition on Y :

$$Y^{AB}\Omega_{AB} = 0, \quad \Omega_{AB} = \begin{pmatrix} 0 & -I \\ I & 0 \end{pmatrix}. \quad (4.80)$$

This also implies that the bi-twistors Z_i must satisfy:

$$Z_i^A Z_{i+1}^B \Omega_{AB} = 0. \quad (4.81)$$

Note that (4.81) is projectively well-defined, so we can construct the 3d momentum twistor as a familiar 4d momentum twistor $Z_i = (\lambda_i, \mu_i)$ subject to the constraint:

$$\langle\langle i, i+1 \rangle\rangle := Z_i^A Z_{i+1}^B \Omega_{AB} = \langle \mu_i \lambda_{i+1} \rangle - \langle \mu_{i+1} \lambda_i \rangle = 0. \quad (4.82)$$

We now need to identify the relation between λ_i and λ'_i . Recall that in three dimensions, a massless momentum can be parameterized as $p_i = E_i(1, \sin \theta_i, \cos \theta_i)$, where E_i is the energy. In bi-spinor notation, we can deduce:

$$\lambda'_{ia} \lambda'_{ib} = p_{iab} = E_i \begin{pmatrix} -1 + \cos \theta_i & \sin \theta_i \\ \sin \theta_i & -1 - \cos \theta_i \end{pmatrix} \rightarrow \lambda'_{ia} = i\sqrt{2E_i} \begin{pmatrix} -\sin \frac{\theta_i}{2} \\ \cos \frac{\theta_i}{2} \end{pmatrix}. \quad (4.83)$$

Now since Z_i is defined projectively, the components of Z_i must have well-defined projective scalings. This is not possible with $Z_i = (\lambda'_i, \mu_i)$ because p_i is not invariant under the scaling $\lambda'_i \rightarrow t_i \lambda'_i$. Consequently, $y_i = p_i - p_{i+1}$ cannot have any nice homogenous scaling property and neither can μ_i , since the latter is defined through the incidence relation $\mu_i^a = y_i^{ab} \lambda'_{ib}$.

The resolution is to parameterize the 3d kinematics in a fashion that is similar to 4d. We define

$$\lambda_{ia} = \begin{pmatrix} -\sin \frac{\theta_i}{2} \\ \cos \frac{\theta_i}{2} \end{pmatrix}, \quad \tilde{\lambda}_{ia} = -2E_i \lambda_{ia} \quad (4.84)$$

such that we now have $p_i = \lambda_i \tilde{\lambda}_i$. For simplicity, we set $\tilde{E}_i = -2E_i$ in the following. Note

that the number of degrees of freedom for each particle is still 2 and that p_i is now invariant under the following scaling rules:

$$\lambda_i \rightarrow t_i \lambda_i, \quad \tilde{E}_i \rightarrow t_i^{-2} \tilde{E}_i. \quad (4.85)$$

Since p_i (and hence y_i) is invariant, μ_i has the same scaling property as λ_i through the new incidence relation

$$\mu_i^a = y_i^{ab} \lambda_{ib} = y_{i+1}^{ab} \lambda_{ib} : \quad \mu_i \rightarrow t_i \mu_i. \quad (4.86)$$

With the incidence relation (4.86) and the symmetry of the y_i -matrices, the constraint (4.82) is automatically satisfied

$$\langle \mu_i \lambda_{i+1} \rangle - \langle \mu_{i+1} \lambda_i \rangle = \lambda_{ia} y_i^{ab} \lambda_{i+1,b} - \lambda_{i+1,a} y_{i+1}^{ab} \lambda_{ib} = 0. \quad (4.87)$$

Thus we have deduced a suitable form of 3d momentum twistor which has a well defined projective property. It has many of the same properties as its 4d cousin, for example (4.10) holds, and one can directly derive the 3d versions of the relations (4.11):

$$\begin{aligned} \tilde{\lambda}_i &= \frac{\langle i+1, i \rangle \mu_{i-1} + \langle i, i-1 \rangle \mu_{i+1} + \langle i-1, i+1 \rangle \mu_i}{\langle i-1, i \rangle \langle i, i+1 \rangle}, \\ \tilde{\eta}_{iA} &= \frac{\langle i+1, i \rangle \eta_{i-1,A} + \langle i, i-1 \rangle \eta_{i+1,A} + \langle i-1, i+1 \rangle \eta_{iA}}{\langle i-1, i \rangle \langle i, i+1 \rangle}. \end{aligned} \quad (4.88)$$

where we define $\tilde{\eta}_i := \eta'_i \sqrt{\tilde{E}_i}$.

In summary, we have found that the new momentum space variables

$$\lambda_i = \frac{1}{\sqrt{\tilde{E}_i}} \lambda'_i, \quad \tilde{\lambda}_i = \sqrt{\tilde{E}_i} \lambda'_i, \quad \tilde{\eta}_i = \eta'_i \sqrt{\tilde{E}_i} \quad (4.89)$$

facilitate the introduction of 3d momentum supertwistors $\mathcal{Z}_i = (\lambda_i, \mu_i | \eta_i)$, which are just like the 4d ones but subject to the constraints (4.82). Also, in addition to the $SL(4)$ -invariant $\langle ijkl \rangle$ defined in (4.43), we now have a 2-bracket invariant

$$\langle\langle ij \rangle\rangle := Z_i^A Z_j^B \Omega_{AB}. \quad (4.90)$$

As noted in (4.82), the projection from 4d momentum twistors to 3d ones is defined by $\langle\langle i, i+1 \rangle\rangle = 0$. The 4-brackets and 2-brackets are related via a version of the Schouten identity:

$$\langle ijkl \rangle = \langle\langle ij \rangle\rangle \langle\langle kl \rangle\rangle + \langle\langle ik \rangle\rangle \langle\langle lj \rangle\rangle + \langle\langle il \rangle\rangle \langle\langle jk \rangle\rangle. \quad (4.91)$$

This follows from the identity $\epsilon_{ABCD} = -\Omega_{AB}\Omega_{CD} - \Omega_{AC}\Omega_{DB} - \Omega_{AD}\Omega_{BC}$. Note that the RHS of (4.91) has the same form as the 2d Schouten identity for angle-brackets, but the LHS has the non-vanishing contraction with the Levi-Civita symbol because the momentum twistors are 4-component objects.

As a side-remark, we note that just as the parameterization in (4.84) can be viewed as a descendant from the 4d spinor helicity variables, it also has another 2d sibling: the 2d momentum twistors that correspond to taking $\theta = 0$ or π in (4.84):

$$\lambda_i|_{\theta_i=0} = \begin{pmatrix} 0 \\ 1 \end{pmatrix} =: \lambda^+, \quad \tilde{\lambda}^+ = \tilde{E}_i \lambda^+, \quad \lambda_i|_{\theta_i=\pi} = \begin{pmatrix} -1 \\ 0 \end{pmatrix} =: \lambda^-, \quad \tilde{\lambda}^- = \tilde{E}_i \lambda^-. \quad (4.92)$$

The superscript (+, -) indicates which of the two distinct light-cone directions contains the corresponding momentum:

$$\lambda_i^+ \tilde{\lambda}_i^+ = p_i^+ = \begin{pmatrix} 0 & 0 \\ 0 & \tilde{E}_i \end{pmatrix}, \quad \lambda_i^- \tilde{\lambda}_i^- = p_i^- = \begin{pmatrix} \tilde{E}_i & 0 \\ 0 & 0 \end{pmatrix}. \quad (4.93)$$

These 2d momentum variables have been used to study scattering amplitudes of planar $\mathcal{N} = 4$ SYM limited to 2d kinematics [108, 109].

4.5.3 Derivation of ABJM Momentum Twistor Space Grassmannian

We are now ready to convert the integral formula in (4.76) to momentum twistor space.¹⁴ First we change variables $B'_{\alpha i} = \sqrt{\tilde{E}_i} B_{\alpha i}$, $\lambda'_i = \tilde{\lambda}_i / \sqrt{\tilde{E}_i}$, $\eta'_i = \tilde{\eta}_i / \sqrt{\tilde{E}_i}$, so that only the variables in (4.84) appear in the bosonic delta functions:

$$\mathcal{L}_{2\tilde{k};\tilde{k}} = J_E \int \frac{d^{2\tilde{k}^2} B}{GL(\tilde{k}) m_1 m_2 \cdots m_{\tilde{k}}} \delta^{\tilde{k}(\tilde{k}+1)/2}(B_{\alpha i} B_{\beta j} g^{ij}) \delta^{2\tilde{k}}(B \cdot \tilde{\lambda}) \delta^{(3\tilde{k})}(B \cdot \tilde{\eta}), \quad (4.94)$$

where the factor

$$J_E = \frac{\prod_{i=1}^n \tilde{E}_i^{\tilde{k}/2}}{(\tilde{E}_1 \tilde{E}_2 \tilde{E}_3 \cdots \tilde{E}_{\tilde{k}} \tilde{E}_{\tilde{k}+1} \cdots \tilde{E}_{n-2} \tilde{E}_{n-1})^{1/2}} \quad (4.95)$$

¹⁴A similar attempt was initiated in [110] with a different definition of 3d momentum twistors. As a result, projectivity was not well defined.

comes from the scaling of the measure and the minors. The $2\tilde{k}$ -dimensional metric g^{ij} is

$$g^{ij} = \begin{pmatrix} \tilde{E}_1 & 0 & 0 & 0 \\ 0 & \tilde{E}_2 & 0 & 0 \\ 0 & 0 & \ddots & 0 \\ 0 & 0 & 0 & \tilde{E}_{2k} \end{pmatrix}. \quad (4.96)$$

Just as in 4d, the delta function $\delta^{2\tilde{k}}(B \cdot \tilde{\lambda})$ requires B to be orthogonal to the $\tilde{\lambda}$ -plane, and by momentum conservation ($\sum_i \lambda_i \tilde{\lambda}_i = 0$), the B -plane must therefore contain the λ -plane. We can use this to gauge-fix part of the $GL(\tilde{k})$ as in 4d:

$$B_{\alpha i} = \begin{pmatrix} B_{\hat{\alpha} i} \\ \lambda_i^1 \\ \lambda_i^2 \end{pmatrix}, \quad (4.97)$$

where $\hat{\alpha} = 1, \dots, k$ and $k = \tilde{k} - 2$. With this gauge choice, the remaining delta functions become¹⁵

$$\delta^{\tilde{k}(\tilde{k}+1)/2}(B_{\alpha i} B_{\beta j} g^{ij}) \delta^{3\tilde{k}}(B \cdot \tilde{\eta}) \rightarrow \delta^3(\mathcal{P}) \delta^6(\mathcal{Q}) \delta^{k(k+1)/2}(B_{\hat{\alpha} i} B_{\hat{\beta} j} g^{ij}) \delta^{2k|3k}(B_{\hat{\alpha}} \cdot \tilde{\Lambda}), \quad (4.98)$$

where $\tilde{\Lambda} = (\tilde{\lambda}|\tilde{\eta})$, \mathcal{P} is the total momentum, and \mathcal{Q} is the total supermomentum.

Now we can follow the steps from the $\mathcal{N} = 4$ SYM analysis in Section 4.3 to convert the Grassmannian integral to one with momentum twistor external data:

1. The relation between the momentum space data and the momentum twistor variables allow us to introduce a new variable $C_{\hat{\alpha} i} = B_{\hat{\alpha} j} Q_{ji}$, with Q defined in (4.30) (see also (F.2)).
2. Rewrite the minors using (4.26).
3. To invert the relation $B_{\hat{\alpha} j} Q_{ji}$, we use translation invariance T_k to fix $B_{\hat{\alpha} 1} = B_{\hat{\alpha} 2} = 0$, thus obtaining $B_{\hat{\alpha} \hat{j}} = C_{\hat{\alpha} \hat{i}} (Q^{-1})_{\hat{i} \hat{j}}$, with $\hat{i} = 3, \dots, n$. A simple expression for Q^{-1} is given in (F.13), and we verify its form in Appendix F.2. This allows us to change variables from $B_{\hat{\alpha} \hat{j}}$ to $C_{\hat{\alpha} \hat{j}}$. We restore the integration variables to include $C_{\hat{\alpha} 1}, C_{\hat{\alpha} 2}$ by introducing $\delta^{2k}(C \cdot \lambda)$.

¹⁵Note that for $\alpha = \tilde{k} - 1, \tilde{k}$, we have $\lambda_i B_{\hat{\beta} j} g^{ij} = \lambda_i B_{\hat{\beta} i} \tilde{E}_i = \tilde{\lambda}_i B_{\hat{\beta} i}$

This brings us to the following final form of the Grassmannian integral ($n = 2k + 4$):

$$\mathcal{L}_{n;k} = J \times \delta^3(\mathcal{P}) \delta^{(6)}(\mathcal{Q}) \times \int \frac{d^{kn}C}{GL(k)} \frac{\delta^{k(k+1)/2} \left(C_{\hat{\alpha}\hat{i}}(Q^{-1})_{\hat{i}\hat{j}} C_{\hat{\beta}\hat{k}}(Q^{-1})_{\hat{k}\hat{l}} g^{\hat{j}\hat{l}} \right) \delta^{4k|3k}(C \cdot \mathcal{Z})}{M_2 M_3 \cdots M_{k+3}}, \quad (4.99)$$

where $\mathcal{Z}_i = (Z_i | \eta_i)$ and

$$J = (\langle 12 \rangle \langle 23 \rangle \cdots \langle n1 \rangle)^k \frac{\prod_{i=1}^n \tilde{E}_i^{(k+2)/2}}{\tilde{E}_{k+2}^{(k+2)/2} \prod_{i=1}^{k+1} \left(\tilde{E}_i^{1/2} \langle i, i+1 \rangle \langle n-i-1, n-i \rangle \tilde{E}_{n-i}^{1/2} \right)^i}. \quad (4.100)$$

It is straightforward to verify that the $GL(1)$ weight of the integral in (4.99) cancels. It should be noted that here and in the remainder of this section, the angle-brackets $\langle ij \rangle$ are now composed of the λ -spinors, not the λ' 's.

There is an unsatisfactory feature in (4.99): the sum in the constraint $CQ^{-1}CQ^{-1}g = 0$ only runs over $\hat{i}, \hat{j} = 3, \dots, n$, and therefore $(Q^{-1}Q^{-1}g)^{\hat{i}\hat{j}}$ cannot be interpreted as an orthogonal constraint on the Grassmannian C . This is because an orthogonal Grassmannian is defined with a metric G^{ij} whose indices run over the full n -dimensional space. However, using the delta function support we can rewrite $CQ^{-1}CQ^{-1}g$ in terms of a non-degenerate effective metric G^{ij} specified by the external data. To see this note that on the support of the $\delta(C \cdot \lambda)$, we have

$$C_{\hat{\alpha}\hat{i}}(Q^{-1})_{\hat{i}\hat{j}} = \sum_{i=2}^{\hat{j}-1} C_{\hat{\alpha}i} \langle i \hat{j} \rangle. \quad (4.101)$$

For example, for $k = 1$, we have $\hat{i}, \hat{j} = 3, \dots, 6$ and

$$C_{\hat{\alpha}\hat{i}}(Q^{-1})_{\hat{i}\hat{j}} = \begin{pmatrix} C_{\hat{\alpha}2} \langle 23 \rangle \\ C_{\hat{\alpha}2} \langle 24 \rangle + C_{\hat{\alpha}3} \langle 34 \rangle \\ C_{\hat{\alpha}2} \langle 25 \rangle + C_{\hat{\alpha}3} \langle 35 \rangle + C_{\hat{\alpha}4} \langle 45 \rangle \\ C_{\hat{\alpha}2} \langle 26 \rangle + C_{\hat{\alpha}3} \langle 36 \rangle + C_{\hat{\alpha}4} \langle 46 \rangle + C_{\hat{\alpha}5} \langle 56 \rangle \end{pmatrix}. \quad (4.102)$$

Note that $C_{\hat{\alpha}1}$ and $C_{\hat{\alpha}6}$ do not appear in (4.102). We can use $C \cdot \lambda = 0$ to get an expression in terms of a ‘conjugate’ set of $C_{\hat{\alpha}i}$ ’s, e.g.

$$C_{\hat{\alpha}\hat{i}}(Q^{-1})_{\hat{i}\hat{j}} = - \begin{pmatrix} C_{\hat{\alpha}1} \langle 13 \rangle + C_{\hat{\alpha}4} \langle 43 \rangle + C_{\hat{\alpha}5} \langle 53 \rangle + C_{\hat{\alpha}6} \langle 63 \rangle \\ C_{\hat{\alpha}1} \langle 14 \rangle + C_{\hat{\alpha}5} \langle 54 \rangle + C_{\hat{\alpha}6} \langle 64 \rangle \\ C_{\hat{\alpha}1} \langle 15 \rangle + C_{\hat{\alpha}6} \langle 65 \rangle \\ C_{\hat{\alpha}1} \langle 16 \rangle \end{pmatrix}. \quad (4.103)$$

To reveal the symmetric form of the effective (inverse) metric \tilde{G}^{ij} defined via $C_{\hat{\alpha}i}C_{\hat{\beta}j}\tilde{G}^{ij} = (C_{\hat{\alpha}}Q^{-1})(C_{\hat{\beta}}Q^{-1})g$, we take the symmetric (in $\hat{\alpha}$ and $\hat{\beta}$) product of two copies of $C_{\hat{\alpha}i}(Q^{-1})_{ij}$, one in the form (4.102) and one in the conjugate form (4.103). For $k = 1$, we find

$$\tilde{G}^{ij} = \frac{1}{2} \begin{pmatrix} 0 & 0 & -\langle 1|2|3\rangle & -\langle 1|2+3|4\rangle & -\langle 1|2+3+4|5\rangle & 0 \\ 0 & 0 & 0 & \langle 2|3|4\rangle & \langle 2|3+4|5\rangle & \langle 2|3+4+5|6\rangle \\ * & 0 & 0 & 0 & \langle 3|4|5\rangle & \langle 3|4+5|6\rangle \\ * & * & 0 & 0 & 0 & \langle 4|5|6\rangle \\ * & * & * & 0 & 0 & 0 \\ 0 & * & * & * & 0 & 0 \end{pmatrix}, \quad (4.104)$$

where the terms denoted by $*$ are related to the ones explicitly written via symmetry, $\tilde{G}^{ji} = \tilde{G}^{ij}$. The notation $\langle i|l|j\rangle = \langle i|p_l|j\rangle$ uses $\lambda_i g^{il} \lambda_l = p_i$ (only l summed over). To rewrite the entries of the effective matrix in terms of the momentum twistors, note that

$$\langle i|(p_i + p_{i+1} + \dots + p_{j-1})|j\rangle = \langle i|(y_i - y_j)|j\rangle = Z_i^A Z_j^B \Omega_{AB} =: \langle\langle ij\rangle\rangle \quad (4.105)$$

The constraints (4.82) on the external data is $\langle\langle i, i+1\rangle\rangle = 0$, so in terms of the double-bracket (4.105), we can write the effective metric as

$$\tilde{G}^{ij} = \langle\langle ij\rangle\rangle \quad \text{for } 2 \leq i < j \leq n, \quad \tilde{G}^{1j} = -\langle\langle 1j\rangle\rangle \quad \text{for } 2 \leq j \leq n. \quad (4.106)$$

This defines a non-degenerate metric only for $n > 4$, since for $n = 4$ the only non-trivial elements are $C_1\langle\langle 13\rangle\rangle C_3$ and $C_2\langle\langle 24\rangle\rangle C_4$ which vanishes under the support of $\delta(C \cdot Z)$.

While the metric is non-degenerate for $n > 4$, it is not manifestly cyclic symmetric. Let us first inspect the orthogonality condition:

$$0 = \sum_{1 \leq i, j \leq n} C_{\hat{\alpha}i} C_{\hat{\beta}j} \tilde{G}^{ij} = \sum_{3 \leq i < j \leq n} C_{\hat{\alpha}i} C_{\hat{\beta}j} \langle\langle ij\rangle\rangle + (\hat{\alpha} \longleftrightarrow \hat{\beta}). \quad (4.107)$$

The second equality is obtained using $C \cdot Z = 0$. Now, to see that the orthogonality constraint is indeed cyclic invariant, one uses $C \cdot Z = 0$ to show that $\sum_{4 \leq i < j \leq n+1} C_{\hat{\alpha}i} C_{\hat{\beta}j} \langle\langle ij\rangle\rangle = \sum_{3 \leq i < j \leq n} C_{\hat{\alpha}i} C_{\hat{\beta}j} \langle\langle ij\rangle\rangle$, with the understanding that $n+1$ equals 1. This suffices to prove that the condition $CGC^T = 0$ is cyclic invariant.

Next, we can simplify the sum of n cyclic copies of the orthogonality condition to find

an equivalent, manifestly cyclic invariant, form of the metric:

$$\left\{ \begin{array}{l} G^{i,i+2} = \frac{k}{n} \langle\langle i, i+2 \rangle\rangle \\ G^{i,i+3} = \frac{k-1}{n} \langle\langle i, i+3 \rangle\rangle \\ \vdots \\ G^{i,i+k+1} = \frac{1}{n} \langle\langle i, i+k+1 \rangle\rangle \end{array} \right. \quad (4.108)$$

while $G^{ij} = 0$ for all other cases.

We then have the final form for the cyclically invariant momentum twistor Grassmannian integral for 3d ABJM. It is an orthogonal Grassmannian whose metric (4.108) depends on the external data:

$$\mathcal{L}_{n;k} = J \times \delta^3(\mathcal{P}) \delta^{(6)}(\mathcal{Q}) \times \int \frac{d^{kn}C}{GL(k)} \frac{\delta^{\frac{k(k+1)}{2}} \left(C_{\hat{\alpha}i} G^{ij} C_{\hat{\beta}j} \right) \delta^{4k|3k}(C \cdot \mathcal{Z})}{M_2 M_3 \cdots M_{k+3}}, \quad (4.109)$$

with $n = 2k + 4$ and the Jacobian J given in (4.100). Note that the integral is indeed projectively invariant under rescaling of $Z_i \rightarrow t_i Z_i$ due to the form of the effective metric G^{ij} in (4.106).

The momentum twistor space Grassmannian integral for ABJM theory and $\mathcal{N} = 4$ SYM both have $4k$ bosonic delta functions $\delta^{4k}(C \cdot \mathcal{Z})$, but in addition the ABJM integral (4.109) has the extra orthogonal constraint. In $\mathcal{N} = 4$ SYM, the $(k(n-k)-4k)$ remaining degrees of freedom in the momentum twistor Grassmannian are localized by the minors. For ABJM, $k(k+1)/2$ of the $(k(n-k)-4k)$ degrees of freedom are localized by the orthogonal constraint, so the dimension of the integral (4.109) is

$$2(k+2)k - k^2 - 4k - \frac{1}{2}k(k+1) = \frac{k(k-1)}{2}, \quad (4.110)$$

the same as the dimension (4.78) of the momentum space Grassmannian integral (4.76). In particular, we note that for $n = 6$ (i.e. $k = 1$) the integral localizes completely. Because the orthogonality constraint is quadratic, there are two solution branches that the integral localizes on and we must add them to obtain the $n = 6$ tree-level ABJM superamplitude. This matches the observation that there is only one BCFW-diagram for the $n = 6$ ABJM amplitude, but the kinematic constraint is quadratic, so the diagram yields a two-term contribution. Those are the two terms given by the two branches of the orthogonal Grassmannian. In the following, we study the orthogonality condition and evaluate the integral (4.109) explicitly for $n = 6$.

4.5.4 The 6-point ABJM Amplitude in Momentum Twistor Space

For $n = 6$, the integral (4.109) becomes

$$\mathcal{L}_{6;1} = J_{234} \times \delta^3(\mathcal{P}) \delta^{(6)}(\mathcal{Q}) \int \frac{d^6 c}{GL(1)} \frac{\delta(c_i G^{ij} c_j) \delta^4(c \cdot Z) \delta^{(3)}(c \cdot \eta)}{c_2 c_3 c_4}, \quad (4.111)$$

where the Jacobian is given by (4.100) and is

$$J_{234} = \frac{\langle 12 \rangle \langle 23 \rangle \langle 34 \rangle \langle 45 \rangle \langle 56 \rangle \langle 61 \rangle \prod_{i=1}^6 \tilde{E}_i^{3/2}}{\tilde{E}_3^{3/2} \tilde{E}_1^{1/2} \langle 12 \rangle \langle 45 \rangle \tilde{E}_5^{1/2} \tilde{E}_2 \langle 23 \rangle^2 \langle 34 \rangle^2 \tilde{E}_4}. \quad (4.112)$$

If we had picked a representation of the original momentum space Grassmannian integral with a different product of 3 consecutive minors in the denominator, the integral $\mathcal{L}_{6;1}$ would have a denominator $c_i c_{i+1} c_{i+2}$ and the associated Jacobian $J_{i,i+1,i+2}$ would be obtained from (4.112) by relabeling of the lines.

Orthogonality Constraint and Symmetry Under $i \rightarrow i + 2$

In the momentum space Grassmannian (4.76), the orthogonality condition $B' \cdot B'^T = 0$ implies the following relation among the minors:

$$m'_i m'_{i+1} = (-1)^{\tilde{k}-1} m'_{i+\tilde{k}} m'_{i+1+\tilde{k}}, \quad (4.113)$$

with $\tilde{k} = k + 2$ and indices mod n . The relation (4.113) is key for proving that the Grassmannian integral (4.111) has the appropriate cyclic invariance under $i \rightarrow i + 2$.

The equivalent relation for the minors of the momentum twistor space Grassmannian will depend on the external data. Let us work out what it is for $n = 6$ and how it can be used to prove that our momentum twistor Grassmannian (4.111) has cyclic symmetry $i \rightarrow i + 2$.

Using $C \cdot Z = 0$, direct evaluation of the orthogonality condition gives

$$\begin{aligned} 0 &= c_i G^{ij} c_j = \frac{1}{6} \left(c_1 \langle\langle 13 \rangle\rangle c_3 + c_2 \langle\langle 24 \rangle\rangle c_4 + c_3 \langle\langle 35 \rangle\rangle c_5 + c_4 \langle\langle 46 \rangle\rangle c_6 + c_5 \langle\langle 51 \rangle\rangle c_1 + c_6 \langle\langle 62 \rangle\rangle c_2 \right) \\ &= \frac{1}{2} c_3 \langle\langle 35 \rangle\rangle c_5 - \frac{1}{2} c_2 \langle\langle 26 \rangle\rangle c_6. \end{aligned} \quad (4.114)$$

Since the metric G^{ij} is cyclic invariant, other forms of the constraint can be obtained from cyclic symmetry: there are three distinct ones:

$$c_3 \langle\langle 35 \rangle\rangle c_5 = c_2 \langle\langle 26 \rangle\rangle c_6, \quad c_4 \langle\langle 46 \rangle\rangle c_6 = c_3 \langle\langle 31 \rangle\rangle c_1, \quad c_5 \langle\langle 51 \rangle\rangle c_1 = c_4 \langle\langle 42 \rangle\rangle c_2. \quad (4.115)$$

It follows from the first two identities in (4.115) that

$$c_1 c_2 = \frac{\langle\langle 35 \rangle\rangle \langle\langle 46 \rangle\rangle}{\langle\langle 26 \rangle\rangle \langle\langle 31 \rangle\rangle} c_4 c_5 = \frac{\langle 3456 \rangle}{\langle 6123 \rangle} c_4 c_5. \quad (4.116)$$

The second equality follows from (4.91). The property (4.116) is the equivalent of (4.113) in momentum twistor space. The other relations $c_i c_{i+1} \propto c_{i+3} c_{i+4}$ (indices mod 6) are obtained from cyclic relabeling of (4.116).

Let us now examine the cyclic symmetry $i \rightarrow i + 2$. The only part that changes in the integral of (4.111) is the product $c_2 c_3 c_4$, which becomes $c_4 c_5 c_6$. It follows from a cyclic version of (4.116) that

$$\frac{1}{c_2 c_3 c_4} = \frac{\langle 1234 \rangle}{\langle 4561 \rangle} \frac{1}{c_4 c_5 c_6} \quad (4.117)$$

It is not hard to see that the factor $\langle 1234 \rangle / \langle 4561 \rangle$ is exactly compensated by the non-trivial Jacobian: by (4.112) and its version with $i \rightarrow i + 2$

$$\frac{J_{456}}{J_{234}} = \frac{\langle 12 \rangle \tilde{E}_2 \langle 23 \rangle^2 \tilde{E}_3 \langle 34 \rangle}{\langle 45 \rangle \tilde{E}_5 \langle 56 \rangle^2 \tilde{E}_6 \langle 61 \rangle} = \frac{\langle\langle 13 \rangle\rangle \langle\langle 24 \rangle\rangle}{\langle\langle 46 \rangle\rangle \langle\langle 51 \rangle\rangle} = \frac{\langle 1234 \rangle}{\langle 4561 \rangle}. \quad (4.118)$$

Here we use the form (4.105) of the $Sp(4)$ -product to write

$$\langle\langle i, i + 2 \rangle\rangle = \langle i | p_{i+1} | i + 2 \rangle = \langle i, i + 1 \rangle \tilde{E}_{i+1} \langle i + 1, i + 2 \rangle. \quad (4.119)$$

Then, with the identity (4.91), we conclude that

$$\frac{J_{234}}{c_2 c_3 c_4} = \frac{J_{456}}{c_4 c_5 c_6} \quad (4.120)$$

and that the $n = 6$ integral is invariant under $i \rightarrow i + 2$; the non-trivial orthogonality condition and the overall Jacobian factor nicely conspire to give this result.

Evaluation of the $n = 6$ Integral

To evaluate the integral (4.111), we first use the bosonic delta function constraints for the six-point momentum twistor space Grassmannian, which fixes four of the integrations. As in Section 4.4.1, we use the 5-term Schouten identity (4.42) to expand the constraint $C \cdot Z = 0$

on a basis of four Z 's, although now we find it convenient to solve for c_2, c_3, c_5, c_6 :

$$\begin{aligned} c_2 &= \frac{c_1 \langle 3561 \rangle + c_4 \langle 3564 \rangle}{\langle 2356 \rangle}, & c_3 &= \frac{c_1 \langle 5612 \rangle + c_4 \langle 5642 \rangle}{\langle 2356 \rangle}, \\ c_5 &= \frac{c_1 \langle 6123 \rangle + c_4 \langle 6423 \rangle}{\langle 2356 \rangle}, & c_6 &= \frac{c_1 \langle 1235 \rangle + c_4 \langle 4235 \rangle}{\langle 2356 \rangle}. \end{aligned} \quad (4.121)$$

Evaluating the delta-function this way will generate a Jacobian factor of $1/\langle 2356 \rangle$. The orthogonal constraint (4.114) becomes

$$0 = c_i G^{ij} c_j = \frac{\langle\langle 42 \rangle\rangle \langle 3456 \rangle}{2 \langle 2356 \rangle} \left(c_4^2 - c_1^2 \frac{\langle\langle 31 \rangle\rangle^2 \langle 5612 \rangle}{\langle 1234 \rangle \langle 3456 \rangle} \right). \quad (4.122)$$

We fix the $GL(1)$ gauge by setting $c_1 = \langle 2356 \rangle$; the result is going to be independent of the gauge, but this choice will simplify the other c_i 's. The solution to (4.122) is then:

$$c_4^\pm = \pm \frac{\langle\langle 31 \rangle\rangle \langle 5612 \rangle \langle 2356 \rangle}{\sqrt{D}}, \quad (4.123)$$

where $D = \langle 1234 \rangle \langle 3456 \rangle \langle 5612 \rangle = -\prod_{i=1}^6 \langle\langle i, i+2 \rangle\rangle$.

The Grassmannian integral localizes on the two solutions (4.123):

$$I_i = \int \frac{\delta(c_i G^{ij} c_j) \delta^4(c \cdot Z) \delta^{(3)}(c \cdot \eta)}{c_i c_{i+1} c_{i+2}} = \sum_{s=\pm 1} \frac{2 \langle 2356 \rangle}{2 c_4^s \langle\langle 42 \rangle\rangle \langle 3456 \rangle} \frac{\langle 2356 \rangle}{\langle 2356 \rangle} \frac{\delta^{(3)}(c \cdot \eta)}{c_i c_{i+1} c_{i+2}} \Big|_{c_4=c_4^s}, \quad (4.124)$$

where i depends on the organization of the external states (i.e. which 3 minors we selected at the starting point in momentum space). It is implicitly understood that on the RHS, $c_1 = \langle 2356 \rangle$ and $c_{2,3,5,6}$ are given by (4.121) with c_4 as in (4.123). The factor $2 \langle 2356 \rangle / 2 c_4^s \langle\langle 42 \rangle\rangle \langle 3456 \rangle$ is the Jacobian of the orthogonality condition (see footnote 3), the second $\langle 2356 \rangle$ in the numerator is the gauge-fixing Jacobian, and the $1/\langle 2356 \rangle$ comes from evaluating $\delta^4(c \cdot Z)$. The prefactors readily simplify and we get

$$I_i = \frac{\delta^{(3)}(c \cdot \eta)}{\sqrt{D} c_i c_{i+1} c_{i+2}} \Big|_{c_4=c_4^+} - \frac{\delta^{(3)}(c \cdot \eta)}{\sqrt{D} c_i c_{i+1} c_{i+2}} \Big|_{c_4=c_4^-}. \quad (4.125)$$

It is clear from (4.121) and (4.123) that the individual c_i 's are expressions with square roots. It may be worrisome to see such denominator terms arise from the Grassmannian integral; after all, we would expect the denominators to be a product of physical poles. However, the

expectation is warranted; for each i , just write

$$\frac{1}{c_i^\pm} = \frac{c_i^\mp}{c_i^\pm c_i^\mp}, \quad \text{where} \quad c_i^\pm := c_i|_{c_4=c_4^\pm} \quad \text{for } i = 2, 3, 5, 6. \quad (4.126)$$

The combinations $c_i^+ c_i^-$ are manifestly free of any square roots. Furthermore, after applications of the Schouten identities (4.42) and (4.91), one finds that each $c_i^+ c_i^-$ has a nice factorized form involving only 4-brackets:

$$\begin{aligned} c_1^+ c_1^- &= \langle 2356 \rangle^2, & c_2^+ c_2^- &= \frac{\langle 5613 \rangle \langle 6134 \rangle \langle 2356 \rangle}{\langle 6234 \rangle}, & c_3^+ c_3^- &= \frac{\langle 1245 \rangle \langle 5612 \rangle \langle 2356 \rangle}{\langle 2345 \rangle}, \\ c_4^+ c_4^- &= \frac{\langle 1235 \rangle \langle 5612 \rangle \langle 2356 \rangle^2}{\langle 2456 \rangle \langle 2345 \rangle}, & c_5^+ c_5^- &= \frac{\langle 6123 \rangle \langle 6134 \rangle \langle 2356 \rangle}{\langle 3456 \rangle}, & c_6^+ c_6^- &= \frac{\langle 1235 \rangle \langle 1245 \rangle \langle 2356 \rangle}{\langle 2456 \rangle}. \end{aligned} \quad (4.127)$$

Choosing $i = 2$ in (4.125) and using (4.127), we find

$$\begin{aligned} I_2 &= \sum_{s=\pm} \frac{\langle\langle 24 \rangle\rangle^2 \delta^{(3)}(c^{(s)} \cdot \eta)}{\langle 1234 \rangle \langle 5612 \rangle^2 \langle 1245 \rangle \langle 3461 \rangle \langle 2356 \rangle^3} \\ &\quad \times \left[\langle\langle 35 \rangle\rangle (\langle 1236 \rangle \langle 2456 \rangle - \langle 5612 \rangle \langle 2346 \rangle) + s\sqrt{D} (\langle\langle 26 \rangle\rangle \langle\langle 35 \rangle\rangle + \langle\langle 25 \rangle\rangle \langle\langle 36 \rangle\rangle) \right]. \end{aligned} \quad (4.128)$$

The result (4.128) for the 6-point amplitude has two terms because the orthogonal Grassmannian has two branches. To compare, the BCFW calculation of the 6-point amplitude involves only one diagram, but it gives rise to two terms, just as in (4.128), because the on-shell condition for 3d BCFW is not linear in the shift parameter z . See Chapter 11 of [34] for a review of 3d BCFW and its application in ABJM theory.

The expression (4.128) is probably not the ideal form of the 6-point residue, since its expected properties are not manifest. For example, the result for the $n = 6$ ABJM superamplitude should have $i \rightarrow i + 2$ cyclic symmetry of the integral, as discussed in Section 4.5.4; dressing (4.128) with the Jacobian from (4.112) should make it invariant under $i \rightarrow i + 2$, but this is not obvious.

Another point of concern about (4.128) are the apparent higher-order poles from the denominator-factors $\langle 5612 \rangle^2$ and $\langle 2356 \rangle^3$. The former is not too worrisome: using the identity (4.91) gives $\langle 5612 \rangle = -\langle\langle 51 \rangle\rangle \langle\langle 62 \rangle\rangle = -\langle 56 \rangle \tilde{E}_6 \langle 61 \rangle^2 \tilde{E}_1 \langle 12 \rangle$. Numerator factors can then cancel the individual angle brackets so that there are not double poles. The triple-pole at $\langle 2356 \rangle = 0$ would appear to be a worse problem because $\langle 2356 \rangle = \langle 23 \rangle \langle 56 \rangle y_{63}^2 \propto (p_6 + p_1 + p_2)^2$, which is not just a simple product of angle-brackets. However, it is not hard to show that the numerator factors conspire to cancel the extra powers in $\langle 2356 \rangle$ so that at most we have a simple pole at $\langle 2356 \rangle = 0$. A detailed argument is given in Appendix H. We leave further analysis of the momentum twistor form of the $n = 6$ ABJM amplitude for

future work.

Singularities of the Residues

As a warm up, let us briefly review how poles of the NMHV residues could be understood as boundaries of cells in the $\mathcal{N} = 4$ SYM Grassmannian. Choose a contour γ_{abcde} such that the integral (4.38) picks up the residue where $n-5$ c_i 's with $i \neq a, b, c, d, e$ vanish. The remaining five c_i 's are then fixed by the four bosonic delta functions $\delta^4(c \cdot Z)$ and the $GL(1)$ scaling, as discussed in Section 4.4.1; the result is the 5-bracket $[abcde]$. Its five poles can be described in the Grassmannian integral by forcing an extra c_i to be zero (as discussed in Section 4.4.4): for example, if $c_a = 0$, the delta-function $\delta^4(c \cdot Z)$ says that Z_b, Z_c, Z_d , and Z_e are linearly dependent, and hence $\langle bcde \rangle = 0$. This is precisely one of the five poles of the residue $[abcde]$.

Now consider the ABJM momentum twistor space Grassmannian (4.111) for $n = 6$. Since the integral is completely fixed by the bosonic delta functions and $GL(1)$, there is no contour to choose and the result is simply two terms that are conjugate to each other, one for each of the two branches determined by the orthogonal constraint. Let us gauge-fix the $GL(1)$ by setting $c_1 = 1$ and then analyze the constraints of the bosonic delta-functions when $c_2 = 0$. Via (4.114) and (4.115), the orthogonality condition with $c_2 = 0$ can be written

$$c_5 \langle\langle 51 \rangle\rangle = c_4 \langle\langle 42 \rangle\rangle c_2 = 0. \quad (4.129)$$

So we must have $c_5 = 0$, or $\langle\langle 51 \rangle\rangle = 0$. Examining each in turn:

- $c_2 = c_5 = 0$: using Ω_{AB} to dot Z_3 and Z_4 into the constraint $c \cdot Z = 0$, we find

$$\langle\langle 13 \rangle\rangle + c_6 \langle\langle 63 \rangle\rangle = 0 \quad \text{and} \quad \langle\langle 14 \rangle\rangle + c_6 \langle\langle 64 \rangle\rangle = 0. \quad (4.130)$$

For this to hold true with non-vanishing c_6 requires $\langle 6134 \rangle = 0$. The relations in $c \cdot Z = 0$ can then be solved to find

$$c_3 = \frac{\langle\langle 51 \rangle\rangle}{\langle\langle 35 \rangle\rangle}, \quad c_4 = \frac{\langle 6123 \rangle}{\langle 2346 \rangle}, \quad c_6 = \frac{\langle\langle 13 \rangle\rangle}{\langle\langle 36 \rangle\rangle}. \quad (4.131)$$

Thus $c_2 = c_5 = 0$ leaves the four other c_i non-zero but imposes the constraint $\langle 6134 \rangle = 0$ on the external data. This is precisely one of the poles in (4.128).

- $c_2 = 0$ and $\langle\langle 51 \rangle\rangle = 0$. Dotted Z_5 into $c \cdot Z = 0$ now gives $c_3 \langle\langle 35 \rangle\rangle = 0$.

If $c_3 = 0$, then $c \cdot Z = 0$ gives $c_4 \langle\langle 41 \rangle\rangle = 0$ and $c_4 \langle\langle 46 \rangle\rangle = 0$. If also $c_4 = 0$ then

we get a lower-dimensional subspace ($c_2 = c_3 = c_4 = 0$). If $c_4 \neq 0$, we must have $\langle\langle 41 \rangle\rangle = \langle\langle 46 \rangle\rangle = 0$ which in addition to $\langle\langle 51 \rangle\rangle = 0$ renders multiple 4-brackets to be zero.

If instead $c_3 \neq 0$, we must have $\langle\langle 35 \rangle\rangle = 0$. Consistency of $c \cdot Z = 0$ then requires $\langle 6134 \rangle = 0$ and this combined with $\langle\langle 51 \rangle\rangle = \langle\langle 35 \rangle\rangle = 0$ puts several constraints on the external data. The remaining conditions in $c \cdot Z = 0$ do not completely fix the rest of the c_i 's.

We conclude from the above that the three ‘boundaries’ $c_i = c_{i+3} = 0$ in the $n = 6$ orthogonal Grassmannian integral (4.111) correspond to poles of the form $\langle i+1, i+2, i+4, i+5 \rangle = 0$. These are exactly the three different 3-particle poles $P_{i+2, i+3, i+4}^2$ of the amplitudes: for example $P_{123}^2 = y_{14}^2 \propto \langle 6134 \rangle$. On the other hand, boundaries of the form $c_i = c_{i+1} = 0$ impose constraints among two-brackets (e.g. $\langle\langle 51 \rangle\rangle = \langle\langle 41 \rangle\rangle = \langle\langle 46 \rangle\rangle = 0$) which are akin to soft limits. Thus, as in the 4d case, we find that the cell boundaries of the Grassmannian correspond to poles in the residues.

The fact that locality is partially hidden in the orthogonal constraint was already observed in the derivation of the twistor string formula for ABJM theory [111],¹⁶ where locality is achieved as the momentum space Grassmannian is localized onto a Veronese map [41], $B_{\alpha,i}(a_i, b_i) = a_i^{\tilde{k}-\alpha} b_i^{\alpha-1}$. This reduces a $\text{Gr}(k, n)$ down to a $\text{Gr}(2, n)$ Grassmannian, parameterized by (a_i, b_i) . At 6-point, this localization was achieved by the orthogonal constraint. For higher-points, only part of the orthogonal constraint is relevant to the localization to the Veronese map. Thus we anticipate that for higher-points, the effective metric will continue to play an important role for the realization of locality.

4.6 Outlook

In this chapter, we presented a detailed review of the relationship between Grassmannian integral formulas of different external data and provided a new derivation to establish their equivalence. Using the new approach, we derived the momentum twistor version of the Grassmannian integral for ABJM theory. Contrary to the momentum space representation, which is an orthogonal Grassmannian with constant metric, the momentum twistor space representation corresponds to an orthogonal Grassmannian whose metric depends on the external data.

There are a number of interesting questions that can be tackled at this point. Recently the planar amplitudes of $\mathcal{N} = 4$ SYM have been identified as a single geometric object, the

¹⁶A twistor string whose vertex operators give the corresponding formula was later presented in [112].

amplituhedron [45, 46]. It is defined in the Grassmannian $\text{Gr}(k, k+4)$ via

$$Y_\alpha^I = C_{+, \alpha i} Z_{+i}^I, \quad (4.132)$$

where $C_{+, \alpha i}$ are cells in the positive Grassmannian¹⁷ $\text{Gr}(k, n)$ and Z_{+i}^I are $(k+4)$ -component vectors, $i = 1, \dots, n$, built linearly from the momentum supertwistors (see [45] for details). The array of n vectors Z_{+i}^I are viewed as elements in the positive Grassmannian $\text{Gr}(k+4, n)$. The amplituhedron is then the “volume-form” in this space, and it has logarithmic singularities at the boundaries of Y . It would be very appealing to derive this definition from the momentum twistor space Grassmannian integral. As a first step, one should be able to prove that the BCFW terms in momentum twistor space are associated with dimension $4k$ positive cells in $\text{Gr}(k, n)$. In principle, this is accomplished by the momentum twistor space on-shell diagrams introduced by He and Bai [100], where the individual cells are associated with diagrams that are again iteratively built from the fundamental 3-point vertices. On the other hand, from our analysis one might expect the existence of a straightforward map from cells in the momentum space Grassmannian to cells in the momentum twistor space Grassmannian. However as the minors of the two Grassmannians are related by a multiplicative string of spinor brackets, a priori it is not clear that positivity in one Grassmannian can be related to that of the other, even for the top-cell. Thus we see that positivity of the BCFW terms in momentum twistor space is non-trivial result, and should warrant further investigation.

Given that we have derived the momentum twistor space Grassmannian for ABJM theory, one can ask if there exists a geometric entity like the amplituhedron for ABJM? Supporting evidence for its existence includes the realization that BCFW recursion relations for the theory exists both at tree- and at loop-level, and when represented in terms of on-shell diagrams, stratifies the positive orthogonal Grassmannian. Unlike $\mathcal{N} = 4$ SYM, where positivity ensures locality, we have already seen that the orthogonal condition plays an important role as well. What is unclear is whether or not the condition is to be viewed as a condition on the cells, or on the space Y where the amplituhedron lives, perhaps both. Another interesting question is if there exist on-shell diagrams for cells in ABJM momentum twistor space Grassmannian such as those found for $\mathcal{N} = 4$ SYM [100]. One of the remarkable results in the on-shell diagram approach for cells of the momentum space Grassmannian, is that the gluing and merging of diagrams preserves orthogonality [37, 42]. In momentum twistor space, the orthogonality is now defined with a momentum twistor dependent metric. It would be very interesting if an iterative way of constructing cells exists such that the

¹⁷The positive Grassmannian, or non-negative Grassmannian to be precise, refers to the property that the $k \times n$ matrices are real-valued with all minors are greater or equal to zero.

orthogonality property of the smaller cells ensures that of the higher-dimensions ones.

In this chapter, we also studied residue theorems for the NMHV level in momentum twistor space and showed that an abstract homological point of view offered a clear geometric description. For amplitudes beyond NMHV, the combinatorics and geometry become much more difficult, and it is no longer the case that every momentum twistor cell of the appropriate dimension ($d = 4k$) has support for generic external data. Composite singularities become the norm, even in momentum twistor space, so the residue calculation outlined in Appendix G cannot be applied directly. Moreover, whereas the entries in the $k = 1$ matrix (4.38) can be interpreted as homogeneous coordinates on \mathbb{CP}^{n-1} , higher k Grassmannians do not have such simple geometric structure. Even the locations of poles become more complicated for $k > 1$ due to the non-linear dependence of the minors on the matrix entries. Instead of cutting out hyperplanes as in Section 4.4.2, the minors vanish on generally complicated surfaces. Understanding the geometric and homological structure of such spaces in a general sense remains a subject of active research in the mathematics community.

Despite the inherent mathematical challenges, the BCFW bridge decompositions of [37] suggest a possible route forward. The technique provides a robust way to generate coordinates on any cell of $\text{Gr}(k, n)$ with the useful property that all singularities of the integration measure are manifestly of the form $d\alpha/\alpha$ (similar to the dc/c structure of (4.39)). This eliminates the issue of composite residues at the cost of requiring multiple charts to cover all singularities.¹⁸ The existence of such a convenient representation of the Grassmannian integral offers compelling motivation to pursue higher k generalizations, and it will almost certainly lead to further insights regarding residues, residue theorems, superamplitudes, and locality constraints for all k and n .

¹⁸Until recently it was not known how to compare the orientations of those charts, but the resolution of this problem is the subject of [52] and is covered in the next chapter.

Chapter 5

Orientations of BCFW Charts on the Grassmannian

5.1 Motivation and Preview

Scattering amplitudes in 4d planar $\mathcal{N} = 4$ super Yang-Mills (SYM) theory can be formulated as contour integrals in the space of $k \times n$ matrices, modulo multiplication by a $GL(k)$ matrix; this is the Grassmannian manifold $\text{Gr}(k, n)$ [37]. Reformulating scattering amplitudes in this new framework has led to many interesting and unexpected mathematical structures in $\mathcal{N} = 4$ SYM such as on-shell diagrams [37, 100, 113] and the amplituhedron [45, 46, 114]. Many of the results extend also to 3d $\mathcal{N} = 6$ ABJM theory [85, 86] where several novel properties have emerged [42, 44, 51].

This chapter will focus on planar $\mathcal{N} = 4$ SYM theory, where the n -particle $N^k\text{MHV}$ tree amplitude can be obtained by evaluating the following integral:

$$\mathcal{A}_n^{(k)} = \mathcal{A}_n^{\text{MHV}} \oint_{\Gamma} \frac{d^{k \times n} C}{GL(k) M_1 M_2 \dots M_n} \delta^{4k|4k}(C \cdot \mathcal{Z}). \quad (5.1)$$

The prefactor $\mathcal{A}_n^{\text{MHV}}$ is the n -particle MHV amplitude, C is a $k \times n$ matrix of full rank, and \mathcal{Z} encodes the external data (momentum, particle type, etc.) as super-momentum twistors. In the denominator of the measure, M_i is the i^{th} consecutive k -minor of C , which means that it is the determinant of the submatrix of C with ordered columns $i, i + 1, \dots, i + k - 1 \pmod{n}$. The contour on which the integral should be evaluated is designated by Γ . The result is a sum over residues computed at poles of the integrand. There are generally many families of contours which produce equivalent representations of the amplitude due to residue theorems.

Each contour can be thought of as a product of circles wrapping around poles of the

integrand, the points where certain minors vanish. The minors are degree- k polynomials in the variables of integration, so the pole structure is generally very difficult to describe in the formulation (5.1). However, a technique was presented in [37] for generating charts on the space such that any individual codimension-1 residue occurs at a simple logarithmic singularity. Using one of those charts, the measure on a d -dimensional submanifold can be decomposed into a product of $d\alpha/\alpha = \text{dlog } \alpha$ quantities. We call this measure ω for future reference:

$$\omega = \frac{d^{k \times n} C}{GL(k) M_1 M_2 \dots M_n} \rightarrow \text{dlog } \alpha_d \wedge \text{dlog } \alpha_{d-1} \wedge \dots \wedge \text{dlog } \alpha_1. \quad (5.2)$$

Advantages to this formulation are that such charts are easy to generate and that every codimension-1 residue can be reached as a dlog singularity using only a small atlas of charts. A potential disadvantage is that directly relating two distinct charts is non-trivial; this could lead to sign ambiguities when combining individual residues into the amplitude. This is especially important because the residues contain non-local singularities that should cancel in the tree amplitude sum. Previously, such divergences were shown to appear in pairs, so they at least cancel mod 2 [37]. In Section 5.4 of this chapter, we demonstrate that for doubly-appearing poles the cancellation is exact,¹ which follows from the main result of this chapter: the Master Algorithm introduced in Section 5.3. However, we observe the presence of other non-physical singularities that appear to contribute individually in some Grassmannian representations of tree amplitudes but not in others. We describe the sources of such poles and explain how momentum conservation allows one to eliminate those apparently problematic singularities.

Summary of Results

The key development of this chapter is a systematic algorithm that generates the relative sign between any two BCFW charts on a submanifold, or *cell*, of the Grassmannian. Each chart is defined by a sequence of transpositions $(a_1 b_1)(a_2 b_2) \dots (a_d b_d)$ acting on a permutation labeling a 0-dimensional cell. Equivalently, each chart can be represented by a path through the poset (partially ordered set) of Grassmannian cells. Every transposition $(a_i b_i)$ corresponds to a factor of $\text{dlog } \alpha_i$ in (5.2).

To get a sense of the result, it is illustrative to consider the simple example of two charts defined by the sequences $(ab)(cd)$ and $(cd)(ab)$ with $a < b < c < d < a+n$. In the poset of cells, these sequences define distinct paths from a 0-dimensional cell labeled by σ_0 to a 2-dimensional cell labeled by σ , shown in Figure 5.1 with edges labeled by the corresponding transpositions:

¹The relative signs between NMHV residues were derived in [51], but that method does not easily generalize to higher- k amplitudes.

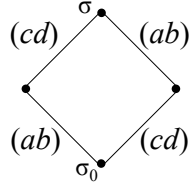


Figure 5.1: Two distinct sequences of transpositions connecting the 0-dimensional cell σ_0 to the 2-dimensional cell σ .

If we associate the coordinate α_1 with (ab) and α_2 with (cd) , then the dlog forms generated by the sequences are, respectively,

$$\omega = \text{dlog } \alpha_1 \wedge \text{dlog } \alpha_2, \quad \text{and} \quad \omega' = \text{dlog } \alpha_2 \wedge \text{dlog } \alpha_1. \quad (5.3)$$

Clearly the two forms differ by an overall sign, so the two coordinate charts are oppositely oriented. We can encode this property in the poset by weighting the edges with ± 1 such that the product of the edge weights around the loop in Figure 5.1 is -1 . One choice of suitable signs is shown in Figure 5.2. Then the relative orientation is given by the product of edge signs along the two paths.

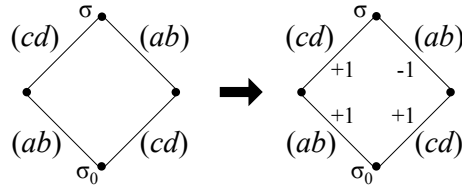


Figure 5.2: A choice of edge weights such that the product around the loop is -1 .

We show in Section 5.3.3 that the relative orientation between *any* two charts is equal to the product of edge signs around a closed loop in the poset. All the edges can be weighted such that the product of signs around every quadrilateral is -1 , just as in the example 5.2.² The closed loop is obtained by concatenating each input path (blue and green solid lines in Figure (5.3 A)) together with a sawtooth path connecting their 0d cells (thick red line in (5.3 A)) times -1 for each 1d cell along the connecting path. We call this method the **Master Algorithm**.

To prove that the **Master Algorithm** correctly yields the relative orientation, we introduce two preliminary algorithms in Section 5.3.1. When the two paths meet at a common 0d cell, illustrated in (5.3 B) with blue and green solid lines, Algorithm 1 splits the big loop into smaller loops, e.g. using the dashed black lines in (5.3 B), for which the relative orientations

²A technique developed by T. Lam and D. Speyer for assigning edge weights is presented in Appendix J [47].

can be computed directly from the corresponding plabic networks.³ If the paths end in different 0d cells, e.g. (5.3 C), Algorithm 2 additionally computes the relative sign between the source cells: We then use Algorithms 1 and 2 in Section 5.3.2 to demonstrate that the big

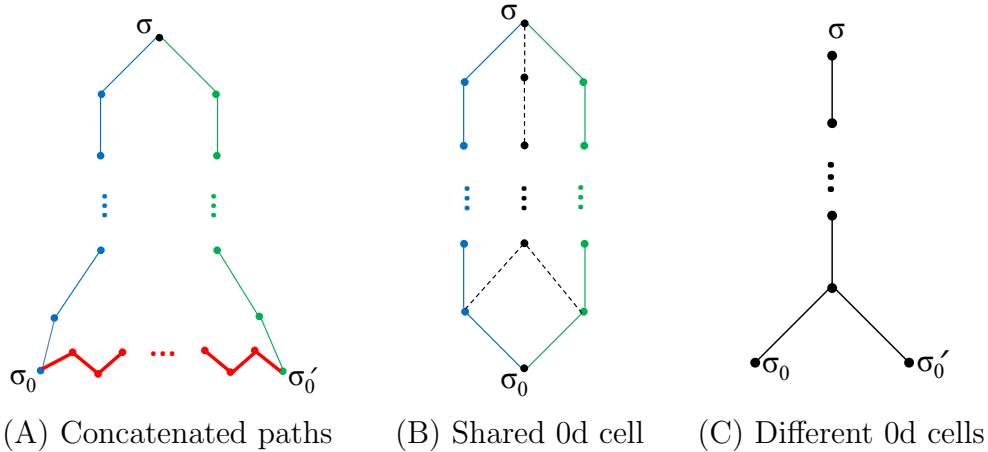


Figure 5.3: Different types of paths through the poset of cells.

loop (5.3 A) can always be split up into quadrilaterals, each of which contributes a factor of -1 to the overall sign. Finally in Section 5.3.3 it is shown that if the edges are appropriately decorated with ± 1 , then only those that make up the loop contribute to the end result (in addition to -1 from each 1d cell along the sawtooth path).

In Section 5.4, we show that the edge-weighting rules can also be used to compute relative signs between distinct residues by requiring further that all residue theorems are mutually consistent. Consequently, residues contributing to the tree amplitude are always decorated with signs so that all non-physical singularities that appear in pairs cancel exactly in the sum of residues. In the context of the on-shell BCFW recursion relations described in [37], this forces every term to have an appropriate sign whereby all non-local poles are guaranteed to cancel. A similar argument demonstrates the existence of a boundary operator that manifestly squares to zero. Some individual non-physical poles appear with unit multiplicity in the boundary of amplitude representations and thus do not cancel, so we identify the origin of those poles and demonstrate that the associated residues vanish. In addition, we present an interpretation of charts corresponding to decompositions with non-adjacent transpositions. We review the necessary background in Section 5.2 before presenting the algorithms in Section 5.3, and a few details are relegated to appendices.

During the development of this analysis, a different method for determining relative orientations was proposed independently by J. Bourjaily and A. Postnikov using determinants

³We thank R. Karpman for many helpful ideas and discussions regarding the details of the graph transformations.[115]

of certain large matrices. We computed the orientations of 500 distinct charts on the 10d cell $\{5, 3, 8, 9, 6, 7, 12, 10, 14, 11\} \in \text{Gr}(3, 10)$ with both methods and found perfect agreement [48]. The algorithms presented in this chapter have also been verified by checking a variety of charts whose orientations are known by other methods. The cancellation of all doubly-appearing poles in the tree amplitude has been confirmed explicitly for all $n = 5, \dots, 13$ and $k = 3, \dots, \lfloor n/2 \rfloor$, and the elimination of all individual non-physical poles using the criteria defined in Section 5.4 have been checked for the same set of parameters. All of the algorithms described here have been implemented in Mathematica as an extension of the *positroids* package included with the arXiv version of [116].

5.2 Background

5.2.1 Positroid Stratification

The positroid stratification is a decomposition of the Grassmannian $\text{Gr}(k, n)$ into submanifolds called *positroid cells* (or just *cells*). Cells can be classified according to the ranks of submatrices constructed out of cyclically consecutive columns of a representative matrix. The *top cell* of $\text{Gr}(k, n)$ is the unique cell of highest dimension, $d = k(n - k)$. All maximal $(k \times k)$ minors are non-vanishing in the top cell, so all chains of consecutive columns will be full rank. For example, a representative matrix of the top cell of $\text{Gr}(2, 4)$ is

$$C = \begin{pmatrix} 1 & 0 & c_{13} & c_{14} \\ 0 & 1 & c_{23} & c_{24} \end{pmatrix}, \quad (5.4)$$

where $c_{ij} \in \mathbb{C}$ are coordinates on the manifold such that none of the 2×2 minors vanish. All four parameters must be fixed to specify a point in the top cell, which is consistent with the expected dimension $d = 2(4 - 2) = 4$.

Lower dimensional cells are reached by fixing relations among the entries so that additional linear dependencies arise among consecutive columns. From a given cell, the accessible codimension-1 submanifolds are called the *boundaries* of that cell. The extra linear relations imply that various minors vanish in the measure of (5.1). Thus going to the boundary should be interpreted as taking a residue at the corresponding pole. Note that choosing a particular representative matrix amounts to selecting a chart on the cell, so some poles may not be accessible in certain charts. In the example above, the boundary where columns \vec{c}_2 and \vec{c}_3 are parallel is accessible by setting $c_{13} = 0$, but there is no way to reach the boundary where columns \vec{c}_1 and \vec{c}_2 are parallel in the stated chart. The latter boundary could be accessed in a $GL(2)$ -equivalent chart where a different set of columns were set to the identity.

A partial order can be defined on the set of positroid cells by setting $C \prec C'$ whenever C is a codimension-1 boundary of C' [117]. The poset structure is interesting for a number of reasons, several of which will be mentioned throughout the text. One such reason is that the poset of positroid cells in $\text{Gr}(k, n)$ is isomorphic to a poset of *decorated permutations*. Decorated permutations are similar to standard permutations of the numbers $1, \dots, n$, but differ in that k of the entries are shifted forward by n . To simplify the notation, we will use often ‘permutation’ to mean ‘decorated permutation’ since only the latter are relevant to us. Permutations will be written single-line notation using curly brackets; an example is given in (5.5). When referencing specific elements of a permutation, we will use the notation $\sigma(i)$ to mean the i^{th} element of the permutation σ , and with the understanding that $\sigma(i+n) = \sigma(i) + n$. A decorated permutation encodes the ranks of cyclically consecutive submatrices by recording, for each column \vec{c}_a , the first column c_b with $a \leq b \leq a+n$ such that $\vec{c}_a \in \text{span}(\vec{c}_{a+1}, \vec{c}_{a+2}, \dots, \vec{c}_b)$. The first inequality is saturated when $\vec{c}_a = 0$, and the second is saturated when \vec{c}_a is linearly independent of all other columns. Continuing with the example (5.4), the top cell of $\text{Gr}(2, 4)$ corresponds to the permutation

$$\sigma_{\text{top}} = \{3, 4, 5, 6\}, \quad (5.5)$$

which says that $1 \rightarrow 3$, $2 \rightarrow 4$, $3 \rightarrow 5 \equiv 1$, and $4 \rightarrow 6 \equiv 2$. In terms of the linear dependencies among columns of a representative matrix, it means $\vec{c}_1 \in \text{span}(\vec{c}_2, \vec{c}_3)$, $\vec{c}_2 \in \text{span}(\vec{c}_3, \vec{c}_4)$, $\vec{c}_3 \in \text{span}(\vec{c}_4, \vec{c}_5) \equiv \text{span}(\vec{c}_4, \vec{c}_1)$, and $\vec{c}_4 \in \text{span}(\vec{c}_5, \vec{c}_6) \equiv \text{span}(\vec{c}_1, \vec{c}_2)$.

Going to the boundary of a cell involves changing the linear relations among consecutive columns, so in permutation language, the boundary is accessed by exchanging two entries in σ . The transposition operation that swaps the elements at positions a and b is denoted by (ab) , with $a < b < a+n$; we call this the *boundary operation*. Note that σ only has positions $1, \dots, n$, but b can be greater than n . To account for this, we use

$$\sigma'(a) = \sigma(b) = \sigma(b-n) + n \quad \text{and} \quad \sigma'(b) = \sigma(a) \Rightarrow \sigma'(b-n) = \sigma(a) - n. \quad (5.6)$$

In the example (5.4), taking the boundary where $c_{13} = 0$ lands in a cell with linear dependencies specified by

$$\sigma' = \{4, 3, 5, 6\}. \quad (5.7)$$

This corresponds to exchanging the first and second elements of σ_{top} , i.e. the transposition (12).

Not all exchanges are allowed; for instance, applying the same transposition twice would

revert back to the initial cell, which is clearly not a boundary. The allowed boundary transpositions satisfy the following criteria:

$$a < b \leq \sigma(a) < \sigma(b) \leq a+n \quad \text{and} \quad \sigma(q) \notin (\sigma(a), \sigma(b)) \quad \forall q \in (a, b), \quad (5.8)$$

where (a, b) means the set $\{a + 1, b + 2, \dots, b - 1\}$. We will call (ab) an *adjacent* transposition if all $q \in (a, b)$ satisfy $\sigma(q) \equiv q \pmod n$ [37]. The reason for this distinction will become clear in the next section. A *strictly adjacent* transposition is of the form $(a \ a+1)$. For notational purposes, we define (ab) to act on the right, so if σ is a boundary of $\tilde{\sigma}$, then we write $\sigma = \tilde{\sigma} \cdot (ab)$. Of course, (ab) is its own inverse, so acting on the right with (ab) again yields the *inverse boundary operation* $\sigma \cdot (ab) = \tilde{\sigma}$. The boundary operation reduces the dimension by one, while the inverse boundary operation increases the dimension by one. Although the notation is identical, it should be clear what we mean from the context. Taking additional (inverse) boundaries leads to expressions like $\rho = \sigma \cdot (a_1 b_1)(a_2 b_2) \dots$, which means first exchange $\sigma(a_1)$ and $\sigma(b_1)$, then swap the elements at positions a_2 and b_2 , etc.⁴

5.2.2 Plabic Graphs

Permutations and positroid cells can be represented diagrammatically with *plabic* (planar-bicolored) *graphs* and *plabic networks*.⁵ *Plabic graphs* are planar graphs embedded in a disk, in which each vertex is colored either black or white. Any bicolored graph can be made bipartite by adding oppositely-colored bivalent vertices on edges between two identically-colored vertices, so we will assume all graphs have been made bipartite. Some edges are attached to the boundary; we will call these *external legs* and number them in clockwise order $1, 2, \dots, n$. If a monovalent leaf is attached to the boundary, it will be called a *lollipop* together with its edge. *Plabic networks* are plabic graphs together with weights (t_1, t_2, \dots, t_e) assigned to the edges. The weights are related to coordinates on the corresponding cell, as will be discussed in the next subsection.

Given a plabic graph G , one can define a *trip permutation* by starting from an external leg a and traversing the graph, turning (maximally) left at each white vertex and (maximally) right at each black vertex until the path returns to the boundary at some vertex b . When

⁴To avoid any confusion with accessing elements of the permutation, e.g. $\sigma(i)$, we use the \cdot after σ to indicate that σ is a permutation, and (ab) is a transposition. The \cdot operation is implicit between neighboring transpositions.

⁵Physical interpretations of certain plabic networks, also known as ‘on-shell diagrams,’ have been explored in several recent papers, including [37, 100].

$a \neq b$, the permutation associated with this trip has

$$\sigma_G(a) = \begin{cases} b & b > a \\ b+n & b < a \end{cases}. \quad (5.9)$$

We will explain the case $a = b$ momentarily.

For tree amplitudes, we will be concerned with *reduced* plabic graphs. A plabic graph is reduced if it satisfies the following after deleting all lollipops [118]:

1. It has no leaves;
2. No trip is a cycle;
3. No trip uses a single edge twice;
4. No two trips share two edges e_1 and e_2 in the same order.

It follows that any external leg a for which $\sigma_G(a) \equiv a \pmod n$ must be a lollipop [118]. Specifically, we define $\sigma_G(a) = a$ to be a black lollipop, and $\sigma_G(a) = a+n$ to be a white lollipop.

Thus each reduced plabic graph/network corresponds to a unique decorated permutation. However, the correspondence is not a bijection; rather each permutation labels a family of reduced plabic graphs/networks. Members of each family are related by *equivalence moves* that modify the edge weights but leave the permutation unchanged [37, 119]:

(E1) $GL(1)$ rotation: At any vertex, one can perform a $GL(1)$ rotation that uniformly scales the weights on every attached edge, e.g. Figure 5.4 shows the transformation for a scaling factor f .

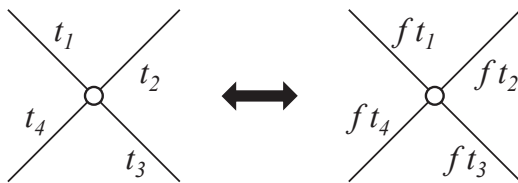


Figure 5.4: A $GL(1)$ transformation with scaling factor f .

(E2) Merge/delete: Any bivalent vertex whose edges both have weight 1 can be eliminated by merging its neighbors into one combined vertex and deleting the bivalent vertex and its edges, e.g. Figure 5.5.



Figure 5.5: A merge operation.

If one of its neighbors is the boundary, then the bivalent vertex should be merged with the boundary instead. The inverse operation can also be used to ‘unmerge’ a vertex or boundary.

(E3) Square move: A four-vertex square with one pattern of coloring is equivalent to the four-vertex square with opposite coloring. The edge weights in Figure 5.6 are related (using the sign conventions of [113]):

$$t'_1 = \frac{t_3}{t_1 t_3 + t_2 t_4}, \quad t'_2 = \frac{t_4}{t_1 t_3 + t_2 t_4}, \quad t'_3 = \frac{t_1}{t_1 t_3 + t_2 t_4}, \quad t'_4 = \frac{t_2}{t_1 t_3 + t_2 t_4}. \quad (5.10)$$

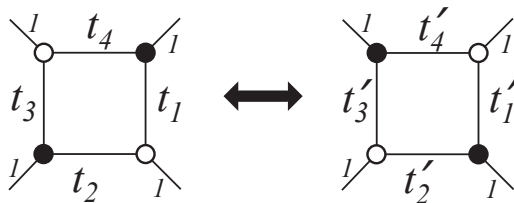


Figure 5.6: A square move operation.

From the plabic network, one can also read off a representative $k \times n$ matrix for the corresponding positroid cell, which is called the *boundary measurement matrix* (or *boundary measurement map*). Several related methods exist for defining boundary measurements such as using perfect orientations [37, 113, 119] or perfect matchings [113, 118, 120]. The equivalence moves above can be derived by requiring that the boundary measurements are unchanged by each transformation. In the next subsection, we will show how to construct the boundary measurements systematically for the types of plabic networks relevant to amplitudes. We refer the reader to the above references for more details, though we caution that the transformation rules are presented slightly differently.

These three moves are sufficient to transform any plabic network into any other in its equivalence class. In addition, using these moves one can always fix all but d of the edge weights to unity in any network that represents a d -dimensional cell; throughout the rest of this chapter, edges with unspecified weights will have weight 1. As we will see shortly, certain planar networks lead to especially convenient parameterizations of positroid cells. The equivalence moves will allow us to compare the resulting oriented forms.

5.2.3 Bridge Decompositions and Charts

To write down a coordinate chart on a given cell, it is sufficient to construct a representative matrix with the appropriate linear dependencies among its columns. However, in a general chart the boundary structure could be very difficult to identify. Fortunately, there is a straightforward method to construct charts with simple dlog forms as in (5.2) [37]; we review this technique below and how it relates to paths in the poset of cells. Some paths through the poset do not correspond to any such charts, so we suggest an interpretation for those paths in Section 5.2.3 and explain the consequences for residues in Section 5.4.1.

Standard BCFW Bridge Decompositions

Positroid cells of dimension zero in $\text{Gr}(k, n)$ correspond to unique plabic graphs made solely out of lollipops with edge weight 1. The k legs with $\sigma(a) = a+n$ have white vertices while the rest are black. The boundary measurement matrix is zero everywhere except the submatrix composed out of the k columns corresponding to the white vertices, which together form a $k \times k$ identity matrix. There are no degrees of freedom, so the differential form (5.2) is trivial, $\omega = 1$.

Since there is a unique representative plabic network for each 0d cell, we will build higher-dimensional representatives out of the set of 0d networks. In the poset, higher-dimensional cells can be reached from 0d cells by repeatedly applying the inverse boundary operation defined below (5.8). Equivalently, a d -dimensional cell can be decomposed into a sequence of adjacent transpositions acting on a 0d permutation, e.g.⁶

$$\{3, 5, 4, 6\} = \{5, 6, 3, 4\} \cdot (24)(23)(12). \quad (5.11)$$

This is called a *BCFW decomposition* and leads to a convenient graphical representation. In a planar network, an adjacent transposition $(a_i b_i)$ amounts to simply adding a white vertex on leg a_i , a black vertex on leg b_i , and an edge between them with weight α_i as illustrated in Figure 5.7. This is called a *(BCFW) bridge*. Note that if one of the legs is initially a lollipop, then the resulting leaf should be deleted after adding the bridge [118, 119].

The example (5.11) generates the sequence of graphs shown in Figure 5.8. Many simplifications are possible using the equivalence moves (E1)-(E3).

Adding a BCFW bridge affects the trip permutation by exchanging $\sigma_G(a) \leftrightarrow \sigma_G(b)$ as

⁶The transposition (24) is adjacent because it acts on a permutation whose third element is self-identified.

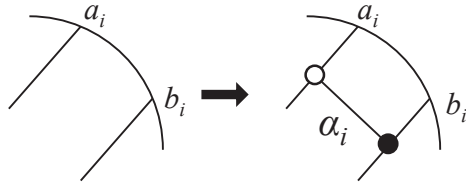


Figure 5.7: Adding a BCFW bridge.

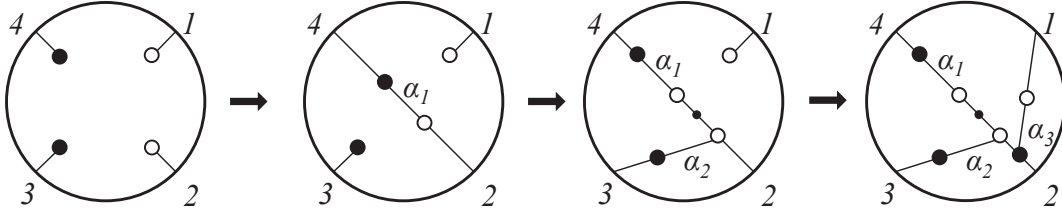


Figure 5.8: The sequence of diagrams produced by (5.11). We have added a black vertex between the first two bridges to make the graph bipartite; it is drawn slightly smaller to distinguish it from the bridge vertices.

desired, and the boundary measurement matrix transforms in a simple way [37],

$$c_b \rightarrow c_b + \alpha_i c_a. \quad (5.12)$$

One can easily check that the linear dependencies of the shifted matrix agree with the expected permutation as long as $(a_i b_i)$ is an adjacent transposition. If ω_{i-1} is the differential form associated with the initial cell, then after adding the bridge, the new form is

$$\omega_i = \text{dlog } \alpha_i \wedge \omega_{i-1}. \quad (5.13)$$

This prescription provides a robust way to generate coordinates on any cell in $\text{Gr}(k, n)$.

There are generally many ways to decompose a d -dimensional permutation σ into a sequence of adjacent transpositions acting on a 0d cell. In fact, no single chart covers all boundaries of a generic cell. However, an atlas of at most n standard BCFW charts is sufficient to cover all boundaries [37]. Every such chart defines a unique path through the poset from σ to some σ_0 . In the example (5.11), the path was

$$\sigma = \{3, 5, 4, 6\} \xrightarrow{(12)} \{5, 3, 4, 6\} \xrightarrow{(23)} \{5, 4, 3, 6\} \xrightarrow{(24)} \{5, 6, 3, 4\} = \sigma_0. \quad (5.14)$$

Not all BCFW decompositions of σ end in the same 0d cell, however. Another BCFW

decomposition of $\{3, 5, 4, 6\}$ ends in $\sigma'_0 = \{5, 2, 7, 4\}$:

$$\sigma = \{3, 5, 4, 6\} \xrightarrow{(12)} \{5, 3, 4, 6\} \xrightarrow{(46)} \{5, 2, 4, 7\} \xrightarrow{(34)} \{5, 2, 7, 4\} = \sigma'_0. \quad (5.15)$$

The important point is that every BCFW decomposition corresponds to a unique path of length d that starts at σ and ends in a 0d cell. The converse is not true; some paths of length d that start at σ and end in a 0d cell do not correspond to any BCFW decomposition.

Generalized Decompositions

When evaluating residues, one will often encounter paths through the poset that do not coincide with any single standard chart. These paths contain edges that represent non-adjacent transpositions. Continuing with the earlier example, the following path ends in the same 0d cell as (5.11), but the first transposition (13) crosses a non-self-identified leg:

$$\sigma = \{3, 5, 4, 6\} \xrightarrow{(13)} \{4, 5, 3, 6\} \xrightarrow{(24)} \{4, 6, 3, 5\} \xrightarrow{(14)} \{5, 6, 3, 4\} = \sigma_0. \quad (5.16)$$

Nevertheless, this path is certainly a possible route when evaluating residues since every codimension-1 boundary is accessible from some adjacent chart [37]. We could, for instance, take the decomposition from (5.11), and take $\alpha_2 \rightarrow 0$. It is easy to see from the boundary measurement matrix that this yields the desired linear dependencies among columns:

$$\begin{pmatrix} 1 & \alpha_3 & 0 & 0 \\ 0 & 1 & \alpha_2 & \alpha_1 \end{pmatrix} \xrightarrow{\alpha_2 \rightarrow 0} \begin{pmatrix} 1 & \alpha_3 & 0 & 0 \\ 0 & 1 & 0 & \alpha_1 \end{pmatrix}. \quad (5.17)$$

The generalization to any path through the poset is clear; each successive step involves computing the residue at a logarithmic singularity in some chart. Thus every path corresponds to some dlog form, not just the paths for which we have explicit plabic graphical representations. We will call these *generalized decompositions* and their coordinates *generalized charts*. In practice, computing residues along a particular path through the poset can always be done using standard adjacent charts, though it may involve changing coordinates at several steps along the way. As we will see in Section 5.4.1, the sign of the resulting residue depends only on the path taken, and not on the choice of reference charts along the way.

5.3 Relating Distinct Charts

Recall that a decomposition for a d -dimensional cell C corresponds to a sequence of transpositions applied to a permutation σ_0 labeling a 0-dimensional cell C_0 . Each sequence defines a particular path through the poset with endpoints at C and C_0 . In this section, we will show that the relative sign between the dlog forms generated by two distinct charts can be obtained systematically. We will first show this result for standard BCFW charts constructed using only adjacent transpositions. Subsequently, we will discuss the generalized situation where we do not always have a simple graphical representation; the convention for deriving signs will be extended to cover the additional possibilities while maintaining consistency with the standard setup. The extended conventions will also lead to a simpler method for comparing charts.

5.3.1 Standard BCFW Charts

There are two cases that we need to address depending on whether the decompositions end in identical 0d cells or distinct ones. We will cover the identical case first and then deal with the other situation.

Charts with Identical 0d Cells

We assume first that the 0d cell labeled by σ_0 is the same for both paths. The d -dimensional cell labeled by σ is connected to σ_0 by two sequences of transpositions

$$\sigma = \sigma_0 \cdot (a_1 b_1)(a_2 b_2) \dots (a_d b_d) = \sigma_0 \cdot (a'_1 b'_1)(a'_2 b'_2) \dots (a'_d b'_d). \quad (5.18)$$

Graphically, the concatenation of the two paths creates a closed loop of length $2d$ in the poset, shown schematically in Figure 5.9 with one path denoted by a blue solid line and the other by a green dashed line.

The relative orientation of the two dlog forms corresponding to the sequences can be obtained by a simple algorithm. Before presenting that result, we will need the following lemma:

Lemma 1. *The top cell can be reached from any cell, C , of dimension d by a sequence of $k(n - k) - d$ strictly adjacent transpositions.*

Proof. Let σ be the permutation labeling $C \in \text{Gr}(k, n)$. When σ contains two neighboring elements satisfying $\sigma(i) > \sigma(i + 1)$ (with $\sigma(n + 1) = \sigma(1) + n$), this is called an *inversion*. Such an inversion can be removed by applying the (strictly adjacent) transposition $(i \ i + 1)$.

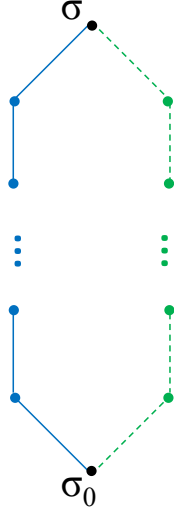


Figure 5.9: Two paths representing sequences of transpositions connecting the permutations σ_0 and σ . Together the paths form a closed loop.

Since all entries in σ_{top} are ordered, one can reach the top cell by iteratively eliminating all inversions. \square

For example, the top cell of $\text{Gr}(2, 6)$ can be reached from the 5-dimensional cell labeled by $\{2, 3, 4, 6, 7, 11\}$ by the sequence of transpositions $(6\ 7)(1\ 2)(2\ 3)$:

$$\{2, 3, 4, 6, 7, 11\} \xrightarrow{(6\ 7)} \{5, 3, 4, 6, 7, 8\} \xrightarrow{(1\ 2)} \{3, 5, 4, 6, 7, 8\} \xrightarrow{(2\ 3)} \{3, 4, 5, 6, 7, 8\}. \quad (5.19)$$

Using this procedure, any BCFW sequence can be extended to reach the top cell using only strictly adjacent transpositions. We thank R. Karpman for pointing this out.

Since $(i, i + 1)$ does not cross any legs, the resulting sequence will be a valid BCFW sequence. Therefore, we may assume without loss of generality that the cell on which we seek to compare orientations is the top cell because two sequences which lead to a cell of lower dimension can be trivially extended to top cell sequences by appending the same transpositions to both paths. This will not affect the relative sign of the forms since both will have identical pieces appended to them.

We turn now to the sign-comparison algorithm. The idea is to compare each BCFW chart to specially chosen reference charts whose relative orientation is easy to compute. They are chosen so that at each iteration, the loop in the poset (initially of length $2d$) is shortened. Then the final relative orientation is the product over all the intermediate orientations.

Algorithm 1

Input: Two BCFW sequences of length $d = k(n - k)$: $\mathbf{w} = (a_1b_1)(a_2b_2) \dots (a_db_d)$ and $\mathbf{w}' = (a'_1b'_1)(a'_2b'_2) \dots (a'_db'_d)$

Output: ± 1

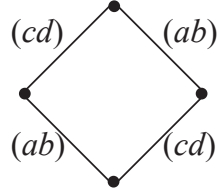
Procedure:

- 1) Let j be the smallest index such that $(a_jb_j) \neq (a'_jb'_j)$. The transpositions with $i > j$ yield a closed loop of length $\ell \leq 2d$. If there is no such position, then the paths are identical, so return $+1$.
- 2) Let σ label the j -dimensional cell reached by the sequence of transpositions $(a_1b_1)(a_2b_2) \dots (a_jb_j)$ and σ' label that reached by $(a'_1b'_1)(a'_2b'_2) \dots (a'_jb'_j)$. Using the following rules, construct reference charts to which the initial charts should be compared. Comparing the two reference charts produces a known sign; the relevant parts are displayed with each step, and their relative signs are derived in Appendix I. There are several cases to consider (with $a < b < c < d < a+n$):

i) $(a_jb_j) = (ab)$, $(a'_jb'_j) = (cd)$

The j -dimensional cells σ and σ' have a shared $(j + 1)$ -dimensional neighbor $\tilde{\sigma} = \sigma \cdot (cd) = \sigma' \cdot (ab)$. Let \mathbf{u} be the sequence generated by Lemma 1 for the cell labeled by $\tilde{\sigma}$. Then the reference sequences and relative sign are:

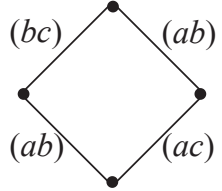
- Ref. sequence 1: $\tilde{\mathbf{w}} = (a_1b_1)(a_2b_2) \dots (a_{j-1}b_{j-1})(ab)(cd)\mathbf{u}$
- Ref. sequence 2: $\tilde{\mathbf{w}}' = (a'_1b'_1)(a'_2b'_2) \dots (a'_{j-1}b'_{j-1})(cd)(ab)\mathbf{u}$
- The relative sign between reference charts is -1 .



ii) $(a_jb_j) = (ab)$, $(a'_jb'_j) = (ac)$

In this case, cells σ and σ' have a shared $(j + 1)$ -dimensional neighbor $\tilde{\sigma} = \sigma \cdot (bc) = \sigma' \cdot (ab)$. Let \mathbf{u} be the sequence generated by Lemma 1 for the cell labeled by $\tilde{\sigma}$. Then the reference sequences and relative sign are:

- Ref. sequence 1: $\tilde{\mathbf{w}} = (a_1b_1)(a_2b_2) \dots (a_{j-1}b_{j-1})(ab)(bc)\mathbf{u}$
- Ref. sequence 2: $\tilde{\mathbf{w}}' = (a'_1b'_1)(a'_2b'_2) \dots (a'_{j-1}b'_{j-1})(ac)(ab)\mathbf{u}$
- The relative sign between reference charts is -1 .

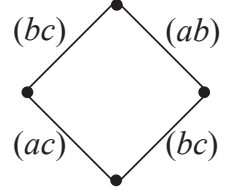


iii) $(a_jb_j) = (ac)$, $(a'_jb'_j) = (bc)$

Once again, cells σ and σ' have a shared $(j + 1)$ -dimensional neighbor

$\tilde{\sigma} = \sigma \cdot (bc) = \sigma' \cdot (ab)$. Let \mathbf{u} be the sequence generated by Lemma 1 for the cell labeled by $\tilde{\sigma}$. Then the reference sequences and relative sign are:

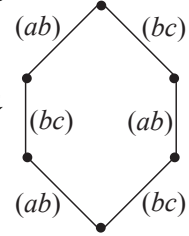
- Ref. sequence 1: $\tilde{\mathbf{w}} = (a_1b_1)(a_2b_2) \dots (a_{j-1}b_{j-1})(ac)(bc)\mathbf{u}$
- Ref. sequence 2: $\tilde{\mathbf{w}}' = (a'_1b'_1)(a'_2b'_2) \dots (a'_{j-1}b'_{j-1})(bc)(ab)\mathbf{u}$
- The relative sign between reference charts is -1 .



iv) $(\mathbf{a}_j\mathbf{b}_j) = (ab)$, $(\mathbf{a}'_j\mathbf{b}'_j) = (bc)$

Using only adjacent transpositions, σ and σ' do not have a common $(j+1)$ -dimensional neighbor. However, certain neighbors of σ and σ' do have a common neighbor of dimension $(j+2)$. Specifically, let $\tilde{\sigma} = \sigma \cdot (bc)$ and $\tilde{\sigma}' = \sigma' \cdot (ab)$. Then $\tilde{\sigma}$ and $\tilde{\sigma}'$ have a common $(j+2)$ -dimensional neighbor $\rho = \tilde{\sigma} \cdot (ab) = \tilde{\sigma}' \cdot (bc)$. Let \mathbf{u} be the sequence generated by Lemma 1 for the cell labeled by ρ . Then the reference sequences and relative sign are:

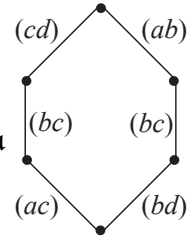
- Ref. sequence 1: $\tilde{\mathbf{w}} = (a_1b_1)(a_2b_2) \dots (a_{j-1}b_{j-1})(ab)(bc)(ab)\mathbf{u}$
- Ref. sequence 2: $\tilde{\mathbf{w}}' = (a'_1b'_1)(a'_2b'_2) \dots (a'_{j-1}b'_{j-1})(bc)(ab)(bc)\mathbf{u}$
- The relative sign between reference charts is $+1$.



v) $(\mathbf{a}_j\mathbf{b}_j) = (ac)$, $(\mathbf{a}'_j\mathbf{b}'_j) = (bd)$

Similar to the previous case, σ and σ' do not have a common $(j+1)$ -dimensional neighbor using only adjacent transpositions. Nonetheless, with $\tilde{\sigma} = \sigma \cdot (bc)$ and $\tilde{\sigma}' = \sigma' \cdot (bc)$, then $\tilde{\sigma}$ and $\tilde{\sigma}'$ have a common $(j+2)$ -dimensional neighbor $\rho = \tilde{\sigma} \cdot (cd) = \tilde{\sigma}' \cdot (ab)$. Let \mathbf{u} be the sequence generated by Lemma 1 for the cell labeled by ρ . Then the reference sequences and relative sign are:

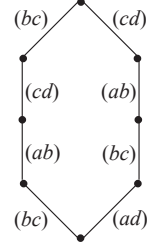
- Ref. sequence 1: $\tilde{\mathbf{w}} = (a_1b_1)(a_2b_2) \dots (a_{j-1}b_{j-1})(ac)(bc)(cd)\mathbf{u}$
- Ref. sequence 2: $\tilde{\mathbf{w}}' = (a'_1b'_1)(a'_2b'_2) \dots (a'_{j-1}b'_{j-1})(bd)(bc)(ab)\mathbf{u}$
- The relative sign between reference charts is -1 .



vi) $(\mathbf{a}_j\mathbf{b}_j) = (bc)$, $(\mathbf{a}'_j\mathbf{b}'_j) = (ad)$

In this case, we must look further to find a shared cell above σ and σ' using only adjacent transpositions. They have a shared $(j+3)$ -dimensional great-grandparent $\tilde{\rho} = \sigma \cdot (ab)(cd)(bc) = \sigma' \cdot (bc)(ab)(cd)$. Let \mathbf{u} be the sequence generated by Lemma 1 for the cell labeled by $\tilde{\rho}$. Then the reference sequences and relative sign are:

- Ref. sequence 1: $\tilde{\mathbf{w}} = (a_1 b_1)(a_2 b_2) \dots (a_{j-1} b_{j-1})(bc)(ab)(cd)(bc)\mathbf{u}$
- Ref. sequence 2: $\tilde{\mathbf{w}}' = (a'_1 b'_1)(a'_2 b'_2) \dots (a'_{j-1} b'_{j-1})(ad)(bc)(ab)(cd)\mathbf{u}$
- The relative sign between reference charts is -1 .



- 3) Repeat this algorithm to compare \mathbf{w} to $\tilde{\mathbf{w}}$ and \mathbf{w}' to $\tilde{\mathbf{w}}'$.
- 4) Return the product of the relative sign from step (2) times the result of each comparison in step (3).

The relative orientation of any two BCFW charts with identical endpoints can be compared with this algorithm. In the second part of the proof below, we show that the signs and reference charts presented in step (2i) are correct; this should also serve as an illustrative example of the algorithm in action.

Proof. We need to show that the algorithm will terminate in a finite number of iterations, and that the sign generated at each step is correct.

- We will first show that the algorithm will terminate after a finite number of iterations. The reference sequences constructed in step (2) are chosen so that when the algorithm is called again in step (3) to compare \mathbf{w} to $\tilde{\mathbf{w}}$, the new inputs satisfy $(a_i b_i) = (a'_i b'_i)$ for all $i \leq j$. The same is true for the comparison of \mathbf{w}' and $\tilde{\mathbf{w}}'$. Step (1) searches for the first point at which the input sequences differ, so by construction, the next position will be at least $j + 1$, which is larger than in the previous iteration. Since j is bounded by d , the algorithm will eventually terminate.
- Next we will explain the results presented in step (2i). Since $a < b < c < d < a + n$, the two transpositions can be applied in either order without violating the adjacent requirement of BCFW sequences. Therefore σ and σ' have a common neighbor $\tilde{\sigma}$, and both $(a_1 b_1)(a_2 b_2) \dots (a_{j-1} b_{j-1})(ab)(cd)\mathbf{u}$ and $(a'_1 b'_1)(a'_2 b'_2) \dots (a'_{j-1} b'_{j-1})(cd)(ab)\mathbf{u}$ are valid BCFW sequences for the top cell. Moreover, since $(a'_i b'_i) = (a_i b_i)$ for all $i < j$, their corresponding forms differ only in positions j and $j + 1$:

$$\begin{aligned}
 \omega &= \text{dlog } \alpha_d \wedge \text{dlog } \alpha_{d-1} \dots \wedge \text{dlog } \alpha_{j+2} \wedge \text{dlog } \alpha_{j+1} \wedge \text{dlog } \alpha_j \wedge \text{dlog } \alpha_{j-1} \dots \wedge \text{dlog } \alpha_1, \\
 \omega' &= \text{dlog } \alpha_d \wedge \text{dlog } \alpha_{d-1} \dots \wedge \text{dlog } \alpha_{j+2} \wedge \text{dlog } \beta_{j+1} \wedge \text{dlog } \beta_j \wedge \text{dlog } \alpha_{j-1} \dots \wedge \text{dlog } \alpha_1,
 \end{aligned}
 \tag{5.20}$$

where α_j and α_{j+1} are the weights associated with (ab) and (cd) in the first sequence, while β_j and β_{j+1} are associated with (cd) and (ab) in the second sequence. To determine the relationship between the two forms, we will use the plabic graph representations of the transpositions as BCFW bridges. Focusing on the j and $j + 1$ parts of the graphs in Figure 5.10, the only differences are the labels of the j^{th} and $(j + 1)^{\text{th}}$ bridges. The left and right diagrams can only be equivalent if $\beta_j = \alpha_{j+1}$ and $\beta_{j+1} = \alpha_j$, which implies

$$\omega' = \text{dlog } \alpha_d \wedge \dots \wedge \text{dlog } \alpha_{j+2} \wedge \text{dlog } \alpha_j \wedge \text{dlog } \alpha_{j+1} \wedge \text{dlog } \alpha_{j-1} \dots \wedge \text{dlog } \alpha_1 = -\omega. \quad (5.21)$$

Thus the relative sign between the reference charts is -1 .

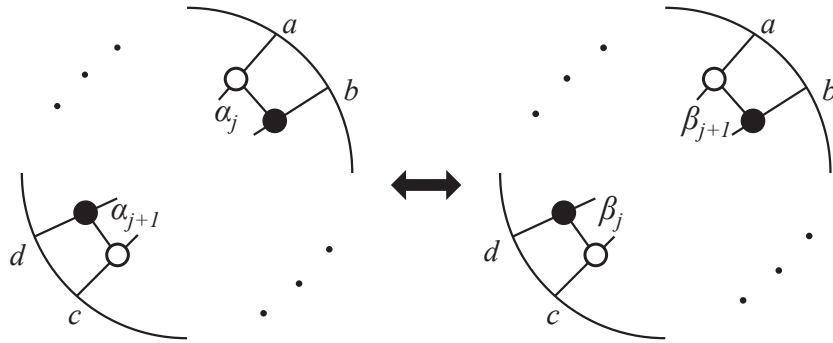


Figure 5.10: Graphs representing the sequences defined in step (2i) of Algorithm 1.

The remaining cases are described in Appendix I. □

Thus we now have an algorithm that correctly computes the relative signs for BCFW forms generated from identical 0d cells.

Charts with Distinct 0d Cells

The next step will be to extend the result to decompositions that terminate in distinct 0d cells. Let us start with the simplest case: finding the relative sign between two charts on a 1d cell labeled by σ_1 . Since it is 1-dimensional, all but two entries in σ are self-identified mod n . The two non-trivial positions can be labeled a and b such that $a < b < a + n$.

As illustrated in Figure 5.11, the 1d cell has exactly two boundaries, which can be accessed respectively by (ab) or $(b a + n)$, so the two BCFW sequences whose charts we will

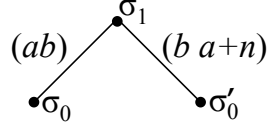


Figure 5.11: Boundaries of a 1-dimensional cell σ_1 .

compare are (ab) and $(b a+n)$. It is straightforward to find the relative orientations of the corresponding forms,

$$\omega_1 = \text{dlog } \alpha \quad \text{and} \quad \omega'_1 = \text{dlog } \beta, \quad (5.22)$$

using basic plabic graph manipulations. Figure 5.12 demonstrates that several $GL(1)$ rotations (E1) combined with a merge and unmerge with the boundary (E2) are sufficient to discover that $\beta = 1/\alpha$. Therefore, the forms are oppositely oriented, i.e. $\omega'_1 = -\omega_1$.

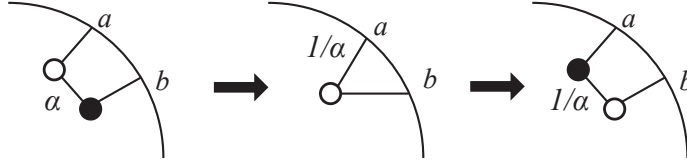


Figure 5.12: A sequence of equivalence moves relating the two representative graphs for a 1d cell.

More generally, we could consider charts on d -dimensional cells whose corresponding BCFW sequences are identical everywhere except for the first transposition, e.g. Figure 5.13. The associated forms are

$$\begin{aligned} \omega_d &= \text{dlog } \alpha_d \wedge \text{dlog } \alpha_{d-1} \wedge \dots \wedge \text{dlog } \alpha_1, \\ \omega'_d &= \text{dlog } \alpha_d \wedge \text{dlog } \alpha_{d-1} \wedge \dots \wedge \text{dlog } \beta_1. \end{aligned} \quad (5.23)$$

To construct a pair of sequences like these, we could find a Lemma 1 sequence, \mathbf{u} , for the 1d cell in Figure 5.11 and compare the two charts defined by $\sigma_0 \cdot (ab)\mathbf{u}$ and $\sigma'_0 \cdot (b a+n)\mathbf{u}$. Since BCFW sequences such as \mathbf{u} use only adjacent transpositions, no bridge will ever be attached to legs a and b further from the boundary than the first bridge (ab) , resp., $(b a+n)$. Therefore, one can apply very similar logic as in the 1d case⁷ to find that $\beta_1 = 1/\alpha_1$, so $\omega'_d = -\omega_d$.

⁷The only difference being that the merge/unmerge moves may be with other vertices instead of the boundary.

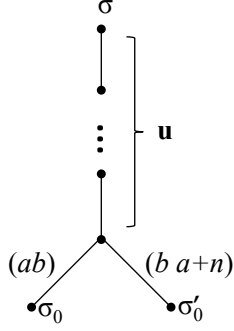


Figure 5.13: Two sequences that are identical except for the first transposition.

We can easily extend this to any two charts whose 0d endpoints share a common 1d neighbor, σ_1 , by applying Algorithm 1. Each sequence can be related to a reference sequence with the same 0d cell, but which goes through σ_1 and then follows some arbitrarily chosen path, say \mathbf{u} , to the top cell. If the same path is chosen to compare to both charts, then the relative orientation of the reference charts is -1 .

Finally, this can be extended to any two charts terminating in arbitrarily separated 0d cells by iterating the previous step together with Algorithm 1. We combine this into Algorithm 2.

Algorithm 2

Input: Two BCFW sequences of length $d = k(n - k)$: $\mathbf{w} = (a_1 b_1)(a_2 b_2) \dots (a_d b_d)$ and $\mathbf{w}' = (a'_1 b'_1)(a'_2 b'_2) \dots (a'_d b'_d)$; and their 0d endpoints: σ_0 and σ'_0 .

Output: ± 1

Procedure:

- 1) If $\sigma_0 = \sigma'_0$, compute the relative sign of the two forms using Algorithm 1. Return the result.
- 2) Else, let a be the smallest index such that $\sigma_0(a) < \sigma'_0(a)$, and let b be the smallest index such that $\sigma_0(b) > \sigma'_0(b)$. We assume that $a < b$; if not, then the roles of σ_0 and σ'_0 should be exchanged. Let $\tilde{\sigma} = \sigma_0 \cdot (ab)$, whose boundaries are σ_0 and $\tilde{\sigma}_0 = \tilde{\sigma} \cdot (b a+n)$, and define \mathbf{u} to be the Lemma 1 sequence from $\tilde{\sigma}$ to the top cell. Construct two reference sequences: $\tilde{\mathbf{w}} = (ab)\mathbf{u}$ and $\tilde{\mathbf{w}}' = (b a+n)\mathbf{u}$.
- 3) Repeat this algorithm to compare (\mathbf{w}, σ_0) to $(\tilde{\mathbf{w}}, \sigma_0)$, and (\mathbf{w}', σ'_0) to $(\tilde{\mathbf{w}}', \tilde{\sigma}_0)$.
- 4) Return the product of the results from step (3) times -1 due to the relative sign between $\tilde{\mathbf{w}}$ and $\tilde{\mathbf{w}}'$.

Proof. Assuming that the cells and edges in step (2) exist, the sign at each iteration is valid because it uses Algorithm 1 to compare charts with identical 0d cells, and it returns -1 for each pair of sequences that differ only in the first position. It remains to show that step (2) is correct. Since all entries in the permutations labeling 0d cells are self-identified mod n , the definitions of a and b imply that:

$$\sigma_0(a) = a, \quad \sigma_0(b) = b+n, \quad \sigma'_0(a) = a+n, \quad \text{and} \quad \sigma'_0(b) = b. \quad (5.24)$$

There exists another 0d cell $\tilde{\sigma}_0$, which is identical to σ_0 except

$$\tilde{\sigma}_0(a) = \sigma_0(a)+n = a+n = \sigma'_0(a) \quad \text{and} \quad \tilde{\sigma}_0(b) = \sigma_0(b)-n = b = \sigma'_0(b). \quad (5.25)$$

The new cell $\tilde{\sigma}_0$ has two important properties:

- The first is that σ_0 and $\tilde{\sigma}_0$ have a common 1d neighbor, $\tilde{\sigma} = \sigma_0 \cdot (ab) = \tilde{\sigma}_0 \cdot (b \ a+n)$. Since all other entries in σ_0 and $\tilde{\sigma}_0$ are self-identified mod n , both (ab) and $(b \ a+n)$ are adjacent. Thus the cells and reference sequences of step (2) are uniquely defined and satisfy the standard adjacency requirements.
- The second is that $\tilde{\sigma}_0$ differs from σ'_0 at fewer sites than σ_0 differs. If there are $m \geq 1$ locations where $\sigma_0(i) - \sigma'_0(i) \neq 0$, then there are only $m - 2$ locations where $\tilde{\sigma}_0(i) - \sigma'_0(i) \neq 0$. Since all entries in 0d cells are self-identified mod n , and k entries are greater than n , then m must be even and no larger than $2k$. Hence, Algorithm 2 will complete after at most k iterations.

Therefore, Algorithm 2 computes the correct sign. □

Therefore Algorithms 1 and 2 are together sufficient to find the relative orientation of any two standard BCFW charts.

5.3.2 Generalized Decompositions

The plabic graph representation explained in Section 5.2.3 is convenient for the study of standard BCFW charts. They are a subset of the generalized decompositions, so the rules for defining reference charts and relative signs in Algorithms 1 and 2 will still apply. Since cases (i)-(vi) in step (2) of Algorithm 1 cover all possible comparisons, the techniques introduced in the previous section are in fact sufficient to find the relative orientation of *any* two charts.

However, there is an advantage to studying the generalized charts more closely. Cases (iv)-(vi) in Algorithm 1 were distinctly different than the other three cases because the

reference charts required two or three steps to meet at a common cell as opposed to only one step in the earlier cases. Comparing the reference paths of the first three cases shows that they define quadrilaterals, while cases (iv) and (v) define hexagons, and (vi) defines an octagon. The relevant sections of the poset are depicted in Figure 5.14 with the solid lines indicating the paths used in Algorithm 1, and the dashed lines showing the additional edges that were not used (the finely dotted lines indicate edges that do not always exist). We include the quadrilaterals from cases (i)-(iii) for completeness.

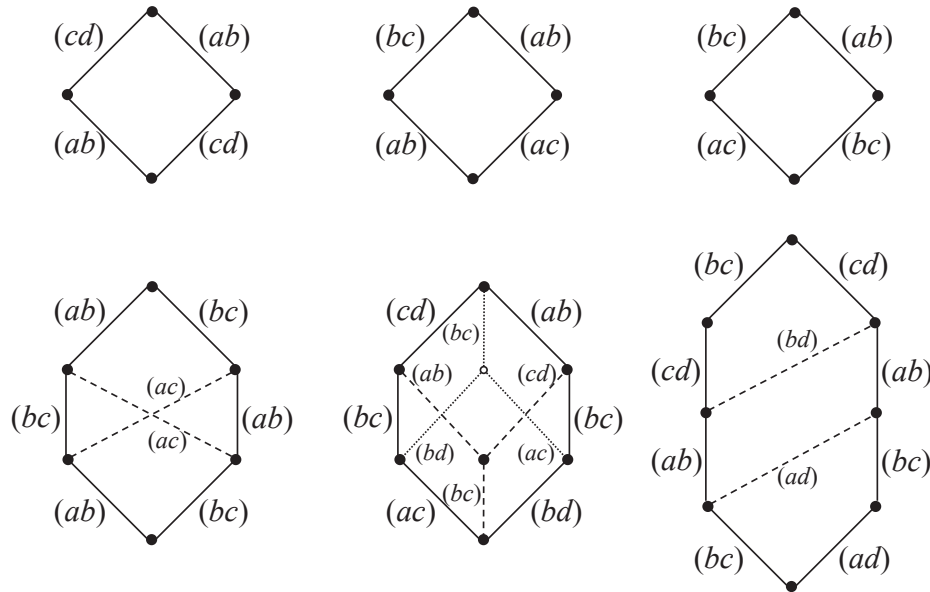


Figure 5.14: Reference paths from Algorithm 1 and interior quadrilaterals.

The extra transpositions permitted in generalized charts allow the hexagons and octagons to be refined into quadrilaterals. Some of the internal quadrilaterals are equivalent to those from cases (i)-(iii), but there are also new ones. The relative orientation of two charts which differ only by one of the new quadrilaterals needs to be determined. To fix the signs, we require that the refined polygons produce the same signs as above when split into charts that differ by the interior quadrilaterals.

The hexagon from case (iv) can be split into a pair of quadrilaterals two ways. Either way, the top quadrilateral appears in one of the first three cases, which implies that the relative orientation around the lower quadrilateral must be -1 in order to agree with the overall sign of $+1$ derived in Appendix I.

In case (v), the edges shown with dashed lines always exist, so the hexagon can be split into three quadrilaterals. The one on the lower left is equivalent to case (iii), the lower right is equivalent to case (ii), and the top quadrilateral is identical to case (i). Hence the product of the three individual signs is $(-1)^3 = -1$, in agreement with the result found in Appendix

I. In some situations, the hexagon can also be split up using the finely dotted lines. Then the top two hexagons are equivalent to cases (ii) and (iii), which implies that the relative orientation around the lower quadrilateral must also be -1 .

Finally, the octagon from case (vi) can be also be split into three quadrilaterals. The top one matches case (iii), and the middle is equivalent to case (ii), so the relative orientation around the lower one must be -1 to agree with Appendix 1. This is unsurprising considering that the two transpositions are completely disjoint, so applying them in opposite order would suggest that the forms differ by a minus signs, similar to example 5.2 in the Preview.

This exhausts all possible quadrilaterals that could appear in the poset. Hence the relative orientation between any two charts that differ by a quadrilateral is -1 . A significant consequence of this result is the existence of a boundary operator which manifestly squares to zero, as we discuss further in Section 5.4.

5.3.3 The Master Algorithm

Before proceeding to discuss various applications, we present a more efficient method to compute the relative orientation of any two charts. In each iteration of Algorithm 1, every edge in the reference charts enters into two comparisons (once to the corresponding initial chart, and once to the other reference chart), while the edges in the initial charts enter only one comparison (to the associated reference chart). Therefore, if we assign ± 1 to each *edge* such that the product of signs around any quadrilateral is -1 , then the signs on the reference chart edges will appear twice and hence square to 1, while the product of signs on the initial chart edges will combine to produce the same overall sign as found by Algorithm 1. One method for producing a consistent set of edge signs is presented in Appendix J [47].

When changing 0d cells with Algorithm 2, one should think of taking a closed loop that traverses down and back each branch in Figure 5.13, thus encountering each edge twice. Consequently, every edge sign appears twice, thus squaring to 1, so the only sign from this step will be -1 due to the relative sign between the reference charts. However, one can easily check that applying Algorithm 1 will introduce one additional copy of each branch, so those edges should be included in the overall loop. The result of chaining several of these together is a sawtooth path between the two 0d cells (the bold red line in Figure 5.15) that contributes signs from each edge along the way and a minus sign for each 1d cell along the path. Schematically, the combined loop will look like Figure 5.15. This method for computing signs is summarized in the Master Algorithm.

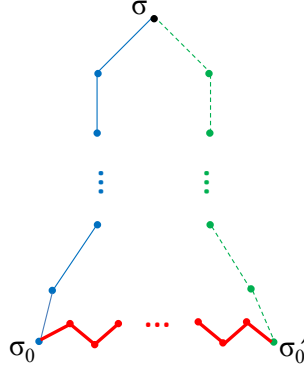


Figure 5.15: The two 0d cells at the end of the paths are connected by a sawtooth path between 1d and 0d cells. Combining this path with the input paths yields a closed loop.

Master Algorithm

Input: Two BCFW sequences of length $d = k(n - k)$: $\mathbf{w} = (a_1 b_1)(a_2 b_2) \dots (a_d b_d)$ and $\mathbf{w}' = (a'_1 b'_1)(a'_2 b'_2) \dots (a'_d b'_d)$

Output: ± 1

Procedure:

- 1) If both BCFW paths terminate in the same 0-dimensional cell, then the relative orientation is given by the product of edge signs along the paths. Equivalently, it is the product of signs around the closed loop of length $2d$ obtained by traversing down one path and back up the other.
- 2) If they terminate in different 0d cells, then the relative orientation also depends on the signs along a path connecting the two 0d cells. One can obtain such a path by a sawtooth pattern between 0d and 1d cells. The sign of this path is given by the product of edge signs along the path, times $(-1)^{m/2}$, where m is the number of locations i satisfying $\sigma_0(i) - \sigma'_0(i) \neq 0$ ($m/2$ is the number of 1d cells in the sawtooth path). Thus the relative orientation is given by the product of signs along each BCFW path, times the connecting path sign. Equivalently, it is the product of signs around the closed loop obtained by concatenating the three paths in Figure 5.15, times the signs for the 1d cells.

So far, all the charts have been assumed to have minimal length, i.e. $k(n - k)$ for charts on the top cell. In other words, each transposition in the sequence increases the dimension by 1. However, the [Master](#) Algorithm indicates that *any* path through the poset can be

compared to any other path, even if they zig-zag up and down.

The algorithm has been verified by implementing it in Mathematica and applying it to a variety of charts whose orientations are known by other methods. This includes pairs of randomly generated NMHV charts of the type studied in [51], as well as higher k charts whose matrix representatives have identical $GL(k)$ gauge fixings; the latter can be compared by directly equating the entries. In addition, the orientations of 500 distinct charts on the 10d cell $\{5, 3, 8, 9, 6, 7, 12, 10, 14, 11\} \in \text{Gr}(3, 10)$ were computed using an independent method due to J. Bourjaily and A. Postnikov [48]. The results agreed perfectly with our algorithm.

5.4 Applications

In the remainder of this chapter, we will discuss several areas in which the relative orientations are important. The end results are not surprising; they were anticipated and used in several previous works. The new contribution of this section will be to put these ideas on firm combinatorial footing, so for example, spurious poles in the tree contour will cancel exactly instead of mod 2 as in [37].

5.4.1 Comparing Residue Orientations

We have shown that any two charts can be compared by taking the product of edge signs around a closed loop in the poset of cells. This applies to any charts, even those corresponding to generalized decompositions with non-adjacent transpositions. As explained in Section 5.2.3, one can follow any path through the poset by taking residues out of order in standard BCFW charts and changing coordinates as needed. Due to the Master Algorithm, the final sign on the residue depends only on the path, not on the intermediate choices of charts. We will demonstrate this with a convincing example.

There is a standard chart on $\{4, 3, 6, 5\}$ obtained by the path P_1 :

$$\{4, 3, 6, 5\} \xrightarrow{(23)} \{4, 6, 3, 5\} \xrightarrow{(14)} \{5, 6, 3, 4\}. \quad (5.26)$$

Both transpositions are adjacent. The corresponding matrix representative and form are

$$C = \begin{pmatrix} 1 & 0 & 0 & \alpha_1 \\ 0 & 1 & \alpha_2 & 0 \end{pmatrix} \quad \omega = \text{dlog } \alpha_2 \wedge \text{dlog } \alpha_1. \quad (5.27)$$

Taking either coordinate to vanish lands in a codimension-1 boundary, so we are allowed to take them to zero in either order. There is also a non-adjacent path P_2 that ends in the

same 0d cell:

$$\{4, 3, 6, 5\} \xrightarrow{(14)} \{5, 3, 6, 4\} \xrightarrow{(23)} \{5, 6, 3, 4\}. \quad (5.28)$$

We will now evaluate the 0d residue along both paths using the coordinate chart (5.27), ignoring the delta functions in (5.1). The convention for evaluating residues is to take a contour around $\alpha_i = 0$ only when α_i is the first variable in the form. Along P_1 we first take $\alpha_2 \rightarrow 0$ and then $\alpha_1 \rightarrow 0$, which is the order they appear in the form; hence the residue is $+1$. We can follow P_2 by taking $\alpha_1 \rightarrow 0$ first, so we pick up a factor of -1 from reversing the order of the wedge product. Thus the residue along P_2 is -1 . The relative sign is -1 , exactly as our algorithm predicts because the paths differ by a quadrilateral.

In terms of edge signs, there is a \mathbb{Z}_2 symmetry at every vertex that allows us to flip the signs on all the attached edges without changing the overall sign of any closed loop. Since the product of signs around a quadrilateral is -1 , we can use the symmetry to fix the edge signs so they exactly agree with the above computation at each step as in Figure 5.16. The generalization to more complicated charts is straightforward.

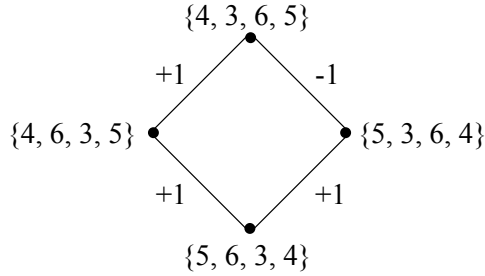


Figure 5.16: A set of edge weights that locally match the signs obtained by direct computation.

5.4.2 Boundary Operator

Define the signed boundary operator ∂ acting on a cell C to be the sum of all boundaries of C weighted by the ± 1 weight on the edge connecting each boundary to C ,

$$\partial C = \sum_i w(C, C'_i) C'_i, \quad (5.29)$$

where the sum is over all cells C'_i in the boundary of C and $w(C, C'_i) = \pm 1$ is the weight on the edge between C and C'_i . Equivalently, we could take the sum over all cells of the

appropriate dimension and define $w(C, C'_i) = 0$ whenever there is no edge between them.⁸ Applying the boundary operator again therefore yields a sum of codimension-2 boundaries of C , each one weighted by the product of the sign on the edge connecting it to its parent times the sign on its parent from the first application of ∂ :

$$\partial^2 C = \sum_i \sum_{j(i)} w(C, C'_i) w(C'_i, C''_{j(i)}) C''_{j(i)}, \quad (5.30)$$

where i runs over boundaries C'_i of C and $j(i)$ runs over boundaries $C''_{j(i)}$ of C'_i . In order for this result to vanish, every codimension-2 cell must appear twice and with opposite signs.

We will first show that each cell appears twice,⁹ and then it will be clear from our setup that that signs are opposite. Let σ be the permutation labeling C . Each edge represents a transposition acting on σ , so codimension-2 cells will arise from pairs of transpositions $(ab)(cd)$. If a, b, c, d are all distinct, then the transpositions can be applied in either order and thus each cell appears twice. If only three are distinct, then there are a few cases to consider:

$$\begin{aligned} (ac)(ab) &\equiv (ab)(bc) & \sigma(a) < \sigma(c) < \sigma(b) \\ (ac)(bc) &\equiv (bc)(ab) & \sigma(b) < \sigma(a) < \sigma(c) \\ (bc)(ac) &\equiv (ab)(bc) \text{ and } (ab)(ac) \equiv (bc)(ab) & \sigma(a) < \sigma(b) < \sigma(c). \end{aligned} \quad (5.31)$$

Thus there are two unique routes from C to every codimension-2 cell in $\partial^2 C$. Each pair of routes defines a quadrilateral in the poset, which we have seen implies a relative minus sign between the residues. Hence the boundary operator manifestly squares to zero.

5.4.3 Locality of Tree Contours

The n -particle N^k MHV tree amplitude can be computed as a linear combination of residues of (5.1) with coefficients ± 1 . Each residue appearing in the amplitude corresponds to a $4k$ -dimensional cell, whose the remaining degrees of freedom are fixed by the $4k$ bosonic delta functions in (5.1). A *tree contour* is defined as any choice of contour on the top cell that produces a valid representation of the tree amplitude; there are many equivalent representations due to residue theorems. Tree-level BCFW recursion relations [121, 122, 123] written in terms of on-shell diagrams [37] provide one technique to find an appropriate set of cells, but the on-shell diagram formulation does not generate the relative signs between

⁸This is not a unique definition since the edge weights can be flipped without affecting signs around closed loops, but any consistent set of signs such as those defined in Appendix J will be sufficient for our purposes.

⁹See also Section 6.3 of [37] for a similar proof that they appear twice.

them. This will be resolved shortly.

The tree amplitude diverges for certain configurations of the external momenta; these are called local poles — physically, they are interpreted as factorization channels in which an internal propagator goes on-shell such that the diagram splits into two on-shell subamplitudes \mathbf{L} and \mathbf{R} , e.g. all cyclic permutations of Figure 5.17.

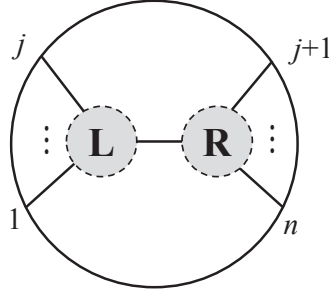


Figure 5.17: A factorization channel representing a physical, local pole.

In the Grassmannian residue representation, such poles correspond to cells of dimension $(4k - 1)$, i.e. boundaries of the $4k$ -dimensional cells. The amplitude is not manifestly local in this formulation, meaning that some boundary cells translate to non-local poles, which are momentum configurations with non-physical divergences. A key feature of the tree contour is that all of the local poles appear precisely once in the residue representation of the amplitude, while non-local poles appear twice [37]. It was conjectured that the two appearances of each non-local pole should come with opposite signs so they cancel in the sum, similar to the vanishing of ∂^2 . We are now equipped to prove that claim.

The boundary operator (5.29) can be used to define signed residue theorems. Even though the sign of each term in (5.29) is not fixed, the *relative* sign between any two cells in the boundary, say C'_1 and C'_2 , will always agree whenever they both appear in the boundary of a cell. It is easy to see that this is true if C'_1 and C'_2 share a common boundary since they form a quadrilateral in the poset. The edges connecting C'_1 and C'_2 to their shared boundary are the same no matter which C is used in the initial boundary operation, so the relative sign between the edges connecting C to C'_1 and C'_2 must not depend on that choice either. There is one situation in which they may not share a boundary, but in that case there will always be a third cell C'_3 which has common boundaries with both of them; cf. case (v) in Section 5.3.2. Now following the intuition of [37], we find residue theorems by requiring that the boundary of every $(4k + 1)$ -dimensional cell vanishes:

$$\partial C^{(4k+1)} = \sum_i w\left(C^{(4k+1)}, C_i^{(4k)}\right) C_i^{(4k)} = 0. \quad (5.32)$$

We define the tree contour to encircle each enclosed singularity of the measure exactly once, so any residue appearing in the amplitude will have a coefficient ± 1 . The residue theorems (5.32) can change which poles are included in the contour, but they will never cause residues to appear more than once. This implies that the relative sign between any two cells in the amplitude must match the relative sign of those cells in the residue theorems. Therefore, by the same logic that showed $\partial^2 = 0$, it follows that any $(4k - 1)$ -dimensional cell appearing twice in the boundary of the tree amplitude will show up with opposite signs. Hence every doubly-appearing pole cancels in the sum.

Note that we have presented these results in terms of the momentum twistor representation in which the amplitude is a linear combination of $4k$ -dimensional cells. The method works analogously in the twistor version where the amplitude is described by $(2n - 4)$ -dimensional cells. We have checked numerically that this choice of signs correctly cancels all paired poles for BCFW representations of the tree amplitude with $n = 5, \dots, 13$ and $k = 3, \dots, \lfloor n/2 \rfloor$.

5.4.4 Other Non-Physical Poles

After canceling all pairs of poles as described above, all remaining terms in the boundary sum will have unit multiplicity as expected for local poles. However, some of the surviving boundaries may yet correspond to non-physical divergences. For example, one representation of the 7-particle N^2 MHV amplitude (accessible by `treeContour[7,4]` in the *positroids* package [116]) has 52 terms in the boundary. Eight of them appear twice and hence cancel in the sum leaving 36 unit multiplicity poles. One of those poles is labeled by the permutation $\{4, 5, 6, 8, 9, 10, 14\}$ and can be represented graphically diagram in Figure 5.18. The diagram does not indicate any internal propagators going on-shell, so it does not represent a physical singularity of the form of Figure 5.17.

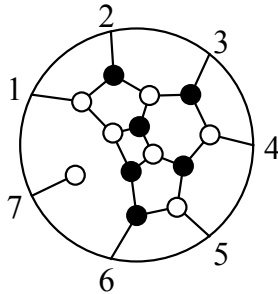


Figure 5.18: A diagram for the permutation $\{4, 5, 6, 8, 9, 10, 14\}$. It represents an unphysical, nonlocal singularity.

Since the boundary of the amplitude is ultimately expected to contain all (and only)

physical poles, it is therefore not surprising that some Grassmannian representations of the amplitude do not contain a pole of this form. However, we must then explain how such a diagram can apparently contribute to the boundary of *any* representations. In fact, we will see that momentum conservation forces this diagram to vanish.

To illustrate the result, let us group legs 6 and 7 together in Figure 5.18 so that it looks schematically like Figure 5.17. We add two bivalent vertices on leg 6 and group those vertices with leg 7 in the subamplitude \mathbf{L} shown in Figure 5.19. The other subamplitude \mathbf{R} contains all other vertices from Figure 5.18. No extra internal propagators have gone on-shell since leg 6 was already an on-shell external propagator and adding the two bivalent vertices does not affect the momentum flowing through them.

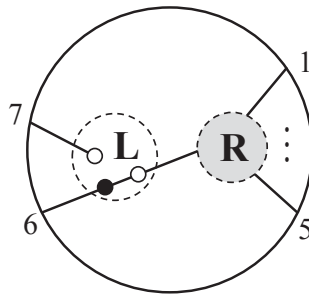


Figure 5.19: Grouping legs 6 and 7 in Figure 5.18 leads to a diagram of the form in Figure 5.17.

Recall that momentum conservation requires both \mathbf{L} and \mathbf{R} to be on-shell subamplitudes in Figure 5.17, but in Figure 5.19 the left-hand subamplitude (Figure 5.20) does not have support for generic “external” momenta and therefore vanishes. Consequently, the whole diagram in Figure 5.18 is identically zero and can be neglected in the boundary sum whenever it appears.

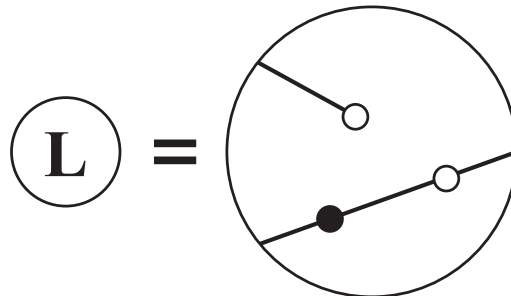


Figure 5.20: A closeup of the left-hand subamplitude in Figure 5.19.

The example in Figure 5.19 is a special case of a much more general phenomenon wherein an apparently valid boundary term with unit multiplicity actually vanishes after taking into

account momentum conservation on the left and right subamplitudes independently. Any boundary labeled by a permutation with a self-identified element will have a lollipop in its diagram and thus vanish by the same logic as above. In addition, for Grassmannian amplitude representations with large enough k and n there will be many lollipop-free boundary diagrams that factorize in the form of Figure 5.17 yet still fail to satisfy momentum conservation on the left or right. Those diagrams evaluate to zero due to the momentum delta functions and can be dropped from the sum. Given an arbitrary diagram of the form of Figure 5.17, it is straightforward to check whether the left and right subamplitudes have kinematical support by computing their respective *intersection numbers* as defined in Section 10 of [37]. If either intersection number is zero, then the whole diagram vanishes and can be dropped from the boundary sum.¹⁰

After removing from the boundary of the amplitude any cells with an unsupported subamplitude, the remaining terms will all correspond to physical, local poles of the form in Figure 5.17 with non-vanishing residues. Note that there exist multiple equivalent representations of amplitudes, so the subamplitudes that appear in the boundaries of different representations of the full amplitude may not be manifestly identical. Residue theorems ensure that as long as the boundary cells can be grouped into subamplitudes as in Figure 5.17, then every amplitude representation will have the same *number* of supported boundaries in every channel of Figure 5.17. We have checked for multiple Grassmannian BCFW representations of n -particle N^k MHV amplitudes with $n = 5, \dots, 13$ and $k = 3, \dots, \lfloor n/2 \rfloor$ that the above method for removing unsupported poles produces boundaries with matching numbers of terms in every factorization channel.

The same principles must be valid for each of the subamplitudes as well, namely they must be local on-shell amplitudes. Therefore, given an arbitrary list of $4k$ -dimensional cells,¹¹ one can determine whether that list represents a physical amplitude by recursively checking that the number of supported boundaries of each subamplitude matches the number of boundaries of a known local BCFW bridge representation of the same amplitude. However, this is not a very efficient solution in practice. We expect there should be a more straightforward method to test whether a given set of cells forms an amplitude directly at the level of those cells and their boundaries. We leave this as an open question for the reader to explore.

¹⁰This is the simplest method to check the kinematical support for subamplitudes with at least four particles. A 3-particle subamplitude is either equivalent to a single black or white 3-vertex, in which case it is non-vanishing due to special 3-particle kinematics, or it is zero as in Figure 5.20.

¹¹Or $(2n - 4)$ -dimensional cells in momentum space.

Appendix A

Euler Density and the WZ Action

We begin by constructing the $d = 2k$ dimensional Euler density for a metric $g_{\mu\nu}$ from its definition:

$$\begin{aligned} E_{2k}(g_{\mu\nu}) &= \frac{1}{2^k} R_{\mu_1\nu_1}{}^{\rho_1\sigma_1} \dots R_{\mu_k\nu_k}{}^{\rho_k\sigma_k} \epsilon_{\rho_1\sigma_1\dots\rho_k\sigma_k} \epsilon^{\mu_1\nu_1\dots\mu_k\nu_k} \\ &= \frac{d!}{2^k} R_{\mu_1\nu_1}{}^{\rho_1\sigma_1} \dots R_{\mu_k\nu_k}{}^{\rho_k\sigma_k} \delta_{[\rho_1}^{\mu_1} \dots \delta_{\sigma_k]}^{\nu_k}. \end{aligned} \quad (\text{A.1})$$

The Euler density can be written in terms of Ricci scalars and Ricci tensors plus terms involving the Weyl tensor using the identity

$$R_{\mu\nu\rho\sigma} = W_{\mu\nu\rho\sigma} + \frac{2}{d-2} (g_{\mu[\rho}R_{\sigma]\nu} - g_{\nu[\rho}R_{\sigma]\mu}) - \frac{2}{(d-2)(d-2)} Rg_{\mu[\rho}g_{\sigma]\nu}, \quad (\text{A.2})$$

where $W_{\mu\nu\rho\sigma}$ is the Weyl tensor. The 8-dimensional Euler density for conformally flat space is then:

$$E_8(g_{\mu\nu}) = -\frac{16}{9}(R_{\mu\nu})^4 + \frac{8}{9}((R_{\mu\nu})^2)^2 + \frac{32}{21}R(R_{\mu\nu})^3 - \frac{344}{441}R^2(R_{\mu\nu})^2 + \frac{208}{3087}R^4 + \text{Weyl-terms}. \quad (\text{A.3})$$

We are interested in the Wess-Zumino action in a flat background, so we pick $e^{-2t\tau}\eta_{\mu\nu}$ and integrate t over the interval $[0, 1]$:

$$\begin{aligned} S_{\text{WZ}} &= \int d^8x \int_0^1 dt \tau E_8(e^{-2t\tau}\eta_{\mu\nu}) \\ &= 48 \int d^8x \left[3(\square^2\tau)(\partial\tau)^4 + 6(\square\tau)^3(\partial\tau)^2 + 36(\square\tau)^2(\partial\partial\tau\partial\tau\partial\tau) + 16(\square\tau)(\partial\partial\partial\tau\partial\tau\partial\tau\partial\tau) \right. \\ &\quad \left. - 12(\square\tau)(\partial\partial\tau)^2(\partial\tau)^2 - 24(\partial\partial\tau\partial\tau\partial\tau)(\partial\partial\tau)^2 \right. \\ &\quad \left. + 12(\square\tau)^2(\partial\tau)^4 - 12(\partial\partial\tau)^2(\partial\tau)^4 - 20(\square\tau)(\partial\tau)^6 + 15(\partial\tau)^8 \right]. \end{aligned} \quad (\text{A.4})$$

Appendix B

Diff×Weyl Invariants in d Dimensions

The diff×Weyl invariants in flat space are constructed as curvature scalars of the ‘hatted’ metric $\hat{g}_{\mu\nu} = e^{-2\tau} \eta_{\mu\nu}$. We need only work with the scalars constructed from the Ricci tensor, Ricci scalar and covariant derivatives thereof, since the Riemann tensor can be eliminated with (A.2).

The results for the diff×Weyl invariants are expressed in terms of the dilaton τ and its derivatives. Since these terms will appear in the dilaton effective action, we use partial integration to simplify the expressions. This is indicated with “ $\xrightarrow{\text{PI}}$ ” below. The 2-derivative terms were discussed in Section 2.2; here we present the details for 4, 6, and 8-derivative Weyl invariants.

4 Derivatives

There are two 4-derivative invariants:

$$\begin{aligned} \sqrt{-\hat{g}} \hat{R}^2 \xrightarrow{\text{PI}} e^{-(d-4)\tau} & \left(4(d-1)^2 (\square\tau)^2 - 4(d-1)^2 (d-2) (\square\tau) (\partial\tau)^2 \right. \\ & \left. + (d-1)^2 (d-2)^2 (\partial\tau)^4 \right), \end{aligned} \tag{B.1}$$

$$\begin{aligned} \sqrt{-\hat{g}} (\hat{R}_{\mu\nu})^2 \xrightarrow{\text{PI}} e^{-(d-4)\tau} & \left(d(d-1) (\square\tau)^2 - \frac{1}{2} (d-2) (3d^2 - 8d + 8) (\square\tau) (\partial\tau)^2 \right. \\ & \left. + \frac{1}{2} (d-2)^2 (d^2 - 4d + 6) (\partial\tau)^4 \right). \end{aligned} \tag{B.2}$$

6 Derivatives

In general dimension d , there are 4 independent 6-derivative invariants:

$$\sqrt{-\hat{g}}\hat{R}^3 \xrightarrow{\text{PI}} e^{-(d-6)\tau}(d-1)^3 \left(8(\square\tau)^3 - 12(d-2)(\square\tau)^2(\partial\tau)^2 + 6(d-2)^2(\square\tau)(\partial\tau)^4 - (d-2)^3(\partial\tau)^6 \right), \quad (\text{B.3})$$

$$\begin{aligned} \sqrt{-\hat{g}}\hat{R}(\hat{R}_{\mu\nu})^2 &\xrightarrow{\text{PI}} \frac{1}{2}e^{-(d-6)\tau}(d-1) \left(4(3d-4)(\square\tau)^3 + 4(d-2)^2(\square\tau)(\partial\partial\tau)^2 \right. \\ &\quad + 8(d-2)^2(\square\tau)(\partial\partial\tau\partial\tau\partial\tau) - 2(d-2)(11d-16)(\square\tau)^2(\partial\tau)^2 \\ &\quad - 2(d-2)^3(\partial\partial\tau)^2(\partial\tau)^2 + (13d-18)(d-2)^2(\square\tau)(\partial\tau)^4 \\ &\quad \left. - (d-2)^3(3d-8)(\partial\tau)^6 \right), \end{aligned} \quad (\text{B.4})$$

$$\begin{aligned} \sqrt{-\hat{g}}\hat{R}\hat{\square}\hat{R} &\xrightarrow{\text{PI}} \frac{1}{2}e^{-(d-6)\tau}(d-1)^2 \left(8(\square^2\tau)(\square\tau) + 12(d-2)(\square\tau)^3 - 16(d-2)(\square\tau)(\partial\partial\tau)^2 \right. \\ &\quad + 8(d-10)(d-2)(\square\tau)(\partial\partial\tau\partial\tau\partial\tau) - 16(d^2-6d-10)(\square\tau)^2(\partial\tau)^2 \\ &\quad + 4(d-2)^2(\partial\partial\tau)^2(\partial\tau)^2 + (5d^2-20d-12)(d-2)(\square\tau)(\partial\tau)^4 \\ &\quad \left. - (d^2-8d+20)(d-2)^2(\partial\tau)^6 \right), \end{aligned} \quad (\text{B.5})$$

$$\begin{aligned} \sqrt{-\hat{g}}(\hat{R}_{\mu\nu})^3 &\xrightarrow{\text{PI}} \frac{1}{8}e^{-(d-6)\tau} \left(-4(d^3-6d^2+4d+4)(\square\tau)^3 + 12d(d-2)^2(\square\tau)(\partial\partial\tau)^2 \right. \\ &\quad + 24d(d-2)^2(\square\tau)(\partial\partial\tau\partial\tau\partial\tau) - 4(2d-3)(d-2)^3(\partial\partial\tau)^2(\partial\tau)^2 \\ &\quad + 4(d-2)(2d^3-17d^2+26d-6)(\square\tau)^2(\partial\tau)^2 \\ &\quad - (d-2)^2(5d^3-55d^2+126d-96)(\square\tau)(\partial\tau)^4 \\ &\quad \left. + (d-2)^4(d^2-13d+32)(\partial\tau)^6 \right). \end{aligned} \quad (\text{B.6})$$

8 Derivatives

At the level of 8 derivatives, we have found 9 independent diff×Weyl invariants:

$$R^4, R^2(R_{\mu\nu})^2, R(R_{\mu\nu})^3, ((R_{\mu\nu})^2)^2, (R_{\mu\nu})^4, (\square R)^2, (\square R_{\mu\nu})^2, R(\nabla_\mu R)^2, (R_{\mu\nu})^2\square R, \quad (\text{B.7})$$

where $\sqrt{-\hat{g}}$ is implicit and we use the shorthand notation

$$\begin{aligned} (R_{\mu\nu})^2 &\equiv R_{\mu\nu}R^{\mu\nu}, \quad (R_{\mu\nu})^3 \equiv R^\mu{}_\nu R^\nu{}_\rho R^\rho{}_\mu, \quad (R_{\mu\nu})^4 \equiv R^\mu{}_\nu R^\nu{}_\rho R^\rho{}_\sigma R^\sigma{}_\mu, \\ (\nabla_\mu R)^2 &\equiv (\nabla_\mu R)(\nabla^\mu R), \quad (\square R_{\mu\nu})^2 \equiv (\square R_{\mu\nu})(\square R^{\mu\nu}). \end{aligned} \quad (\text{B.8})$$

Due to the complexity of the off-shell expressions in general d dimensions, we have opted to

display only the $d = 8$ forms:

$$\hat{R}^4 \xrightarrow{\text{PI}} 38416 \left[(\square\tau)^4 - 12(\square\tau)^3(\partial\tau)^2 + 54(\square\tau)^2(\partial\tau)^4 - 108(\square\tau)(\partial\tau)^6 + 81(\partial\tau)^8 \right], \quad (\text{B.9})$$

$$\begin{aligned} \hat{R}^2(\hat{R}_{\mu\nu})^2 \xrightarrow{\text{PI}} & 784 \left[5(\square\tau)^4 + 9(\square\tau)^2(\partial\partial\tau)^2 + 18(\square\tau)^2(\partial\partial\tau\partial\tau\partial\tau) - 69(\square\tau)^3(\partial\tau)^2 - 54(\square\tau)(\partial\partial\tau)^2(\partial\tau)^2 \right. \\ & \left. + 342(\square\tau)^2(\partial\tau)^4 + 81(\partial\partial\tau)^2(\partial\tau)^4 - 108(\square\tau)(\partial\partial\tau\partial\tau\partial\tau)(\partial\tau)^2 - 756(\square\tau)(\partial\tau)^6 + 567(\partial\tau)^8 \right], \end{aligned} \quad (\text{B.10})$$

$$\begin{aligned} \hat{R}(\hat{R}_{\mu\nu})^3 \xrightarrow{\text{PI}} & 28 \left[13(\square\tau)^4 + 108(\square\tau)(\partial\partial\tau\partial\partial\tau\partial\partial\tau) + 54(\square\tau)^2(\partial\partial\tau)^2 + 648(\square\tau)(\partial\partial\partial\tau\partial\tau\partial\tau\partial\tau) + 1728(\square\tau)^2(\partial\partial\tau\partial\tau\partial\tau) \right. \\ & - 972(\partial\partial\tau\partial\tau\partial\tau)(\partial\partial\tau)^2 + 162(\square^2\tau)(\partial\tau)^4 + 276(\square\tau)^3(\partial\tau)^2 - 1620(\square\tau)(\partial\partial\tau)^2(\partial\tau)^2 + 972(\square\tau)^2(\partial\tau)^4 \\ & \left. + 1215(\partial\partial\tau)^2(\partial\tau)^4 - 1620(\square\tau)(\partial\partial\tau\partial\tau\partial\tau)(\partial\tau)^2 - 3024(\square\tau)(\partial\tau)^6 + 2268(\partial\tau)^8 \right], \end{aligned} \quad (\text{B.11})$$

$$\begin{aligned} ((\hat{R}_{\mu\nu})^2)^2 \xrightarrow{\text{PI}} & 16 \left[25(\square\tau)^4 + 90(\square\tau)^2(\partial\partial\tau)^2 + 81(\partial\partial\tau)^4 + 180(\square\tau)^2(\partial\partial\tau\partial\tau\partial\tau) + 324(\partial\partial\tau\partial\tau\partial\tau)(\partial\partial\tau)^2 \right. \\ & - 390(\square\tau)^3(\partial\tau)^2 - 702(\square\tau)(\partial\partial\tau)^2(\partial\tau)^2 + 324(\partial\partial\tau\partial\tau\partial\tau)^2 + 2151(\square\tau)^2(\partial\tau)^4 \\ & \left. + 1134(\partial\partial\tau)^2(\partial\tau)^4 - 1404(\square\tau)(\partial\partial\tau\partial\tau\partial\tau)(\partial\tau)^2 - 5292(\square\tau)(\partial\tau)^6 + 3969(\partial\tau)^8 \right], \end{aligned} \quad (\text{B.12})$$

$$\begin{aligned} (\hat{R}_{\mu\nu})^4 \xrightarrow{\text{PI}} & 8 \left[31(\square\tau)^4 + 324(\square\tau)(\partial\partial\tau\partial\partial\tau\partial\partial\tau) + 81(\partial\partial\tau)^4 - 135(\square\tau)^2(\partial\partial\tau)^2 + 1944(\square\tau)(\partial\partial\partial\tau\partial\tau\partial\tau\partial\tau) \right. \\ & + 4590(\square\tau)^2(\partial\partial\tau\partial\tau\partial\tau) - 2592(\partial\partial\tau\partial\tau\partial\tau)(\partial\partial\tau)^2 + 486(\square^2\tau)(\partial\tau)^4 + 1221(\square\tau)^3(\partial\tau)^2 \\ & - 3240(\square\tau)(\partial\partial\tau)^2(\partial\tau)^2 + 324(\partial\partial\tau\partial\tau\partial\tau)^2 + 189(\square\tau)^2(\partial\tau)^4 + 1296(\partial\partial\tau)^2(\partial\tau)^4 \\ & \left. - 1620(\square\tau)(\partial\partial\tau\partial\tau\partial\tau)(\partial\tau)^2 - 1512(\square\tau)(\partial\tau)^6 + 1134(\partial\tau)^8 \right], \end{aligned} \quad (\text{B.13})$$

$$\begin{aligned} (\hat{\square}\hat{R})^2 \xrightarrow{\text{PI}} & \frac{196}{3} \left[3(\square^2\tau)^2 + 48(\square^2\tau)(\square\tau)^2 + 48(\square\tau)(\partial\partial\partial\tau)^2 - 60(\square^2\tau)(\partial\partial\tau)^2 + 140(\square\tau)^4 + 192(\square\tau)(\partial\partial\partial\tau\partial\partial\tau\partial\tau) \right. \\ & + 384(\square\tau)(\partial\partial\tau\partial\partial\tau\partial\partial\tau) - 120(\square^2\tau)(\partial\partial\tau\partial\tau\partial\tau) + 108(\partial\partial\tau)^4 - 456(\square\tau)^2(\partial\partial\tau)^2 - 84(\square^2\tau)(\square\tau)(\partial\tau)^2 \\ & + 576(\square\tau)(\partial\partial\partial\tau\partial\tau\partial\tau\partial\tau) + 624(\square\tau)^2(\partial\partial\tau\partial\tau\partial\tau) - 432(\partial\partial\tau\partial\tau\partial\tau)(\partial\partial\tau)^2 + 288(\square^2\tau)(\partial\tau)^4\tau \\ & - 216(\square\tau)^3(\partial\tau)^2 - 72(\square\tau)(\partial\partial\tau)^2(\partial\tau)^2 + 432(\partial\partial\tau\partial\tau\partial\tau)^2 + 2028(\square\tau)^2(\partial\tau)^4 - 864(\partial\partial\tau)^2(\partial\tau)^4 \\ & \left. + 3600(\square\tau)(\partial\partial\tau\partial\tau\partial\tau)(\partial\tau)^2 - 2304(\square\tau)(\partial\tau)^6 + 1728(\partial\tau)^8 \right], \end{aligned} \quad (\text{B.14})$$

$$\begin{aligned} (\hat{\square}\hat{R}_{\mu\nu})^2 \xrightarrow{\text{PI}} & \frac{2}{3} \left[84(\square^2\tau)^2 + 777(\square^2\tau)(\square\tau)^2 + 156(\square\tau)(\partial\partial\partial\tau)^2 - 762(\square^2\tau)(\partial\partial\tau)^2 + 662(\square\tau)^4 \right. \\ & - 8448(\square\tau)(\partial\partial\partial\tau\partial\partial\tau\partial\tau) - 1272(\square\tau)(\partial\partial\tau\partial\partial\tau\partial\partial\tau) - 1524(\square^2\tau)(\partial\partial\tau\partial\tau\partial\tau) + 2376(\partial\partial\tau)^4 \\ & - 2454(\square\tau)^2(\partial\partial\tau)^2 - 3432(\square^2\tau)(\square\tau)(\partial\tau)^2 - 8064(\square\tau)(\partial\partial\partial\tau\partial\tau\partial\tau\partial\tau) - 25080(\square\tau)^2(\partial\partial\tau\partial\tau\partial\tau) \\ & - 5616(\partial\partial\tau\partial\tau\partial\tau)(\partial\partial\tau)^2 + 2016(\square^2\tau)(\partial\tau)^4 - 15012(\square\tau)^3(\partial\tau)^2 + 7488(\square\tau)(\partial\partial\tau)^2(\partial\tau)^2 \\ & - 17712(\partial\partial\tau\partial\tau\partial\tau)^2 + 45444(\square\tau)^2(\partial\tau)^4 - 540(\partial\partial\tau)^2(\partial\tau)^4 \\ & \left. + 59328(\square\tau)(\partial\partial\tau\partial\tau\partial\tau)(\partial\tau)^2 - 64512(\square\tau)(\partial\tau)^6 + 48384(\partial\tau)^8 \right], \end{aligned} \quad (\text{B.15})$$

$$\begin{aligned} \hat{R}(\hat{\nabla}_\mu\hat{R})^2 \xrightarrow{\text{PI}} & -\frac{1372}{3} \left[3(\square^2\tau)(\square\tau)^2 + 14(\square\tau)^4 - 18(\square\tau)^2(\partial\partial\tau)^2 - 18(\square^2\tau)(\square\tau)(\partial\tau)^2 - 108(\square\tau)^2(\partial\partial\tau\partial\tau\partial\tau) \right. \\ & + 27(\square^2\tau)(\partial\tau)^4 - 150(\square\tau)^3(\partial\tau)^2 + 108(\square\tau)(\partial\partial\tau)^2(\partial\tau)^2 + 594(\square\tau)^2(\partial\tau)^4 \\ & \left. - 162(\partial\partial\tau)^2(\partial\tau)^4 + 648(\square\tau)(\partial\partial\tau\partial\tau\partial\tau)(\partial\tau)^2 - 864(\square\tau)(\partial\tau)^6 + 648(\partial\tau)^8 \right], \end{aligned} \quad (\text{B.16})$$

$$\begin{aligned} (\hat{R}_{\mu\nu})^2\hat{\square}\hat{R} \xrightarrow{\text{PI}} & \frac{56}{3} \left[15(\square^2\tau)(\square\tau)^2 + 27(\square^2\tau)(\partial\partial\tau)^2 + 70(\square\tau)^4 + 432(\square\tau)(\partial\partial\partial\tau\partial\partial\tau\partial\tau) + 54(\square^2\tau)(\partial\partial\tau\partial\tau\partial\tau) \right. \\ & - 162(\partial\partial\tau)^4 + 180(\square\tau)^2(\partial\partial\tau)^2 - 117(\square^2\tau)(\square\tau)(\partial\tau)^2 + 432(\square\tau)(\partial\partial\partial\tau\partial\tau\partial\tau\partial\tau) + 216(\square\tau)^2(\partial\partial\tau\partial\tau\partial\tau) \\ & + 297(\square^2\tau)(\partial\tau)^4 - 696(\square\tau)^3(\partial\tau)^2 - 108(\square\tau)(\partial\partial\tau)^2(\partial\tau)^2 + 648(\partial\partial\tau\partial\tau\partial\tau)^2 + 3888(\square\tau)^2(\partial\tau)^4 \\ & \left. - 486(\partial\partial\tau)^2(\partial\tau)^4 + 3888(\square\tau)(\partial\partial\tau\partial\tau\partial\tau)(\partial\tau)^2 - 6048(\square\tau)(\partial\tau)^6 + 4536(\partial\tau)^8 \right]. \end{aligned} \quad (\text{B.17})$$

Appendix C

Dilaton Amplitudes in d Dimensions

Here we list the dilaton amplitudes at $O(p^4)$, $O(p^6)$, and $O(p^8)$ for $n = 4, 5, \dots, 8$ as derived from the general d -dimensional dilaton effective action (2.49):

► $O(p^4)$ amplitudes:

$$\begin{aligned}
 \mathcal{A}_4^{(4)} &= \frac{32}{(d-2)^4} \frac{\alpha}{f^{2d-4}} (s^2 + t^2 + u^2), & \mathcal{A}_5^{(4)} &= \frac{32d}{(d-2)^5} \frac{\alpha}{f^{5d/2-5}} P_5^{(4)}, \\
 \mathcal{A}_6^{(4)} &= \frac{32d(3d-2)}{(d-2)^6} \frac{\alpha}{f^{3d-6}} P_6^{(4)}, & \mathcal{A}_7^{(4)} &= \frac{128d(d-1)(3d-2)}{(d-2)^7} \frac{\alpha}{f^{7d/2-7}} P_7^{(4)}, \\
 \mathcal{A}_8^{(4)} &= \frac{128d(d-1)(3d-2)(5d-6)}{(d-2)^8} \frac{\alpha}{f^{4d-8}} P_8^{(4)}, & & \tag{C.1}
 \end{aligned}$$

where $P_n^{(4)} \equiv \sum_{1 \leq i < j \leq n} s_{ij}^2$.

► $O(p^6)$ amplitudes:

$$\begin{aligned}
 \mathcal{A}_4^{(6)} &= \frac{128}{(d-2)^4} \frac{\beta}{f^{2d-4}} (s^3 + t^3 + u^3), \\
 \mathcal{A}_5^{(6)} &= \frac{128(d+2)}{(d-2)^5} \frac{\beta}{f^{5d/2-5}} P_5^{(6)}, \\
 \mathcal{A}_6^{(6)} &= \frac{64(d+2)}{(d-2)^6} \frac{\beta}{f^{3d-6}} \left(4d P_{6,A}^{(6)} + (d+2) P_{6,B}^{(6)} \right), \\
 \mathcal{A}_7^{(6)} &= \frac{256d(d+2)}{(d-2)^7} \frac{\beta}{f^{7d/2-7}} \left((3d-2) P_{7,A}^{(6)} + (d+2) P_{7,B}^{(6)} \right), \\
 \mathcal{A}_8^{(6)} &= \frac{256d(d+2)(5d-2)}{(d-2)^8} \frac{\beta}{f^{4d-8}} \left(2(d-2) P_{8,A}^{(6)} + (d+2) P_{8,B}^{(6)} \right), & & \tag{C.2}
 \end{aligned}$$

where $P_{n,A}^{(6)} = \sum_{1 \leq i < j \leq n} s_{ij}^3$ and $P_{n,B}^{(6)} = \sum_{1 \leq i < j < k \leq n} s_{ijk}^3$.

► $O(p^8)$ amplitudes:

$$\begin{aligned}
\mathcal{A}_4^{(8)} &= \frac{1}{f^{2d-4}} \frac{32}{(d-2)^4} (9\gamma + \tilde{\gamma}) (s^4 + t^4 + u^4), \\
\mathcal{A}_5^{(8)} &= \frac{1}{f^{\frac{5d}{2}-5}} \frac{32}{(d-2)^5} \left([9(d+4)\gamma + d\tilde{\gamma}] P_{5,A}^{(8)} + 8\tilde{\gamma} P_{5,B}^{(8)} \right) \\
\mathcal{A}_6^{(8)} &= \frac{1}{f^{3d-6}} \frac{16}{(d-2)^6} \left(4 [9(d+4)(d+1)\gamma + d(d-1)\tilde{\gamma}] P_{6,A}^{(8)} + [9(d+4)^2\gamma + d^2\tilde{\gamma}] P_{6,B}^{(8)} \right. \\
&\quad \left. + 16(d+6)\tilde{\gamma} P_{6,C}^{(8)} + 16d\tilde{\gamma} P_{6,D}^{(8)} \right) \\
\mathcal{A}_7^{(8)} &= \frac{1}{f^{\frac{7d}{2}-7}} \frac{64(d+1)}{(d-2)^7} \left(d [27(d+4)\gamma + (3d+4)\tilde{\gamma}] P_{7,A}^{(8)} + [9(d+4)^2\gamma + d(d-8)\tilde{\gamma}] P_{7,B}^{(8)} \right. \\
&\quad \left. + 16(d+6)\tilde{\gamma} P_{7,C}^{(8)} + 16d\tilde{\gamma} P_{7,D}^{(8)} \right) \\
\mathcal{A}_8^{(8)} &= \frac{1}{f^{4d-8}} \frac{64(d+1)}{3(d-2)^8} \left(2d [81(2d^2+7d-4)\gamma + (18d^2+7d-4)\tilde{\gamma}] P_{8,A}^{(8)} \right. \\
&\quad + d [81(d+4)^2\gamma + (9d^2+4d+8)\tilde{\gamma}] P_{8,B}^{(8)} \\
&\quad + [27(d+1)(d+4)^2\gamma + d(3d^2-29d-16)\tilde{\gamma}] P_{8,C}^{(8)} \\
&\quad \left. + 288(5d+2)\tilde{\gamma} P_{8,D}^{(8)} + 24d(5d+2)\tilde{\gamma} P_{8,E}^{(8)} \right), \tag{C.3}
\end{aligned}$$

where

$$P_{5,A}^{(8)} = \sum_{1 \leq i < j \leq 5} s_{ij}^4, \quad P_{5,B}^{(8)} = s_{12}^2 s_{34}^2 + \text{perms}, \tag{C.4}$$

$$\begin{aligned}
P_{6,A}^{(8)} &= \sum_{1 \leq i < j \leq 6} s_{ij}^4, & P_{6,B}^{(8)} &= \sum_{1 \leq i < j < k \leq 6} s_{ijk}^4, \\
P_{6,C}^{(8)} &= s_{12}^2 s_{34}^2 + \text{perms}, & P_{6,D}^{(8)} &= s_{123}^2 s_{45}^2 + \text{perms}
\end{aligned} \tag{C.5}$$

$$\begin{aligned}
P_{7,A}^{(8)} &= \sum_{1 \leq i < j \leq 7} s_{ij}^4, & P_{7,B}^{(8)} &= \sum_{1 \leq i < j < k \leq 7} s_{ijk}^4, \\
P_{7,C}^{(8)} &= s_{12}^2 s_{34}^2 + \text{perms}, & P_{7,D}^{(8)} &= s_{123}^2 s_{456}^2 + \text{perms},
\end{aligned} \tag{C.6}$$

$$\begin{aligned}
P_{8,A}^{(8)} &= \sum_{1 \leq i < j \leq 8} s_{ij}^4, & P_{8,B}^{(8)} &= \sum_{1 \leq i < j < k \leq 8} s_{ijk}^4, & P_{8,C}^{(8)} &= \sum_{1 \leq i < j < k < l \leq 8} s_{ijkl}^4, \\
P_{8,D}^{(8)} &= s_{12}^2 s_{34}^2 + \text{perms}, & P_{8,E}^{(8)} &= s_{123}^2 s_{456}^2 + \text{perms}.
\end{aligned} \tag{C.7}$$

Here “+perms” includes all *inequivalent* permutations of the external particle labels.

Appendix D

Free Massive Scalar: 1-Loop Dilaton Scattering

Here we provide some practical details of the calculation of the 1-loop dilaton scattering amplitudes in the example of the free massive scalar in d -dimensions.

Consider a 1-loop diagram with the n external outgoing momenta p_1, p_2, \dots, p_n in canonical order; all other diagrams of the same topology are obtained from the one with canonical ordering by simple permutations of the momentum labels in the result. Momentum conservation is enforced as $\sum_{i=1}^n p_i^\mu = 0$ with all momenta outgoing as in Figure D.1.

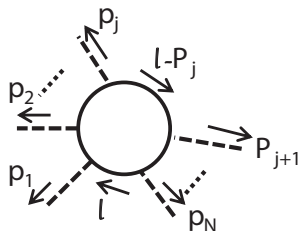


Figure D.1: All external momenta are outgoing. Loop momentum flows clockwise.

The n external φ 's connect to a Φ -loop via $\Phi^2\varphi^k$ terms generated by expanding the action (2.71) with $\Omega = f^{(d-2)/2} - \varphi$, as discussed in Section 2.5.1. We denote a canonical diagram with V vertices by $\{N_1, N_2, \dots, N_V\}$, where N_j are the number of external φ 's at the j^{th} vertex and $\sum_{j=1}^V N_j = n$. For example, two distinct box diagrams for $n = 6$ are shown in Figure D.2.

Let ℓ be the loop momentum flowing into the vertex associated with p_1 . The momentum of the j^{th} internal propagator (going out of the j^{th} vertex) is $\ell - \mathcal{P}_j$, where by momentum conservation $\mathcal{P}_j \equiv \sum_{r=1}^{N_1+N_2+\dots+N_j} p_r$.

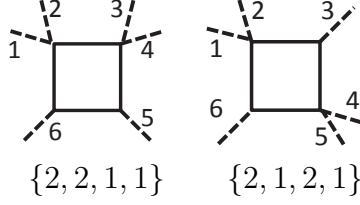


Figure D.2: Two distinct $n = 6$ box diagrams with canonical labels.

The expression for a canonical diagram $\{N_1, N_2, \dots, N_V\}$ can be written

$$I_{\{N_1, N_2, \dots, N_V\}} = \frac{1}{S} \int \frac{d^d \ell}{(2\pi)^d} \prod_{j=1}^V V_{N_j} \frac{-i}{(\ell - \mathcal{P}_j)^2 + M^2}, \quad (\text{D.1})$$

where V_{N_j} is the vertex factor (2.75) associated with the j^{th} vertex. The symmetry factor S takes into account exchanges of identical internal propagators. All diagrams we consider have $S = 1$ except the bubble diagrams with exactly two vertices, which have $S = 2$.

It is useful to Feynman-parameterize (D.1) as

$$I_{\{N_1, N_2, \dots, N_V\}} = \frac{(-1)^{V+N}}{S} \frac{M^{2V}}{f^N} \left(\prod_{n=0}^{N_j-1} \binom{\frac{4}{d-2} - n}{n} \right) \int \frac{d^d \ell}{(2\pi)^d} \left(\prod_{j=1}^V \int_0^1 dx_j \right) \frac{\Gamma(V) \delta\left(1 - \sum_{k=1}^V x_k\right)}{\left[\sum_{m=1}^V x_m ((\ell - \mathcal{P}_m)^2 + M^2) \right]^V}. \quad (\text{D.2})$$

We are interested in the low-energy expansion of the amplitudes, so we expand the integrals (D.2) in the Mandelstam invariants of the external momenta. Practically this is done by shifting the loop-momentum ℓ such that the integrand can be expanded in powers of $\mathbb{P}^2/(\ell^2 + M^2)$, where

$$\mathbb{P}^2 \equiv \left(\sum_{m=1}^V x_m \mathcal{P}_m \right)^2 - \sum_{m=1}^V x_m \mathcal{P}_m^2. \quad (\text{D.3})$$

A little algebra shows that the $O(p^{2k})$ part of the diagram is

$$I_{\{N_1, N_2, \dots, N_V\}}^{O(p^{2k})} = \frac{(-1)^{V+N}}{S} \frac{M^{2V}}{f^N} \frac{\Gamma(V+k)}{k!} \left(\prod_{n=0}^{N_j-1} \binom{\frac{4}{d-2} - n}{n} \right) \left(\int \frac{d^d \ell}{(2\pi)^d} \frac{1}{[\ell^2 + M^2]^{V+k}} \right) \times \left[\left(\prod_{j=1}^V \int_0^1 dx_j \right) (\mathbb{P}^2)^k \delta\left(1 - \sum_{k=1}^V x_k\right) \right]. \quad (\text{D.4})$$

The momentum integral is finite for $V + k > d/2$ and gives (in Euclidean signature)

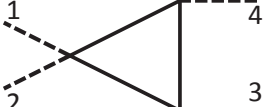
$$\begin{aligned} \int_{-\infty}^{\infty} \frac{d^d \ell}{(2\pi)^d} \frac{1}{[\ell^2 + M^2]^{V+k}} &= \int d\Omega_{d-1} \int_0^{\infty} \frac{d\ell}{(2\pi)^d} \frac{\ell^{d-1}}{[\ell^2 + M^2]^{V+k}} \\ &= \frac{1}{(4\pi)^{d/2} M^{2(V+k-d/2)}} \frac{\Gamma(V+k-d/2)}{\Gamma(V+k)} \end{aligned} \quad (\text{D.5})$$

So we arrive at the Mathematica-friendly expression:

$$\begin{aligned} I_{\{N_1, N_2, \dots, N_V\}}^{O(p^{2k})} & \\ &= \frac{(-1)^{V+N}}{S} \frac{\Gamma(V+k-d/2)}{k!} \frac{M^{d-2k}}{f^N (4\pi)^{d/2}} \left(\prod_{n=0}^{N_j-1} \left(\frac{4}{d-2} - n \right) \right) \left[\left(\prod_{j=1}^V \int_0^{1-\sum_{q=1}^{j-1} x_q} dx_j \right) (\mathbb{P}^2)^k \right]. \end{aligned} \quad (\text{D.6})$$

To obtain the full contribution from diagrams of a given topology $\{N_1, N_2, \dots, N_V\}$, we must sum over inequivalent permutations of the external momenta, i.e. over arrangements of the external momentum labels not related by cyclic permutations or reflection symmetry. The final result can be written in terms of a basis of Mandelstam polynomials which are fully symmetric in the external momenta, e.g. the $O(p^8)$ basis of (C.4)-(C.7).

Example: 4-point amplitude. Consider the 4-point amplitude at $\mathcal{O}(p^8)$ in $d = 8$ dimensions. There are 3 types of diagrams, a bubble, a triangle and a square. The canonical diagram $\{2, 1, 1\}$ gives

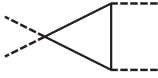
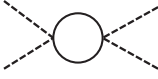
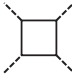


$$= \frac{s^4}{612\,360 (4\pi)^4 f^{12}}. \quad (\text{D.7})$$

There are $\binom{4}{2} = 6$ distinct permutations of the momentum labels of this diagram, and summing them gives the result in the first row of Table D.1. The sum of the contributions from the three classes of diagrams in the table gives the 4-point 1-loop amplitude at $\mathcal{O}(p^8)$ in $8d$, as also listed in (2.57),

$$\mathcal{A}_4^{(8)} = \frac{17}{3\,061\,800 (4\pi)^4 f^{12}}. \quad (\text{D.8})$$

Table D.1: Diagrams contributing to the 4-point 1-loop amplitude at $\mathcal{O}(p^8)$ in $8d$.

Diagram	Unique Permutations	Symmetry Factor	Partial Amplitude at $\mathcal{O}(p^8)$ in $8d$
	6	1	$\frac{s^4 + t^4 + u^4}{612\,360 (4\pi)^4 f^{12}}$
	3	2	$\frac{s^4 + t^4 + u^4}{382\,725 (4\pi)^4 f^{12}}$
	3	1	$\frac{s^4 + t^4 + u^4}{765\,450 (4\pi)^4 f^{12}}$

Appendix E

Conformal Anomaly

The conformal anomaly in four-dimensional CFTs in the presence of background metric and gauge field is well-known (see, for example, [124] for a summary). The goal here is to show how this result arises from imposing the WZ consistency condition [78] and compatibility with the anomaly for the global $U(1)$ symmetry associated with the background gauge field.

The trace anomaly $\langle T_\mu^\mu \rangle$ should be a function only of the background fields $g_{\mu\nu}$, A_μ , and their derivatives. Since the gauge symmetry is broken, it is conceivable that one could have new gauge-noninvariant contributions to the trace anomaly in addition to the standard W^2 , E_4 , $(F_{\mu\nu})^2$, and $\square R$ terms.¹ The possible new quantities should be constructed out of the following list with various choices of the coefficients d_i :

$$\begin{aligned}
& d_1 \nabla_\mu (R) A^\mu + d_2 R \nabla_\mu A^\mu + d_3 \nabla_\mu \square A^\mu + d_4 R^{\mu\nu} \nabla_\mu A_\nu + d_5 R (A_\mu)^2 + d_6 R_{\mu\nu} A^\mu A^\nu \\
& + d_7 \nabla_\mu (A^\mu) \nabla_\nu (A^\nu) + d_8 \nabla_\mu (A^\nu) \nabla_\nu (A^\mu) + d_9 \nabla_\mu (A_\nu) \nabla^\mu (A^\nu) + d_{10} A_\mu \nabla_\nu \nabla^\nu A^\mu \\
& + d_{11} A^\nu \nabla_\mu \nabla_\nu A^\mu + d_{12} (A_\mu)^2 \nabla_\nu A^\nu + d_{13} A^\mu A^\nu \nabla_\mu A_\nu + d_{14} (A_\mu)^4 .
\end{aligned} \tag{E.1}$$

We will find, however, that none of these possibilities are allowed in the trace anomaly.

WZ consistency conditions

The full action S should satisfy the Wess-Zumino consistency conditions [78] (see also [125] for further discussion). In particular, since the Weyl variation of S is the trace anomaly, the WZ conditions amount to the requirement

$$\int d^4x \left(\sigma_2 \delta_{\sigma_1} - \sigma_1 \delta_{\sigma_2} \right) \sqrt{-g} \langle T_\mu^\mu \rangle = 0 . \tag{E.2}$$

¹The $\square R$ “anomaly” is non-physical because it can be removed by a local counterterm, but we include it here for completeness.

The usual anomalies, W^2 , E_4 , $(F_{\mu\nu})^2$, and $\square R$, satisfy that constraint, but it remains to check whether any combination of the terms in (E.1) might also work. In fact, one can verify that each of the following independently satisfies the constraint:

$$\begin{aligned}
K_1 &= \nabla_\mu \left(3R^{\mu\nu} A_\nu - R A^\mu + 3\square A^\mu \right), \\
K_2 &= \nabla_\mu \left(A^\nu \nabla_\nu A^\mu \right), \\
K_3 &= \nabla_\mu \left(A^\mu \nabla_\nu A^\nu \right), \\
K_4 &= A_\mu \nabla_\nu (F^{\mu\nu}), \\
K_5 &= \nabla_\mu \left(A^\mu (A_\nu)^2 \right), \\
K_6 &= (A_\mu)^4.
\end{aligned} \tag{E.3}$$

Therefore based on the WZ consistency conditions alone, the trace anomaly can take the form

$$cW^2 - aE_4 + b'\square R + \kappa_0(F_{\mu\nu})^2 + \kappa_1 K_1 + \kappa_2 K_2 + \kappa_3 K_3 + \kappa_4 K_4 + \kappa_5 K_5 + \kappa_6 K_6, \tag{E.4}$$

where the first four terms are the standard conformal anomalies in the presence of a background gauge field and curved background for a theory with central charges c and a [124]. The coefficient of $(F_{\mu\nu})^2$ is generally an independent physical quantity, although for $\mathcal{N} = 1$ theories it is fixed in terms of c and a .

Constraints on $\langle T_\mu^\mu \rangle$ from the gauge anomaly

Just as the Weyl anomaly does not depend on either τ or β , the gauge anomaly (3.3) should also be a function of just the background fields. Thus there cannot be gauge dependent fields in (E.4); under a gauge variation those terms generate τ -dependent contributions to the gauge anomaly. To illustrate this point, let us consider an example. Suppose $\kappa_6 \neq 0$, so $\langle T_\mu^\mu \rangle$ includes an $(A)^4$ anomaly. Since $\sqrt{-g}(A)^4$ is Weyl invariant, the action whose variation produces this anomaly is simply

$$S_{\text{WZ}, A^4} = \kappa_6 \int d^4x \sqrt{-g} \tau (A)^4. \tag{E.5}$$

Now consider a gauge variation of this action, which should produce the gauge anomaly as in (3.3)

$$\delta_\alpha S_{\text{WZ}, A^4} \sim \kappa_6 \int d^4x \sqrt{-g} \tau (A)^3 \nabla \alpha, \tag{E.6}$$

which is τ -dependent. The other new quantities have similar issues; in fact, no linear combination of K_1, \dots, K_6 in (E.3) is gauge invariant. This forces us to set $\kappa_1 = \kappa_2 = \dots = \kappa_6 = 0$ so that the trace anomaly is gauge invariant.

Since none of the new possibilities can contribute, we find that the trace anomaly for any $\mathcal{N} = 1$ superconformal theory is

$$\langle T_\mu{}^\mu \rangle = cW^2 - aE_4 + b'\square R - 6c(F_{\mu\nu})^2, \quad (\text{E.7})$$

where the coefficient $\kappa_0 = -6c$ of the last term is fixed by supersymmetry as in [26, 22, 75] (though with different normalization for the gauge field).

Appendix F

Matrix Q Details

F.1 Derivation of $\det Q$

Let $Q_{ij}^{(0)}$ be the full (degenerate) $n \times n$ transformation matrix from B to C variables, i.e. $C_{\hat{\alpha}j} = B_{\hat{\alpha}i} Q_{ij}^{(0)}$. It can be obtained from (4.25) as

$$Q_{ij}^{(0)} = \frac{\partial C_{\hat{\alpha}i}}{\partial B_{\hat{\alpha}j}}. \quad (\text{F.1})$$

Define $Q_{ij}^{(m)}$ to be the $(n-m) \times (n-m)$ matrix obtained from $Q_{ij}^{(0)}$ by deleting the first m rows and m columns. For example, the matrix needed in (4.31) is obtained by deleting the first two rows and columns:

$$Q = Q^{(2)} = \begin{pmatrix} \frac{\langle 42 \rangle}{\langle 23 \rangle \langle 34 \rangle} & \frac{1}{\langle 34 \rangle} & 0 & 0 & \cdots & 0 \\ \frac{1}{\langle 34 \rangle} & \frac{\langle 53 \rangle}{\langle 34 \rangle \langle 45 \rangle} & \frac{1}{\langle 45 \rangle} & 0 & \cdots & 0 \\ 0 & \frac{1}{\langle 45 \rangle} & \ddots & \ddots & \ddots & \vdots \\ 0 & 0 & \ddots & & & 0 \\ \vdots & \vdots & 0 & \frac{1}{\langle n-2, n-1 \rangle} & \frac{\langle n, n-2 \rangle}{\langle n-2, n-1 \rangle \langle n-1, n \rangle} & \frac{1}{\langle n-1, n \rangle} \\ 0 & \cdots & 0 & 0 & \frac{1}{\langle n-1, n \rangle} & \frac{\langle 1, n-1 \rangle}{\langle n-1, n \rangle \langle n1 \rangle} \end{pmatrix}. \quad (\text{F.2})$$

With the definition $Q^{(n)} = 1$, we will prove the following claim by induction:

Claim: For $i > 0$, $\det Q^{(n-i)} = (-1)^{i-1} \frac{\langle 1, n-i \rangle}{\langle n-i, n-i+1 \rangle \cdots \langle n1 \rangle}$.

(F.3)

Proof: For $i = 1$, we trivially have

$$Q^{(n-1)} = \left(\frac{\langle 1, n-1 \rangle}{\langle n-1, n \rangle \langle n1 \rangle} \right) \implies \det Q^{(n-1)} = \frac{\langle 1, n-1 \rangle}{\langle n-1, n \rangle \langle n1 \rangle}, \quad (\text{F.4})$$

i.e. the determinant satisfies the claim (F.3).

For $i = 2$, the determinant of

$$Q^{(n-2)} = \begin{pmatrix} \frac{\langle n, n-2 \rangle}{\langle n-2, n-1 \rangle \langle n-1, n \rangle} & \frac{1}{\langle n-1, n \rangle} \\ \frac{1}{\langle n-1, n \rangle} & \frac{\langle 1, n-1 \rangle}{\langle n-1, n \rangle \langle n1 \rangle} \end{pmatrix}. \quad (\text{F.5})$$

is calculated easily with a single application of the Schouten identity, and the answer is

$$\det Q^{(n-2)} = -\frac{\langle 1, n-2 \rangle}{\langle n-2, n-1 \rangle \langle n-1, n \rangle \langle n1 \rangle}. \quad (\text{F.6})$$

The result satisfies the claim. This establishes the base of the induction.

For the inductive argument, assume that the claim (F.3) is satisfied for all $i < m < n$. We will prove it for $i = m$. The matrix $Q^{(n-m)}$ is of the form

$$Q^{(n-m)} = \begin{pmatrix} A & B & 0 & 0 & \cdots & 0 \\ B & C & D & 0 & \cdots & \vdots \\ 0 & D & & & & \\ 0 & 0 & & & & \\ \vdots & \vdots & & & Q^{(n-m+2)} & \\ 0 & 0 & & & & \end{pmatrix} \quad (\text{F.7})$$

with

$$A = \frac{\langle n-m+2, n-m \rangle}{\langle n-m, n-m+1 \rangle \langle n-m+1, n-m+2 \rangle}, \quad B = \frac{1}{\langle n-m+1, n-m+2 \rangle} \quad \text{etc.} \quad (\text{F.8})$$

To evaluate the determinant, we expand on the first row of (F.7), and subsequently on the second row, to find

$$\det Q^{(n-m)} = A \det Q^{(n-m+1)} - B^2 \det Q^{(n-m+2)}. \quad (\text{F.9})$$

By the inductive hypothesis, we may replace the two determinants on the right-hand side

and obtain:

$$\begin{aligned}
\det Q^{(n-m)} &= (-1)^m \left[\frac{\langle n-m+2, n-m \rangle}{\langle n-m, n-m+1 \rangle \langle n-m+1, n-m+2 \rangle} \frac{\langle 1, n-m+1 \rangle}{\langle n-m+1, n-m+2 \rangle \cdots \langle n1 \rangle} \right. \\
&\quad \left. + \frac{1}{\langle n-m+1, n-m+2 \rangle^2} \frac{\langle 1, n-m+2 \rangle}{\langle n-m+2, n-m+3 \rangle \cdots \langle n1 \rangle} \right] \\
&= \frac{(-1)^m}{\langle n-m+1, n-m+2 \rangle} \frac{\langle 1, n-m+1 \rangle \langle n-m+2, n-m \rangle + \langle 1, n-m+2 \rangle \langle n-m, n-m+1 \rangle}{\langle n-m, n-m+1 \rangle \cdots \langle n1 \rangle} \\
&= (-1)^{m-1} \frac{\langle 1, n-m \rangle}{\langle n-m, n-m+1 \rangle \cdots \langle n1 \rangle}.
\end{aligned} \tag{F.10}$$

In the last line we used the Schouten identity. Thus by induction we have proven the claim (F.3). \square

The determinant given in (4.31) is simply the result for $i = n - 2$, so

$$|\det Q^{(2)}| = \frac{\langle 12 \rangle}{\langle 23 \rangle \cdots \langle n1 \rangle} = \frac{\langle 12 \rangle^2}{\langle 12 \rangle \cdots \langle n1 \rangle}. \tag{F.11}$$

F.2 Verification of Q^{-1}

The square, symmetric matrix Q is given by (for $\hat{i}, \hat{p} \in [3, n]$)

$$Q_{\hat{i}\hat{p}} = \begin{cases} \frac{\langle \hat{i}+1, \hat{i}-1 \rangle}{\langle \hat{i}-1, \hat{i} \rangle \langle \hat{i}, \hat{i}+1 \rangle}, & \hat{p} = \hat{i} \\ \frac{1}{\langle \hat{i}, \hat{i}+1 \rangle}, & \hat{p} = \hat{i} + 1 \\ \frac{1}{\langle \hat{i}-1, \hat{i} \rangle}, & \hat{p} = \hat{i} - 1 \\ 0, & \text{else.} \end{cases} \tag{F.12}$$

The determinant is non-vanishing as shown above, so it is invertible. We claim that its inverse is given by (for $\hat{p}, \hat{j} \in [3, n]$)

$$Q_{\hat{p}\hat{j}}^{-1} = \begin{cases} -\frac{\langle 1\hat{j} \rangle \langle 2\hat{p} \rangle}{\langle 12 \rangle}, & \hat{j} \geq \hat{p} \\ -\frac{\langle 1\hat{p} \rangle \langle 2\hat{j} \rangle}{\langle 12 \rangle}, & \hat{j} \leq \hat{p}. \end{cases} \tag{F.13}$$

It is straightforward to verify the claim by a direct computation of $Q_{\hat{i}\hat{p}} Q_{\hat{p}\hat{j}}^{-1}$. The sum over \hat{p}

produces three terms due to the three non-zero entries in each row of (F.12).

$$\begin{aligned}
Q_{i\hat{p}}Q_{\hat{p}\hat{j}}^{-1} &= \frac{1}{\langle \hat{i}-1, \hat{i} \rangle} \left\{ \begin{array}{l} -\frac{\langle 1\hat{j} \rangle \langle 2, \hat{i}-1 \rangle}{\langle 12 \rangle}, \quad \hat{j} \geq \hat{i} \\ -\frac{\langle 1, \hat{i}-1 \rangle \langle 2\hat{j} \rangle}{\langle 12 \rangle}, \quad \hat{j} < \hat{i} \end{array} \right\}_{\hat{p}=\hat{i}-1} \\
&+ \frac{\langle \hat{i}+1, \hat{i}-1 \rangle}{\langle \hat{i}-1, \hat{i} \rangle \langle \hat{i}, \hat{i}+1 \rangle} \left\{ \begin{array}{l} -\frac{\langle 1\hat{j} \rangle \langle 2, \hat{i} \rangle}{\langle 12 \rangle}, \quad \hat{j} \geq \hat{i} \\ -\frac{\langle 1, \hat{i} \rangle \langle 2\hat{j} \rangle}{\langle 12 \rangle}, \quad \hat{j} < \hat{i} \end{array} \right\}_{\hat{p}=\hat{i}} \\
&+ \frac{1}{\langle \hat{i}, \hat{i}+1 \rangle} \left\{ \begin{array}{l} -\frac{\langle 1\hat{j} \rangle \langle 2, \hat{i}+1 \rangle}{\langle 12 \rangle}, \quad \hat{j} > \hat{i} \\ -\frac{\langle 1, \hat{i}+1 \rangle \langle 2\hat{j} \rangle}{\langle 12 \rangle}, \quad \hat{j} \leq \hat{i} \end{array} \right\}_{\hat{p}=\hat{i}+1}.
\end{aligned} \tag{F.14}$$

Examining the limits on \hat{j} in each term, we see that there are three cases that should be considered: $\hat{j} < \hat{i}$, $\hat{j} = \hat{i}$, $\hat{j} > \hat{i}$. We begin with $\hat{j} < \hat{i}$. Taking the relevant pieces from each of the three terms in (F.14), we find

$$\begin{aligned}
Q_{i\hat{p}}Q_{\hat{p}\hat{j}}^{-1}|_{\hat{j}<\hat{i}} &= -\frac{\langle 2\hat{j} \rangle \langle 1, \hat{i}-1 \rangle \langle \hat{i}, \hat{i}+1 \rangle + \langle 2\hat{j} \rangle \langle 1\hat{i} \rangle \langle \hat{i}+1, \hat{i}-1 \rangle + \langle 2\hat{j} \rangle \langle 1, \hat{i}+1 \rangle \langle \hat{i}-1, \hat{i} \rangle}{\langle 12 \rangle \langle \hat{i}-1, \hat{i} \rangle \langle \hat{i}, \hat{i}+1 \rangle} \\
&= -\frac{-\langle 2\hat{j} \rangle \langle 1, \hat{i}+1 \rangle \langle \hat{i}-1, \hat{i} \rangle + \langle 2\hat{j} \rangle \langle 1, \hat{i}+1 \rangle \langle \hat{i}-1, \hat{i} \rangle}{\langle 12 \rangle \langle \hat{i}-1, \hat{i} \rangle \langle \hat{i}, \hat{i}+1 \rangle} = 0,
\end{aligned} \tag{F.15}$$

where we used the Schouten identity to combine the first two terms. Note that when $\hat{i} = n$, the third term in (F.15) would not be present in the sum as there is no $\hat{p} = n+1$. This does not lead to any inconsistencies because $\langle 1, n+1 \rangle \equiv \langle 1, 1 \rangle = 0$, so the term vanishes anyway. A similar computation shows that the product also vanishes for $\hat{j} > \hat{i}$ (here the first $\hat{i} = 3$ term vanishes as needed since there is no $\hat{p} = 2$).

Thus we are left to consider the case when $\hat{j} = \hat{i}$. Replacing all the \hat{j} 's with \hat{i} 's, we find

$$\begin{aligned}
Q_{i\hat{p}}Q_{\hat{p}\hat{j}}^{-1}|_{\hat{j}=\hat{i}} &= -\frac{\langle 1\hat{i} \rangle \langle 2, \hat{i}-1 \rangle \langle \hat{i}, \hat{i}+1 \rangle + \langle 1\hat{i} \rangle \langle 2\hat{i} \rangle \langle \hat{i}+1, \hat{i}-1 \rangle + \langle 2\hat{i} \rangle \langle 1, \hat{i}+1 \rangle \langle \hat{i}-1, \hat{i} \rangle}{\langle 12 \rangle \langle \hat{i}-1, \hat{i} \rangle \langle \hat{i}, \hat{i}+1 \rangle} \\
&= -\frac{-\langle 1\hat{i} \rangle \langle 2, \hat{i}+1 \rangle \langle \hat{i}-1, \hat{i} \rangle + \langle 2\hat{i} \rangle \langle 1, \hat{i}+1 \rangle \langle \hat{i}-1, \hat{i} \rangle}{\langle 12 \rangle \langle \hat{i}-1, \hat{i} \rangle \langle \hat{i}, \hat{i}+1 \rangle} = 1,
\end{aligned} \tag{F.16}$$

where we have used the Schouten identity once to combine the first two terms, and again to combine the remaining terms (as above, the respective $\hat{i} = 3, n$ terms cause no issues). Hence $Q_{i\hat{p}}Q_{\hat{p}\hat{j}}^{-1} = \delta_{i\hat{j}}$, so Q^{-1} is the inverse of Q as claimed.

Appendix G

Calculations of Higher-Dimensional Residues

We present here a more detailed evaluation of the NMHV residues of the momentum twistor Grassmannian integral (4.16).

The starting point is the integral (4.39) with contour γ_{abcde} , as defined in Section 4.4.1. To begin with, fix the $GL(1)$ redundancy by setting

$$c_a = c_a^{(0)} \neq 0. \quad (\text{G.1})$$

We can use a delta-function $\delta(c_a - c_a^{(0)})$ to enforce this choice. It comes with a Jacobian factor $c_a^{(0)}$ that compensates the little-group scaling.

Next we turn our attention to the bosonic delta functions $\delta^4(c_i Z_i)$. They enforce the condition $\sum_{i=1}^n c_i Z_i = 0$. Since the Z_i 's are 4-component vectors, we can use Cramer's rule (4.42) to write all Z_j for $j \notin \{b, c, d, e\}$ in terms of $Z_b, Z_c, Z_d,$ and Z_e :

$$\langle bcde \rangle Z_j = - \left(\langle cdej \rangle Z_b + \langle dejb \rangle Z_c + \langle ejbc \rangle Z_d + \langle jbcd \rangle Z_e \right). \quad (\text{G.2})$$

For generic external data, $Z_b, Z_c, Z_d,$ and Z_e are linearly independent, so for $\sum_{i=1}^n c_i Z_i = 0$ to hold, the coefficients of each must vanish. This gives four constraints

$$\begin{aligned} c_b &= \sum_{j \neq b, c, d, e} c_j \frac{\langle cdej \rangle}{\langle bcde \rangle} =: c_b^{(0)}, & c_c &= \sum_{j \neq b, c, d, e} c_j \frac{\langle dejb \rangle}{\langle bcde \rangle} =: c_c^{(0)}, \\ c_d &= \sum_{j \neq b, c, d, e} c_j \frac{\langle ejbc \rangle}{\langle bcde \rangle} =: c_d^{(0)}, & c_e &= \sum_{j \neq b, c, d, e} c_j \frac{\langle jbcd \rangle}{\langle bcde \rangle} =: c_e^{(0)}. \end{aligned} \quad (\text{G.3})$$

Thus we can write

$$\delta^4(c_i Z_i) = \frac{1}{\langle bcde \rangle} \prod_{i=b,c,d,e} \delta(c_i - c_i^{(0)}). \quad (\text{G.4})$$

Now, enforcing a delta function $\delta(z - z_0)$ can also be done by re-interpreting the integral as a contour integral $\oint \frac{dz}{z - z_0}$ with a contour that surrounds only z_0 . We can therefore write the NMHV Grassmannian integral as

$$\mathcal{I}_{n;1}^{\gamma_{abcde}}(\mathcal{Z}) = \oint_{\Gamma_{abcde}} \frac{d^{1 \times n} C}{\prod_{i=a,b,c,d,e} (c_i - c_i^{(0)}) \prod_{j \neq a,b,c,d,e} c_j} \times \frac{\delta^{(4)}(c_i \eta_i)}{c_a c_b c_c c_d c_e}, \quad (\text{G.5})$$

where Γ_{abcde} is the n -dimensional contour that encircles each $c_{a,b,c,d,e}^{(0)}$ as well as $c_j = 0$ for each $j \neq a, b, c, d, e$. This contour extends the $(n - 5)$ -dimensional contour γ_{abcde} to encircle the delta function singularities in the other five dimensions.

It is straightforward to evaluate the contour integral (G.5) and obtain the residue. By the choice of contour Γ_{abcde} , all c_i 's vanish on the pole except $c_{a,b,c,d,e}$, so we find from (G.1) and (G.3) that

$$c_a c_b c_c c_d c_e \rightarrow \left(\frac{c_a^{(0)}}{\langle bcde \rangle} \right)^5 \langle abcd \rangle \langle bcde \rangle \langle cdea \rangle \langle deab \rangle \langle eabc \rangle. \quad (\text{G.6})$$

Including all the Jacobian factors, the residue is therefore:

$$\frac{c_a^{(0)} \delta^{(4)} \left(\left(\frac{c_a^{(0)}}{\langle bcde \rangle} \right) \left(\langle bcde \rangle \eta_a + \langle cdea \rangle \eta_b + \langle deab \rangle \eta_c + \langle eabc \rangle \eta_d + \langle abcd \rangle \eta_e \right) \right)}{\langle bcde \rangle \left(\frac{c_a^{(0)}}{\langle bcde \rangle} \right)^5 \langle bcde \rangle \langle cdea \rangle \langle deab \rangle \langle eabc \rangle \langle abcd \rangle}. \quad (\text{G.7})$$

We can pull out the multiplicative factor from the fermionic delta function, which combines with the Jacobians to exactly cancel the extra factor in the denominator. Hence the residue is simply the result given in (4.44): $\mathcal{I}_{n;1}^{\gamma_{abcde}} = [abcde]$. Note that this is independent of the gauge choice $c_a^{(0)}$. The expression (4.44) is manifestly antisymmetric in the five labels a, b, c, d, e .

We label the residue by the $n - 5$ values $i_1, i_2, \dots, i_{n-5} \neq a, b, c, d, e$ as $\{i_1, i_2, \dots, i_{n-5}\}$. This label is fully anti-symmetric and is related to the five-bracket via

$$\mathcal{I}_{n;1}^{\gamma_{abcde}} = \frac{1}{(n - 5)!} \varepsilon^{abcde i_1 i_2 \dots i_{n-5}} \{i_1, i_2, \dots, i_{n-5}\} = [abcde]. \quad (\text{G.8})$$

To see this, we recall the following results from the calculus of higher-dimensional contour integrals.¹

Suppose we have a set of m functions $f_i(x)$ of m complex variables $x = x_1 \dots, x_m$, which have an isolated common zero at the origin $f_i(0) = 0$ and are holomorphic in a neighborhood of a ball around the origin. Let $g(x)$ be holomorphic in the same region and non-vanishing at $x = 0$. Then we have a meromorphic m -form

$$\omega = \frac{g(x)dx^1 \wedge \dots \wedge dx^m}{f_1(x) \dots f_m(x)} \quad (\text{G.9})$$

which has a simple pole at the origin. We define the residue:

$$\text{Res}_{x=0} = (2\pi i)^{-m} \int_{\Gamma} \omega = \frac{g(0)}{\mathcal{J}_f(0)}, \quad (\text{G.10})$$

where $\mathcal{J}_f(x)$ is the Jacobian determinant for the functions f

$$\mathcal{J}_f(x) = \frac{\partial(f_1, \dots, f_m)}{\partial(x_1, \dots, x_m)}. \quad (\text{G.11})$$

The contour Γ is given by

$$\Gamma = \{x : |f_i(x)| = \epsilon_i\} \quad (\text{G.12})$$

and oriented such that

$$d(\arg f_1) \wedge \dots \wedge d(\arg f_m) \quad (\text{G.13})$$

is positively oriented with respect to the volume form in (G.9). In other words, any sign that would be produced by (G.13) is compensated by reversing one of the circles in Γ . Therefore, the only signs can come from the Jacobian (G.11).

Now we are set to compute residues of the form (G.10). From (G.5), we have

$$g(c) = (2\pi i)^{-(n-5)} \frac{\delta^{(4)}(c_i \eta_i)}{c_a c_b c_c c_d c_e}, \quad (\text{G.14})$$

where we have absorbed some numerical factors in the normalization for future simplicity. As a convention, we assign the first five functions $f_1(c), \dots, f_5(c)$ to the delta function

¹The derivation given here is similar to the example given in Section 2.3 of [82]; see also Section 5.1 of [40]. For a mathematical reference, see Chapter 5 of [126].

singularities, i.e.

$$f_1 = c_a - c_a^{(0)}, \quad f_2 = c_b - c_b^{(0)}, \quad f_3 = c_c - c_c^{(0)}, \quad f_4 = c_d - c_d^{(0)}, \quad f_5 = c_e - c_e^{(0)}. \quad (\text{G.15})$$

The rest of the f_i 's are assigned to the $n - 5$ c_j 's that vanish at the location of the pole encircled by Γ such that $f_i = 0$ corresponds to the vanishing of the j^{th} minor of C .

The contour is oriented such that we first take $f_1 \rightarrow 0$, then $f_2 \rightarrow 0$, etc, which we can use to define a labeling of the residues by the indices of the c_i 's; for example, we can assign them in increasing order

$$f_6 = c_1, f_7 = c_2, f_8 = c_3, \dots \rightarrow \text{Res} = \{1, 2, 3, \dots\}, \quad (\text{G.16})$$

or with a different ordering τ on the labels $i \neq a, b, c, d, e$,

$$\begin{aligned} f_6 = c_{\tau(1)}, f_7 = c_{\tau(2)}, f_8 = c_{\tau(3)}, \dots \rightarrow \text{Res} &= \{\tau(1), \tau(2), \tau(3), \dots\} \\ &= \text{sgn}(\tau) \times \{1, 2, 3, \dots\}, \end{aligned} \quad (\text{G.17})$$

where $\text{sgn}(\tau)$ is the signature of the permutation of the $(n - 5)$ indices $i \neq a, b, c, d, e$. The antisymmetry of the Jacobian \mathcal{J}_f in (G.10) implies that the residue labels are antisymmetric in their indices. Similarly, the residue is antisymmetric in the labels a, b, c, d, e . It follows that the result is (G.8).

Appendix H

Pole Structure of 6-Point ABJM Amplitude

The result (4.128) appears to have a triple-pole at $\langle 2356 \rangle = 0$. We show here that it is actually no worse than at most a simple pole.

We first note that it follows directly from (4.91) that

$$\langle 2356 \rangle = 0 \quad \longleftrightarrow \quad \langle\langle 25 \rangle\rangle \langle\langle 63 \rangle\rangle + \langle\langle 26 \rangle\rangle \langle\langle 35 \rangle\rangle = 0, \quad (\text{H.1})$$

and employing the Schouten identity we also have

$$0 = \langle\langle 14 \rangle\rangle \langle 2356 \rangle = -\langle\langle 13 \rangle\rangle \langle 5642 \rangle - \langle\langle 15 \rangle\rangle \langle 6423 \rangle = \langle\langle 13 \rangle\rangle \langle\langle 52 \rangle\rangle \langle\langle 64 \rangle\rangle + \langle\langle 15 \rangle\rangle \langle\langle 63 \rangle\rangle \langle\langle 42 \rangle\rangle. \quad (\text{H.2})$$

Thus, by (H.1) and (H.2), the D that appears in the localization of the c_i 's become a perfect square

$$D = -\langle\langle 13 \rangle\rangle \langle\langle 24 \rangle\rangle \langle\langle 35 \rangle\rangle \langle\langle 46 \rangle\rangle \langle\langle 51 \rangle\rangle \langle\langle 62 \rangle\rangle \xrightarrow{\langle 2356 \rangle \rightarrow 0} \langle\langle 13 \rangle\rangle^2 \langle\langle 52 \rangle\rangle^2 \langle\langle 46 \rangle\rangle^2. \quad (\text{H.3})$$

Now, we examine how each c_i^\pm behaves in the limit $\langle 2356 \rangle = \epsilon \rightarrow 0$. With our gauge choice $c_1 = \langle 2356 \rangle$ it is clear that $c_1^\pm = O(\epsilon)$ and by (4.123) we also have $c_4^\pm = O(\epsilon)$. Now, the four other c_i 's are given by (4.121) and they may appear to be finite as $\epsilon \rightarrow 0$; however, an extra cancellation can occur between the two terms in the numerator. To see this, consider the example of c_3^\pm :

$$c_3^\pm = \frac{\langle 5612 \rangle}{\sqrt{D}} \left(\sqrt{D} \mp \langle\langle 13 \rangle\rangle \langle\langle 52 \rangle\rangle \langle\langle 64 \rangle\rangle \right) \xrightarrow{\langle 2356 \rangle = \epsilon \rightarrow 0} \begin{cases} O(\epsilon) \\ O(1) \end{cases}, \quad (\text{H.4})$$

where the limit follows from (H.3) and the outcome, $O(\epsilon)$ and $O(1)$, depends on the relative

sign \pm between the two terms and the sign of $\langle\langle 13 \rangle\rangle \langle\langle 52 \rangle\rangle \langle\langle 64 \rangle\rangle$. This will be the same for c_2 , c_5 , and c_6 , and it can easily be demonstrated, using (H.1) and (H.2), that in the limit $\langle 2356 \rangle = \epsilon \rightarrow 0$, we will either have

$$c_2^+, c_3^+, c_5^+, c_6^+ = O(\epsilon) \quad \text{and} \quad c_2^-, c_3^-, c_5^-, c_6^- = O(1) \quad (\text{H.5})$$

or vice versa. Suppose $\langle\langle 13 \rangle\rangle \langle\langle 52 \rangle\rangle \langle\langle 64 \rangle\rangle$ is such that we have the case (H.5): then

$$\frac{\delta^{(3)}(c^+ \cdot \eta)}{c_2^+ c_3^+ c_4^+} \xrightarrow{\langle 2356 \rangle = \epsilon \rightarrow 0} \frac{O(\epsilon^3)}{O(\epsilon^3)} \sim O(1), \quad (\text{H.6})$$

while

$$\frac{\delta^{(3)}(c^- \cdot \eta)}{c_2^- c_3^- c_4^-} \xrightarrow{\langle 2356 \rangle = \epsilon \rightarrow 0} \frac{O(\epsilon^3) \text{ or } O(\epsilon^2) \text{ or } O(\epsilon^1) \text{ or } O(1)}{O(\epsilon)}, \quad (\text{H.7})$$

i.e. it is no worse than $O(1/\epsilon)$, which signifies the (expected) simple pole. Thus we have shown that despite the apparent $1/\epsilon^3$ pole in the limit $\langle 2356 \rangle = \epsilon \rightarrow 0$ of the $n = 6$ result (4.128), there is at most a simple pole.

Appendix I

Details for Algorithm 1

In this appendix, we derive the reference sequences and compute the relative signs for step (2) of Algorithm 1. Many of the transformations presented here were computed independently by R. Karpman who found agreement with these results [115].

i) (ab) vs. (cd)

This case was discussed in the main text so we do not repeat the argument here.

ii) (ab) vs. (ac)

These transpositions share a leg, so they do not commute as simply as in the previous case. Nonetheless, in this case we can use the fact that both (ab) and (ac) are allowed transpositions on the initial permutation to find a common parent cell. Specifically, since (ab) was the last transposition before σ , we know $a < b \leq \sigma(a) < \sigma(b) \leq a+n$ and there is no $q \in (a, b)$ such that $\sigma(q) \in (\sigma(a), \sigma(b))$. Similarly from (ac) we know $a < c \leq \sigma'(a) < \sigma'(c) \leq a+n$ and there is no $q \in (a, c)$ such that $\sigma'(q) \in (\sigma'(a), \sigma'(c))$. Moreover, since σ and σ' come from the same initial permutation, we also know that $\sigma(a) = \sigma'(b)$, $\sigma(b) = \sigma'(c)$, $\sigma(c) = \sigma'(a)$, and $\sigma(q) = \sigma'(q)$ for all other legs.

To show that (bc) can be applied to σ , we need to show that $\sigma(c) < \sigma(b)$ and that there is no $q \in (b, c)$ such that $\sigma(q) \in (\sigma(c), \sigma(b))$. The condition that $\sigma(c) < \sigma(b)$ is satisfied since it is equivalent to $\sigma'(a) < \sigma'(c)$, and since no legs are touched between b and c , the condition on $q \in (a, c)$ implies that no $q \in (b, c)$ has $\sigma(q) \in (\sigma(c), \sigma(b))$. Thus (bc) is an allowed transposition on σ , so the path $\tilde{\mathbf{w}}$ exists.

We also need to show that (ab) can be applied to σ' , so we must show $\sigma'(b) < \sigma'(a)$ and that there is no $q \in (a, b)$ such that $\sigma'(q) \in (\sigma'(b), \sigma'(a))$. Since $b \in (a, c)$, we must have either $\sigma'(b) < \sigma'(a) < \sigma'(c)$ or $\sigma'(a) < \sigma'(c) < \sigma'(b)$. Since $\sigma(a) < \sigma(b) \Rightarrow \sigma'(b) < \sigma'(c)$, only the former condition is allowed, hence $\sigma'(b) < \sigma'(a)$. Furthermore, there is no

$q \in (a, b)$ such that $\sigma'(q) \in (\sigma'(b), \sigma'(c))$, and $(\sigma'(b), \sigma'(a))$ is a subset of that range. Hence (ab) is allowed on σ' , and $\tilde{\mathbf{w}}'$ exists.

Note that the above analysis was valid for any charts, not just adjacent ones. However, to compute the relative sign, we will focus on the restricted set of charts for which all $q \in (a, c)$ satisfy $\sigma'(q) \equiv q \pmod n$, namely the standard BCFW charts. The corresponding plabic graphs can be manipulated to a common layout using the equivalence moves (E1) and (E2). The results are displayed in Figure I.1.

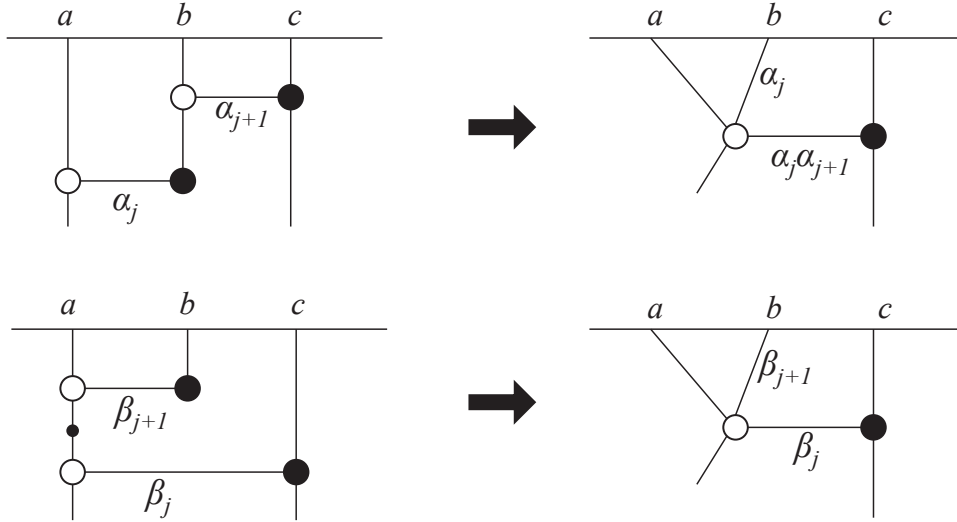


Figure I.1: Graph manipulations used to compare the transposition sequences in case (ii).

We find that the graphs are equivalent only with the identifications

$$\beta_j = \alpha_j \alpha_{j+1}, \quad \beta_{j+1} = \alpha_j. \quad (\text{I.1})$$

Plugging this into the dlog forms and using that

$$\text{dlog } \alpha_j \wedge \text{dlog}(\alpha_j \alpha_{j+1}) = \text{dlog } \alpha_j \wedge (\text{dlog } \alpha_j + \text{dlog } \alpha_{j+1}) = -\text{dlog } \alpha_{j+1} \wedge \text{dlog } \alpha_j, \quad (\text{I.2})$$

we find that the two forms are oppositely oriented.

iii) (ac) vs. (bc)

This situation is analogous to case (ii), so we can skip directly to comparing the graphs. Restricting again to the standard BCFW situation where $\sigma(q) \equiv q \pmod n$ for

all $q \in (a, c)$, we can perform a sequence of merge/delete and $GL(1)$ rotations on the corresponding plabic graphs as in Figure I.2.

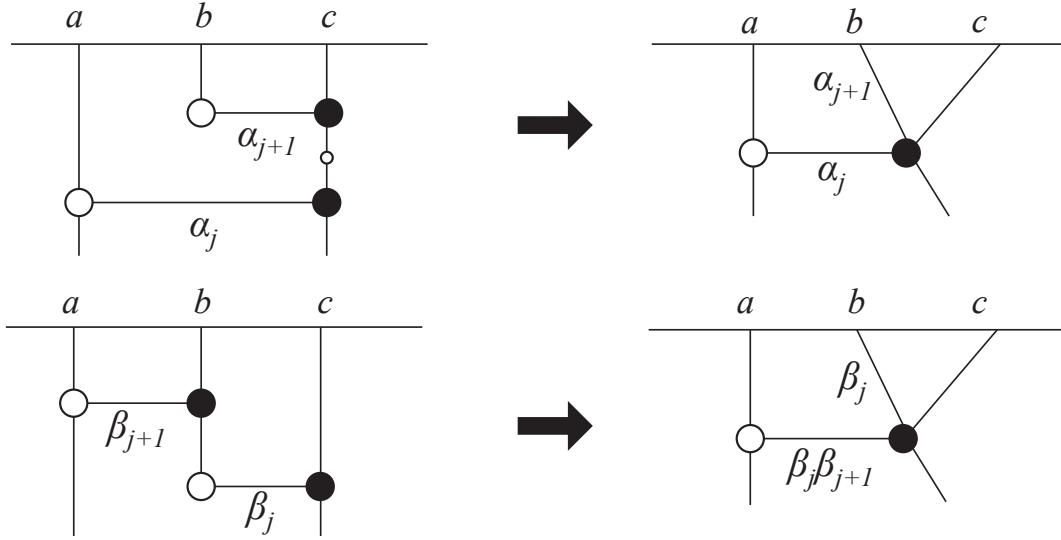


Figure I.2: Graph manipulations used to compare the transposition sequences in case (iii).

We therefore identify

$$\beta_j = \alpha_{j+1}, \quad \beta_{j+1} = \alpha_j / \alpha_{j+1}. \quad (\text{I.3})$$

Then using that $\text{dlog}(\alpha_j / \alpha_{j+1}) = \text{dlog} \alpha_j - \text{dlog} \alpha_{j+1}$, we find that the two forms are oppositely oriented.

iv) (ab) vs (bc)

Using only adjacent transpositions, σ and σ' do not have a common parent cell. However, we can show that $\rho = \sigma \cdot (bc)(ab) = \sigma' \cdot (ab)(bc)$ is a shared grandparent. From the initial (ab) , we know $a < b \leq \sigma(a) < \sigma(b) \leq a+n$, while from the initial (bc) , we have $b < c \leq \sigma'(b) < \sigma'(c) \leq b+n$. From their shared origin cell, we also have $\sigma(a) = \sigma'(c)$, $\sigma(b) = \sigma'(a)$, and $\sigma(c) = \sigma'(b)$. We will focus on adjacent charts wherein $\sigma(q) = \sigma'(q) \equiv q \pmod n$ for all $q \in (a, b) \cup (b, c)$. The general case is covered in Section 5.3.2.

Since $\sigma'(b) < \sigma'(c)$ is equivalent to $\sigma(c) < \sigma(a)$, and $\sigma(a) < \sigma(b)$, we can apply (bc) to reach $\tilde{\sigma} = \sigma \cdot (bc)$. Now $\tilde{\sigma}(b) < \tilde{\sigma}(a) < \tilde{\sigma}(c)$, so (ab) is a valid transposition, which arrives at ρ . Hence the reference chart $\tilde{\mathbf{w}}$ exists.

On the other side, $\sigma(a) < \sigma(b)$ is equivalent to $\sigma'(c) < \sigma'(a)$, and $\sigma'(b) < \sigma'(c)$, so (ab) can be applied to σ' , yielding $\tilde{\sigma}' = \sigma' \cdot (ab)$. Since $\tilde{\sigma}'(a) < \tilde{\sigma}'(c) < \tilde{\sigma}'(b)$, we can apply (bc) , which also arrives at ρ . Thus $\tilde{\mathbf{w}}'$ is also a valid reference chart.

Finally, we can compare the plabic graphs to find their relative orientation. After performing a square move (E3) on the bottom right diagram in Figure I.3, we find

$$\beta_j = \frac{\alpha_{j+1}\alpha_{j+2}}{\alpha_j + \alpha_{j+2}}, \quad \beta_{j+1} = \alpha_j + \alpha_{j+2}, \quad \beta_{j+2} = \frac{\alpha_j\alpha_{j+1}}{\alpha_j + \alpha_{j+2}}. \quad (\text{I.4})$$

Chugging through a bit of algebra, the result is a positive relative orientation.

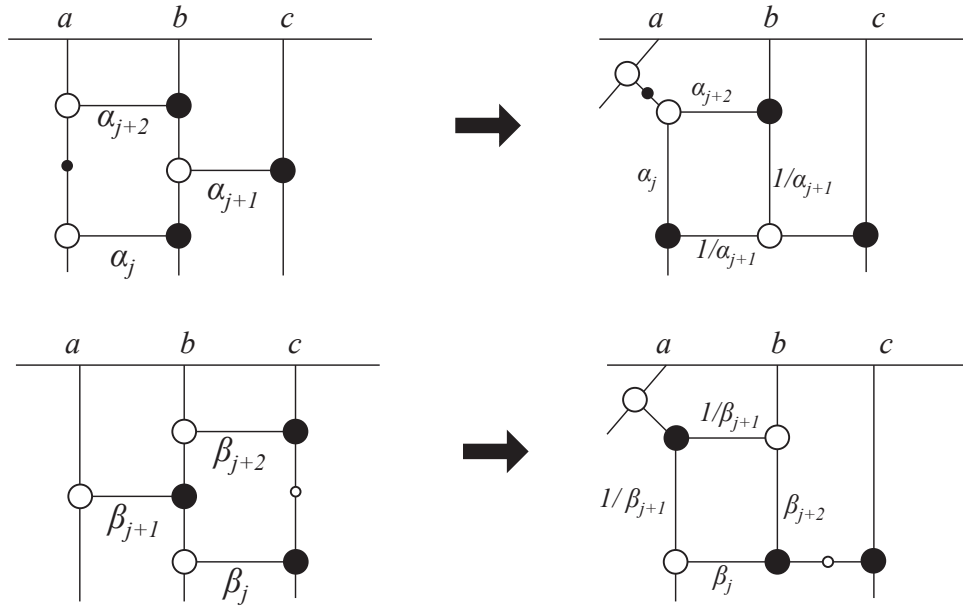


Figure I.3: Simple graph manipulations used to compare the transposition sequences in case (iv). A square move is required to complete the transformation.

v) (ac) vs. (bd)

There is no way to find a common parent using only adjacent transpositions. However, there is a common grandparent $\rho = \sigma \cdot (bc)(cd) = \sigma' \cdot (bc)(ab)$. Since σ and σ' come from a shared origin, we have the following: $a < c \leq \sigma(a) < \sigma(c) \leq a+n$ and $b < d \leq \sigma'(b) < \sigma'(d) \leq b+n$; and $\sigma(a) = \sigma'(c)$, $\sigma(b) = \sigma'(d)$, $\sigma(c) = \sigma'(a)$, and $\sigma(d) = \sigma'(b)$. We focus on adjacent charts, so $\sigma(q) = \sigma'(q) \equiv q \pmod{n}$ for all indices $q \in (a, d) \setminus \{b, c\}$. In addition, $\sigma(b) = \sigma'(d) = b+n$ and $\sigma'(c) = \sigma(a) = c$.

Since $\sigma(b) = b+n > a+n \geq \sigma(c)$, the transposition (bc) is allowed, which leads to

$\tilde{\sigma} = \sigma \cdot (bc)$. Then $\tilde{\sigma}(a) < \tilde{\sigma}(b) < \tilde{\sigma}(c) = b+n$ and $\tilde{\sigma}(d) = \sigma(d) = \sigma'(b) < b+n$. Therefore (cd) is also allowed, and we arrive at ρ . Therefore $\tilde{\mathbf{w}}$ is a valid reference chart.

For σ' , we use that $\sigma'(c) = c < d \leq \sigma'(b)$, so (bc) is allowed. Thus with $\tilde{\sigma}' = \sigma' \cdot (bc)$, we have that $c = \tilde{\sigma}'(b) < \tilde{\sigma}'(c) < ts'(d)$ and $\tilde{\sigma}'(a) = \sigma'(a) = \sigma(c) > c$. Hence we can apply (ab) , which yields ρ , so $\tilde{\mathbf{w}}'$ is a good reference chart.

To compute the relative sign, we study the plabic graphs in Figure I.4. They are equivalent under the identifications

$$\beta_j = \alpha_{j+1}\alpha_{j+2}, \quad \beta_{j+1} = \alpha_{j+1}, \quad \beta_{j+2} = \alpha_j/\alpha_{j+1}. \quad (\text{I.5})$$

Plugging this into ω' , one finds that the two forms are oppositely oriented.

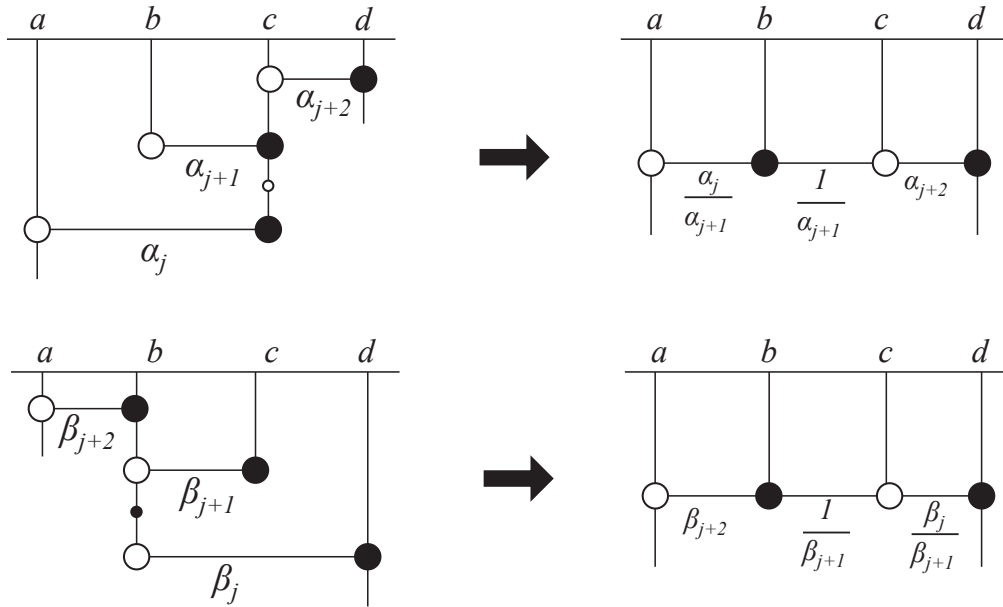


Figure I.4: Graph manipulations used to compare the transposition sequences in case (v).

vi) (bc) vs. (ad)

From the point of view of a graph embedded in a disk, these bridges can be added in either order, i.e. there are no intersecting edges in Figure I.5. However, the adjacency requirement forbids applying (ad) after (bc) . Thus we must look further to find a meeting point, $\tilde{\rho}$, for their reference charts. We will focus on adjacent charts, leaving the general case for Section 5.3.2.

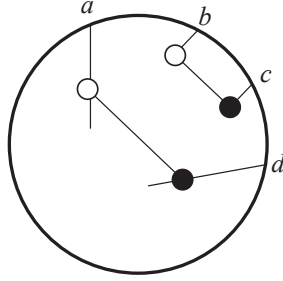


Figure I.5: An on-shell diagram with bridges (ad) and (bc) .

Since $b, c \in (a, d)$, we know $\sigma(b), \sigma(c) \equiv c, b \pmod{n}$, so it follows that $\sigma(b) = c$ and $\sigma(c) = b+n$. Then since $\sigma(a) = \sigma'(d) \geq d > c = \sigma(b)$, we can next apply (ab) . Similarly, $\sigma(d) = \sigma'(a) \leq a+n < b+n = \sigma(c)$, we could also apply (cd) ; this is unaffected by applying (ab) , so we apply it next to arrive at $\rho = \sigma \cdot (ab)(cd)$. Finally, (bc) is allowed because the permutations satisfy both $\rho(b) = \sigma(a) = \sigma'(d) > \sigma'(a) = \sigma(d) = \rho(c)$ and $c < d \leq \sigma'(a) < \sigma'(d) \leq a+n < b+n$. Hence $\tilde{\mathbf{w}}$ is a valid reference chart.

From σ' , we are certainly allowed to apply (bc) after (ad) , thus arriving at $\tilde{\sigma} = \sigma' \cdot (bc)$. We can add (ab) and then (cd) by essentially the same argument as above. Therefore both $\tilde{\mathbf{w}}$ and $\tilde{\mathbf{w}}'$ are valid reference charts.

We compare the plabic graphs to find the relative sign. One can either use the equivalence moves (E1)-(E3) or repeatedly apply the transformation rules from cases (ii)-(iv) to derive Figure I.6. The graphs are equivalent after the following identifications:

$$\beta_j = \frac{\alpha_j \alpha_{j+1} \alpha_{j+2} \alpha_{j+3}}{\alpha_j + \alpha_{j+3}}, \quad \beta_{j+1} = \alpha_j + \alpha_{j+3}, \quad \beta_{j+2} = \frac{\alpha_j \alpha_{j+1}}{\alpha_j + \alpha_{j+3}}, \quad \beta_{j+3} = \frac{\alpha_j \alpha_{j+2}}{\alpha_j + \alpha_{j+3}}. \quad (\text{I.6})$$

Rearranging the corresponding forms demonstrates that the relative orientation of the reference charts is -1 .

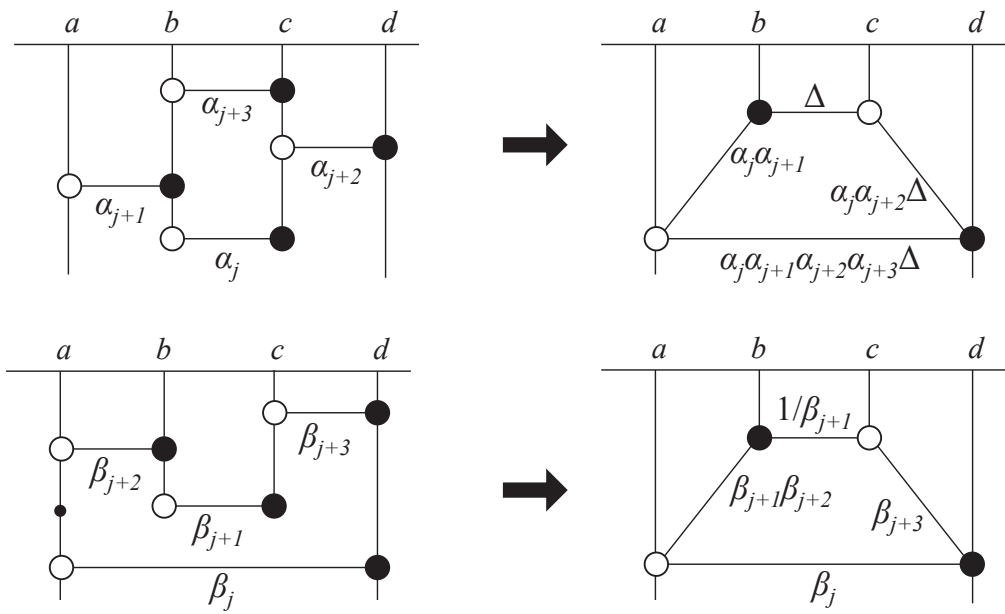


Figure I.6: Graph manipulations used to compare the transposition sequences in case (vi), where we have defined $\Delta = 1/(\alpha_j + \alpha_{j+3})$.

Appendix J

Assigning Edge Weights

In this appendix we provide one technique for assigning weights ± 1 to every edge in the poset such that the product of signs around every quadrilateral is -1 . The method was developed by T. Lam and D. Speyer [47].

J.1 Reduced Words

Each decorated permutation can equivalently be represented by one or more *reduced words*: minimal-length sequences of *letters* which obey certain equivalence relations. In this case, the letters s_i are generators of the affine permutation group \tilde{S}_n . They are defined with the following properties and relations:

$$\begin{aligned} s_i &:= \begin{cases} \sigma(i) \rightarrow \sigma(i+1) \\ \sigma(i+1) \rightarrow \sigma(i) \end{cases} & 1 \leq i \leq n, & s_{i+n} \equiv s_i, \\ s_i^2 &\equiv 1, & s_i s_{i+1} s_i \equiv s_{i+1} s_i s_{i+1}, & s_i s_j \equiv s_j s_i, \quad |i-j| > 1. \end{aligned} \tag{J.1}$$

We will refer to the relations in the second line as, respectively, the *reduction move*, the *braid move*, and the *swap move*. As we showed in Lemma 1, any d -dimensional cell C in $\text{Gr}(k, n)$ can be reached from the top cell by a sequence of $k(n-k) - d$ transpositions s_i , and that sequence defines a reduced word labeling C . There are generally many distinct reduced words for a given cell, but they are equivalent due to the relations in (J.1).

Any two cells C and C' of dimensions d and $d+1$, which share an edge in the poset, i.e. are related by a single boundary operation, are straightforwardly connected in the language of reduced words. Given a reduced word f of length $\delta = k(n-k) - d$ on the lower-dimensional cell C , there is a unique reduced word f' on C' of length $\delta' = \delta - 1$ obtained by deleting a single letter from f [127]. Specifically, for $f = s_{i_1} s_{i_2} \dots s_{i_j} \dots s_{i_\delta}$, there is a unique s_{i_j} such that

$f' = s_{i_1} s_{i_2} \dots \hat{s}_{i_j} \dots s_{i_\delta}$, where the hat denotes deletion. It is easy to construct a (generally non-reduced) word t such that $f' \equiv tf$; one can check that $t = s_{i_1} s_{i_2} \dots s_{i_{j-1}} s_{i_j} s_{i_{j-1}} \dots s_{i_2} s_{i_1}$ accomplishes the desired effect by repeated reduction moves. Given that the two cells are also related by a transposition of the form (ab) , it is not surprising that repeated application of the relations (J.1) shows that $t \equiv s_a s_{a+1} \dots s_{b-2} s_{b-1} s_{b-2} \dots s_{a+1} s_a$, which is a reduced word representation of (ab) .

J.2 Decorating Edges

Choose a representative reduced word for every cell in the poset; we will refer to this as the *standard word* on that cell. This is similar to choosing a particular Lemma 1 sequence for each cell. From a cell C labeled by the standard word f , every cell C' that has C as a boundary can be reached by deleting some s_{i_j} from f . This yields a word f' on C' as explained above. If f' is identical to the standard word on C' , then weight the corresponding edge with $(-1)^j$. It is easy to check that deleting two letters $s_{i_{j_1}}$ and $s_{i_{j_2}}$ in opposite orders will produce the desired factor of -1 around a quadrilateral. For one order, we would find $(-1)^{i_{j_1}+i_{j_2}}$, while for the other order we would find $(-1)^{i_{j_1}+i_{j_2}-1}$, so they differ by -1 .

However, it is not always possible to delete both transpositions in either order. One may have to delete different transpositions to reach the same cell by two different routes. Moreover, the final reduced word in each case may be different. Thus, we need to find the sign difference between two reduced words. Any two reduced words can be mutated into each other using just the braid and swap moves defined in (J.1). By decorating these rules with ± 1 , we can find the desired difference between the words. In fact, we already determined those signs in Appendix I because the generators act as adjacent transpositions. The braid move is simply a special case of (iv), so it should be decorated with a $+1$, and the swap move is a special case of (i), so it should be decorated with a -1 . Hence, the relative sign between two words is the number of swaps required to transform one into the other.

The number of swaps can be determined directly from the *inversion list* of each word. A reduced word creates a unique ordering on the set of inversions in the permutation labeling the cell (not all orderings are possible). The number of swap moves needed to transform one word into another is the number of pairs of inversions (i, j) and (k, l) , with all i, j, k, l distinct, in different order in the two inversion lists.

Bibliography

- [1] J. Polchinski, *Scale and Conformal Invariance in Quantum Field Theory*, *Nucl. Phys.* **B303** (1988) 226.
- [2] A. B. Zamolodchikov, *Irreversibility of the Flux of the Renormalization Group in a 2D Field Theory*, *JETP Lett.* **43** (1986) 730–732.
- [3] A. Dymarsky, Z. Komargodski, A. Schwimmer and S. Theisen, *On Scale and Conformal Invariance in Four Dimensions*, *JHEP* **10** (2015) 171, [[1309.2921](#)].
- [4] K. Farnsworth, M. A. Luty and V. Prelipina, *Scale Invariance plus Unitarity Implies Conformal Invariance in Four Dimensions*, [[1309.4095](#)].
- [5] Z. Komargodski and A. Schwimmer, *On Renormalization Group Flows in Four Dimensions*, *JHEP* **12** (2011) 099, [[1107.3987](#)].
- [6] Z. Komargodski, *The Constraints of Conformal Symmetry on RG Flows*, *JHEP* **07** (2012) 069, [[1112.4538](#)].
- [7] J. L. Cardy, *Conformal Invariance and Statistical Mechanics*, in *Les Houches Summer School in Theoretical Physics: Fields, Strings, Critical Phenomena Les Houches, France, June 28-August 5, 1988*, pp. 0169–246, 1989.
- [8] C. Holzhey, F. Larsen and F. Wilczek, *Geometric and renormalized entropy in conformal field theory*, *Nucl. Phys.* **B424** (1994) 443–467, [[hep-th/9403108](#)].
- [9] T. Azeyanagi, T. Nishioka and T. Takayanagi, *Near Extremal Black Hole Entropy as Entanglement Entropy via AdS(2)/CFT(1)*, *Phys. Rev.* **D77** (2008) 064005, [[0710.2956](#)].
- [10] B. Chen and J.-q. Wu, *Universal relation between thermal entropy and entanglement entropy in conformal field theories*, *Phys. Rev.* **D91** (2015) 086012, [[1412.0761](#)].
- [11] R. C. Myers and A. Sinha, *Seeing a c-theorem with holography*, *Phys. Rev.* **D82** (2010) 046006, [[1006.1263](#)].
- [12] R. C. Myers and A. Sinha, *Holographic c-theorems in arbitrary dimensions*, *JHEP* **01** (2011) 125, [[1011.5819](#)].
- [13] D. L. Jafferis, *The Exact Superconformal R-Symmetry Extremizes Z*, *JHEP* **05** (2012) 159, [[1012.3210](#)].

- [14] D. L. Jafferis, I. R. Klebanov, S. S. Pufu and B. R. Safdi, *Towards the F-Theorem: $N=2$ Field Theories on the Three-Sphere*, *JHEP* **06** (2011) 102, [[1103.1181](#)].
- [15] I. R. Klebanov, S. S. Pufu and B. R. Safdi, *F-Theorem without Supersymmetry*, *JHEP* **10** (2011) 038, [[1105.4598](#)].
- [16] I. R. Klebanov, S. S. Pufu, S. Sachdev and B. R. Safdi, *Entanglement Entropy of 3-d Conformal Gauge Theories with Many Flavors*, *JHEP* **05** (2012) 036, [[1112.5342](#)].
- [17] H. Liu and M. Mezei, *A Refinement of entanglement entropy and the number of degrees of freedom*, *JHEP* **04** (2013) 162, [[1202.2070](#)].
- [18] I. R. Klebanov, T. Nishioka, S. S. Pufu and B. R. Safdi, *Is Renormalized Entanglement Entropy Stationary at RG Fixed Points?*, *JHEP* **10** (2012) 058, [[1207.3360](#)].
- [19] M. J. Duff, *Twenty years of the Weyl anomaly*, *Class. Quant. Grav.* **11** (1994) 1387–1404, [[hep-th/9308075](#)].
- [20] S. Deser and A. Schwimmer, *Geometric classification of conformal anomalies in arbitrary dimensions*, *Phys. Lett.* **B309** (1993) 279–284, [[hep-th/9302047](#)].
- [21] A. Cappelli, D. Friedan and J. I. Latorre, *C theorem and spectral representation*, *Nucl. Phys.* **B352** (1991) 616–670.
- [22] D. Anselmi, D. Z. Freedman, M. T. Grisaru and A. A. Johansen, *Nonperturbative formulas for central functions of supersymmetric gauge theories*, *Nucl. Phys.* **B526** (1998) 543–571, [[hep-th/9708042](#)].
- [23] D. Anselmi, J. Erlich, D. Z. Freedman and A. A. Johansen, *Positivity constraints on anomalies in supersymmetric gauge theories*, *Phys. Rev.* **D57** (1998) 7570–7588, [[hep-th/9711035](#)].
- [24] J. L. Cardy, *Is There a c Theorem in Four-Dimensions?*, *Phys. Lett.* **B215** (1988) 749–752.
- [25] M. A. Luty, J. Polchinski and R. Rattazzi, *The a-theorem and the Asymptotics of 4D Quantum Field Theory*, *JHEP* **01** (2013) 152, [[1204.5221](#)].
- [26] A. Schwimmer and S. Theisen, *Spontaneous Breaking of Conformal Invariance and Trace Anomaly Matching*, *Nucl. Phys.* **B847** (2011) 590–611, [[1011.0696](#)].
- [27] G. 't Hooft, *Naturalness, chiral symmetry, and spontaneous chiral symmetry breaking*, *NATO Sci. Ser. B* **59** (1980) 135.
- [28] H. Elvang, D. Z. Freedman and M. Kiermaier, *A simple approach to counterterms in $N=8$ supergravity*, *JHEP* **11** (2010) 016, [[1003.5018](#)].
- [29] J. J. Heckman and T. Rudelius, *Evidence for C-theorems in 6D SCFTs*, *JHEP* **09** (2015) 218, [[1506.06753](#)].

- [30] C. Cordova, T. T. Dumitrescu and K. Intriligator, *Anomalies, Renormalization Group Flows, and the a-Theorem in Six-Dimensional (1,0) Theories*, [1506.03807](#).
- [31] C. Cordova, T. T. Dumitrescu and X. Yin, *Higher Derivative Terms, Toroidal Compactification, and Weyl Anomalies in Six-Dimensional (2,0) Theories*, [1505.03850](#).
- [32] W. Nahm, *Supersymmetries and their Representations*, *Nucl. Phys.* **B135** (1978) 149.
- [33] C. R. Graham, R. Jenne, L. J. Mason and G. A. J. Sparling, *Conformally invariant powers of the Laplacian. I. Existence*, *J. London Math. Soc. (2)* **46** (1992) 557–565.
- [34] H. Elvang and Y.-t. Huang, *Scattering Amplitudes*, [1308.1697](#).
- [35] S. J. Parke and T. R. Taylor, *An Amplitude for n Gluon Scattering*, *Phys. Rev. Lett.* **56** (1986) 2459.
- [36] L. J. Dixon, *A brief introduction to modern amplitude methods*, in *Proceedings, 2012 European School of High-Energy Physics (ESHEP 2012): La Pommeraye, Anjou, France, June 06-19, 2012*, pp. 31–67, 2014. [1310.5353](#). DOI.
- [37] N. Arkani-Hamed, J. L. Bourjaily, F. Cachazo, A. B. Goncharov, A. Postnikov and J. Trnka, *Scattering Amplitudes and the Positive Grassmannian*. Cambridge University Press, 2012.
- [38] G. 't Hooft, *A Planar Diagram Theory for Strong Interactions*, *Nucl. Phys.* **B72** (1974) 461.
- [39] J. M. Drummond, J. M. Henn and J. Plefka, *Yangian symmetry of scattering amplitudes in N=4 super Yang-Mills theory*, *JHEP* **05** (2009) 046, [[0902.2987](#)].
- [40] N. Arkani-Hamed, F. Cachazo, C. Cheung and J. Kaplan, *A Duality For The S Matrix*, *JHEP* **03** (2010) 020, [[0907.5418](#)].
- [41] N. Arkani-Hamed, J. Bourjaily, F. Cachazo and J. Trnka, *Unification of Residues and Grassmannian Dualities*, *JHEP* **01** (2011) 049, [[0912.4912](#)].
- [42] Y.-T. Huang and C. Wen, *ABJM amplitudes and the positive orthogonal grassmannian*, *JHEP* **02** (2014) 104, [[1309.3252](#)].
- [43] J. Kim and S. Lee, *Positroid Stratification of Orthogonal Grassmannian and ABJM Amplitudes*, *JHEP* **09** (2014) 085, [[1402.1119](#)].
- [44] Y.-t. Huang, C. Wen and D. Xie, *The Positive orthogonal Grassmannian and loop amplitudes of ABJM*, *J. Phys.* **A47** (2014) 474008, [[1402.1479](#)].
- [45] N. Arkani-Hamed and J. Trnka, *The Amplituhedron*, *JHEP* **10** (2014) 030, [[1312.2007](#)].

- [46] N. Arkani-Hamed and J. Trnka, *Into the Amplituhedron*, *JHEP* **12** (2014) 182, [[1312.7878](#)].
- [47] T. Lam and D. E. Speyer. Private communication.
- [48] J. L. Bourjaily. Private communication.
- [49] H. Elvang and T. M. Olson, *RG flows in d dimensions, the dilaton effective action, and the a -theorem*, *JHEP* **03** (2013) 034, [[1209.3424](#)].
- [50] N. Bobev, H. Elvang and T. M. Olson, *Dilaton effective action with $N = 1$ supersymmetry*, *JHEP* **04** (2014) 157, [[1312.2925](#)].
- [51] H. Elvang, Y.-t. Huang, C. Keeler, T. Lam, T. M. Olson, S. B. Roland et al., *Grassmannians for scattering amplitudes in $4d$ $\mathcal{N} = 4$ SYM and $3d$ ABJM*, *JHEP* **12** (2014) 181, [[1410.0621](#)].
- [52] T. M. Olson, *Orientations of BCFW Charts on the Grassmannian*, *JHEP* **08** (2015) 120, [[1411.6363](#)].
- [53] H. Casini, M. Huerta and R. C. Myers, *Towards a derivation of holographic entanglement entropy*, *JHEP* **05** (2011) 036, [[1102.0440](#)].
- [54] N. Boulanger and J. Erdmenger, *A Classification of local Weyl invariants in $D=8$* , *Class. Quant. Grav.* **21** (2004) 4305–4316, [[hep-th/0405228](#)].
- [55] H. Elvang, D. Z. Freedman, L.-Y. Hung, M. Kiermaier, R. C. Myers and S. Theisen, *On renormalization group flows and the a -theorem in $6d$* , *JHEP* **10** (2012) 011, [[1205.3994](#)].
- [56] T. Maxfield and S. Sethi, *The Conformal Anomaly of $M5$ -Branes*, *JHEP* **06** (2012) 075, [[1204.2002](#)].
- [57] A. Bhattacharyya, L.-Y. Hung, K. Sen and A. Sinha, *On c -theorems in arbitrary dimensions*, *Phys. Rev.* **D86** (2012) 106006, [[1207.2333](#)].
- [58] S. M. Paneitz, *A quartic conformally covariant differential operator for arbitrary pseudo-Riemannian manifolds (summary)*, *SIGMA Symmetry Integrability Geom. Methods Appl.* **4** (2008) Paper 036, 3.
- [59] E. S. Fradkin and A. A. Tseytlin, *One Loop Beta Function in Conformal Supergravities*, *Nucl. Phys.* **B203** (1982) 157.
- [60] E. S. Fradkin and A. A. Tseytlin, *Asymptotic Freedom in Extended Conformal Supergravities*, *Phys. Lett.* **B110** (1982) 117–122.
- [61] E. S. Hung and R. C. Myers. Unpublished notes.
- [62] T. Branson, *Q -curvature and spectral invariants*, *Rend. Circ. Mat. Palermo (2) Suppl.* (2005) 11–55.

- [63] A. Juhl, *Explicit formulas for GJMS-operators and Q-curvatures*, *Geom. Funct. Anal.* **23** (2013) 1278–1370.
- [64] D. E. Diaz, *Polyakov formulas for GJMS operators from AdS/CFT*, *JHEP* **07** (2008) 103, [[0803.0571](#)].
- [65] J. M. Martín-García, “xact: efficient tensor computer algebra.” <http://www.xact.es>.
- [66] D. Anselmi, *Quantum irreversibility in arbitrary dimension*, *Nucl. Phys.* **B567** (2000) 331–359, [[hep-th/9905005](#)].
- [67] G. M. Shore, *Dimensional Regularization of Gauge Theories in Spherical Space-Time: Free Field Trace Anomalies*, *Annals Phys.* **117** (1979) 121.
- [68] E. J. Copeland and D. J. Toms, *The Conformal Anomaly in Higher Dimensions*, *Class. Quant. Grav.* **3** (1986) 431.
- [69] A. Cappelli and G. D’Appollonio, *On the trace anomaly as a measure of degrees of freedom*, *Phys. Lett.* **B487** (2000) 87–95, [[hep-th/0005115](#)].
- [70] J. S. Dowker, *Entanglement entropy for even spheres*, [1009.3854](#).
- [71] J. S. Dowker, *Entanglement entropy for odd spheres*, [1012.1548](#).
- [72] I. L. Buchbinder and S. M. Kuzenko, *Nonlocal Action for Supertrace Anomalies in Superspace of $N = 1$ Supergravity*, *Phys. Lett.* **B202** (1988) 233–237.
- [73] S. M. Kuzenko, *Super-Weyl anomalies in $N=2$ supergravity and (non)local effective actions*, *JHEP* **10** (2013) 151, [[1307.7586](#)].
- [74] K. A. Intriligator and B. Wecht, *The Exact superconformal R symmetry maximizes a* , *Nucl. Phys.* **B667** (2003) 183–200, [[hep-th/0304128](#)].
- [75] D. Cassani and D. Martelli, *Supersymmetry on curved spaces and superconformal anomalies*, *JHEP* **10** (2013) 025, [[1307.6567](#)].
- [76] M. T. Grisaru, H. N. Pendleton and P. van Nieuwenhuizen, *Supergravity and the S Matrix*, *Phys. Rev.* **D15** (1977) 996.
- [77] M. T. Grisaru and H. N. Pendleton, *Some Properties of Scattering Amplitudes in Supersymmetric Theories*, *Nucl. Phys.* **B124** (1977) 81.
- [78] J. Wess and B. Zumino, *Consequences of anomalous Ward identities*, *Phys. Lett.* **B37** (1971) 95.
- [79] F. Baume and B. Keren-Zur, *The dilaton Wess-Zumino action in higher dimensions*, *JHEP* **11** (2013) 102, [[1307.0484](#)].
- [80] Y. Nakayama, *On ϵ -conjecture in a -theorem*, *Mod. Phys. Lett.* **A27** (2012) 1250029, [[1110.2586](#)].

- [81] Y. Nakayama, *Scale invariance vs conformal invariance*, *Phys. Rept.* **569** (2015) 1–93, [[1302.0884](#)].
- [82] L. J. Mason and D. Skinner, *Dual Superconformal Invariance, Momentum Twistors and Grassmannians*, *JHEP* **11** (2009) 045, [[0909.0250](#)].
- [83] N. Arkani-Hamed, F. Cachazo and C. Cheung, *The Grassmannian Origin Of Dual Superconformal Invariance*, *JHEP* **03** (2010) 036, [[0909.0483](#)].
- [84] N. Arkani-Hamed, J. L. Bourjaily, F. Cachazo, A. Hodges and J. Trnka, *A Note on Polytopes for Scattering Amplitudes*, *JHEP* **04** (2012) 081, [[1012.6030](#)].
- [85] O. Aharony, O. Bergman, D. L. Jafferis and J. Maldacena, *$N=6$ superconformal Chern-Simons-matter theories, $M2$ -branes and their gravity duals*, *JHEP* **10** (2008) 091, [[0806.1218](#)].
- [86] K. Hosomichi, K.-M. Lee, S. Lee, S. Lee and J. Park, *$N=5,6$ Superconformal Chern-Simons Theories and $M2$ -branes on Orbifolds*, *JHEP* **09** (2008) 002, [[0806.4977](#)].
- [87] J. M. Drummond, J. Henn, G. P. Korchemsky and E. Sokatchev, *Dual superconformal symmetry of scattering amplitudes in $N=4$ super-Yang-Mills theory*, *Nucl. Phys.* **B828** (2010) 317–374, [[0807.1095](#)].
- [88] S. Lee, *Yangian Invariant Scattering Amplitudes in Supersymmetric Chern-Simons Theory*, *Phys. Rev. Lett.* **105** (2010) 151603, [[1007.4772](#)].
- [89] A. Henriques and D. E. Speyer, *The multidimensional cube recurrence*, *Adv. Math.* **223** (2010) 1107–1136.
- [90] T. Lam, *Electroid varieties and a compactification of the space of electrical networks*, *ArXiv e-prints* (Feb., 2014) , [[1402.6261](#)].
- [91] V. P. Nair, *A Current Algebra for Some Gauge Theory Amplitudes*, *Phys. Lett.* **B214** (1988) 215.
- [92] I. M. Gel'fand and G. E. Shilov, *Generalized functions. Vol. 1*. Academic Press [Harcourt Brace Jovanovich, Publishers], New York-London, 1964 [1977].
- [93] A. Hodges, *Eliminating spurious poles from gauge-theoretic amplitudes*, *JHEP* **05** (2013) 135, [[0905.1473](#)].
- [94] P. Orlik and H. Terao, *Arrangements of hyperplanes*, vol. 300 of *Grundlehren der Mathematischen Wissenschaften [Fundamental Principles of Mathematical Sciences]*. Springer-Verlag, Berlin, 1992. 10.1007/978-3-662-02772-1.
- [95] A. Brandhuber, P. Heslop and G. Travaglini, *One-Loop Amplitudes in $N=4$ Super Yang-Mills and Anomalous Dual Conformal Symmetry*, *JHEP* **08** (2009) 095, [[0905.4377](#)].

- [96] H. Elvang, D. Z. Freedman and M. Kiermaier, *Dual conformal symmetry of 1-loop NMHV amplitudes in $N=4$ SYM theory*, *JHEP* **03** (2010) 075, [[0905.4379](#)].
- [97] J. M. Drummond and J. M. Henn, *All tree-level amplitudes in $N=4$ SYM*, *JHEP* **04** (2009) 018, [[0808.2475](#)].
- [98] M. Bullimore, L. J. Mason and D. Skinner, *Twistor-Strings, Grassmannians and Leading Singularities*, *JHEP* **03** (2010) 070, [[0912.0539](#)].
- [99] J. Broedel and S. He, *Dual conformal constraints and infrared equations from global residue theorems in $N=4$ SYM theory*, *JHEP* **06** (2010) 054, [[1004.2400](#)].
- [100] Y. Bai and S. He, *The Amplituhedron from Momentum Twistor Diagrams*, *JHEP* **02** (2015) 065, [[1408.2459](#)].
- [101] T. Bargheer, F. Loebbert and C. Meneghelli, *Symmetries of Tree-level Scattering Amplitudes in $N=6$ Superconformal Chern-Simons Theory*, *Phys. Rev.* **D82** (2010) 045016, [[1003.6120](#)].
- [102] D. Gang, Y.-t. Huang, E. Koh, S. Lee and A. E. Lipstein, *Tree-level Recursion Relation and Dual Superconformal Symmetry of the ABJM Theory*, *JHEP* **03** (2011) 116, [[1012.5032](#)].
- [103] A. E. Lipstein and L. Mason, *Amplitudes of 3d Yang Mills Theory*, *JHEP* **01** (2013) 009, [[1207.6176](#)].
- [104] P. A. M. Dirac, *Wave equations in conformal space*, *Annals Math.* **37** (1936) 429–442.
- [105] G. Mack and A. Salam, *Finite component field representations of the conformal group*, *Annals Phys.* **53** (1969) 174–202.
- [106] S. L. Adler, *Massless, Euclidean quantum electrodynamics on the five-dimensional unit hypersphere*, *Phys. Rev.* **D6** (1972) 3445–3461.
- [107] R. Marnelius and B. E. W. Nilsson, *Manifestly Conformally Covariant Field Equations and a Possible Origin of the Higgs Mechanism*, *Phys. Rev.* **D22** (1980) 830.
- [108] T. Goddard, P. Heslop and V. V. Khoze, *Uplifting Amplitudes in Special Kinematics*, *JHEP* **10** (2012) 041, [[1205.3448](#)].
- [109] S. Caron-Huot and S. He, *Three-loop octagons and n -gons in maximally supersymmetric Yang-Mills theory*, *JHEP* **08** (2013) 101, [[1305.2781](#)].
- [110] D. Gang, Y.-t. Huang, E. Koh, S. Lee and A. E. Lipstein. Unpublished notes.
- [111] Y.-t. Huang and S. Lee, *A new integral formula for supersymmetric scattering amplitudes in three dimensions*, *Phys. Rev. Lett.* **109** (2012) 191601, [[1207.4851](#)].
- [112] O. T. Engelund and R. Roiban, *A twistor string for the ABJ(M) theory*, *JHEP* **06** (2014) 088, [[1401.6242](#)].

- [113] S. Franco, D. Galloni and A. Mariotti, *The Geometry of On-Shell Diagrams*, *JHEP* **08** (2014) 038, [[1310.3820](#)].
- [114] S. Franco, D. Galloni, A. Mariotti and J. Trnka, *Anatomy of the Amplituhedron*, *JHEP* **03** (2015) 128, [[1408.3410](#)].
- [115] R. Karpman. Private communication.
- [116] J. L. Bourjaily, *Positroids, Plabic Graphs, and Scattering Amplitudes in Mathematica*, [1212.6974](#).
- [117] A. Knutson, T. Lam and D. E. Speyer, *Positroid varieties: juggling and geometry*, *Compos. Math.* **149** (2013) 1710–1752.
- [118] T. Lam, “Notes on the totally nonnegative Grassmannian.”
- [119] A. Postnikov, *Total positivity, Grassmannians, and networks*, [math/0609764](#).
- [120] R. Karpman, *Bridge graphs and Deodhar parametrizations for positroid varieties*, *ArXiv e-prints* (Nov., 2014) , [[1411.2997](#)].
- [121] R. Britto, F. Cachazo and B. Feng, *New recursion relations for tree amplitudes of gluons*, *Nucl. Phys.* **B715** (2005) 499–522, [[hep-th/0412308](#)].
- [122] R. Britto, F. Cachazo, B. Feng and E. Witten, *Direct proof of tree-level recursion relation in Yang-Mills theory*, *Phys. Rev. Lett.* **94** (2005) 181602, [[hep-th/0501052](#)].
- [123] A. Brandhuber, P. Heslop and G. Travaglini, *A Note on dual superconformal symmetry of the $N=4$ super Yang-Mills S -matrix*, *Phys. Rev.* **D78** (2008) 125005, [[0807.4097](#)].
- [124] J. Erdmenger and H. Osborn, *Conserved currents and the energy momentum tensor in conformally invariant theories for general dimensions*, *Nucl. Phys.* **B483** (1997) 431–474, [[hep-th/9605009](#)].
- [125] A. Cappelli and A. Coste, *On the Stress Tensor of Conformal Field Theories in Higher Dimensions*, *Nucl. Phys.* **B314** (1989) 707.
- [126] P. Griffiths and J. Harris, *Principles of algebraic geometry*. Wiley-Interscience [John Wiley & Sons], New York, 1978.
- [127] A. Björner and F. Brenti, *Combinatorics of Coxeter groups*, vol. 231 of *Graduate Texts in Mathematics*. Springer, New York, 2005.